JET PROPULSION

A publication of the

AMERICAN ROCKET SOCIETY

Research and Development

VOLUME 28 NOVEMBER 1958 SCIENCE & TECHNOLOGY

Missile Metal Machining

The picture below shows a guided missile component of A-286 alloy being machined on a 48" Monarch Air Gage Tracer Lathe at Diversey Engineering. Nowhere else can you get such extensive facilities for contour machining of Titanium, Inconel, A-286, Haynes Stellite and Zirconium.

LARGEST FACILITIES . . . exclusively devoted to your Guided Missile, Rocket, and Jet hardware problems in missile metal machining. Currently in production are accumulators, nozzles, nose sections, bulkheads, rings, cones, and rocket motor parts, all of them involving intricate and difficult machining techniques.

Write or phone for information on your designs and blueprints.

SEND FOR FREE BOOKLET

LEADERS IN CONTOUR MACHINING

Diversey ENGINEERING COMPANY

10550 WEST ANDERSON PLACE
FRANKLIN PARK, ILLINOIS • *A Suburb of Chicago*

FROM NOSE TO NOZZLE, FROM FIN TO FIN, CONTOUR TURNED PARTS—WITH PRECISION BUILT IN

JET PROPULSION

A publication of the

AMERICAN ROCKET SOCIETY

Research and Development

IRWIN HERSEY—DIRECTOR OF PUBLICATIONS

EDITOR MARTIN SUMMERFIELD

ASSISTANT EDITOR BARBARA NOWAK

ART EDITOR JOHN CULIN

ASSOCIATE EDITORS

ALI BULENT CAMBEL, *Northwestern University*
IRVIN GLASSMAN, *Princeton University*
M. H. SMITH, *Princeton University*

CONTRIBUTORS

MARSHALL FISHER, *Princeton University*
GEORGE F. McLAUGHLIN

ADVERTISING PRODUCTION MANAGER

WALTER BRUNKE

ADVERTISING & PROMOTION MANAGER

WILLIAM CHENOWETH

ADVERTISING REPRESENTATIVES

D. C. Emery & Associates
155 East 42 St., New York, N. Y.
Telephone: Yukon 6-6855

James C. Galloway & Co.
6535 Wilshire Blvd., Los Angeles, Calif.
Telephone: Olive 3-3223

Jim Summers & Associates
35 E. Wacker Dr., Chicago, Ill.
Telephone: Andover 3-1154

R. F. Pickrell & Associates
318 Stephenson Bldg., Detroit, Mich
Telephone: Trinity 1-0790

Louis J. Bresnick
304 Washington Ave., Chelsea 50, Mass.
Telephone: Chelsea 3-3335

John W. Foster
239 4th Ave., Pittsburgh, Pa.
Telephone: Atlantic 1-2977

Scope of JET PROPULSION

This Journal is a publication of the American Rocket Society devoted to the advancement of the field of jet propulsion through the dissemination of original papers disclosing new knowledge or new developments. As used herein, the term "jet propulsion" embraces all engines that develop thrust by rearward discharge of a jet through a nozzle or duct; and thus it includes air-consuming engines and underwater systems as well as rockets. JET PROPULSION is open to contributions dealing not only with propulsion but with other aspects of jet-propelled flight, such as flight mechanics, guidance, telemetering, and research instrumentation. Increasing emphasis will be given to the scientific problems of extraterrestrial flight.

Information for Authors

Manuscripts must be as brief as the proper presentation of the ideas will allow. Exclusion of dispensable material and conciseness of expression will influence the Editors' acceptance of a manuscript. In terms of standard-size double-spaced typed pages, a typical maximum length is 22 pages of text (including equations), 1 page of references, 1 page of abstract, and 12 illustrations. Fewer illustrations permit more text, and vice versa. Greater length will be acceptable only in exceptional cases.

Short manuscripts, not more than one quarter of the maximum length stated for full articles, may qualify for publication as Technical Notes or Technical Comments. They may be devoted to new developments requiring prompt disclosure or to comments on previously published papers. Such manuscripts are usually published within two months of the date of receipt.

Sponsored manuscripts are published occasionally as an ARS service to the industry. A manuscript that does not qualify for publication according to the above-stated requirements as to subject, scope or length, but which nevertheless deserves widespread distribution among jet propulsion engineers, may be printed as an extra part of the Journal or as a special supplement, if the author or his sponsor will reimburse the Society for actual publication costs. Estimates are available on request. Acknowledgment of such financial sponsorship appears as a footnote on the first page of the article. Publication is prompt since such papers are not in the ordinary backlog.

Manuscripts must be double spaced on one side of paper only with wide margins to allow for instructions to printer. Include a 100 to 200 word abstract. State the authors' positions and affiliations in a footnote on the first page. Equations and symbols may be handwritten or typewritten; clarity for the printer is essential. Greek letters and unusual symbols should be identified in the margin. If handwritten, distinguish between capital and lower case letters, and indicate subscripts and superscripts. References are to be grouped at the end of the manuscript and are to be given as follows: for journal articles: authors first, then title, journal, volume, year, page numbers; for books: authors first, then title, publisher, city, edition, and page or chapter numbers. Line drawings must be clear and sharp to make clear engravings. Use black ink on white paper or tracing cloth. Lettering should be large enough to be legible after reduction. Photographs should be glossy prints, not matte or semi-matte. Each illustration must have a legend; legends should be listed in order on a separate sheet.

Manuscripts must be accompanied by written assurance as to security clearance in the event the subject matter lies in a classified area or if the paper originates under government sponsorship. Full responsibility rests with the author.

Submit manuscripts in duplicate (original plus first carbon, with two sets of illustrations) to the Editor, Martin Summerfield, Professor of Aeronautical Engineering, Princeton University, Princeton, N. J. Preprints of papers presented at ARS national meetings are automatically considered for publication.

JET PROPULSION is published monthly by the American Rocket Society, Inc., and the American Interplanetary Society at 20th & Northampton Sts., Easton, Pa., U. S. A. Editorial offices: 500 Fifth Ave., New York 36, N. Y. Price: $12.50 per year, $2.00 per single copy. Second-class mail privileges authorized at Easton, Pa. Notice of change of address should be sent to the Secretary, ARS, at least 30 days prior to publication. Opinions expressed herein are the authors and do not necessarily reflect the views of the Editors or of the Society

Recent Advances in Transient Surface Temperature Thermometry

J. GORDON HALL and A. HERTZBERG

Cornell Aeronautical Laboratory, Inc., Buffalo, N. Y.

Dr. Hall, a research aerodynamicist at the Cornell Aeronautical Laboratory, has had many years of experience in shock tube investigations. He was educated in Canada (B.A., 1950, University of British Columbia; M.S., 1951 and Ph.D., 1954, University of Toronto). After receiving his doctorate he was a research associate and assistant professor at the Institute of Aerophysics, University of Toronto. He moved to the Cornell Aeronautical Laboratory this year.

Mr. Hertzberg, presently Assistant Department Head of Aerodynamic Research at the Cornell Aeronautical Laboratory, is well known for his work and publications on the development of the shock tube as a tool for various basic studies. Trained in aeronautical engineering at Virginia Polytechnic Institute (B.Ae.E., 1943) and Cornell (M.Ae.E., 1949), he has been associated with Cornell Aeronautical Laboratory most of his career.

Nomenclature

C = specific heat capacity
e = film voltage
I = film current
k = heat conductivity
K = thermal diffusivity, $k/\rho c$
l = film thickness
q = rate of heat transfer per unit area
t = time
T = film temperature
$\bar{T}$ = average temperature through film
R = film resistance
R_t = film resistance at temperature T_t
x = distance normal to film measured from exposed surface
α = temperature coefficient of resistance
β = $\sqrt{\rho_B k_B C_B}$
ρ = mass density
δ = $\sqrt{Kt}$ = characteristic thermal diffusion depth
τ = variable of integration; time

Subscripts

F refers to film
B refers to backing material

Introduction

METHODS of determining transient surface temperatures with a time resolution of the order of 1 microsec or better are of interest today in various fields of scientific and engineering research. Until about 1953, the principal advances toward reliable techniques for such measurement were made in connection with two problems: Determination of cylinder wall temperature variations in reciprocating engines, and determination of the surface temperature history of gun barrels subjected to continuous firing. In 1939, Meier in Germany (1),[1] following an earlier suggestion by Pfriem (2), successfully used a 2-μ thick gold film as a surface resistance thermometer to record quasi-steady cylinder wall temperatures. The gold film was evaporated in spiral form onto a thin insulating layer of aluminum oxide electrolytically deposited on an aluminum base plug. Around 1941, Hackemann in Germany developed a rugged thermocouple for gun barrel application (3). This consisted of a 2-μ thick nickel film, plated and ground on the end of an encased steel wire. Imbedded in the gun barrel with the nickel film flush with the bore, the thermocouple had very rapid response and sensed a temperature close to the bore surface temperature. In subsequent years, American workers developed improved versions of this instrument (4 to 8). In a design described by Bendersky (6), the film thickness was reduced to 1μ thereby lowering the response time to $\frac{1}{4}$ microsec.

Around 1953, a new demand for a microsecond response instrument arose in the field of shock tube and hypersonic shock tunnel research, where it was necessary to determine heat transfer rates at the surface of aerodynamic models in quasi-steady gas flows of durations ranging from 1 millisec to 20 microsec. One approach taken here was to measure model surface temperature change with time and from this calculate the corresponding heat transfer. Although the Bendersky-type thermocouple had sufficiently fast response for the measuring times involved, it was considered too insensitive for general application. This difficulty was overcome by depositing thin films directly on dielectric models or inserts which experienced measurable surface temperature rise in the brief flow times available. Films of sub-micron thickness were tried in this way as both thermocouples and resistance thermometers. The latter method proved generally superior and has been subsequently developed with a high degree of success.

Another successful approach to shock tube heat transfer determination involved the development of relatively thick film surface calorimeters. These retain essentially all the heat absorbed during the short flow time and provide a direct indication of surface heat transfer rate.

The purpose of the present article is to review the foregoing advances in transient surface temperature thermometry and calorimetry which have been made over a period of about the past five years. As the developments during this period have been made largely in the field of shock tube research, the discussion of the thin and thick film techniques which follows makes frequent reference to shock tube heat transfer application.

Thin Film Surface Thermometer Techniques

The possibility of using very thin metallic films on dielectric bodies for transient surface temperature measurement in shock tube flows was apparently considered in several laboratories at about the same time. Early development of the techniques involved (1953–1954) was done at Princeton and Lehigh Universities (9,10) and at the Cornell Aeronautical Laboratory, Inc. (11). The early studies (e.g., (11)) achieved greater success using the surface film as a resistance thermometer rather than as an evaporated thermocouple (requiring two overlapping films). Erosion difficulties were experi-

Received Sept. 19, 1958.

[1] Numbers in parentheses indicate References at end of paper.

enced with the latter, and, in addition, its sensitivity was relatively low. Accordingly, there was an initial concentration of effort on the resistance thermometer, and its development proceeded rapidly. While some success has been obtained with the evaporated thermocouple (12f), it appears to have been largely abandoned for shock tube use. In what follows, primary consideration is given to use of the thin film as a resistance thermometer, although much of what is said applies with little or no change to the film thermocouple.

The thermal response characteristics of the thin film can be determined from the classical theory of one-dimensional heat flow (13), and detailed analyses have been given by several authors (11,14,15). Film thicknesses used, of the order of 0.1 μ, are ordinarily much smaller than the characteristic thermal diffusion depth δ of the film metal for the shortest times of interest.[2] Thus temperature gradients in the film may be neglected. The film senses the instantaneous surface temperature of the dielectric backing, but some response lag relative to zero film thickness occurs because of the small but finite film heat capacity. The magnitude of this response lag is illustrated by considering a suddenly applied heat transfer rate varying inversely as the square root of time. In the ideal case of zero film thickness l the surface temperature instantly jumps to a new constant value. For a finite film thickness, the backing surface temperature attains 94 per cent of the ideal value in a time $t = 100\,\tau_R$, where

$$\tau_R = \frac{\rho_F^2 C_F^2 l^2}{\rho_B C_B k_B}$$

is a characteristic time parameter of the film plus backing (15). With a 0.1 μ platinum film on quartz, for example, τ_R is about 3.5×10^{-8} sec, and the response is extremely fast. In the shock tube or shock tunnel, a suddenly applied constant rate of heat transfer is of interest. In this case, the surface temperature for zero film thickness increases as the square root of time. With a finite film thickness, 90 per cent of the ideal temperature rise is attained in a time of $100\,\tau_R$. For testing times large compared to $100\,\tau_R$ the film heat capacity effects may be neglected.

The technology of the preparation of thin films has been fairly well developed and reported in the literature. The methods of applying films to pyrex, glass or quartz surfaces include sputtering and evaporation under vacuum (16 to 20), the painting technique using commercial metallic paints such as Hanovia preparations (11,21) and the use of metallic foils (10,21). The sputtering and evaporation methods provide good control of film thickness and uniformity on plane surfaces but are somewhat difficult to apply with sharply curved surfaces. After deposition of the metal on glass by sputtering or evaporation, it is common to bake the element at a temperature close or equal to the softening temperature of the backing (around 1100 to 1200 F for pyrex or quartz), after which it is allowed to cool slowly. The baking ensures some penetration of metal into the backing which provides a strong metal-to-glass bond and greatly increases the resistance of the film to abrasion. Electrical leads may be soft-soldered to the film with suitable flux. Platinum, gold and rhodium have been the metals most used for sputtering or evaporation followed by baking. Reference (20) reports that evaporated platinum films on glass without baking are easily removed, whereas chromium, with its affinity for oxygen, which is believed important for bonding, forms a film very resistant to corrosion and abrasion. Similar results were observed in tests of (21) where, in addition, evaporated rhodium films (unbaked) were also found very durable.

In the painting method the metallic solution is applied with a brush, pen or air brush. Then, the element is baked in a vented oven at a temperature near the softening point of the backing. During the baking process, the vehicle holding the metallic particles in suspension is driven off, and the particles react with a reducing agent to produce a smooth film. As with sputtered or evaporated elements, the baking produces a film which is very durable. An important advantage of the painting method is its simplicity, but film thickness and uniformity cannot be controlled to the degree possible with evaporation or sputtering. Provided the film thickness is small compared to the thermal diffusion depth δ, precise control or knowledge of thickness is unimportant. Uniformity of thickness is desirable to provide uniform heating if the electrical pulse method of calibration is used. Reference (21) reports that film resistance (thickness) is easily repeatable to ± 50 per cent, and temperature coefficients of film resistance are repeatable to ± 5 per cent using Hanovia platinum 05-X paint.

The use of bonded metallic foils becomes attractive where the film cannot be sputtered, evaporated or baked. Gold, copper and nickel foils are available commercially in thicknesses ranging upward from 0.1 micron. Gold foils have proved very satisfactory where erosion is not a problem (10). In shock tunnel tests with foils mounted at the stagnation point of a sphere, bonded nickel foil was found very durable and gold foil extremely fragile (21).

Electrical stability of the film is necessary for its use as a resistance thermometer. The natural and artificial aging of thin metal films has been extensively studied over the years (see for example (22)). With sputtered, evaporated and painted films baked at high temperatures as described, the films produced are usually quite stable. A slow increase of resistance with time is sometimes observed (e.g., (11)) which, while not a problem for short measuring times, is bothersome if it necessitates too frequent calibration.

Because the physical properties of thin films are dependent on film thickness and can differ markedly from the bulk metal values (e.g., (17,20,38)), calibration of the thin film resistance thermometer is necessary for its quantitative use. Over the usual range of application, involving maximum temperature increases up to the order of a few hundred deg C, the film resistance-temperature relation can be assumed linear.[3] The film resistance R is then given by

$$R = R_i[1 + \alpha(T - T_i)]$$

where R_i is the film resistance at initial temperature T_i, and α is a constant coefficient which is determined by standard laboratory methods. Measured values of α are always less than for the bulk metal, and typical values for sputtered or evaporated platinum and gold films might lie in the range 0.0015 to 0.0025 per deg C.

The principal aerodynamic application of the thin film as a resistance thermometer has been to heat transfer measurements in the shock tube and shock tunnel. Local surface heat transfer rates are calculated from the measured surface temperature histories by means of classical heat conduction theory. In the short flow times of the shock tube/tunnel, the depth of heat penetration into the film backing material is small, and the local heat flow may be assumed one-dimensional. Neglecting the response lag due to thermal capacity of the film, the instantaneous surface heat transfer rate $q(t)$ is then given by (see for example (18))

$$q(t) = \frac{\beta}{\sqrt{\pi}} \int_0^t \frac{1}{\sqrt{t - \tau}} \frac{dT}{d\tau}\, d\tau \quad \ldots\ldots\ldots\ldots [1]$$

where $\beta = \sqrt{\rho_B k_B C_B}$ is a constant which characterizes the backing material. In terms of film voltage e Equation [1] becomes

$$q(t) = \frac{\beta}{IR_i\alpha\sqrt{\pi}} \int_0^t \frac{1}{\sqrt{t - \tau}} \frac{de}{d\tau}\, d\tau \quad \ldots\ldots\ldots [2]$$

[2] The thermal diffusion depth $\delta = \sqrt{K_F t}$ is a measure of the depth of heat penetration in time t.

[3] In tests reported in (23) the linear resistance-temperature relation was observed to hold to within ± 2 F from 70 F up to the highest test temperature used, 850 F.

Thus, calculation of q from the film voltage history requires the value of β/α.

If there is some penetration of film particles into the backing material during the film baking process, values of β determined from bulk properties of the backing may be unreliable. Calibration is therefore desirable, and several methods for determining β under known heat flow conditions are used. A common technique (18,24) is to apply a sudden and known constant rate of heat input to the backing using a step function electric current through the film. The current is obtained with a long time constant, capacitor discharge. From the theoretical solution for this case ($T \backsim \sqrt{t}$) and an oscilloscope record of film voltage variation with time, the overall constant β/α may be determined. For heat transfer measurement only, a separate determination of α is unnecessary. The repeatability of this calibration technique is reported to be ± 5 per cent (18,25).

A second calibration procedure to determine β/α involves flush mounting the element in a suitable aerodynamic model which is then subjected to a known heat transfer rate by aerodynamic heating in a shock tube flow (11). The known theoretical heat transfer rate and recorded film voltage again determine β/α. A repeatability of ± 5 per cent is reported also with this method (11).

Experience has shown that with some glass backing materials, such as fused quartz and pyrex, measured values of β agree reasonably well with bulk values and do not vary greatly from one sample to the next. Consequently, for some applications assumption of an average value for β (about 0.074 BTU/ft² F sec$^{1/2}$ for quartz and pyrex) may be sufficiently accurate, and calibration can be avoided. In this case only the straightforward determination of α is required to obtain heat transfer data.

A preferable form of Equation [2] for numerical evaluation of heat transfer from oscillographs of film voltage variation with time is

$$q(t) = \frac{\beta}{\alpha I R_i \sqrt{\pi}} \left[\frac{e(t)}{t^{1/2}} + \frac{1}{2} \int_0^t \frac{e(t) - e(\tau)}{(t-\tau)^{3/2}} \, d\tau \right]$$

which does not involve measurement of slopes. Reference (11) gives an expression for q which includes a first order correction for film response lag where such is required.

Shock tube and shock tunnel studies of hypersonic heat transfer distributions over models instrumented with thin films are currently being carried out by a number of research groups (19,25 to 33). Typical film geometry for these applications is rectangular with dimensions of the order of 1 to 2 cm by 1 to 2 mm. With a typical film resistance of 50 ohms, constant current of 20 ma and resistant coefficient α of 0.002 per deg C, a film output voltage of 2 mv per deg C of temperature rise is obtained. The heat transfer rates measured in shock tunnels range roughly from one to several hundred BTU/ft²/sec. With flow durations of the order of 1 millisec, film temperature rise at the higher heating rates does not usually exceed 200 C. The overall accuracy of temperature rise measurement as estimated by various investigators at the present time varies from ± 5 to ± 10 per cent, and that for heat transfer rate from ± 5 to ± 15 per cent. These limits indicate that heat transfer rates can now be measured in the shock tube and shock tunnel with an accuracy which possibly exceeds that attainable in conventional hypersonic tunnels.

Another application of the thin film in shock tube research is as a shock wave detector (9). The film is mounted flush in the shock tube wall and provides a very fast electrical pulse for trigger purposes on passage of the shock wave.

One limit to quantitative accuracy of the film thermometer as described above is imposed by the onset of thermal ionization of the gas at high temperatures (19,26,28,34). When ionization occurs, it appears that the film resistance is partially short-circuited by the electrically conducting gas, and the film voltage is no longer a known and simple function of the film temperature. Attempts have been made to eliminate the effects of ionization by evaporation of a thin insulating layer over the metallic film. In one instance, a $\frac{1}{4}$-μ silicon monoxide layer was evaporated and subsequently baked to obtain a more durable and better insulating layer of silicon dioxide (19). Further experimentation with this technique is required before the usefulness of thin films in ionized flows is fully established.

With its fast response, high sensitivity and ruggedness, it is to be expected that the thin film surface resistance thermometer will find useful application in fields other than shock tube and shock tunnel research. One example of this is its application as a total temperature transducer to study stagnation temperature fluctuations in a jet engine inlet during flight (23). The transducer consists of a thin film (painted) on the spherical head of a pyrex probe. Stagnation point heat transfer rate is deduced from the measured surface temperature, and from the heat transfer rate the stagnation temperature can be calculated. The instrument is designed to sense total temperature fluctuations in the range -65 to 1000 F lasting for 1 millisec. The probe operates continuously at 500 F and can withstand 1000 F for $\frac{1}{2}$ min.

Another example of thin film application is the hot film anemometer (35) which operates in a similar way to the well-known hot wire instrument. Reference (35) describes a film anemometer consisting of a pyrex probe with a 30 deg wedge tip on which a 0.2 × 1 mm platinum film is deposited. The film is heated by electric current to a temperature above the stream recovery temperature, and its resistance serves to indicate the rate of heat loss to the stream. Advantages claimed for the film anemometer over the conventional hot wire are increased signal/noise ratio, improved high-frequency response and excellent mechanical characteristics.

Thick Film Surface Calorimeter Techniques

Although the thin film resistance thermometer has a rather wide range of application in aerodynamic heat transfer measurement, its successful use becomes difficult under certain extreme conditions. These conditions include very high heat transfer rates and/or long flow times giving excessive surface temperature rise, high electrical interference such as may be present with arc driven tunnels, flow ionization as mentioned above and excessive erosion by foreign particles in the gas stream. The shortcomings of the thin film in these respects may be reduced by increasing the film thickness. With the thin film, the thickness l is much smaller than the characteristic metal diffusion depth δ, and the film retains essentially no heat. If l is increased to a value equal to or greater than δ, practically all the heat entering the exposed film surface is retained, and the film functions as a surface calorimeter (36). Practical upper and lower limits on l are set by the need for measurable film temperature rise and the need for minimum heat loss to the dielectric backing, respectively. Reference (36) shows that $l = \delta$ is a practical compromise such that the heat loss may be neglected with small error. The surface heat transfer rate may then be expressed as

$$q(t) = \rho_F C_F l \frac{d\bar{T}(t)}{dt}$$

where

$$\bar{T}(t) = \frac{1}{l} \int_0^l T(x, t) \, dx$$

is the average temperature through the film at time t. Hence, if the average film temperature $\bar{T}$ is measured as a function of time, the instantaneous heat transfer rate is given by the local slope of $\bar{T}$ vs. t. Although the mechanics of data reduction are thus simpler for the thick than for the thin film, the measurement of slopes is inherently inaccurate. It

might be noted that with $l = \delta$, the thick film may still be thin by usual standards. With platinum, and a measuring time of 100 microsec for example, the value of δ is about 50 μ.

One method of measuring $\bar{T}$ is to use the film as a resistance thermometer. To a first order approximation, it may be shown (36) that the film resistance R is directly proportional to $\bar{T}$, in which case q is given in terms of film voltage e by

$$q(t) = \frac{\rho_F C_F l}{\alpha I R_i} \frac{de}{dt} \quad [3]$$

Second and higher order corrections to R due to the initially nonlinear temperature distribution through the film become negligible in a short time. A particular resistance calorimeter for stagnation point heat transfer measurements described in (36) consists of a curved platinum strip (bulk metal) of dimensions 0.636×0.475 cm soldered to a thin platinum film painted and baked on the nose of a pyrex model. With the strip thickness used, about 30 μ, the resistance is of the order of 4×10^{-3} ohms, and relatively large currents of the order of 5 to 10 amp are necessary for adequate voltage output. Bulk metal properties are used to determine the value of the constant $\rho_F C_F l/\alpha R_i$ in Equation [3], and a direct calibration check is also made with electrical heating methods. The maximum calorimeter resistance change is limited to about 25 per cent to avoid possible significant error from variation of $\rho_F C_F l/\alpha R_i$ with temperature.

This instrument has been used to measure stagnation point heat transfer rates in the shock tube ranging from 1000 to 35,000 BTU/ft^2/sec with flow durations of the order of 25 to 50 microsec (33,36). The maximum surface temperature rise on pyrex with these conditions is around 2800 C, well above the melting point. The low resistance of the calorimeter makes it less susceptible to ionization effects than the thin film, while its increased thickness gives it greater durability. The latter is particularly important at model stagnation points if foreign particles which cause erosion are present in the gas stream.

Another type of surface calorimeter which has reportedly proved very successful under extreme conditions is the variable reluctance instrument (12e,37). This is used in arc driven or "hot-shot" tunnels where electrical interference is very high and is designed to measure heat transfer rates in the range of 10 to 1000 BTU/ft^2/sec with flow durations up to 20 millisec. In this gage, a calorimeter sensing element 0.18 in. in diameter and accurately flush with the surface varies the reluctance in a magnetic circuit. A voltage output proportional to the average temperature rise through the element is obtained, and the slope of a voltage-time record gives heat transfer rate. The sensing element and inductance coils are housed in a cylinder of 0.25 in. diameter and 0.5 in. length. Calibration with a repeatability in the range of 2 to 5 per cent is accomplished using alternating hot and cool jets of water with an accurately known temperature difference. The gage is reported to have a response time well under 1 millisec and an accurate reading duration of about $\frac{1}{10}$ sec (12e). The sensing surface is reported to withstand a small amount of melting and to normally endure 20 to 50 tunnel runs with good repeatability (12e). It is noted that the low impedance of this calorimeter permits its use a few feet from a million amp arc discharge.

For some applications, a practical alternative to the surface calorimeter, where surface temperature rise is excessive for the thin film resistance thermometer, might be the Bendersky-type nickel-steel thermocouple (6). This is a very rugged and fast instrument of sufficiently low thermal sensitivity that the (steel) surface temperature rise is only about one tenth that for glass.

Conclusions

The present review has covered some advances in transient surface temperature thermometry and calorimetry made during the past five years in the field of shock tube and shock tunnel heat transfer research. Two basic techniques successfully evolved for shock tube heat transfer measurement are thin film surface thermometry and thick film surface calorimetry. The former method records instantaneous surface temperature from which instantaneous heat transfer rate is calculated. The latter method records total heat input at the surface, and instantaneous heat transfer rate is given by the corresponding time rate of change.

The most successful type of thin film instrument is presently the thin film resistance thermometer, which is simple, sensitive, rugged, and which has microsecond response. In present applications, where the surface temperature does not exceed about 200 C, the film resistance thermometer is capable of 5 per cent accuracy in measurement of surface temperature and heat transfer rate. Extension of its quantitative use to ionized flows is a matter of current research. Its desirable characteristics have led to its application in fields other than shock tube research.

The surface calorimeter has inherent low sensitivity and electrical impedance, and is advantageous under conditions of extreme surface temperature rise or high electrical interference. Its increased thickness makes it more durable than the thin film, and its low impedance renders it less susceptible to flow ionization effects. Both resistance and variable reluctance surface calorimeters have been successfully developed for extreme conditions where use of the thin film resistance thermometer would not be feasible.

References

1 Meier, Adolf, "Recording Rapidly Changing Cylinder-Wall Temperatures," *Forschung auf dem Gebiete des Ingenieurwesens*, vol. 10, no. 1, Jan.-Feb. 1939, pp. 41–54; translated in NACA TM 1013, May 1942.

2 Pfriem, H., "Zur Messung schnell wechselnder Temperaturen in der Zylinderwand von Kolbenmaschinen," *Forschung auf dem Gebiete des Ingenieurwesens*, vol. 6, no. 4, July-Aug. 1935, p. 195.

3 Hackemann, P., "Method for Measuring Rapidly Changing Surface Temperatures and Its Application to Gun Barrels," British Theor. Res. Tr. 1/46, Armament Res. Dept.

4 St. Clair, C. R., Jr., "The Measurement of the Bare Surface Temperature of Gun Barrels," Purdue Univ. Report no. 273-MG, June 15, 1945.

5 "Surface Temperature Measurement," Armour Research Foundation Report no. 5, Project no. 122-7721, Aug. 8, 1952.

6 Bendersky, D., "A Thermocouple for Measuring Transient Temperatures," *Mechanical Engineering*, vol. 75, no. 2, Feb. 1953, pp. 117–121.

7 Chenoweth, J. M., Brock, J. E., St. Clair, C. R. and Kawkins, G. A., "Gun Barrel Measurement Involves Rapidly Fluctuating Temperatures," *Instruments*, vol. 26, Nov. 1953, p. 1714.

8 "Development of Fabrication Techniques for a Special Thermocouple to Measure Transient Surface Temperatures," Midwest Research Institute Phase Report no. 2, Dec. 1955.

9 Blackman, V. H., "Vibrational Relaxation in O_2 and N_2," Princeton Univ. Dept. of Physics, NR 061-20, May 1955; *also Journal of Fluid Mechanics*, vol. 1, 1956, p. 61.

10 Chabai, A. J. and Emrich, R. J., "Measurement of Wall Temperature and Heat Flow in the Shock Tube," *Journal of Applied Physics*, vol. 26, June 1955, p. 779.

11 Vidal, R. J., "Model Instrumentation Techniques for Heat Transfer and Force Measurements in a Hypersonic Shock Tunnel," C.A.L. Report no. AD-917-A-1, Feb. 1956, WADC TN 56-315, AD 97238.

12 Private Communication with: a) J. Rabinowicz, C.I.T., Jan. 22, 1958; b) Y. Yoler, G. E. Phila., Jan. 21, 1958; c) D. Bershader, LMSD, Calif., Feb. 5, 1958; d) R. Emrich, Lehigh Univ., Jan. 27, 1958; e) M. R. Mulkey, ARO, Inc., Jan. 28, and June 24, 1958; f) J. J. Jones, NACA, Langley Field, Jan. 20, 1958.

13 Carslaw and Jaeger, "Conduction of Heat in Solids," Clarendon Press, Oxford, 1947.

14 Bershader, D. and Allport, J., "On the Laminar Boundary Layer Induced by a Traveling Shock Wave," Princeton Univer-

sity Dept. of Physics Technical Report II-22, May 1956.

15 Bromberg, R., "Use of the Shock Tube Wall Boundary Layer in Heat Transfer Studies," JET PROPULSION, vol. 26, Sept. 1956, p. 737; *also* Ramo-Wooldridge Report no. 20280, May 19, 1955.

16 Strong, J., "Procedures in Experimental Physics," Prentice-Hall, New York, 1946.

17 Holand, J., "Vacuum Deposition of Thin Films," Wiley and Sons, New York, 1956.

18 Rabinowicz, J., Jessey, M. E. and Bartsch, C. A., "Resistance Thermometer for Heat Transfer Measurements in a Shock Tube," GALCIT Hypersonic Research Project, Memo no. 33, July 2, 1956.

19 Nagamatsu, H. T. and Geiger, R. E., "A Fast Response Device for Measuring Heat Transfer," General Electric, Schenectady, Turbine Machinery Instrumentation, 2nd Annual Seminar, Schenectady, N. Y., May 15–16, 1957.

20 Winding, C. C., Topper, L. and Baus, B. V., "Metal Film Resistance Thermometers for Measuring Surface Temperatures," *Industrial and Engineering Chemistry*, vol. 47, no. 3, March 1955, pp. 386–392.

21 Vidal, R. J., "A Resistance Thermometer for Transient Surface Temperature Measurements," presented at American Rocket Society Meeting, Sept. 24–26, 1956.

22 Belser, R. B., "Electrical Resistance of Thin Metal Films Before and After Artificial Aging by Heating," *Journal of Applied Physics*, vol. 28, no. 1, Jan. 1957, pp. 109–116.

23 Vidal, R. J. and Hilton, J. H., "The Construction and Application of a Rapid Response Resistance Thermometer Probe," C.A.L. Report no. IM-1062-A-1, April 1956.

24 Bartlett, G. E., Logan, J. G., Vidal, R. J. and Wittliff, C. E., "Investigation of Stagnation Point Heat Transfer in the C.A.L. Hypersonic Shock Tunnel," C.A.L. Report no. AA-966-A-1, Nov. 1955.

25 Wittliff, C. E. and Rudinger, G., "Summary of Instrumentation Development and Aerodynamic Research in a Hypersonic Shock Tunnel," C.A.L. Report AD-917-A-2, Aug. 1958, WADC TR 58-401, Part I, AD 155 758.

26 Vitale, A. J., Kaegi, E. M., Diaconis, N. S. and Warren, W. R., "Results from Aerodynamic Studies of Blunt Bodies in Hypersonic Flows of Partly Dissociated Air," General Electric Missile and Ordnance Systems Dept., Phila., Document no. 58 SD 214, Feb. 1958; *also* 1958 Heat Transfer and Fluid Mechanics Inst., Stanford Univ. Press, 1958.

27 Wittliff, C. E., Wilson, M. R. and Hertzberg, A., "The Tailored-Interface Hypersonic Shock Tunnel," ASME-ARS Aviation Conference, Dallas, Texas, March 16–20, 1958.

28 Hartunian, R., Russo, A. and Marrone, P., "Boundary-Layer Transition and Heat Transfer in Shock Tubes," 1958 Heat Transfer and Fluid Mechanics Inst., Stanford Univ. Press, June 1958, p. 114.

29 Rabinowicz, J., "Aerodynamic Studies in the Shock Tube," GALCIT Hypersonic Research Project, Memo no. 38, June 1957.

30 Rabinowicz, J., "Measurements of Turbulent Heat Transfer Rates on the Aft Portion and Blunt Base of a Hemisphere-Cylinder in the Shock Tube," GALCIT Hypersonic Research Project, Memo no. 41, Nov. 1957; *also* JET PROPULSION, vol. 28, no. 9, Sept. 1958.

31 Rose, P. H., Adams, M. C. and Probstein, R. F., "Turbulent Heat Transfer on Highly Cooled Blunt Nosed Bodies of Revolution in Dissociated Air," 1958 Heat Transfer and Fluid Mechanics Inst., Standford Univ. Press, p. 143; *also* AVCO Research Report no. 14, Dec. 1957.

32 van der Noordoa, R. S. L., "Heat Transfer Measurements from Ionized Argon Produced by Strong Shock Waves," M.A.Sc. Thesis, Feb. 1957, Cornell Univ., Ithaca, N. Y.

33 Rose, R. H. and Stark, W. I. "Stagnation Point Heat Transfer Measurements in Dissociated Air," AVCO Research Report no. 3, April 1957; *also Journal of Aeronautical Sciences*, vol. 25, no. 2, Feb. 1958.

34 Jahn, R. G. and Weimer, D. K., "On the Performance of Thin-Film Gauges in High-Temperature Shock Tube Flows," *Journal of Applied Physics*, vol. 29, no. 4, April 1958, p. 741.

35 Ling, S. C. and Hubbard, P. G., "The Hot-Film Anemometer: A New Device for Fluid Mechanics Research," *Journal of Aeronautical Sciences*, vol. 23, no. 9, 1956, pp. 890–891.

36 Rose, R. H., "Development of the Calorimeter Heat Transfer Gage for Use in Shock Tubes," AVCO Research Report no. 17, Feb. 1958.

37 Perry, R. W. and MacDermott, W. N., "Development of the Spark-Heated Hypervelocity, Blowdown Tunnel—Hotshot," AEDC TR 58-6, June 1958.

38 Simpson, T. B. and Winding, C. C., "Properties of Evaporated Metal Films Related to Their Use for Surface Temperature Measurements," *Journal of the American Institute of Chemical Engineers*, vol. 2, no. 113, 1956.

Project Snooper, A Program for Unmanned Interplanetary Reconnaissance

Martin I. Willinski[1] and Elsie C. Orr[2]

Rocketdyne, A Division of North American Aviation, Inc., Canoga Park, Calif.

A program for the unmanned reconnaissance of the solar system at a moderate cost, in the near future, is suggested. A nonreturn, nuclear powered ion rocket propelled reconnaissance vehicle weighing 3300 lb is described. A vehicle weight statement, drawings and a description of a possible mission trajectory are included.

Presented at the ARS Spring Meeting, Washington, D. C., April 4–7, 1957.

[1] Senior Research Engineer, Advance Design Section. Member ARS.

[2] Computing Engineer, Advance Design Section. Member ARS.

Nomenclature

A	=	mass number of element
a	=	vehicle acceleration, g
c	=	exhaust velocity, ft/sec
e	=	ionic charge, esu
I	=	ion beam current, amp
j	=	ion current density, amp/cm^2
k	=	unit conversion factors
M	=	vehicle weight, lb
m	=	mass of ion, gm
P	=	ion exhaust beam power, w
V	=	accelerating voltage, v

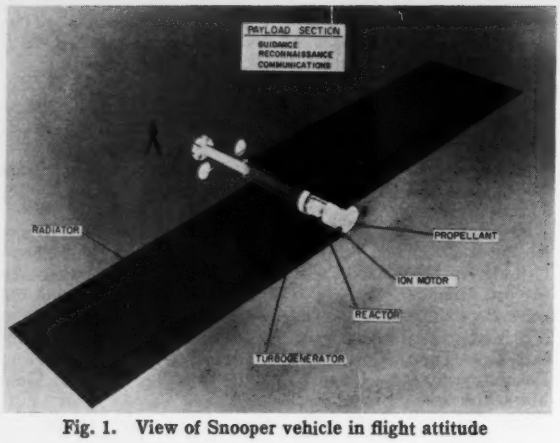

Fig. 1. View of Snooper vehicle in flight attitude

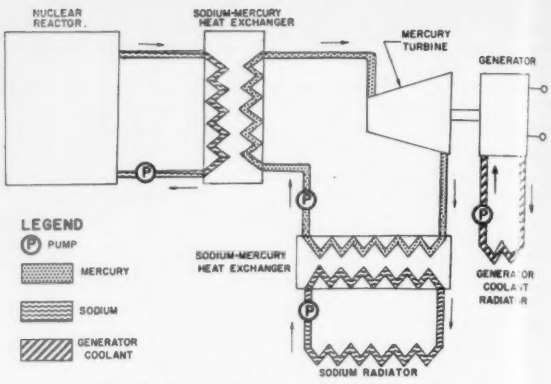

Fig. 2 Ion rocket power supply system

x = accelerating gap distance, cm
$\ddot{r}$ = radial acceleration
$\dot{r}$ = radial velocity
∂ = partial differential symbol
ξ = angle from final take-off point to Earth's heliocentric velocity
θ = angle from final take-off point to vehicle
$\ddot{\theta}$ = angular acceleration of vehicle
$\dot{\theta}$ = angular velocity of vehicle
β = angle from hyperbola axis to cut-off point
α = angle from hyperbola axis to asymptote
φ = angle from hyperbola axis to cut-off velocity

Introduction

THE primary aim of space travel in the near future is the acquisition of knowledge. Obviously, it is desirable to obtain this information at a minimum expenditure of both money and manpower. The acceptance of this requirement leads logically to a system for utilizing robot, instrumented, nonreturn space vehicles. Project Snooper is such a system. Snooper reconnaissance vehicles (Fig. 1) operating in satellite orbits about other planets of the solar system, would gather and transmit information about these planets to Earth. This can be accomplished using current electronic technology. The inclusion of humans in such vehicles, although possibly allowing the collection of more information, would greatly add to the complexity and cost of the system to meet the requirements for crew provision and return to Earth.

The main task in the development of the Snooper reconnaissance system is then reduced to achieving a low weight, interorbital space vehicle which can be placed in an Earth satellite orbit with a feasible conventional rocket booster; perhaps similar to the type necessary for an intercontinental ballistic missile. To satisfy this requirement, as well as that for carrying a reasonable size reconnaissance payload, a propulsion system of specific impulse one hundred times greater than that available with conventionally powered rockets is required. Only the photon and ion rocket principles provide sufficiently high specific impulse. The photon rocket must be removed from consideration because its temperature and power requirements cannot be satisfied using our present technical knowledge. The ion rocket alone is suitable for propelling the robot Snooper vehicle.

An ion rocket is a device for obtaining thrust through the high velocity expulsion of electrically accelerated ionized particles. In the case of Snooper, the source of electrical power is a closed system nuclear powered turbogenerator. The powerplant would provide most of its electrical power output to the propulsion system during powered flight. All of its power would be available to the payload when the propulsion system is not operating, so that the powerplant could be considered part of the useful payload.

Once developed, fleets of Snooper vehicles would have the capability of gathering the information necessary both to motivate further space exploration and to achieve practical manned space travel at minimum cost, maximum expediency.

Nuclear Powerplant

Power Source

A nuclear powerplant was selected for the reconnaissance vehicle after a comparison with a solar energy powerplant. The difficulties associated with packaging the solar mirrors of a solar energy powerplant for the boost period, the varying amount of solar energy received as a function of distance from the sun, and the inability to operate in shadow excluded further consideration of a solar energy powerplant.

The low weight requirement of the nuclear powerplant for this application appears possible if radiation shielding is omitted. This is permissible in the Snooper vehicle because it is unmanned. On the basis of published data (1)[3] on current reactor design and performance, the estimated weight of the unshielded Snooper vehicle reactor appears to be reasonable.

For the system assumed in this paper, a sodium coolant is used. There are, of course, other possible reactor coolants depending on the exact reactor type used (2,3).

The Snooper propulsion system requires that the thermodynamic system have an output sufficient to produce 147 kw of electrical power. To do this the reactor must have a thermal output of approximately 1 megawatt. This requirement for reactor power, along with the total probable thrust duration, is a fortunate circumstance, for it appears that there would be sufficiently low consumption of fissionable material in the reactor to allow long term operation without further addition of fuel. This should allow considerable simplification in the reactor design.

Thermodynamic System

In the system illustrated in Fig. 2, the sodium reactor coolant is passed through a heat exchanger to boil the turbine working fluid, in a single-fluid Rankine cycle. Mercury was selected as the turbine working fluid because it allows the system to operate at a moderate pressure at high temperature, in comparison for example, with steam.

Heat Rejection System

The heat rejection system of this powerplant may be considered one of the major problem areas in the design of ion propulsion systems. Each heat generating component in the entire vehicle system must eventually have its heat rejected from the vehicle by radiation, the only means for rejecting

[3] Numbers in parentheses indicate References at end of paper.

heat in the vacuum of space without mass ejection. Radiator sections would be constructed of thin gage aluminum sheet (0.010 in. or thinner if feasible) upon which are brazed, at approximately 2-in. intervals, $\frac{1}{4}$-in. diam thin walled copper tubes for coolant flow. These tubes run parallel to the longitudinal axis of the vehicle, thereby requiring no bending of the tubes during radiator stowage (Fig. 3). The manifolds would be made of inflatable copper sections, which would be expanded (and remain expanded) when the radiator coolant fluid is initially pumped into the radiator, after it is unwrapped in the Earth satellite orbit. The entire exposed surface of the radiator would be suitably coated, perhaps with soot, to provide a surface having a high emissivity.

Sodium was selected for the radiator coolant fluid because of its excellent heat transfer properties and low density. Upon comparison with mercury, the weight advantage of sodium was found to be quite pronounced, even though a mercury system can operate at approximately constant temperature by using the radiator as a condenser.

The problem of the relative position of the radiator sections with respect to incident rays from the sun was considered. It appears that no radiator hinging or gimballing mechanism is required because the Snooper vehicle would remain essentially in the plane of the ecliptic during its flight.

Electrical Power System

The electrical power system would include an a.c. generator, a rectifier, and a control and distribution system. Both d.c. and a.c. generators were considered for this application. The d.c. generator was rejected on the basis of the low power-to-weight ratio presently obtainable from such machinery. With an a.c. generator, it appears that a power-to-weight ratio of approximately 1 kw per lb can be attained (4). A judicious arrangement of both the electrical and mechanical rotating machinery would be necessary to prevent precessional moments resulting from gyroscopic action.

Propulsion

Principles of Operation

An ion rocket produces thrust by the reaction of a stream of electrically accelerated ions. The acceleration of a mass to a high velocity requires power. The power in the ion exhaust beam is expressed by (5)

$$P = \tfrac{1}{2} k_1 Mac \quad \ldots\ldots [1]$$

This beam power, although less than the power which must be provided by the ion rocket power source, is a measure of the specific power requirements of an ion rocket propulsion system. A general plot of the ratio of required ion beam power to vehicle weight (6) for a range of vehicle accelerations and exhaust velocities is shown in Fig. 4. Applied to ion rockets, this curve provides a means of determining either the maximum vehicle acceleration or the ion exhaust velocity for a given ratio of ion beam power to vehicle weight.

Propellant Selection

One of the primary requirements of an ion rocket propellant is that it have favorable ionization characteristics as nonionized atoms contribute no thrust to the vehicle.

Of all the elements, the alkali metals (lithium, sodium, potassium, rubidium and cesium) have the lowest ionization potentials. Because of this, the alkali atoms may be ionized on incandescent metallic surfaces, such as platinum or tungsten (7), two metals whose respective work functions (6.2 and 4.5 ev) are higher than the ionization potentials of the alkali elements. When an alkali atom contacts an incandescent platinum or tungsten surface it becomes ionized after a stay time of only several microseconds; the probability of an alkali atom being ionized when contacting such a hot surface is essentially unity.

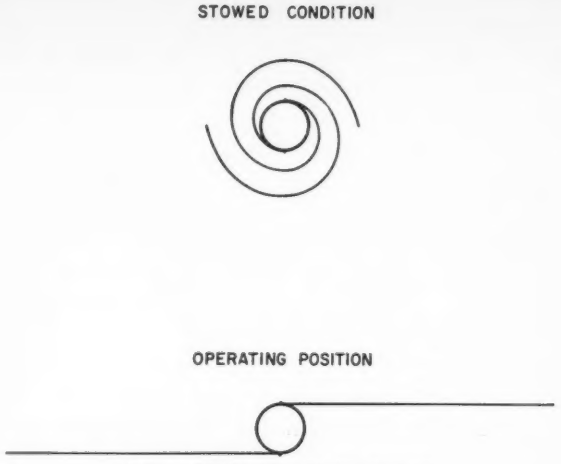

Fig. 3 Method of radiator stowage

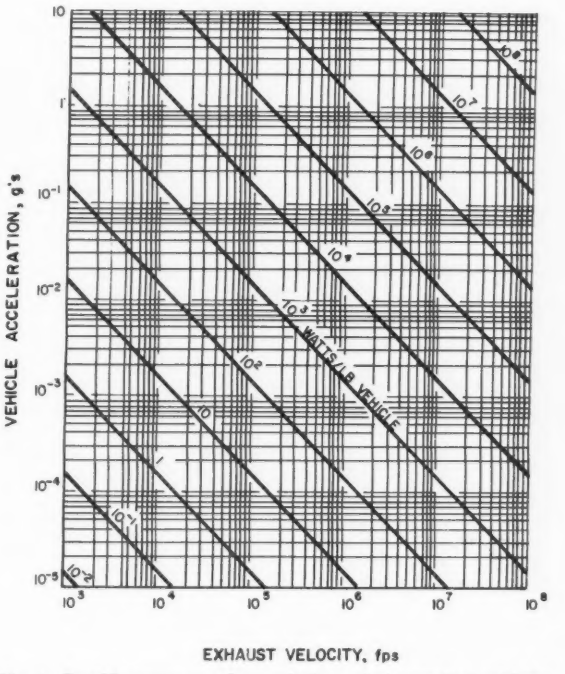

Fig. 4 Specific power requirements for rocket propelled vehicles

Of the alkali metals, cesium and rubidium share the desirable properties of low ionization energy, low heats of fusion and vaporization at relatively low temperatures, and high density.

Another criterion for propellant selection is the required area of the ion source. The accelerating voltage in an ion motor is expressed by (5)

$$V = \frac{k_2 mc^2}{2e} \quad \ldots\ldots [2]$$

From Equations [1 and 2], the ion beam current is

$$I = \frac{k_3 ma}{Ac} \quad \ldots\ldots [3]$$

For a desired value of exhaust velocity (specific impulse) and

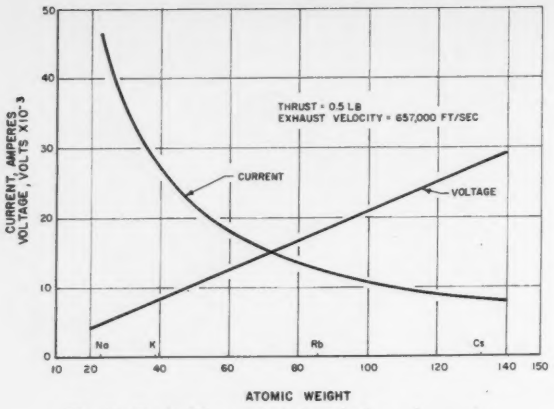

Fig. 5 Typical ion rocket electrical requirements

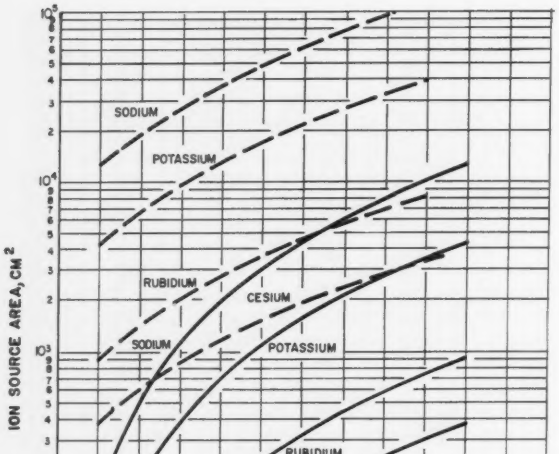

Fig. 6 Typical ion source area requirements

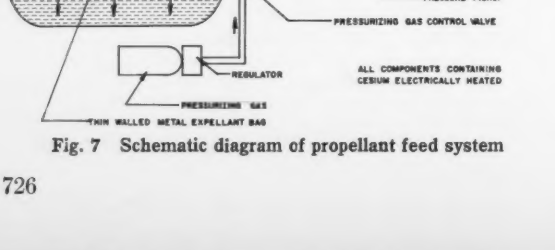

Fig. 7 Schematic diagram of propellant feed system

thrust the voltage and current can be related to the atomic weight as shown in Fig. 5.

The ion current density, based on space charge considerations, is expressed by (7)

$$j = k_4 \sqrt{\frac{V^3}{x^4}\frac{e}{m}} \quad \ldots\ldots\ldots\ldots\ldots\ldots [4]$$

Using Equation [4] and Fig. 5, the required ion source area is given in Fig. 6 for several of the alkali metals. The ratio of the ion source areas of cesium and rubidium from Fig. 6 shows the ion source area for cesium to be approximately 40 per cent that of rubidium for gap distances of 1 to 3 cm. Thus cesium appears to be the most desirable propellant for the Snooper design.

Propellant Feed System

One possible propellant feed system suitable for the Snooper vehicle is shown schematically in Fig. 7. The cesium propellant is stored in the liquid state. Its temperature is maintained at approximately 100 F by an electrically heated blanket surrounding the propellant tank. (The melting point of cesium is 83 F.)

The necessity for operation at exceedingly low vehicle acceleration (approximately 0.1 milligee) indicates the need of a positive expulsion propellant feed system for the Snooper vehicle. This is accomplished by an expandable metal bag, which is slowly inflated by pressurized gas as the propellant is consumed. The liquid cesium passes through a check valve and is then sprayed onto the wall of a vaporizing chamber by means of an atomizer. The vaporizing chamber wall is maintained at a temperature of 1400 to 1500 F, providing a surface on which the atomized liquid cesium is vaporized. (The boiling point of cesium is 1301 F.) The cesium vapor then flows under vapor pressure through a sintered metal restrictor which functions as a precalibrated flow metering system. Two on-off control valves are in the system, immediately downstream of the propellant tank and at the vaporizer respectively. During the startup of the propulsion system, the opening of the on-off valve downstream of the vaporizing chamber is delayed until the design operating vapor pressure is achieved in the vaporizing chamber by introduction of the propellant.

One method of thrust level control which appears possible with this feed system is propellant flow control by varying the reference pressure setting on the pressurizing gas control valve and the wall temperature of the vaporizing chamber (and hence the cesium vapor pressure). The variation in the cesium vapor pressure will change the pressure drop across the restrictor and hence the cesium flow.

Ion Motors

Two ion motors, each of $\frac{1}{6}$-lb thrust and an ion current rating of 2.67 amp are used in the Snooper design. These motors would provide an initial acceleration of 0.1 milligee to the Snooper vehicle.

The motor design is based on one proposed by Dr. E. Stuhlinger of the Army Ballistic Missile Agency, Huntsville, Ala. (7). Cesium propellant, delivered from the propellant feed system, is fed into the motor as a vapor (Fig. 8). After passing through a distributor, the cesium impinges on incandescent tungsten surfaces, which are formed into a series of ionizing grids. The cesium is ionized at these grids and then accelerated through an acceleration gap to a velocity of 657,000 ft per sec by a d.c. potential of 27,500 v. The accelerating or cathode grid has a honeycomb cross-section to allow a nearly uniform electrostatic field in the radial direction.

If only electrically positive particles were ejected, the vehicle would soon attain a large negative charge which would hinder and even prevent the further expulsion of ions. This effect is circumvented in the Snooper propulsion system in

much the same manner as that proposed by Dr. Stuhlinger—by the simultaneous emission of electrons which would mix with the ejected ions forming an electrically neutral plasma. As shown in Fig. 8, a thermionic electron emitting surface along with its associated heating element is mounted on the downstream side of the cathode grid.

Payload

The payload of the Snooper vehicle includes television, radar, communication equipment and auxiliary power supply systems. Devices for measuring cosmic ray and electromagnetic field intensity about the planets as well as solar effects at various distances from the sun could be included. This section would also include provisions in its design for environmental control where necessary, and would be equipped with hydraulic and electrical systems for the actuation and control of antennae, cameras and transducer devices. Much of this equipment would be specially designed to allow operation in a radiation field.

The payload would be designed to accommodate a variety of tasks. Only one of these is discussed here to give an indication of the information gathering potential of the Snooper reconnaissance system. This task is the televising and radar scanning of the surfaces of planets and the transmission of this information to Earth. A general block diagram of the scanning, transmission and receiving system is presented in Fig. 9. Television and televised radar signals would be put on magnetic tape (continuously erased and revised). Following this taping process, the information is coded in order to transmit it in a narrow bandwidth signal. This signal would be received by monitoring stations on the Earth, where essentially the reverse process would take place. This system would reduce significantly the power required for the transmission of information to Earth. Information theory can probably be of great aid in further reducing power requirements and improving the transmission system.

More advanced payload equipment might include small aerodynamic test vehicles (weighing perhaps 100 lb each) which would be decelerated initially out of the observation orbit by a small rocket. The descent of such vehicles, instrumented and carrying telemetering equipment, would allow the collection of considerable atmospheric data. The use of this telemetered information could conceivably lead to the placing of small instrumentation packages on the surfaces of the planets. This package could even carry a television camera-transmitter, possibly like the lightweight portable television camera developed for the U. S. Army, "Creepy-Peepy." The surface exploration package could even be self-propelled and thus deliver highly detailed information about a relatively large area of planetary surface. The possibility of such advanced instrumentation systems indicates some of the reconnaissance potential of Project Snooper.

Trajectory Analysis

In showing the feasibility of the Snooper propulsion system, the ability to move along a reasonable trajectory must be proved. To do this, a trajectory must be established and examined to see if travel times are reasonable, if navigation corrections can be made, etc. Snooper has been designed for solar system reconnaissance. However, to set up a reference trajectory, Mars will be used as a sample objective (8).

It shall be assumed here that Snooper has previously been placed into a close satellite orbit, approximately 300 miles above the surface of Earth by means of chemical fuel rockets. The trajectory of the Snooper vehicle can be divided into four discrete parts, starting from this Earth satellite orbit. The first part of the trajectory is powered flight, sustained until the ion rocket reaches some arbitrary orbit about Earth sufficiently far from the Earth's center of gravity so that an excessive amount of energy need not be expended during the second

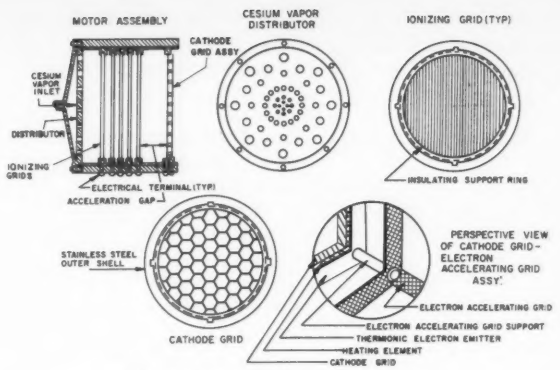

Fig. 8 Ion rocket motor assembly

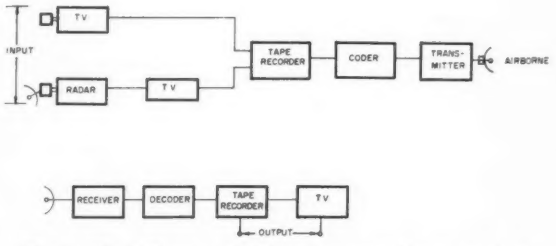

Fig. 9 Block diagram of TV-radar reconnaissance system

part of the trajectory. The second part of the trajectory consists of resumed powered flight sustained until the necessary velocity is obtained to escape the Earth's gravitational field and place the vehicle into the elliptical orbit connecting the solar orbits of Earth and Mars. The third part is the elliptical orbit along which the rocket "coasts." As the ship nears Mars, powered flight is resumed to maneuver the vehicle into a satellite orbit, about Mars, the fourth and last part of the trajectory.

Only the theory describing the first three parts of the trajectory is presented in this report. Approximations have been made for the purpose of simplifying this analysis. Circular, coplanar solar orbits are assumed for Earth and Mars. The perturbing effects of the moons of the two planets are not considered. During powered flight, solar effects are ignored and during the elliptical coasting orbit, the gravitational effects of Earth and Mars are neglected.

To derive equations of motion for the first sections of the trajectory the Lagrangian equation of energy is applied (9)

$$\frac{d}{dt}\left(\frac{\partial T}{\partial \dot{q}_i}\right) - \frac{\partial T}{\partial q_i} - Q_p \qquad i = 1,2 \ldots\ldots\ldots [7]$$

where the q's are the generalized coordinates, the Q's the generalized forces, and T is the energy. The equations of motion are reducible (8) to (Fig. 10)

$$\ddot{r} - r\dot{\theta}^2 + g_E\left(\frac{r_E}{r}\right)^2 = \frac{F\dot{r}}{Mv}$$

$$r\ddot{\theta} + 2\dot{r}\dot{\theta} = \frac{Fr\dot{\theta}}{Mv} \qquad \ldots\ldots\ldots\ldots [8]$$

The solution of the equations of motion must be done by numerical means involving a great deal of computational work.

The initial conditions are imposed by the orbit of departure and the angle of applied thrust.

The vehicle is expected to spiral around the Earth, slowly increasing its energy, moving farther and farther from its original orbit. At some predetermined point the propulsion system is turned off, and the vehicle coasts into a new satellite orbit relatively close to the entry point of the circum-solar ellipse. While the ion rocket is in this new geocentric orbit, its exact position and velocity can be observed from Earth. These observations would then provide new initial conditions from which the interplanetary trajectory can be computed. Information concerning the position at take-off, the thrust duration (to determine cut-off point) and any other pertinent information can then be relayed to the vehicle. The equations of motion are, as before, with the initial conditions a function of the new orbit and desired angle of thrust application.

When the observations and computations have been completed, the vehicle resumes its spiral around the Earth until it builds up enough energy to escape the Earth's gravitational field, and then proceeds into a circum-solar ellipse which has its aphelion in proximity to the solar orbit of Mars (Fig. 11).

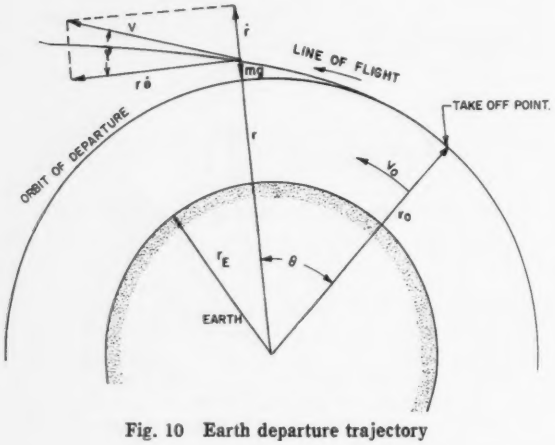

Fig. 10 Earth departure trajectory

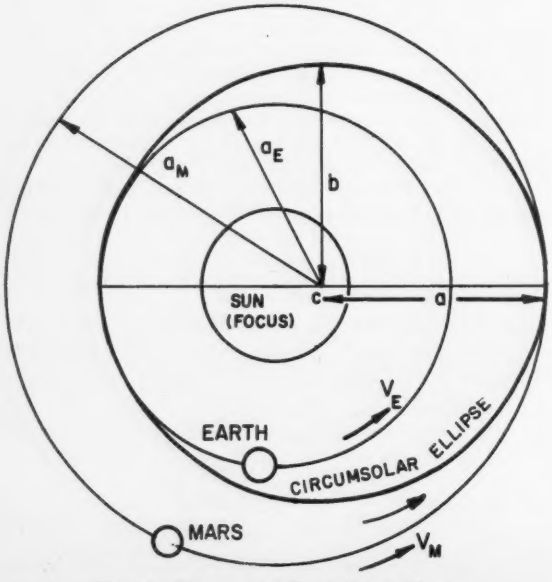

Fig. 11 Circum-solar Earth-Mars ellipse

The cut-off point will be timed so that as the vehicle follows the escape hyperbola, the escape asymptote of the hyperbola is parallel to the Earth's circum-solar orbit and in the same direction. This escape hyperbola leads directly into the desired circum-solar ellipse (Fig. 12).

The point of take-off for the second part of powered flight is determined by the requirement that the escape asymptote be parallel to the orbital motion of the Earth

$$\xi = \theta_2 + 90 \text{ deg} - \beta + 90 \text{ deg} - \alpha$$
$$\xi = \theta_2 - \beta - \alpha + 180 \text{ deg} \quad \ldots\ldots\ldots\ldots [9]$$

The above angles are defined in Fig. 12.

The problem of errors occurring during the various portions of the trajectory is serious. These errors must be corrected in order to ensure the successful completion of any mission. The real problem then, lies in the ability of the vehicle to make corrections for these errors.

In the theory as discussed here only one attempt has been made to compensate for errors. This is done by separating the Earth escape trajectory into two portions. Those errors incurred during spiraling from the first orbit about Earth to the second can be compensated for by accurately determining the initial conditions for the second power flight and then proceeding with the trajectory calculations and corrections.

Guidance

The navigation of the Snooper vehicle would be accomplished with an automatic solar-planetary navigation system. Star triangulation does not appear to be usable because of the exceedingly small parallax of the stars. In turn, however, the stars would provide an extremely accurate reference system. A solar-planetary navigation system will enable the vehicle's position to be determined at any instant by observing the angles between the planets and the sun.

A highly accurate chronometer would be required based, perhaps, on the exact process of radioactive decay. A continuously available frame of reference such as a gyrostabilized platform will probably be required. In the environment of total or near weightlessness, the drift of a gyro may be greatly

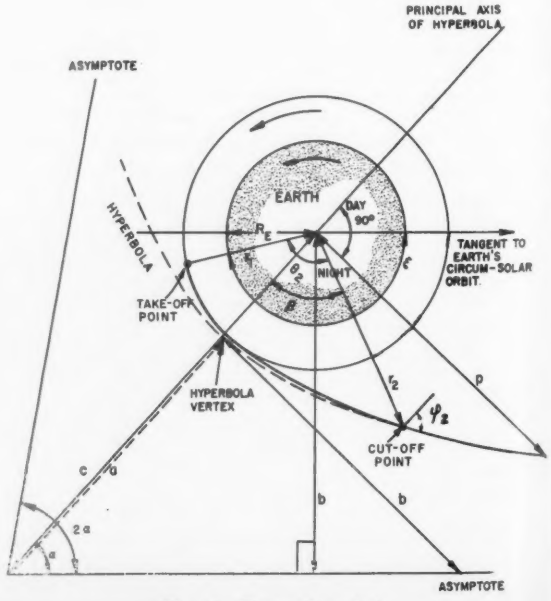

Fig. 12 Escape hyperbola

reduced because of the reduction of significant torque forces. The spatial orientation of the stable platform would be monitored by an automatic star tracking device to maintain the reference axes in the proper spatial direction. The perfect seeing available to any optical instrument in the vehicle's guidance system, operating in the vacuum of space, is a definite advantage in the development of such a system.

Prior to any mission, an elaborate ephemeris of the voyage must be compiled. This information would be fed into the thrust level and vector control systems to achieve the desired trajectory in space.

Vehicle Configuration and Operation

The general configuration of the interorbital vehicle is shown in Fig. 1. The payload section of the vehicle, containing the guidance and payload instrumentation and equipment, would be separated from the nuclear powerplant-ion propulsion section during operation by a telescoping radiation isolation structure. The physical separation of the payload-guidance section from the powerplant nuclear reactor reduces the effects of harmful incident nuclear radiations on the payload and guidance instrumentation. The large, winglike radiators are extended on either side of the vehicle.

The powerplant and propulsion systems of the Snooper form a compact package in the aft section of the vehicle. The nuclear reactor, turbogenerator, propellant storage tank and two ion rocket motors are located here. The ion rocket motors are gimbal mounted outboard of the reactor, and can be rotated to allow deceleration without changing the attitude of the vehicle in space. A preliminary weight estimate of this configuration is presented in Table 1.

Table 1 Preliminary weight statement, Snooper reconnaissance vehicle, lb

Payload and guidance	1500
Reactor, heat exchanger, pumps and turbine	1000
Radiator	280
Generator and electrical system	150
Structure and miscellaneous	150
Propellant	220
Gross weight	3300 lb

The Snooper vehicle would be accelerated into an Earth satellite orbit as the payload of a chemical propellant rocket booster similar to that necessary for a possible intercontinental ballistic missile. During the Earth satellite boost portion of the flight, the radiators are stowed overlay wrapped (Fig. 3), the ion motor mount arms folded, and the radiation isolation structure telescoped to form a compact assembly. A jettisonable bracing system and windshield are utilized to protect the Snooper during its acceleration into an Earth satellite orbit. Once in the orbit, the windshield bracing system is jettisoned along with all mass not a functioning part of the vehicle. Then the radiator sections are unwrapped; the radiation isolation structure is extended, and the ion rocket motor arms are unfolded.

The nuclear power source is now activated and the low thrust ion rocket propulsion system accelerates the Snooper along its trajectory. When the desired orbit about its destination planet has been achieved, the power of the reactor is utilized to operate the automatic data collection and transmission equipment. The apparatus would operate for approximately one year after it has reached its destination orbit, thus allowing sufficient time for the collection of useful data.

Acknowledgments

The authors wish to express their gratitude for the assistance and cooperation of the following persons in the preparation of this report during the spring of 1956; D. Calamore, F. Ferebee, M. Hahn, V. Karpenko, A. Kelly, J. Orr, R. Ragsac, P. Sendler and R. Weir.

References

1 Stephenson, R., "Introduction to Nuclear Engineering," McGraw-Hill, Inc., New York, 1954.

2 Williams, C. et al., "Liquid Metal Fuel Reactors," *Nucleonics*, July 1954.

3 Went, J. J. and De Bruyn, H., "Fluidized- and Liquid-Fuel Reactors with Uranium Oxides," *Nucleonics*, Sept. 1954.

4 Rauch, S. E. and Johnson, L. J., "High-Frequency Alternators," *Electrical Engineering*, Aug. 1954.

5 Spitzer, L., "Interplanetary Travel Between Satellite Orbits," JET PROPULSION, March-April 1952.

6 Shepherd, L. R. and Cleaver, A. V., "The Atomic Rocket, Further Possibilities: The Ion Rocket," *Journal of the British Interplanetary Society*, March 1949.

7 Stuhlinger, E., "Possibilities of Electrical Spaceship Propulsion," Bericht über den V. Internationalen Astronautischen Kongress (Report on the Fifth Int. Astronautical Congress), Aug. 1954.

8 Von Braun, Werbner, "The Mars Project," University of Illinois Press, Urbana, Ill., 1953.

9 Goldstein, H., "Classical Mechanics," Addison-Wesley Publishing Co., Inc., Cambridge, Mass., 1953.

Variational Solution of Fuel Sloshing Modes

H. R. LAWRENCE,[1] C. J. WANG[2] and R. B. REDDY[3]

The Ramo-Wooldridge Corp., Los Angeles, Calif.

The problem of calculating the linearized motion of an incompressible inviscid fluid with a free surface is formulated as a variational principle. It is demonstrated that the variational principle is of the free boundary condition type. A procedure for calculating the natural frequencies and modes of a shallow and a deep tank by applying the Rayleigh-Ritz procedure to solve the variational formulation is discussed. An approximate procedure for calculating the sloshing modes and frequencies of a tank of intermediate depth in terms of the solutions for shallow and deep tanks is suggested. The highly satisfactory convergence and accuracy of the method are demonstrated by comparison with exact methods in the cases of flat bottomed tanks and 90 deg conical bottomed tanks. The results of numerical calculations for conical tanks are

Received Feb. 11, 1958.

[1] Associate Director, Astrovehicles Laboratory, Space Technology Laboratories. Member ARS.

[2] Associate Manager, Aerophysics Department, Space Technology Laboratories. Member ARS.

[3] Member, Technical Staff, Space Technology Laboratories. Member ARS.

presented in the form of mode shape diagrams and frequency charts.

Nomenclature

A, B = constants to be determined
a, b = defined by Equation [25]
E = ψ for shallow tank approximation
F = ψ for deep tank approximation
G = ξ, when the latter is function of r only
g = gravitational or total vertical acceleration
h = height of surface above bottom a positive function of r
J_s = Bessel function of order s of the first kind
L = Lagrangian = $T - V$
N = degree of the polynomial $F(r)$
n = normal to boundary surface
r, z, θ = cylindrical coordinates
S = free surface of liquid
s = number of mode in θ
T = kinetic energy of the liquid
t = time
u = velocity of fluid
V = potential energy of the liquid
x, y, z = rectangular coordinates
α = polynomial coefficients
β = dimensionless frequency defined in Equation [35]
ϵ = phase angle
ζ = z on the fluid surface
λ = frequency parameter
ξ = function of r and z; $\psi = \xi(r, z) \cos s\theta$ (or $\sin s\theta$)
ρ = mass density of fluid
Σ = interface of liquid and tank
σ = circular frequency of time function, rad/sec
τ = volume of the liquid
ϕ = potential function dependent on r, z, θ(or x, y, z) and t
ψ = space part of ϕ; $\phi = \psi(r, z, \theta$; or $x, y, z) \sin(\sigma t + \epsilon)$
Ω = potential energy per unit mass

Introduction

THE flow field of the liquid contained in a tank with a free surface when subjected to a transient acceleration field has been investigated since the middle of the eighteenth century. The basic partial differential equations and the classical treatment by linearization and separation of variables were essentially complete by 1895, as reported in Lamb's first edition of "Hydrodynamics." Renewed interest in this subject has been generated recently by the engineering problems arising in the design of liquid rocket powered missiles. In particular, the design of missile autopilots requires an accurate estimate of the natural frequencies of the sloshing modes which lie within the autopilot effective control frequency band during powered flight. In the development of propellant utilization systems which continually measure the residual propellants remaining in the tanks and adjust the engine mixture ratio accordingly, a knowledge of the dynamic behavior of the propellants is necessary.

Linearization of the equations of motion and the imposition of the free surface boundary condition on a plane are employed in the classical theory. An order analysis to establish the range of validity of these assumptions is required, but will not be attempted here. The classical linearization will be employed with the understanding that the range of validity is unknown from the analytic viewpoint. In practice, experimental data on mode shapes and frequencies seem to indicate that the linearization assumptions lead to satisfactory results for a wide class of problems.

Additional assumptions used in the classical theory and adopted here are: The viscosity and compressibility of the fluid may be neglected, the fluid starts from rest and the forces acting on the fluid may be derived from a potential function. An important consequence of these assumptions is that the flow field of the fluid may be calculated in a relatively straightforward manner if the natural frequencies and sloshing modes are known.

Methods for calculating the sloshing modes have been developed in the classical theory for tanks of circular, elliptical and rectangular cross sections with flat bottom. These solutions make use of the technique of separation of variables in the differential equation. It can be shown that the application of this basic technique cannot lead to further useful solutions.

If the tank is very shallow, the problem becomes two-dimensional regardless of the bottom shape. An exact solution has been developed for a circular tank with a bottom in the form of a parabola (1).[4] If the tank is infinitely deep, the bottom can always be considered as flat, and the equations also reduce to a two-dimensional problem. Such problems may be solved for arbitrary cross sections by a variety of methods. The tank with a nearly flat bottom may be treated analytically by a perturbation analysis (1). Such cases, however, are of minor interest in technical applications.

To develop approximate solutions to the sloshing modes and frequencies for tanks of arbitrary depth and bottom shape requires the development of a technique which is basically different from the classical method of separation of variables. From an examination of similar mathematical problems in other areas of physics, the use of integral equations or variational methods appears to offer promise. In this paper, the application of variational techniques is developed and exploited to produce a general procedure for approximating sloshing modes and frequencies. The method of integral equations has not been studied but is believed to be equally applicable and should be pursued.

The variational method developed here for the three-dimensional problem is solved approximately in terms of the solution of a pair of two-dimensional problems: The very shallow tank and the very deep tank. A variational procedure for solving these special cases is presented. These results are believed to be useful independent of their applications to the three-dimensional problem.

It will be noted that the variational procedures developed here are applicable to tanks with multiconnected free surfaces, such as an annulus as well as simple connected free surfaces.

A more general approach to variational solution of sloshing has been initiated to include the nonlinear aspects of the problem. Results of the study will be reported in a separate paper.

Formulation of Problem as a Variational Principle

The differential equation and boundary conditions for the linearized sloshing problem are developed in the literature (1). A formulation of the problem as a variational principle may be developed from these differential equations. However, the development of a variational principle directly from Hamilton's variational formulation of mechanics is adopted here in order to clarify the assumptions employed in the derivation and to obtain a free boundary conditions statement of the problem. The subject of free boundary conditions in a variational formulation will be discussed after the basic mathematical apparatus has been presented.

If T and V are defined as the kinetic and potential energy, respectively, of the fluid, Hamilton's principle may be written as

$$\delta I = \delta \int_{t_1}^{t_2} L dt = \delta \int_{t_1}^{t_2} (T - V) dt = 0 \quad [1]$$

The kinetic energy of the fluid under small waves can be expressed, to the first order

$$T = \frac{\rho}{2} \int_{\tau} |\nabla \phi|^2 d\tau \quad [2]$$

where ϕ is the velocity potential, and τ represents the volume

[4] Numbers in parenthesis indicate References at end of paper.

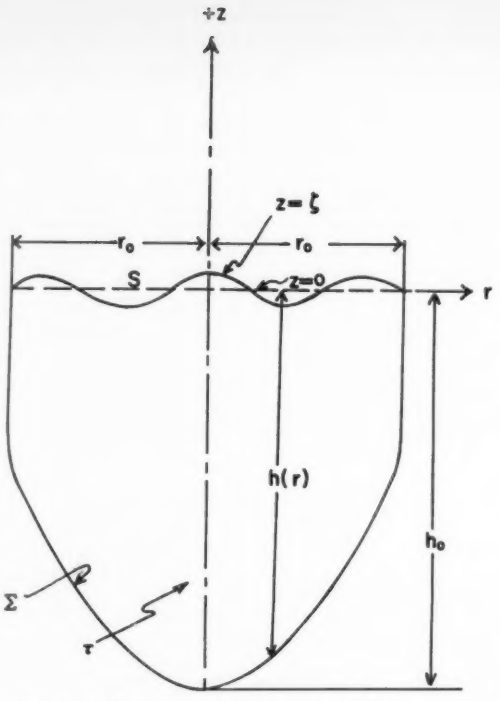

Fig. 1. Axially symmetrical tank and symbols

between the undisturbed surface $z = 0$ denoted by the symbol S and the wetted area of the tank Σ (see Fig. 1).

The potential energy of the fluid can be represented by the following equation

$$V = \int_S \frac{1}{2}\,\zeta(\rho g \zeta dS) \quad \text{[3a]}$$

if the zero potential level is chosen to correspond to the fluid at rest. The symbol ζ denotes the fluid surface height measured from the undisturbed surface. Using the Bernoulli equation, it can be shown that for small waves the following equation holds at the free surface

$$\zeta = -\frac{\phi_t}{g} \quad \text{[3b]}$$

Substituting [3b] into [3a], an expression of the potential energy is obtained in terms of the time derivative of the velocity potential ϕ

$$V = \frac{\rho}{2g}\int_S \phi_t^2 dS \quad \text{[3c]}$$

Using Equations [2 and 3] for the expressions of the kinetic energy and the potential energy and neglecting the fluid density ρ, the Lagrangian may be written as

$$L = \frac{1}{2}\int_\tau |\nabla\phi|^2 d\tau - \frac{1}{2g}\int_S \phi_t^2 dS \quad \text{[4]}$$

Hamilton's principle, Equation [1], will be applied to verify that Equation [4] is indeed the proper Langrangian and to clarify the question of boundary conditions. Upon substituting the expression for the Langrangian, Equation [4], in Equation [1] and carrying out the variational process there results the expression

$$0 = \delta I = -\int_{t_1}^{t_2} dt \int_\tau d\tau \nabla^2\phi\delta\phi + \int_{t_1}^{t_2} dt \int_\Sigma d\Sigma \frac{\partial\phi}{\partial n}\delta\phi + \int_{t_1}^{t_2} dt \int_S dS\left(\frac{\partial\phi}{\partial n} + \frac{1}{g}\phi_{tt}\right)\delta\phi - \frac{1}{g}\int_S dS\phi_t\delta\phi\Big|_{t_1}^{t_2} \quad \text{[5]}$$

In applying Hamilton's principle the variation is assumed to vanish at the end points of the time interval. Thus the last term in [5] vanishes. If the variation δI is to vanish for all admissible variations in the potential function ϕ the following equations must hold

$$\nabla^2\phi = 0 \text{ in volume } \tau \quad \text{[6]}$$

$$\frac{\partial\phi}{\partial n} = 0 \text{ on the wetted surface } \Sigma \quad \text{[7]}$$

$$\frac{\partial\phi}{\partial n} + \frac{1}{g}\phi_{tt} = 0 \text{ on the free surface } S \quad \text{[8]}$$

Equations [6, 7, 8] represent the classical formulation of the linearized problem as a differential equation with boundary conditions (1). The conclusion to be drawn from the preceding analysis is that the problem of calculating a potential function ϕ which satisfies the differential equation and boundary conditions of the linearized theory is equivalent to finding a potential function ϕ which makes the integral

$$I = \frac{1}{2}\int_{t_1}^{t_2} dt\left[\int_\tau |\nabla\phi|^2 d\tau - \frac{1}{g}\int_S \phi^2 dS\right] \quad \text{[9]}$$

an extremum. The importance of this conclusion lies in the fact that not only the differential equation but all necessary boundary conditions are automatically satisfied. There exists an infinite number of variational principles which satisfy the differential equation. However, a variational principle which satisfies the differential equation and the boundary conditions is unique. Such a variational principle is called a free boundary condition variational principle in mathematics literature (4).

The well-known Rayleigh-Ritz procedure will be used to obtain an approximate potential function from the statement that the action integral [9] is an extremum. The potential ϕ is expanded in a series of known functions with undetermined coefficients, and the action I is evaluated. The choice of functions employed in the expansion has an important effect on the accuracy of the results. Since I is thereby represented as a function of the unknown coefficients, the usual methods of finding an extremum may then be used. The functions used in the expansion need not satisfy the boundary conditions in view of the fact that the variational principle is of the free boundary condition type.

The sloshing modes and natural frequencies may be defined as solutions of the extremum problem for the integral I of Equation [9] when the potential is a harmonic function of time or symbolically

$$\phi(x, y, z, t) = \psi(x, y, z)\sin(\sigma t + \epsilon) \quad \text{[10]}$$

Here ψ represents a sloshing mode and σ the natural frequency in radians per sec. Upon substituting expression [10] for ϕ in the action integral [9] and integrating over a single cycle in time, an expression for I is obtained in terms of the function ψ and its gradient.

$$I = \frac{1}{2}\int_\tau |\nabla\psi|^2 dt - \frac{\sigma^2}{2g}\int_S \psi^2 dS \quad \text{[11]}$$

In proceeding to Equation [11], a constant factor $\pi\rho/\sigma$ has been replaced by unity. It is clear that this substitution will not affect the results, since the factor may be absorbed in the definition of the Lagrangian.

The differential equations and boundary conditions for the modes and natural frequencies may be derived either by substitution of the expression [10] for ϕ into Equations [6, 7 and 8] or by carrying out the variation of the expression

for I in Equation [11]. In either case the resulting equations are

$$\nabla^2\psi = 0 \text{ in volume } \tau \quad \text{[6a]}$$

$$\frac{\partial\psi}{\partial n} = 0 \text{ on the wetted surface } \Sigma \quad \text{[7a]}$$

$$\frac{\partial\psi}{\partial n} - \frac{\sigma^2}{g}\psi = 0 \text{ on the free surface } S \quad \text{[8a]}$$

Upon multiplying Equations [6a, 7a and 8a] by ψ, integrating over the regions of validity, and integrating by parts, the following result is obtained

$$\int_\Sigma \psi \frac{\partial\psi}{\partial n}\,d\Sigma + \int_S \psi \frac{\partial\psi}{\partial n}\,dS - \int_\tau |\nabla\psi|^2 d\tau = 0$$

$$\int_\Sigma \psi \frac{\partial\psi}{\partial n}\,d\Sigma = 0$$

$$\int_S \psi \frac{\partial\psi}{\partial n}\,dS - \frac{\sigma^2}{g}\int_S \psi^2 dS = 0$$

The above equations may be solved for σ^2/g to give the result

$$\lambda = \frac{\sigma^2}{g} = \frac{\int_\tau |\nabla\psi|^2 d\tau}{\int_S \psi^2 dS} \quad \text{[12]}$$

It can be shown by direct calculation that the frequency parameter λ is a minimum when the integral expression [11] for I is an extremum.

The condition that the frequency parameter λ be an extremum where λ is defined by Equation [12] thus represents an alternate statement of the variational principles with free boundary conditions.

By using Equation [12], the natural frequency parameter λ can be calculated to second order when the potential ψ is known to first order. This result follows from the fact that the first order error $\delta\lambda$ vanishes when the potential is calculated from a variational principle.

The Shallow Tank Approximation

If the tank under consideration is shallow, i.e., the depth is sufficiently smaller than the distance between mode crests, the calculations can be simplified considerably. Equation [12] can under suitable circumstances be written in the form

$$\lambda = \frac{\int_S dS \int_{-h}^{0} dz(\psi_x^2 + \psi_y^2 + \psi_z^2)}{\int_S dS\psi^2}$$

where h is the depth of the tank. It will be assumed that the potential ψ is independent of z. It is convenient to denote this special potential function by $E(x, y)$ and the frequency parameter by λ_e. Then the previous equation may be simplified to the form

$$\lambda_e = \frac{\int_S dS(E_x^2 + E_y^2)h}{\int_S dSE^2} \quad \text{[13]}$$

The variational principle $\delta\lambda_e = 0$ remains valid with free boundary conditions.

The Deep Tank Approximation

If the tank is cylindrical in shape for depths sufficiently greater than the longest wave length of a sloshing mode, the bottom contour may be ignored. The boundary condition on the surface S as expressed in Equation [8a] becomes

$$\frac{\partial\psi}{\partial z} = \frac{\sigma^2}{g}\psi = \lambda\psi \quad \text{[14]}$$

when Equation [12] is employed. This boundary condition will be satisfied by any function of the form

$$\psi = e^{\lambda_f z}F(x, y) \quad \text{[15]}$$

where λ_f is the frequency parameter for a deep tank. Upon substituting expression [15] for the potential in Equation [12] and assuming the depth of the cylindrical tank to be infinite, the following result is obtained

$$\lambda_f^2 = \frac{\int_S dS \int_{-\infty}^{0} dz e^{2\lambda_f z}(F_x^2 + F_y^2 + \lambda_f^2 F^2)}{\int_S dSF^2}$$

$$2\lambda_f^2 = \frac{\int_S dS(F_x^2 + F_y^2 + \lambda_f^2 F^2)}{\int_S dSF^2}$$

$$\lambda_f^2 = \frac{\int_S dS(F_x^2 + F_y^2)}{\int_S dSF^2} \quad \text{[16]}$$

Equation [16] represents a free boundary variational principle for a deep tank which is cylindrical for a depth sufficiently greater than its maximum cross-sectional dimension.

Tanks of Arbitrary Depth

The potential functions E and F for shallow and deep tanks can be calculated by the Rayleigh-Ritz method from the variational principles $\delta\lambda_e = 0$ and $\delta\lambda_f = 0$ where λ_e and λ_f are defined by Equations [13 and 16], respectively. The calculations necessary to determine these solutions are relatively short, since both cases involve only two dimensions. An approximate solution to the general three-dimensional case may be developed from the two-dimensional cases with little additional labor.

The basic approach is simply to represent the potential for the general case ψ as a linear combination of the potential functions for the shallow and deep tanks.

$$\psi(x, y, z) = AE(x, y) + Be^{\lambda_f z}F(x, y) \quad \text{[17]}$$

Upon substituting the preceding expression for ψ in the variational principle [12], the following formula is obtained

$$\lambda = \frac{\sigma^2}{g} = \frac{\int_S dS \int_{-h}^{0} dz[(AE_x + Be^{\lambda_f z}F_x)^2 + (AE_y + Be^{\lambda_f z}F_y)^2 + \lambda_f^2 B^2 e^{2\lambda_f z}F^2]}{\int_S dS(A^2E^2 + 2ABEF + B^2F^2)}$$

Upon performing the indicated integration, λ may be expressed in the form

$$\lambda = \frac{a_{11}A^2 + 2a_{12}AB + a_{22}B^2}{b_{11}A^2 + 2b_{12}AB + b_{22}B^2} \quad \text{[18]}$$

where a_{ij} and b_{ij} are defined as

$$\begin{aligned}
a_{11} &= \int dSh(E_x^2 + E_y^2) \\
a_{12} = a_{21} &= \int dS\left(\frac{1 - e^{-\lambda_f h}}{2\lambda_f}\right)(E_xF_x + E_yF_y) \\
a_{22} &= \int dS\left(\frac{1 - e^{-2\lambda_f h}}{2\lambda_f}\right)(F_x^2 + F_y^2 + \lambda_f^2F^2) \\
b_{11} &= \int dSE^2 \\
b_{12} = B_{21} &= \int dSEF \\
B_{22} &= \int dSF^2
\end{aligned} \quad \text{[19]}$$

It is evident from Equations [13] that the following identity holds

$$\lambda_e = \frac{a_{11}}{b_{11}} \quad \text{[20]}$$

The frequency parameter λ as expressed in Equation [18] must be an extremum. Upon setting the derivatives with respect to A and B equal to zero, the following results are obtained

$$(a_{11} - \lambda b_{11})A + (a_{12} - \lambda b_{12})B = 0$$
$$(a_{21} - \lambda b_{21})A + (a_{22} - \lambda b_{22})B = 0$$

The condition that the above equations be consistent gives the following quadratic equation for λ.

$$(a_{11} - \lambda b_{11})(a_{22} - \lambda b_{22}) - (a_{12} - \lambda b_{12})(a_{21} - \lambda_{21}) = 0 \quad \ldots\ldots [21]$$

Upon solving Equation [21] for λ, the ratio of the coefficient B/A can be computed

$$\frac{B}{A} = -\frac{(a_{11} - \lambda b_{11})}{(a_{12} - \lambda b_{12})} = -\frac{(a_{21} - \lambda b_{21})}{(a_{22} - \lambda b_{22})} \quad \ldots\ldots [22]$$

The mode shape may then be computed by making use of expression [17] for ψ.

Axially Symmetric Tank

For most missile applications, the tanks are symmetrical about the missile axis. For these tanks, it is convenient to use cylindrical coordinates. The potential function ψ can then be written in the form

$$\psi = \xi(r, z) \cos s\,\theta \quad \ldots\ldots [23]$$

or

$$\psi = \xi(r, z) \sin s\,\theta \quad \ldots\ldots [23a]$$

and the modes may be described by integral values of s. The dependence of ξ on s is not shown explicitly to simplify the notation. Upon substituting expression [23] for ψ in Equation [11], the action integral I becomes

$$I = \int_0^{r_0} dr\,r \int_{-h}^{o} dz \int_o^{2\pi} d\theta \left[(\xi_r^2 + \xi_z^2)\cos^2 s\,\theta + \frac{\xi^2 s^2}{r^2} \sin^2 s\theta \right] - \lambda \int_0^{r_0} dr\,r \int_0^{2\pi} d\theta \xi^2 \cos^2 s\,\theta$$

$$I = \int_0^{r_0} dr\,r \int_{-h}^{o} dz \left[\xi_r^2 + \xi_z^2 + \frac{s^2}{r^2}\xi^2 \right] - \lambda \int_o^{r_0} dr\,r\xi^2 \quad \ldots\ldots [24]$$

where a trivial constant factor π has been omitted. The expression [24] for I is unaltered if Equation [23a] is used in place of Equation [23] for ψ.

The Shallow Tank

For the shallow tank, ξ is assumed to be independent of z, and Equation [24] is further simplified as

$$I = \int_o^{r_0} dr\,r \left\{ h\left[\left(\frac{dG}{dr}\right)^2 + \frac{s^2}{r^2} G^2 \right] - \frac{\sigma^2}{g} G^2 \right\} \quad \ldots\ldots [25]$$

where the potential G is a function of r only.

To solve Equation [25], the unknown function $G(r)$ is first represented by a polynomial, namely

$$G(r) = \sum_{n=0}^{N} \alpha_n \left(\frac{r}{r_0}\right)^{s+2n} \quad \ldots\ldots [26]$$

This is the form of the exact solution for axially symmetric tanks with parabolic bottom (1). The polynomial form for G has been found to give rapid convergence in the treatment of shallow tanks. The presence of s in the exponent is also consistent with the fact that when $s \neq 0$ the singularity of Equation [24] at $r = 0$ requires that $G(r)$ contain no constant term. The depth h will be represented by a polynomial

$$h = h_0 \sum_{i=0}^{K} k_i \left(\frac{r}{r_0}\right)^i \quad \ldots\ldots [27]$$

The polynomial coefficients α_n in Equation [26] must be such that the integral I of Equation [25] has a stationary value. This condition requires that

$$\frac{\partial I}{\partial \alpha_n} = 0 \qquad n = 0, 1, 2, \ldots\ldots N \quad \ldots\ldots [28]$$

which produces a set of $N + 1$ simultaneous homogeneous algebraic equations as follows

$$\sum_{m=0}^{N} \left\{ \left[\sum_{i=0}^{K} \frac{s^2 + (n+m)s + 2nm}{s + n + m + i/2} k_i \right] - \frac{\beta^2/2}{s + n + m + 1} \right\} \alpha_m = 0 \quad \ldots\ldots [29]$$

where

$$\beta^2 = \frac{\sigma^2}{g} \cdot \frac{r_0^2}{h_0} = \text{dimensionless frequency squared}$$

and

$$n = 0, 1, 2, \ldots\ldots N$$

In order that the homogeneous equations be consistent, the determinant of the system must vanish. Thus

$$|A_{nm}| = 0 \quad \ldots\ldots [30]$$

where

$$A_{nm} = \left[\sum_{i=0}^{K} \frac{s^2 + (n+m)s + 2nm}{s + n + m + i/2} k_i \right] - \frac{\beta^2/2}{s + n + m + 1}$$

and n and m $(= 0, 1, 2 \ldots\ldots N)$ denote row and column respectively. The solutions of Equation [30] will yield $(N + 1)$ frequencies with the corresponding mode shapes given by Equations [26 and 29].

Shallow Tank Examples

Parabolic Bottom In the case of a parabolic bottom where

$$h = h_0 \left[1 - \left(\frac{r}{r_0}\right)^2 \right] \quad \ldots\ldots [31]$$

the exact solution (1) consists of terminating hypergeometric series. The variational procedure presented here reproduces the exact solution.

Flat Bottom The flat bottom case has been solved exactly in terms of Bessel functions. The exact value of the lowest radial frequency β for $s = 0$ is 3.8317. In comparison our approximation using a second degree polynomial is 3.8769. The agreement is considered satisfactory.

Conical Bottom Since this case is of considerable practical interest, extensive numerical calculations have been performed and are presented in this paper. The bottom has the simple analytical representation

$$h = h_0 \left(1 - \frac{r}{r_0} \right) \quad \ldots\ldots [32]$$

Four values have been assigned to s, namely 0, 1, 2 and 3. A sixth degree polynomial, i.e., a polynomial with $N = 3$, has been employed in all the cases, yielding in each case four eigenvalues for the dimensionless frequency β. These frequencies and the coefficients of the corresponding normalized polynomials are given in Table 1. The polynomials are plotted in Fig. 2 to give a graphical representation.

In order to assess the effect of the number of terms of the polynomial on the accuracy of the results, polynomials of degrees from 1 to 3 have been used in the calculation of natural frequencies. Results given in Table 2 indicate that polynomials with a very small number of terms are satisfactory,

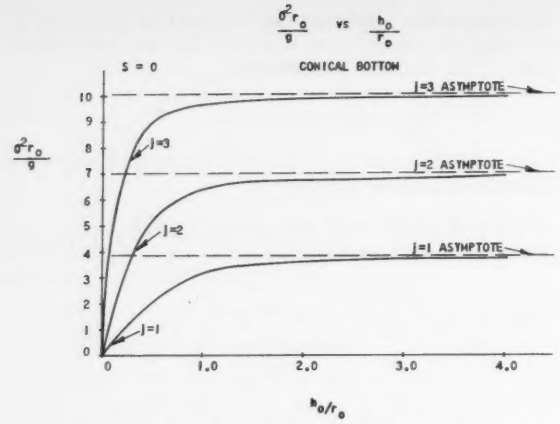

Fig. 2 Frequency vs. depth for a conical bottom ($s = 0$)

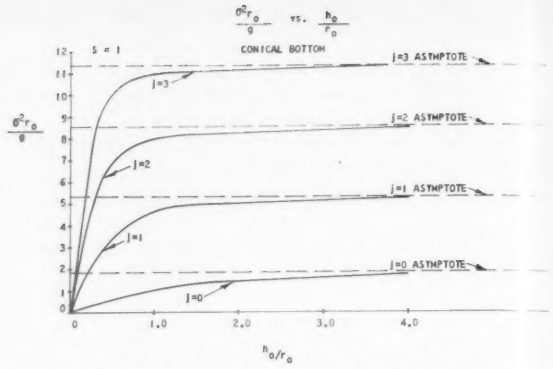

Fig. 3 Frequency vs. depth for a conical bottom ($s = 1$)

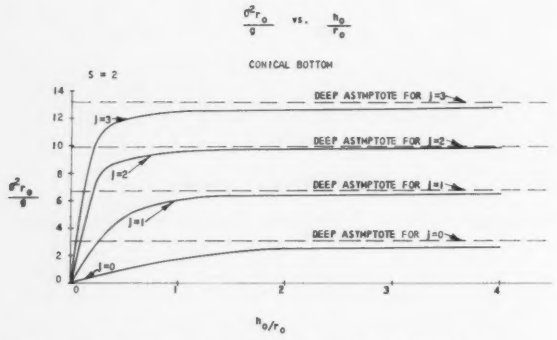

Fig. 4 Frequency vs. depth for a conical bottom ($s = 2$)

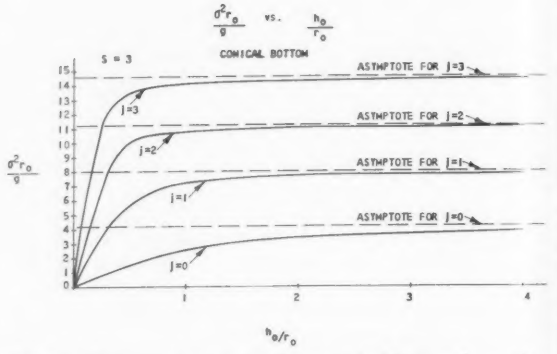

Fig. 5 Frequency vs. depth for a conical bottom ($s = 3$)

Table I Frequencies and normalized polynomial coefficients for shallow tanks with conical bottom

			α_{jn}			
s	j	β_{sj}	$n = 0$	$n = 1$	$n = 2$	$n = 3$
	0	0	0	0	0	0
	1	2.1730	2.1506	−3.0296	−2.1878	0.37387
0	2	3.8078	2.6977	−11.672	0.18296	12.310
	3	5.5218	4.3597	− 47.902	113.74	−73.286
	0	1.1459	1.6241	0.89134	−0.65843	0.27075
	1	2.9029	4.3053	−2.3593	−6.1693	1.1262
1	2	4.5382	7.6674	−17.930	−13.350	27.457
	3	6.2883	19.534	−121.99	214.19	−113.23
	0	1.5424	1.6328	2.7094	−3.5354	1.8067
	1	3.4180	6.6966	2.5563	8.7838	1.2027
2	2	5.1098	14.956	26.217	−29.610	44.987
	3	6.8881	46.118	−264.32	448.01	−233.36
	0	1.8465	2.1129	1.3202	−0.74504	0.26920
	1	3.8511	9.2644	−2.5725	−11.917	1.4863
3	2	5.5776	16.866	2.4142	−109.01	94.316
	3	6.9197	97.010	−484.80	747.51	−363.13

s = circular mode number
j = radial mode number
α_{jn} = coefficients of the polynomial representing the radial wave of the jth mode
β_{sj} = dimensionless frequency

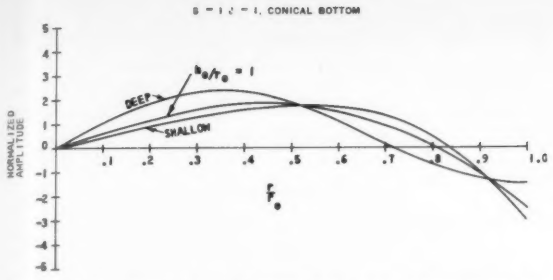

Fig. 6 Comparison of an intermediate wave shape with the asymptotic wave shapes

and the calculated frequencies converge to the correct value rapidly when the number of terms increases.

The polynomials given in Table 1 are normalized so that

$$\int_0^1 d\left(\frac{r}{r_0}\right)\left[G_{sj}\left(\frac{r}{r_0}\right)\right]^2\left(\frac{r}{r_0}\right) = 1 \quad \ldots\ldots\ldots [33]$$

The orthogonality condition for these polynomials is

$$\int_0^1 d\left(\frac{r}{r_0}\right)[G_{sj} \cdot G_{s'j'}]\left(\frac{r}{r_0}\right) = \delta_{ss'}\delta_{jj'}$$

where $\delta_{ss'} = 1$ if $s = s'$, and $\delta_{ss'} = 0$ if $s \neq s'$; $\delta_{jj'} = 1$ if $j = j'$ and $\delta_{jj'} = 0$ if $j \neq j'$, has been used as a check on the numerical calculations.

Circular Tank of Arbitrary Depth

The procedure for obtaining the solution for the tank of arbitrary depth is discussed in the section "Tanks of Arbitrary Depth." For a circular tank, the shallow tank potential $E(x, y)$ becomes $G(r)$, a function of r only, and may be obtained by the method given in the preceding section. The deep tank potential F has been solved (1) exactly in the form

Table 2 Effect of degree of the polynomial on accuracy of the frequency of shallow tanks with conical bottom

		β_{sj}			
s	N	$j = 0$	$j = 1$	$j = 2$	$j = 3$
	0	0			
	1	0	2.1899		
0	2	0	2.1732	3.8645	
	3	0	2.1730	3.8078	5.5218
	0	1.1547			
	1	1.1476	2.9370		
1	2	1.1466	2.9032	4.6177	
	3	1.1459	2.9029	4.5382	6.2883
	0	1.5492			
	1	1.5425	3.4483		
2	2	1.5424	3.4181	5.1843	
	3	1.5424	3.4180	5.1098	6.8881
	0	1.8516			
	1	1.8466	3.8771		
3	2	1.8465	3.8512	5.6742	
	3	1.8465	3.8511	5.5776	6.9197

s = circular mode
N = degree of polynomial
j = radial mode
β_{sj} = dimensionless frequency

The frequency β_{sj} for a given s and j shows rapid convergence with the degree of the polynomial used.

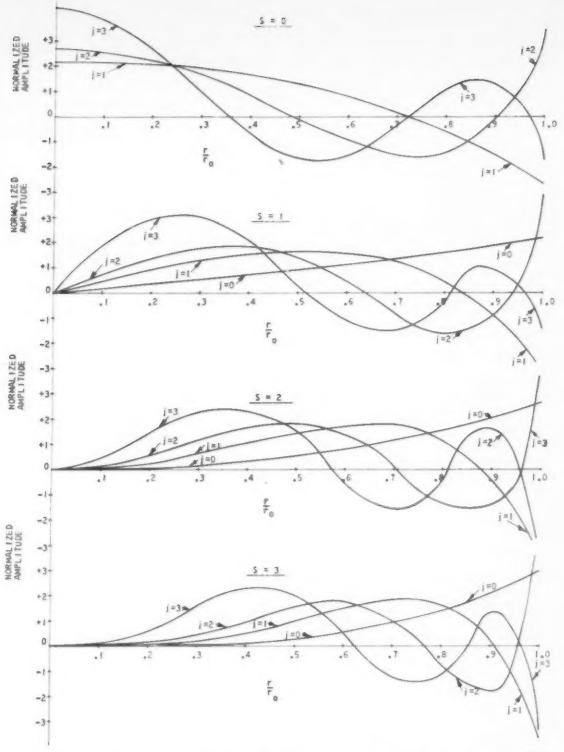

Fig. 7 Normalized wave shapes in a shallow conical tank

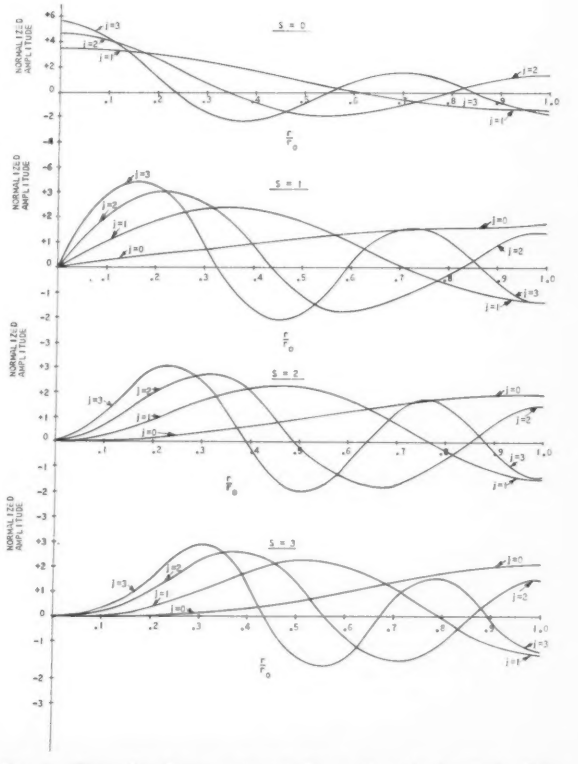

Fig. 8 Normalized wave shapes for a deep tank of circular section

of a Bessel function $J_s(\mu_{sj}\bar{r}/r_0)$, μ_{sj} being the jth zero (2) of $J_s'(\mu_{sj}\bar{r}/r_0)$, where the prime denotes differentiation.

For a circular tank of conical bottom with $h_0/r_0 = 1$, the results obtained by this procedure are given in Figs. 2 through 9. This happens to be a special case which has an exact solution (3) for the lowest mode (i.e., for $s = 1$, $j = 0$). The exact solution gives $\sigma^2 r_0/g = 1$, compared to 0.994 obtained by the present technique. Furthermore, the exact solution gives a linear function of r for the wave amplitude of this mode. The present technique gives a result, as shown in Fig. 4, in close agreement with this.

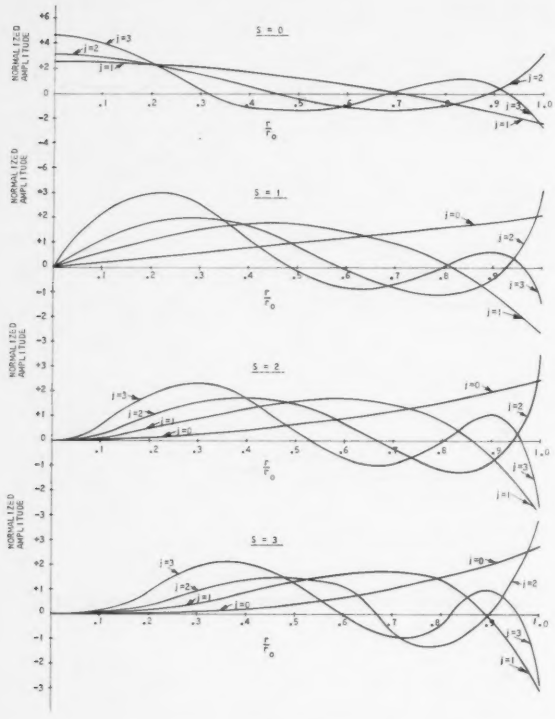

Fig. 9 Normalized wave shapes for a conical tank of 90 deg vertex angle ($h_0/r_0 = 1$)

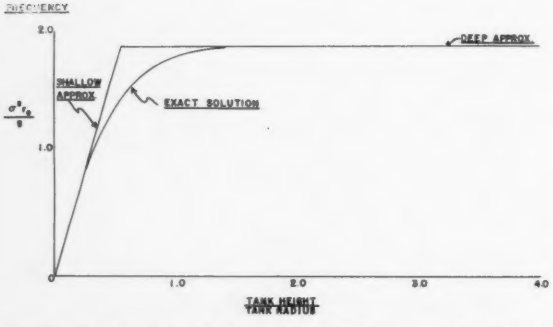

Fig. 10 Exact solution for lowest natural frequency of a circular tank with a flat bottom

Conclusions

1 A variational principle for the approximate calculation of the normal modes of sloshing has been developed, including the specific formulas for the shallow tank, the deep tank and tanks of arbitrary depth.

2 Application of this method to a shallow conical tank shows satisfactorily rapid convergence with the degree of the polynomial used, as shown in Table 2.

3 Application of the method to flat bottomed tanks of arbitrary depth shows satisfactorily accurate results. The error curve in Fig. 11 shows a maximum error of 0.8 per cent for the lowest natural frequency (Fig. 10) when the potential function of the shallow tank is approximated by a fourth degree polynomial. Similarly satisfactory results are obtained for 90 deg conical bottomed tanks.

4 The variational procedure presented in this paper appears to represent an accurate and rapid method for calculating the sloshing modes and frequencies for a wide class of tank geometries. It must be emphasized, however, that the choice of functions used in applying the Rayleigh-Ritz procedure has an important bearing on this conclusion.

References

1 Lamb, Sir Horace, "Hydrodynamics," Dover Publishers, sixth ed., 1945, New York.

2 Smith, D. B., Rodgers, L. M. and Traub, E. H., "Zeros of Bessel Functions," *Journal of the Franklin Institute*, vol. 237, no. 4, April, 1944.

3 Levin, E., "Conical Sloshing," Ramo-Wooldridge Internal Report PA/M-553/1.

4 Courant, R. and Hilbert, D., "Methods of Mathematical Physics, Vol. I," Interscience Publishers, first English ed., 1953, New York.

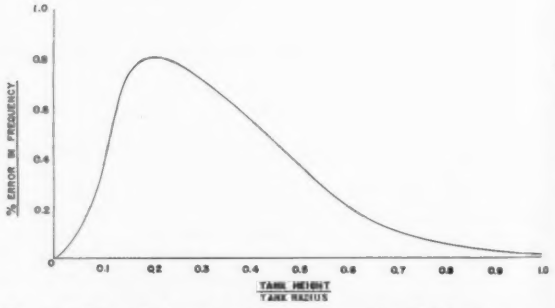

Fig. 11 Error in lowest mode frequency for flat bottom case using fourth degree polynomial approximation

On Catalytic Recombination Rates in Hypersonic Stagnation Heat Transfer[1]

R. GOULARD[2]

Purdue University, West Lafayette, Ind.

Stagnation laminar heat transfer at hypersonic speeds depends on the rate of recombination of the dissociated air behind the detached shock wave. This paper is concerned with the case of a large recombination time compared to the time of diffusion across the boundary layer. The conditions of existence of such a "frozen flow" and its coupling with the dissociation lag behind the shock are discussed. In order to account for finite catalytic recombination rates at the wall, a nonsimilar boundary condition is introduced which can be reduced to similarity for stagnation flow only. In this latter case, Lees' (1)[3] and Fay and Ridell's (2) heat transfer solutions are shown to correspond to the limiting case of an infinitely fast catalyst. The validity of their solutions is extended to the general case of a wall of finite catalytic efficiency, by introducing a correction factor φ. This factor is a simple function of the flight condition, nose geometry and the wall catalytic recombination rate constant. For a given nose material, the percentage of the heat transfer by catalysis is found to increase with the velocity, the nose diameter and the wall temperature and to decrease with altitude. Finally, the experimental values obtained for the catalytic recombination rates of oxygen and nitrogen atoms on various surfaces illustrate numerically the importance of the nature of the wall on the catalytic heat transfer to a missile nose. In particular, the superiority of pyrex over metallic surfaces stresses the need for more experimental values for glassy and ceramic coatings.

Nomenclature

c, c_A = atom mass fraction
c_M = molecular mass fraction
c_p = specific heat of air at constant pressure, cal/gr K
$\tilde{c}_p = \sum_i c_i c_{pi}$ = frozen specific heat, cal/gr K
d = nose diameter, cm
D = ordinary diffusion coefficient, cm²/sec
Dam = Damköhler number (Eq. [35])
f = u/u_e
g = h_s/h_{se}
h = enthalpy, cal/gr
$\tilde{h}$ = frozen enthalpy, cal/gr
h_R = heat of recombination (atoms → molecule), cal/gr (Eq. [32])
j = net mass flux of atoms, gr/cm² sec
k_w = catalytic reaction rate constant (Eqs. [6 and 34])
l = $\mu\rho/\mu_e\rho_e$
Le = Lewis number = $\rho D\tilde{c}_p/\lambda$
m = order of catalytic reaction (Eq. [6])
M = average molecular weight of air, gr/mole
M_A = atomic weight of air, gr/mole
M_M = molecular weight of air, gr/mole
n = molecules per unit volume, cm⁻³
p = pressure, dynes/cm²
q_c = heat transmission by conduction, cal/cm² sec
q_D = heat transmission by diffusion, cal/cm² sec
q = total heat transmission excluding radiation, $q_c + q_D$
q_R = heat transmission by radiation, cal/cm² sec
r_0 = distance from axis of revolution of body, cm
R = nose radius, cm
R_u = universal gas constant, 8.314×10^7 ergs/mole K
s = similarity abscissa
S = Equation [30]
Sc = Schmidt number $\mu/\rho D$
t = time, sec
T = temperature, K
u = velocity along the wall, cm/sec
v = velocity perpendicular to the wall, cm/sec
w_A = rate of generation of atoms, gr/cm³ sec
x = abscissa, (distance along the wall from stagnation point)
y = ordinate (perpendicular to the wall)
z = c/c_e
Z_c = compressibility factor, $\left(p = Z_c\rho\dfrac{R_u}{M_M}T\right)$
β = du_e/dx stream velocity gradient (Eq. [23])
γ = wall recombination efficiency (Eq. [34])
ϵ = Lennard-Jones potential well
η = similarity coordinate
λ = heat conductivity, cal/cm sec K
μ = dynamic viscosity, gr/cm sec
ρ = density, gr/cm³
σ = Lennard-Jones collision diameter, Å
$\bar{\sigma}$ = Prandtl number $\mu\tilde{c}_p/\lambda$
ψ = stream function
φ = correction factor for catalytic effects (Eq. [22])

Subscripts

A = atom
M = molecule
e = stream outside the boundary layer
s = stagnation
w = wall
∞ = ahead of shock

1 Introduction

THE high stagnation temperatures generated by hypersonic flights provoke a chemical process of dissociation behind the shock, followed by a recombination process when the gas expands or flows past a cool body. Consequently, the formulation of the boundary layer problem must account for reacting gas mixtures processes (chemical rates, diffusion) and their effect on thermal properties.

Lees (1) and Fay and Riddell (2) have laid down the general formulation of the boundary layer equations for the case of a dissociating gas. They established the dual process of energy transfer by ordinary molecular conduction and by diffusion of atoms, the latter releasing their energy by recombination in the stream or on the cool wall. Two extreme regimes are possible: The recombination rate may be very fast (thermodynamic equilibrium) or very slow (frozen flow). In the latter case, no recombination takes place in the boundary layer, except possibly at the wall where catalytic reactions may occur. A third case allows for a finite recombination rate in the stream itself (mixed flow). The two extreme cases

[1] Presented at the ARS 12th Annual Meeting, New York, N. Y., Dec. 2–5, 1957 and revised, July 1958. This work has been supported partly by the United States Army, through the Office of Ordnance Research, partly by the McDonnell Aircraft Corporation, under the direction of Dr. H. DeGroff.

[2] Assistant Professor, School of Aeronautical Engineering. Member ARS.

[3] Numbers in parentheses indicate References at end of paper.

present some simplifications: These permitted Lees, on the basis of physical arguments, to further simplify and uncouple the boundary layer equations and finally to present approximate closed form solutions for these two cases. Fay and Riddell, on the other hand, reduced the equations into similar form and, in order to avoid oversimplification, programmed a numerical solution for all possible gas phase recombination rates. Although Lees' closed results underestimate heat transfer, Probstein (3) has shown that they presented a good approximation of Fay and Riddell's more accurate numerical results. This conclusion is also verified on Figs. 2 and 3 of this study.

However, a study of the catalytic recombination process at the wall leads to the conclusion that both Lees' and Fay's assumptions of wall recombination with zero atom concentration represents only the case of an extremely active catalyst. In general, chemical rules require that the rate of recombination at the wall be a power function of the atom concentration ((4) p. 140). As shown by Chambré and Acrivos (5) in the case of incompressible flow past a flat plate, the exact wall conditions generally destroy similarity solutions. A more exact representation of the catalytic process is of special importance, since heat transfer reduction by means of surfaces of low catalytic efficiency may be an attractive possibility for a safe satellite re-entry (6) or for long range hypervelocity vehicles.

This paper is therefore concerned with the effects on stagnation heat transfer of finite catalytic recombination rates in frozen flow.

Although catalytic recombination can be included in the "equilibrium" flow solutions, the high wall temperatures required for its effect to be appreciable are not practical, and this case is not considered here.

2 The Laminar Boundary Layer Equations in Frozen Hypersonic Flow

A frozen process is one in which the chemical reaction time is very long compared to some characteristic mechanical time of the stream. In such flows, the atoms generated by the detached shock wave diffuse towards the cool nose surface recombining ($w_A = 0$). Therefore, the recombination energy release depends entirely on the catalytic properties of the wall. Hence the importance of such frozen regimes when catalytic processes are under study.

The Conservation Equations

Prandtl's dimensional analysis reduces the equations of conservation of atom mass, mixture mass, momentum and energy to the classical form

$$\rho\left(u\frac{\partial c}{\partial x}+v\frac{\partial c}{\partial y}\right)=\frac{\partial}{\partial y}\left(\rho D\frac{\partial c}{\partial y}\right)+w_A \qquad \text{atom mass}$$

$$\frac{\partial}{\partial x}(\rho u r_0)+\frac{\partial}{\partial y}(\rho v r_0)=0 \qquad \text{mixture mass}$$

$$\rho u\frac{\partial u}{\partial x}+\rho v\frac{\partial u}{\partial y}=-\frac{dp_e}{dx}+\frac{\partial}{\partial y}\left(\mu\frac{\partial u}{\partial y}\right) \qquad \text{mom } x$$

$$\rho u\frac{\partial h}{\partial x}+\rho v\frac{\partial h}{\partial y}=\frac{\partial}{\partial y}\left(\lambda\frac{\partial T}{\partial y}\right)+h_R\frac{\partial}{\partial y}\left(\rho D\frac{dc}{dy}\right)+q_R+u\frac{dp_e}{dx}+\mu\left(\frac{\partial u}{dy}\right)^2 \qquad \text{energy}$$

The basic assumption of frozen flow yields immediately: $w_A = 0$. It was also shown by Lees that enthalpy variations can be broken into a chemical energy variation due to the change in mixture composition and an energy variation due to the variation of temperature of the existing components. For a binary atom-molecule mixture

$$dh = \bar{c}_p\,dT + h_R dc$$

It is further convenient in the case of the frozen flow where no reaction takes place in the boundary layer proper, to introduce, after Lees, a *frozen stagnation enthalpy* $\bar{h}_s$ excluding the chemical energy that would be liberated by recombination of the atom fraction ($h_R dc$)

$$d\bar{h}_s = \bar{c}_p dT + d\frac{u^2}{2} = \bar{c}_p\,dT_s$$

If we then multiply the momentum equation by u and add it to the energy expression, we obtain after simplification an expression similar to Von Karman's total energy expression

$$\rho u\frac{\partial \bar{h}_s}{\partial x}+\rho v\frac{\partial \bar{h}_s}{\partial y}=\frac{\partial}{\partial y}\left(\frac{\lambda}{\bar{c}_p}\frac{\partial \bar{h}_s}{\partial y}\right)-\frac{\partial}{\partial y}\left[\mu\left(\frac{1}{\bar{\sigma}}-1\right)\frac{\partial}{\partial y}\left(\frac{u^2}{2}\right)\right]$$

The Similarity Transformation

For compressible viscous flow, a transformation originally devised by Doronitzin has made possible a set of similarity solutions for the compressible boundary layer equations.

In Lees' adaptation of Doronitzin's transformation to the case of a blunt body of revolution, two new coordinates are introduced

$$\eta=\frac{u_e}{(2s)^{1/2}}\int_0^y r_0\,\rho\,dy$$

$$s=\int_0^x \mu_e\rho_e u_e\,r_0^2\,dx$$

In addition, the continuity equation is identically satisfied if we define a stream function ψ such that

$$\psi_y=\rho u r_0 \qquad \psi_x=-\rho v r_0$$

If the dimensionless stream function is defined, $f \equiv \psi/(2s)^{1/2}$, it is then easily verified that

$$\frac{u}{u_e}=\frac{\partial f}{\partial \eta}=f'$$

A dimensionless frozen stagnation enthalpy is introduced: $\bar{g} = \bar{h}_s/\bar{h}_{se}$, and also a dimensionless atom concentration: $z = c/c_e$, where both stream values $\bar{h}_{se}$ and c_e can be assumed constant if thermodynamic equilibrium is achieved in the stagnation area (see the second part of section 5 of this article).

After substitution of the new variables in the equations, we obtain

$$(lf'')'+ff''+\frac{2s}{u_e}\frac{\partial u_e}{\partial s}\left(\frac{\rho_e}{\rho}-f'^2\right)=0 \qquad [1]$$

$$f\bar{g}'+\left(\frac{l}{\bar{\sigma}}\bar{g}'\right)'+\frac{\mu_e^2}{2\bar{h}_{se}}\left[2l\left(1-\frac{1}{\bar{\sigma}}\right)f'f''\right]'=0 \qquad [2]$$

$$2s\frac{\partial z}{\partial s}f'-fz'-\left(\frac{l}{Sc}z'\right)'=0 \qquad [3]$$

This set of equations is similar to Lees, and, provided we also assume in this paper a very cool wall ($T_w \ll T_{es}$), the same boundary conditions exist for both momentum and energy equations

$$f(0)=f'(0)=0 \qquad f(\infty)=1 \qquad \bar{g}(0)\ll 1 \qquad \bar{g}(\infty)=1$$

However, the last equation (atom mass conservation) includes a nonsimilar term in s. This dependence on s is due in general to the nonsimilar form of the boundary condition due to the catalytic process taking place at the wall.

Strictly, the momentum equation also depends on z through

ρ, and the nonsimilar term should be shown in all three equations. However, the solutions we will discuss are those where the contribution of ρ to the momentum equation is neglected, and the terms in s have been left out for simplicity.

Catalysis at the Wall

Existing solutions (1, 2) assume a zero concentration to be a suitable condition at the wall. This does not account for the chemical process of catalytic absorption (4,7) where the catalytic reaction rate is proportional to a power m of the concentration $c_w\rho_w$ at the wall.[4] Since the *net* mass flux of atoms diffusing towards the wall, neglecting thermal diffusion, is

$$j_w = \rho_w D_w \left(\frac{\partial c}{\partial y}\right)_w \quad \ldots\ldots\ldots\ldots\ldots\ldots [4]$$

it follows from the conservation of mass principle that in the steady state

$$j_w = \rho_w D_w \left(\frac{\partial c}{\partial y}\right)_w = k_w(c_w \rho_w)^m \qquad 1 < m < 2 \ldots\ldots [5]$$

which becomes the boundary condition of Equation [3] at the wall. It is clear from this equation that no diffused atom can reach the wall while the concentration c_w is zero, unless the catalytic reaction rate constant k_w becomes infinite. Lees and Fay have thus taken for their treatment of diffusion as the rate controlling process, the limiting case of $k_w \sim \infty$. The other extreme case of a noncatalytic surface ($k_w \sim 0$) implies, since c_w is bounded, that the net flux j_w of atoms toward the wall is zero; it also follows from Equations [8 and 16] that the trivial solution $c(\eta) = c_e$ applies to this case.

In general, if we transpose the wall boundary condition [5] into the new coordinate system η and s, it becomes

$$\left(\frac{\partial c}{\partial \eta}\right)_w = \frac{(2s)^{1/2}}{r_0 u_e} \frac{k_w}{\rho_w^{2-m} D_w} c_w^m \quad \ldots\ldots\ldots\ldots [7]$$

or

$$\left(\frac{\partial z}{\partial \eta}\right)_w = \frac{(2s)^{1/2}}{r_0 u_e} \frac{k_w}{\rho_w^{2-m} D_w} c_e^{m-1} z_w^m \quad \ldots\ldots\ldots\ldots [8]$$

This condition destroys in general the similarity of the equation. A nonsimilar solution to this problem was developed by Chambré and Acrivos (5) in the case of an incompressible flow past a flat plate. In their solution, Chapman and Rubesin's and Lighthill's methods were transposed to this problem. In the case of stagnation flow, however, a simpler similar solution is possible.

The Stagnation Flow With Ordinary Diffusion

The solution of the system of three equations, simultaneous partial differential, nonlinear and coupled to each other is in general an impossible problem, short of numerical solutions.[5] In order to make possible an analytical solution, Lees (1) has introduced a major simplification to this problem: For a highly cooled wall ($\bar{g}_w \ll 1$), the third term of both momentum and energy equations can be dropped with good approximation. This procedure reduces the coupling of these two equations to the dependence of the thermal properties $l = \mu\rho/\mu_e\rho_e$ and $\bar{\sigma}$ on temperature. Lees further advanced that neither l nor $\bar{\sigma}$ were too sensitive to temperature for most of the boundary layer and could be assumed constant

$$\bar{\sigma} = 0.715 \text{(Eucken)} \qquad l = 1$$

Lees' last assumption (l = const) has been long successful in low temperature boundary layer theory where its adoption leads to a convenient uncoupling of momentum and energy equations. It was shown however in (11 and 3) that its validity decreases for higher temperatures, as can also be seen on Fig. 1 of (2). Fortunately, enthalpy wall gradients and concentration wall gradients, and consequently heat transfer, are weak functions of l. This point is illustrated on Figs. 2

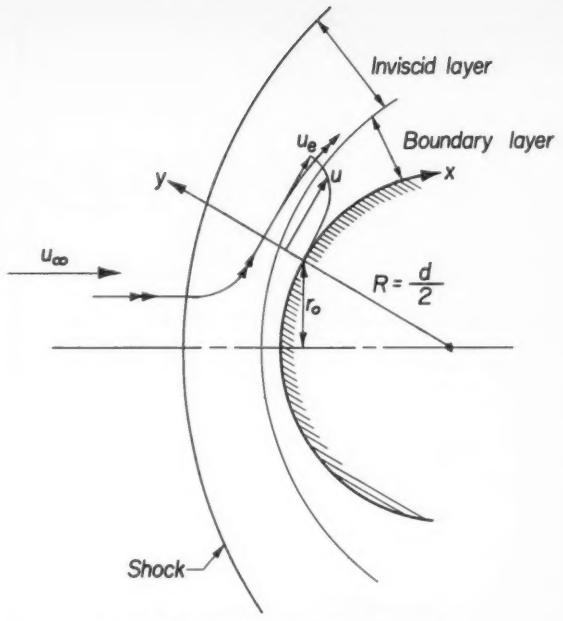

Fig. 1 Stagnation flow past a blunt body

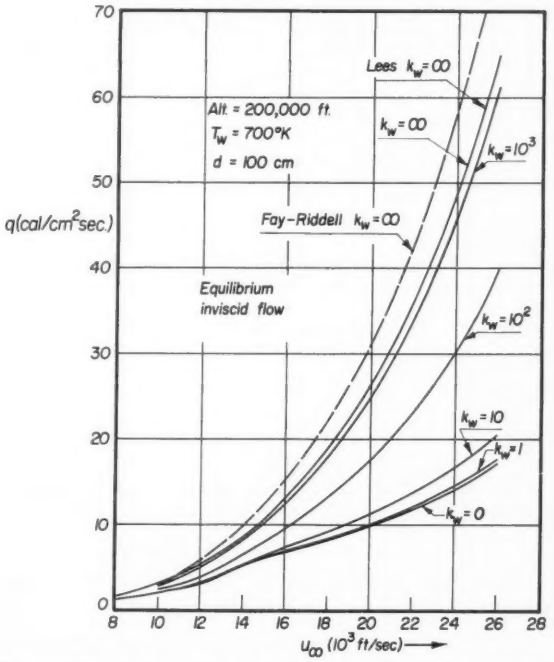

Fig. 2 Stagnation heat transfer at altitude 200,000 ft (assuming the outer edge of the boundary layer in chemical equilibrium)

[4] This expression of surface recombination excludes the opposite surface dissociation reaction and implies therefore a high recombination activation energy and generally a low temperature wall. Scala (8) has shown that this wall condition was correct up to $T_w \simeq 2000$ K. A more general approach is suggested by Rosner (9) in the case of small deviation from equilibrium at arbitrary high wall temperatures.

[5] Such numerical computation has been independently carried out by Scala, including thermal diffusion effects. His results have been recently declassified and are briefly discussed in (8 and 10).

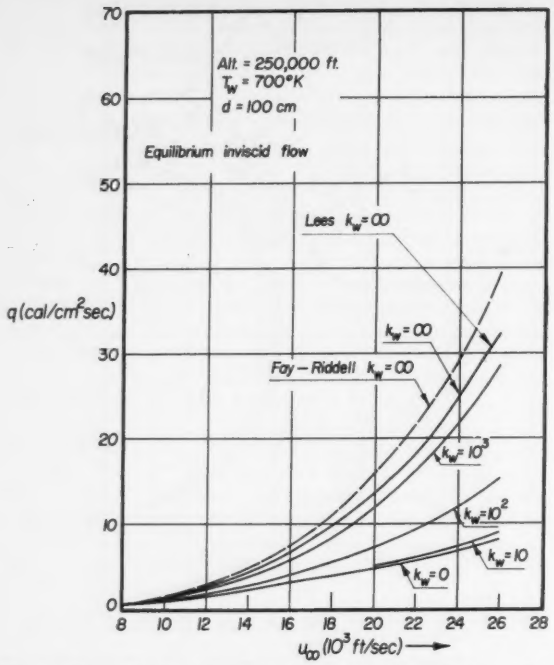

Fig. 3 Stagnation heat transfer at altitude 250,000 ft (assuming the outer edge of the boundary layer in chemical equilibrium)

and 3 of this paper, where in the case of a catalytic wall ($k_w \sim \infty$) the exact numerical results of (2) lie within less than 20 per cent of Lees' results, even for very high stream temperature, i.e., large variations of l across the boundary layer. Lees' assumption $l = 1$ retains therefore a good approximation of the stagnation heat transfer, where the influence of the other physical factors are available in closed form.

The determination of the shear force and total frozen enthalpy reduces therefore in first approximation to the solution of the following set of equations

$$f''' + ff'' = 0$$

$$\bar{g}'' + \bar{\sigma} f \bar{g}' = 0$$

Both equations have been solved by Blasius and Polhausen. In particular, with the present definitions of f, $\bar{g}$, η and $\bar{s}$, one obtains

$$f''(0) = \frac{0.664}{\sqrt{2}} = 0.47 \quad \ldots\ldots [9]$$

$$\bar{g}'(0) = \sqrt{2}\,(0.664)\,\bar{\sigma}^{1/3} = 0.47\,\bar{\sigma}^{1/3} \quad \ldots\ldots [10]$$

Wall Catalysis at Stagnation

For stagnation flow conditions, we introduce the local approximations

$$r_0(x) = x \qquad u_e = \beta x \quad \ldots\ldots [11]$$

where the parameter β depends on flight conditions and nose diameter only (see Eq. [23]).

Substituting into the nonsimilar term of the boundary condition [8], we read

$$\frac{(2s)^{1/2}}{r_0 u_e} = \frac{\left(2\int_0^x \mu_e \rho_e u_e r_0^2 dx\right)^{1/2}}{r_0 u_e} = \frac{\left(2\mu_e \rho_e \beta \frac{x^4}{4}\right)^{1/2}}{\beta x^2} = \left(\frac{\mu_e \rho_e}{2\beta}\right)^{1/2} \quad \ldots\ldots [12]$$

Hence, for stagnation flow, the boundary condition [8] can be written

$$\left(\frac{\partial z}{\partial \eta}\right)_w = \left(\frac{\mu_e \rho_e}{2\beta}\right)^{1/2} \frac{k_w}{\rho_w^{2-m} D_w} c_e^{m-1} z_w^m \quad \ldots\ldots [13]$$

The only s-dependent variables left are the stream properties ρ_e, μ_e and c_e. But the product $\mu_e \rho_e$ can be assumed constant and equal to $\mu_{es}\rho_{es}$ for the high temperatures and nearly constant pressure of the stagnation stream flow (see for instance Fig. 1 of (2)). On the other hand, c_e has been assumed constant in the stagnation area. Furthermore, the practical necessity of a cool wall implies a catalytic reaction of the first order: $m = 1$.[6] In this case, the term in c_e disappears from Equation [13] altogether, and the boundary conditions of Equation [3] are

$$z'(0) = \left(\frac{\mu_{es}\rho_{es}}{2\beta}\right)^{1/2} \frac{k_w}{\rho_w D_w} z(0) \quad \ldots\ldots [14]$$

$$z(\infty) = 1 \quad \ldots\ldots [15]$$

The Continuity Equation Solution

The continuity Equation [3] being entirely similar at stagnation, the nonsimilar term in s can be dropped

$$Sc\, f z' + z'' = 0$$

Integrating this equation in two steps gives

$$z(\eta) - z(0) = z'(0) \int_0^\eta e^{-Sc\int_0^\eta f d\eta} d\eta$$

$$= z'(0) \int_0^\eta \left[\frac{f''(\eta)}{f''(0)}\right]^{Sc} d\eta \quad \ldots\ldots [16]$$

The determination of $z(0)$ and $z'(0)$ comes from the two boundary conditions [14 and 15]. When $\eta \sim \infty$, the numerical value of the integral in Equation [16] was found by Polhausen[7] to be the inverse of $0.47\,Sc^{1/3}$. Hence

$$z'(0) = 0.47\,Sc^{1/3}\,[1 - z(0)] \quad \ldots\ldots [17]$$

Substituting this value of $z'(0)$ in Equation [14] gives the dimensionless concentration at the wall

$$z(0) = \frac{c_w}{c_e} \frac{1}{\left(\frac{\mu_{es}\rho_{es}}{2\beta}\right)^{1/2} \frac{k_w}{0.47\,Sc^{1/3}\,\rho_w D_w} + 1} \quad \ldots\ldots [18]$$

The concentration profiles $z(\eta)$ are then given by Equation [16] using the constant values [17 and 18] for $z(0)$ and $z'(0)$. It is easily verified in expressions [17 and 18] that an infinitely fast catalyst ($k_w \sim \infty$) corresponds to $z(0) = 0$ and $z'(0) = 0.47\,Sc^{1/3}$ (Lees and Fay's values), whereas an infinitely slow catalyst ($k_w = 0$) gives $z(\eta) = z(0) = 1$, and $z'(0) = 0$.

3 Heat Transfer to the Wall

The heat transferred to the cool wall, excluding radiation, results in part from ordinary molecular conduction and in part from recombination at the wall of the atoms diffusing through the boundary layer. The rates of these two processes, per unit time and area, will be called q_c and q_D, respectively.

[6] In addition to this general statement provided by Laidler ((7) pp. 180–181) the first order reaction assumption is verified experimentally for oxygen by Linnett and Marsden. (See section 4 of this article.)

[7] The constant was the Prandtl number $\bar{\sigma}$, and the variable was smaller than η by a ratio $\sqrt{2}$. Hence the factor $0.47 = 0.664/\sqrt{2}$.

Conducted Heat

This fraction of the total heat is

$$q_c = \lambda_w \left(\frac{\partial T}{\partial y}\right)_w = \frac{\lambda_w}{\bar{c}_{pw}} \left(\frac{\partial \bar{h}_s}{\partial y}\right)_w = \frac{\lambda_w}{\bar{c}_{pw}} \bar{h}_{se} \left(\frac{\partial \eta}{\partial y}\right)_w \bar{g}'(0) \ldots [19]$$

since at the wall $\bar{h} = \bar{h}_s$.

Substituting the expressions of η and $\bar{g}'(0)$ (Eqs. [10 and 12])

$$q_c = \frac{\lambda_w}{\bar{c}_{pw}\mu_w} \frac{\mu_w \rho_w}{(\mu_{es}\rho_{es})^{1/2}} (2\beta)^{1/2} (0.47\, \bar{\sigma}_w^{1/3})\, \bar{h}_{se}$$

$$q_c = 0.47\, (2\beta \mu_{es}\rho_{es})^{1/2}\, \bar{\sigma}_w^{-2/3} \bar{h}_{se} \quad \ldots [20]$$

since $l_w = \frac{\mu_w \rho_w}{\mu_s \rho_s} = \frac{\mu_w \rho_w}{\mu_{es}\rho_{es}} = 1$ in Lees' approximation.

Heat Released by Recombination at the Wall

An expression of the heat released by recombination is easily obtained by multiplication of the *net* atom mass flux to the wall j_w (Eq. [4]) by the heat of recombination h_R (Eq. [32])

$$q_D = h_R j_w = h_R k_w c_w \rho_w = k_w h_R c_e z(0)\, \rho_w$$

Substituting the expression [18] for $z(0)$ where

$$\rho_w D_w = \frac{\rho_w D_w}{\mu_w} \mu_w = \frac{\mu_w}{Sc}$$

$$q_D = h_R c_e \rho_w \frac{k_w}{\left(\frac{\mu_{es}\rho_{es}}{2\beta}\right)^{1/2} \frac{k_w Sc}{0.47\, Sc^{1/3}\, \mu_w} + 1}$$

Rearranging

$$q_D = 0.47\, (2\beta \mu_{es}\rho_{es})^{1/2}\, Sc^{-2/3} h_R c_e \frac{1}{1 + \frac{0.47\, Sc^{-2/3}\, (2\beta \mu_{se}\rho_{se})^{1/2}}{\rho_w k_w}} \quad \ldots [21]$$

The interest of this formulation lies in the fact that the effect of the catalytic rate k_w is concentrated in the last fraction. When $k_w \sim \infty$, this fraction tends to unity, and $q_{D(k_w \sim \infty)}$ is equivalent to the previous solutions. This fraction is therefore a correction factor φ[8]

$$\varphi = \frac{1}{1 + \frac{0.47\, Sc^{-2/3}\, (2\beta \mu_{es}\rho_{es})^{1/2}}{\rho_w k_w}} \quad \ldots [22]$$

The expression of q_D becomes

$$q_D = 0.47 (2\beta\, \mu_{es}\, \rho_{es})^{1/2}\, Sc^{-2/3}\, h_R c_e \varphi \quad \ldots [24]$$

[8] Where β may be obtained, for instance, from Probstein (12)

$$\beta = \frac{2u_\infty}{d} \left[\frac{\rho_\infty}{\rho_{es}} \left(2 - \frac{\rho_\infty}{\rho_{es}}\right)\right]^{1/2} \quad \ldots [23]$$

or from Li and Geiger's (13) expression which uses the shock diameter rather than d. Probstein's expression is verified by the experimental results of (14).

Total Heat Transferred to the Wall

The total heat transferred to the wall is the sum of q_c and q_D (Eqs. [20 and 24])

$$q = q_c + q_D = 0.664\, (\beta \mu_{es}\, \rho_{es})^{1/2} (\bar{\sigma}_w^{-2/3}\, \bar{h}_{se} + Sc^{-2/3} h_R c_e \varphi) \ldots [25]$$

Introducing now the Lewis number $Le = \bar{\sigma}/Sc$ and the stream stagnation enthalpy $h_{se} = \bar{h}_{se} + h_R c_e$, we rearrange Equation [25] into

$$q = 0.664\, (\beta \mu_{es}\, \rho_{es})^{1/2}\, \bar{\sigma}_w^{-2/3} h_{se} \left[1 + (Le^{2/3}\, \varphi - 1) \frac{h_R c_e}{h_{se}}\right] \ldots [26]$$

where the correction factor φ is defined in expression [22]. This relation is easily converted into a Nusselt number relation where $Nu_w = q\bar{c}_{pw} x/\lambda_w (h_{es} - h_w)$ and $Re_w = u_e x \rho_w/\mu_w$ based on the wall conditions. One obtains after simplification, still assuming $\mu_e \rho_e/\mu_w \rho_w = 1$, $h_e \gg h_w$

$$\frac{Nu_w}{\sqrt{Re_w}} = 0.664\, \bar{\sigma}_w^{1/3} \left[1 + (Le^{2/3}\, \varphi - 1) \frac{h_R c_e}{h_{se}}\right] \ldots [27]$$

Discussion of Results

Expression [26] corresponds to Lees' results when combining his Equations [19 and 12a] (1). The Nusselt number is also in agreement. Only the catalytic factor φ is added.

Figs. 2 and 3 illustrate, for two typical flight conditions, the effect of flight velocity on the heat transfer q, for different values of the catalytic recombination constant k_w. It is important to note that thermal equilibrium has been assumed at the edge of the boundary layer behind the shock. The validity of this assumption is discussed in section 5 of this article.

The more exact numerical results of Fay and Riddell, as correlated for the case of frozen flow by relation [8] of (9)

$$q = 0.763\, \bar{\sigma}_w^{-0.6}\, (h_{se} - h_w) \left(\frac{\mu_w \rho_w}{\mu_{es}\rho_{es}}\right)^{0.1} (\beta \mu_{es}\rho_{es})^{1/2} \left[1 + (Le^{0.63} - 1) \frac{h_R c_e}{h_{se}}\right] \ldots [28]$$

is also illustrated on Figs. 2 and 3 for the two flight conditions considered. We verify Probstein's comment (3) that for $k_w \sim \infty$, the assumption $\mu_w \rho_w/\mu_{es}\rho_{es} = 1$ reduces the values of heat transfer by 20 per cent at most. It further suggests that Fay and Riddell's equation could be easily fitted with the correction factor φ to account for wall catalytic effects.

To investigate more closely the importance of the catalytic correction factor φ on stagnation heat transfer, it is convenient to analyze the ratio of the heat transferred in the case of any catalyst in general over the heat transferred in the case of an infinitely fast catalyst $q_{k_w \sim \infty}$ (previous solutions)

$$\bar{q} = \frac{q}{q_{k_w \sim \infty}} = \frac{1 + (Le^{2/3}\, \varphi - 1) \frac{h_R c_e}{h_{se}}}{1 + (Le^{2/3} - 1) \frac{h_R c_e}{h_{se}}}$$

$$= 1 - \frac{Le^{2/3} \frac{h_R c_e}{h_{se}}}{1 + (Le^{2/3} - 1) \frac{h_R c_e}{h_{se}}} (1 - \varphi) \ldots [29]$$

However, the catalytic correction factor φ is not a function of the catalytic reaction rate constant k_w only, but also of the flight conditions (see Eq. [22]). It is therefore interesting, from Equations [22 and 29], to represent the variations of $\bar{q}$ directly in terms of k_w for a given set of flight conditions.[9] The results of such calculation are illustrated

[9] The transport properties used in this calculation are discussed in section 4 of this article.

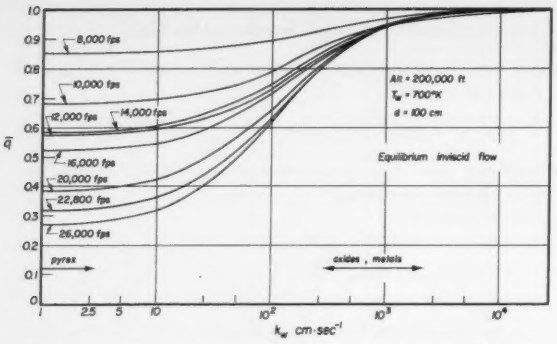

Fig. 4 Reduced heat transfer $\bar{q} = q/q_{kw\sim\infty}$ at 200,000 ft

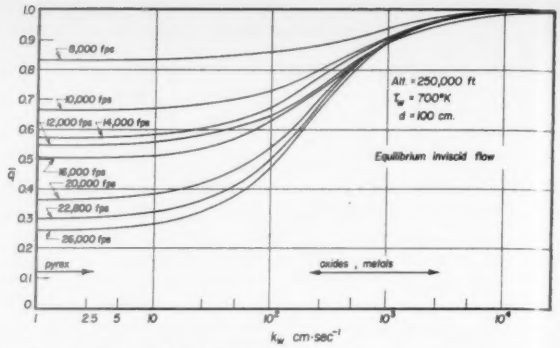

Fig. 5 Reduced heat transfer $\bar{q} = q/q_{kw\sim\infty}$ at 250,000 ft

in Figs. 4 and 5 for two given altitudes, one nose temperature and diameter. Some typical values of k_w are shown on this figure; they correspond to the experimental catalytic data discussed in section 4.

These numerical values illustrate the importance of the wall catalytic effect in typical cases, since the proper choice of the wall material seems to be sufficient to reduce the stagnation heat transfer by a large factor, assuming equilibrium composition of the shock layer at the boundary layer edge.

The Factors of Heat Transfer Reduction in Catalytic Frozen Flow

In addition to the obviously determinant role of k_w, these results and figures point out the effect of the following factors:

1 An increase in *flight velocity* u_∞ increases both heat transfer q and the fraction $\bar{q}$ of this heat due to dissociation. A minor deviation from this trend is observed for $\bar{q}$ in the range of velocities where oxygen is nearly all dissociated but nitrogen is still molecular (around 13,000 ft/sec). For these local conditions, a lesser fraction of the shock energy is converted into chemical energy, resulting in a lesser fraction of energy release by recombination.

2 If we rewrite Equation [22] in the form

$$\varphi = \frac{1}{1 + \dfrac{S}{k_w}}$$

where

$$S = \frac{0.47\ Sc^{-2/3}}{\rho_w}\left[\mu_{es}\rho_{es}\frac{4u_\infty}{d}\left(\frac{\rho_\infty}{\rho_{es}}\left[2 - \frac{\rho_\infty}{\rho_{es}}\right]\right)^{1/2}\right]^{1/2} \quad \ldots [30]$$

it can be seen that the real catalytic variable is the ratio S/k_w, and that any increase in S will have the same effect as a decreased catalytic reaction rate constant k_w. Therefore, a reduced *nose diameter* d will create a reduction of the catalytic effect and a diminution of the heat transfer.

3 The two terms of S/k_w which are affected by a *wall temperature* T_w variation are ρ_w and k_w. Across the boundary layer, the pressure is constant, so that

$$p_w = p_s = \rho_w Z_{cw} R_M T_w = \rho_s Z_{cs} R_M T_s$$

hence ρ_w is proportional to $1/Z_{cw}T_w$ for a given stagnation state. The variation of k_w with temperature is discussed in section 4: k_w is proportional to $T_w^{3/4}$ for pyrex and a much stronger function of T_w for some oxides. Finally, it is easily verified by a short iteration process that Z_{cw} (and z_w, from which it is calculated) is a very weak function of k_w; Z_{cw} doubles at most when k_w increases a hundredfold; hence the variations of Z_{cw} with temperature can be neglected in comparison with those of k_w.

The conclusion is that the ratio S/k_w, being proportional to $1/\rho_w k_w$, increases when the temperature decreases. The increase is mild for pyrex (proportional to $T_w^{1/2}$) and strong for oxides. Correspondingly, Equation [30] shows that the reduced heat transfer $\bar{q}$ decreases. Hence, wall cooling (especially for metal walls) has the double effect of evacuating the heat convected to the wall and preventing chemical energy from releasing more heat at the wall. Conversely, if the wall temperature is allowed to increase, heat transfer by recombination will increase; this inherently unstable situation is discussed by Rosner in (15).

4 Finally, it is difficult to analyze in all cases the effect of a change of *altitude* on the catalytic heat transfer process. This is because nearly all the properties in $\bar{q}$ are affected by a change in altitude. However, it can be stated in gross approximation that for partially dissociated air, above 16,000 ft/sec

$$\mu \sim T \qquad \frac{\rho_\infty}{\rho_{es}}\left(2 - \frac{\rho_\infty}{\rho_{es}}\right) \sim \frac{\rho_\infty}{\rho_{es}}$$

and from Feldman's charts (19)

$$h \sim \frac{u^2_\infty}{2} \qquad T \sim u_\infty \qquad \frac{\rho_{es}}{\rho_\infty} \sim \frac{\sqrt{T}}{\rho_\infty^{1/8}}$$

Hence, the simplified relation

$$(\mu_{es}\rho_{es}\beta)^{1/2} \sim \left(\frac{\rho_\infty}{R}\right)^{1/2} u_\infty^{1.25}$$

and after substitution into q and φ

$$q_{k\sim\infty,\ Le\ =\ 1} \sim \left(\frac{\rho_\infty}{R}\right)^{1/2} u_\infty^{3.25} \quad \ldots\ldots [31a]$$

and

$$\frac{S}{k_w} \sim \frac{T_w}{k_w\sqrt{\rho_\infty R}}\frac{Z_{cw}}{u_\infty^{0.75}} \qquad \text{with } \varphi = \frac{1}{1 + \dfrac{S}{k_w}} \quad \ldots [31b]$$

Relation [31a] has been already established by Kemp and Riddell (6). Relation [31b] illustrates the dependence of the catalytic parameter φ on the ambient density ρ_∞, a strong function of altitude. The beneficial effect of altitude on heat transfer reduction by use of a low catalyst is then substantiated. It can be seen for instance that an increase of density by a factor of 4 due to a change of altitude from 250,000 ft to 200,000 ft will have the same effect on φ as an increase of k_w by a factor of 2 at constant altitude. This result is illustrated by the massive shift along the k_w abcissa of the $\bar{q}$ curves when going from Fig. 5 to Fig. 4.

If the altitude is further reduced from 250,000 to 100,000 ft, the density would be increased more than a hundredfold, and the $\bar{q}$ curves of Fig. 5 would be shifted by one order of magnitude to the left. In this case, all substances with $k_w > 10^2$ would behave as nearly perfect catalysts, as was concluded by Scala in (8).

It is however apparent from this discussion that the non-catalytic character of the wall improves with altitude. Scala's conclusion, illustrated only for an altitude of 100,000 ft in (8 and 10), is therefore too restrictive for the possibilities of heat transfer reduction at higher altitude. This remark is especially important in view of the fact that frozen flow is more likely to take place at higher altitudes.

4 Properties of Dissociated Air

Equilibrium Properties of Dissociated Air

The state and composition of the gas in equilibrium behind the shock is available from many sources. A very convenient reference is the set of charts published by Feldman (19). Hilsenrath and Beckett's (20) composition of argon free air has been adopted: 0.78847 moles of nitrogen and 0.21153 moles of oxygen per mole of air. The standard heat of recombination of nitrogen is 8089 cal/gr (9.76 ev) and that of oxygen is 3686 cal/gr. It has been assumed, after Hirschfelder (21) and Lighthill (22), that the number of degrees of freedom of molecular air was double that of atomic air, resulting in the same specific heat per unit mass: $c_{pM} = c_{pA}$. The heat of recombination is therefore simplified to its standard value

$$h_R = h^\circ_R + (c_{pM} - c_{pA})(T - T^\circ) = h^\circ_R$$

Finally, it is convenient to observe that practically all of the oxygen is dissociated before nitrogen begins to dissociate. The atom concentration c_e can then be used directly in the dissociation energy term $h_R c_e$

for $c_e < 0.2346$ $\quad h_R c_e = h_{RO_2} c_e$ (oxygen only)

for $c_e > 0.2346$ $\quad h_R c_e = h_{RO_2}(0.2346) + h_{RN_2}(c_e - 0.2346)$ (oxygen + nitrogen) .....[32]

Transport Properties of Dissociated Air

Classic experimental techniques fail to give high temperature experimental values for transport properties of air. Although new approaches to this problem are being developed (i.e., shock tube techniques) the bulk of the recently published values rely entirely on extrapolations of low temperature data based on molecular theories of gases (16,17). Since little is known about the atom-molecule interaction potentials of oxygen and nitrogen, these extrapolated values must be considered only as best available guesses.

Among recent estimates, Lees' values (1) were calculated by molecular theory methods on the basis of the following assumptions:

1 High temperature air is assimilated to a binary mixture of atoms and molecules.

2 The molecular models of air atoms and molecules are of the Lennard-Jones 6-12 type, with the following collision diameters and potential wells

$$\sigma_A = 0.80\ \text{Å} \qquad \sigma_{AM} = 3.3\ \text{Å} \qquad \sigma_M = 3.69\ \text{Å}$$

$$\epsilon_A/k = 1.14 \times 10^6\ ^\circ\text{K} \qquad \epsilon_M/k = \epsilon_{AM}/k = 84\ ^\circ\text{K}$$

Lees estimated these numerical values by extrapolation of atom-molecule hydrogen data. His molecular model has been adopted here.

Because of the present uncertainty on the Prandtl, Schmidt and Lewis numbers, the following constant values, used by Lees, Fay and others, have also been used here

$$Sc = 0.485 \qquad Le = 1.4 \qquad \bar{\sigma} = 0.71$$

Finally, the value of viscosity at high temperatures had to be calculated. In this paper, Wilke's semi-empirical relation ((18) p. 533) was used. The lack of collision integrals for the atom species, due to its very large potential well, made it necessary to extrapolate the available collision integrals to lower reduced temperatures. This approach, although approximate, is more consistent with Lees' estimates than using a rigid sphere model for the atoms while retaining a Lennard-Jones model for the molecules.

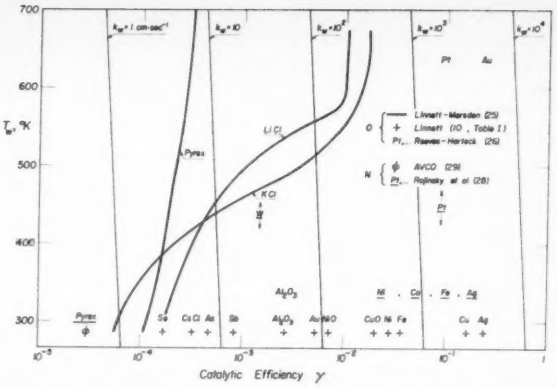

Fig. 6 Catalytic efficiencies for atomic oxygen and atomic nitrogen. The lines of constant k_w (Eq. [34]) are practically the same for oxygen and nitrogen

The Catalytic Recombination of Dissociated Air

THE RECOMBINATION EFFICIENCY γ The catalytic reaction rate constant k_w defined by Equation [5] is not the constant usually chosen to measure a catalytic process. Most chemists rather use the recombination efficiency γ defined as the ratio of the number N_r of atoms recombining on a surface per unit area and time to the total number N of atoms striking the surface per unit area and time

$$\gamma = \frac{N_r}{N} \qquad \text{.....[33]}$$

The number N_r of atoms recombining upon hitting a unit surface per unit time is easily derived from the mass flux at the wall. For a first order process, Equation [5] yields

$$N_r = \frac{j_w}{m_A} = \frac{k_w c_A \rho}{m_A}$$

The total number N of atoms hitting a unit surface per unit time is easily calculated assuming a Maxwellian distribution ((23) Appendix B). In the form given by Langmuir (24)

$$N = \frac{p_A}{(2\pi m_A k T)^{1/2}}$$

where k is Boltzmann's constant. And since $p_A = n_A k T$ and $c_A \rho = n_A m_A$ the catalytic efficiency γ can be written

$$\gamma = \frac{N_r}{N} = \frac{k_w n_A (2\pi m_A k T)^{1/2}}{n_A k T} = k_w \left(\frac{2\pi m_A}{kT}\right)^{1/2} = k_w \left(\frac{2\pi M_A}{R_u T}\right)^{1/2} \qquad \text{.....[34]}$$

RECOMBINATION OF ATOMIC OXYGEN Linnet and Marsden (25) have studied the mechanism of recombination of atomic oxygen on various surfaces. They found that recombination on both glass surfaces and oxides was a first order process.

They further established some experimental values of the catalytic efficiency γ in a temperature range from 0 to 400 C. These values are illustrated on Fig. 6, as well as the additional values given by Linnett in Table 1 of (10) and the qualitative results of Reeves and Harteck (26). For convenient reading of heat transfer charts, lines of constant k_w have been calculated from Equation [34] and are also illustrated.

The catalytic efficiency of several tested materials is low

enough, in the range of temperatures considered, to keep $k_w < 10$. As can be seen from Figs. 4 and 5 such surfaces should allow a substantial reduction in heat transfer. This is especially the case for pyrex, for which Linnett's measurements can be represented[10] between 300 and 700 °K by

$$\gamma \simeq 4 \times 10^{-7} T \qquad (T \text{ in } ^\circ\text{K})$$

Other substances, such as the chlorides and oxides investigated by Linnett have a much stronger positive temperature dependence. Consequently a higher wall temperature, while reducing the temperature gradient and the conducted heat, will increase the recombination heat release at the wall. The possible consequences of these opposite effects on heat transfer instability have been recently discussed by Rosner in this Journal (15).

Also note the possibility of "poisoning" an otherwise catalytic surface with some of the low efficiency elements shown on Fig. 6. As pointed out by Wahlen (27), the adsorption process suggested by Linnett and Marsden would be very sensitive to such poisoning.

Recombination of Atomic Nitrogen The recombination of atomic nitrogen, on various metals in a wide range of temperatures, has been the object of a series of articles by Roginsky, Buben and Schlechter (28). Most metals tested (Pt, Cu, Fe, Ag) seem to be highly catalytic for atomic nitrogen in the whole range of temperature, while a temperature dependence is noted for nickel. Recently, the recombination efficiency of nitrogen on a clean pyrex surface has been measured by Wentink et al. (29), and a value of $\gamma = 3 \times 10^{-5}$ has been obtained. It is interesting to note that the same metals are highly catalytic for both atomic oxygen and nitrogen while pyrex is noncatalytic for both.

It should also be noted that all these measurements were made for partial pressures of atomic nitrogen appreciably smaller ($<10^{-3}$ atm) than for most flight conditions of interest (even at 250,000 ft, $u_\infty = 20{,}000$ ft/sec, partial pressure of nitrogen is 2.8×10^{-2} atm). Catalytic experiments at higher partial pressures are needed.

Recombination of Dissociated Air Although the catalytic recombination values discussed above for pure oxygen and nitrogen show the overall trend of the catalytic phenomena, additional complexity can be expected in the study of the recombination of a mixture of oxygen and nitrogen. As in the case of the gas phase recombination discussed in section 5, fast intermediate reactions between oxygen and nitrogen might very well accelerate the recombination and increase the "bulk" catalytic efficiency γ. No experimental result has been released in this area of research.

5 The Conditions of Existence of Frozen Flow

Recombination in the Boundary Layer

To determine whether atoms will recombine when diffusing across the boundary layer, it is useful to compare, after Fay and Riddell (2), the average time t_{diff} for an atom to diffuse to the wall and the average lifetime t_{chem} of this diffusing atom. A dimensionless Damköhler number can then be introduced

$$Dam = \frac{t_{diff}}{t_{chem}}$$

For large values of this number ($Dam \gg 1$), chemical reactions instantly adjust the diffusing particles to local thermodynamic equilibrium. For small values ($Dam \ll 1$), no recombination takes place before the diffusing atoms hit the wall. By expressing the Damköhler number in terms of flight conditions, it therefore becomes possible to determine the altitude and velocity range in which frozen flow and catalytic phenomena will prevail for a given vehicle.

To obtain this result, a simple formulation of t_{diff} and t_{chem} is required. The diffusion time t_{diff} is easily calculated from classical boundary layer theory. Unfortunately, no reliable expression of the chemical time is available, essentially because the chemical process of air recombination itself is presently not well understood.

As a first step, Fay and Riddell assumed a three-body recombination model

$$\text{atom} + \text{atom} + \text{particle} \rightarrow \text{molecule} + \text{particle}$$

with a recombination rate constant

$$k_r = 5 \times 10^{14} \left(\frac{T}{300}\right)^{-1.5} \qquad \text{cc}^2\,\text{mole}^{-2}\,\text{sec}^{-1} \ldots\ldots [35]$$

This basic assumption led to the definition of a "recombination rate parameter" C similar to the recombination Damköhler number.[11] Frozen flow can then be shown to exist at higher altitudes and lower velocities, as, for instance, in the case of a re-entry vehicle of nose diameter $d = 100$ cm, at 250,000 ft altitude.

Unfortunately, later experimental results indicated that faster air recombination rates occur at high temperatures (30, 31), and it was soon suggested (32) that fast intermediate reactions between nitrogen and oxygen were responsible for the observed high recombination rates. Finally, theoretical work (33,34) indicates the possibility, at low temperature, of recombination rates lower than the present experimental high temperature values. Considering this rather fluid state of information, there is little to be done at the present time to predict the expected range of existence of frozen flow with much accuracy.

Dissociation in the Shock Layer

Because of the interest of high altitudes for frozen flow, some of the problems of low density flight should be briefly examined.

As Adams and Probstein have recently shown (35), the boundary layer thickness at stagnation increases strongly with altitude ($\sim \rho_\infty^{-1/2}$), whereas the shock distance from the nose is a rather mild function of altitude ($\sim \rho_\infty^{-1/6}$). As a result, the inviscid shock layer will tend to disappear above an estimated ratio of the mean free path over the nose radius of 1/100, and in such case, the basic relations of this study should be reconsidered. At 250,000 ft, the mean free path is of the order of a few millimeters, and this problem may arise at this altitude in the case of small diameter noses.

On the other hand, although the shock thickness is still very small in the classical sense of translational collisions, large dissociation relaxation times may prevent the particles from being at thermal equilibrium when reaching the outer edge of the boundary layer. For this problem, we again have to deal with the yet unsolved subject of air chemical kinetics. In general, it can be expected, as shown by Camac et al. (36) in the case of pure oxygen, that low densities and velocities will cause dissociation lag (in Camac's experiments, the relaxation time is inversely proportional to the density ahead of the shock ρ_∞).

It is interesting to note, after Adams, that the same conditions which are favorable for frozen recombination (low

[10] It is to be noted that the temperature T used by Linnett is actually the temperature of the particles hitting the surface and not the surface temperature itself, which can be different at the very low pressure of his experiments. At the relatively higher recovery pressures in hypersonic flight (i.e., partial pressure of oxygen $= 7 \times 10^{-3}$ atm at 250,000 ft., 20,000 ft/sec) no temperature jump is expected at the wall and $T_w = T_{particles}$. We therefore assume implicitly in Fig. 6 that the energy of the particles is the governing factor in their catalytic recombination and not the energy of the wall fixed particles.

[11] C (Eq. [57] of (2)) is different from the Damköhler number, since it is based on flight and nose geometry conditions only and is not inclusive of wall conditions. For instance, a large increase in wall temperature and catalytic efficiency would accentuate the frozen character of the flow (lower Damköhler number) without affecting C.

density and velocity) are also those that promote frozen dissociation. Depending on the chemical constants involved, the atom concentration of the shock heated air, reaching a frozen boundary layer at stagnation, may well be only a fraction of its equilibrium value at that temperature. Consequently, only a fraction of the heat transfer reduction illustrated on Figs. 2 to 5 may actually be achieved by using noncatalytic walls, the rest of this energy being conducted to the wall by molecules which did not have time to dissociate. However, *such coupling is not necessarily rigid*, since shock dissociation is a high temperature process, whereas boundary layer recombination is a low temperature one, possibly much slower (33, 34).

Moreover, the stagnation area extends practically several shock distances from the geometric stagnation point. This situation multiplies the time available for complete stream dissociation by an appreciable factor. In some conditions, it will be possible, having a larger stream atom concentration away from the stagnation point, to accordingly reduce heat transfer by use of a noncatalytic surface. Such a remark is naturally only qualitative, since to drop the assumption c_e = const. introduces a nonsimilar boundary condition in the atom mass conservation equation; the similar solution presented in this paper does not apply to this case.

Acknowledgments

It is a pleasure to acknowledge the many constructive comments that were received from D. E. Rosner in preparing this paper for publication. The cooperation of the scientists of the Avco Research Laboratories, especially F. Riddell and S. Feldman, in discussing the many physical angles of this problem is also gratefully appreciated.

References

1 Lees, L., "Laminar Heat Transfer over Blunt Nosed Bodies at Hypersonic Flight Speeds." JET PROPULSION, vol. 26, April 1956, pp. 259–269.

2 Fay, J. A. and Riddell, F. R., "Theory of Stagnation Point Heat Transfer in Dissociated Air," *Journal of the Aeronautical Sciences*, vol. 25, Feb. 1958, pp. 73–85.

3 Probstein, R. F., "Methods of Calculating the Equilibrium Laminar Heat Transfer Rate at Hypersonic Flight Speeds," JET PROPULSION, vol. 26, June 1956, pp. 497–499.

4 Lewis, B., "Combustion Processes," Vol. II of the High Speed Aerodynamics and Jet Propulsion Series, Princeton University Press, 1956.

5 Chambré, P. L. and Acrivos, A., "On Chemical Surface Reactions in Laminar Boundary Layer Flows," *Journal of Applied Physics*, vol. 27, Nov. 1956, pp. 1322–1328.

6 Kemp, N. H. and Riddell, F. R., "Heat Transfer to Satellite Vehicles Reentering the Atmosphere," JET PROPULSION, vol. 27, Feb. 1957, pp. 132–137.

7 Emmett, T. H., "Catalysis," Reinhold, New York, 1954.

8 Scala, S. M., "Hypersonic Heat Transfer to Catalytic Surfaces," *Journal of the Aeronautical Sciences*, vol. 25, no. 4. April 1958, p. 273.

9 Rosner, D. E., "Boundary Conditions for the Flow of a Multicomponent Gas," JET PROPULSION, vol. 28, Aug. 1958, pp. 555–556.

10 Scala, S. M., "Hypersonic Heat Transfer to Surfaces Having Finite Catalytic Efficiency," General Electric Co. Aerophysics Research Memorandum no. 4, June 1957.

11 Fay, J. A., Riddell, F. R. and Kemp, N. H., "Stagnation Point Heat Transfer in Dissociated Air Flow," JET PROPULSION, vol. 27, June 1957, pp. 672–674.

12 Probstein, R. F., "Inviscid Flow in the Stagnation Point Region of Very Blunt-nosed Bodies at Hypersonic Flight Speeds," WADC TN 56–395, Astia no. AD 97273, Sept. 1956.

13 Li, T. Y., and Geiger, R. E., "Stagnation Point of a Blunt Body in Hypersonic Flow," *Journal of the Aeronautical Sciences*, vol. 24, Jan. 1957, pp. 25–32.

14 Bogdonoff, S. M. and Vas, I. E., "Preliminary Investigations of Spiked Bodies at Hypersonic Speeds," Princeton University, Dept. of Aeronautical Engineering, Report no. 412, March 1958.

15 Rosner, D. E., "Wall Temperature Instability for Convective Heating With Surface Radical Recombination," JET PROPULSION, vol. 28, no. 6, June 1958, p. 402.

16 "Transport Properties in Gases," *Proc. of the Second Biennal Gas Dynamics Symposium*, Aug. 26–28, 1957, Northwestern University Press, Evanston, Ill., 1958.

17 Hansen, C. F., "Approximations for the Thermodynamic and Transport Properties of High Temperature Air," NACA TN 4150, March 1958.

18 Hirschfelder, J. O., Curtiss, C. F. and Bird, R. B., "Molecular Theory of Gases and Liquids," John Wiley & Sons, New York, 1954.

19 Feldman, S., "Hypersonic Gas Dynamic Charts for Equilibrium Air," Avco Research Laboratory, Jan. 1957.

20 Hilsenrath, J. and Beckett, C. W., "Thermodynamic Properties of Argon Free Air to 15,000 °K," National Bureau of Standards, Report 3991, April 1955.

21 Hirschfelder, J. O., "Heat Transfer in Chemically Reacting Mixtures," *Journal of Chemical Physics*, vol. 26, Feb. 1957, pp. 274–281.

22 Lighthill, M. J., "Dynamics of Dissociating Gas—Part I, Equilibrium Flow," vol. 2, part I, Jan. 1957, pp. 1–32.

23 Goulard, R., "On Catalytic Recombination Rates in Hypersonic Stagnation Heat Transfer," ARS Preprint 544-57, Dec. 1957.

24 Langmuir, I., "Phenomena, Atoms and Molecules," Philosophical Library, New York, 1950.

25 Linnett, J. W., and Marsden, D. G. H., "The Kinetics of the Recombination of Oxygen Atoms at a Glass Surface" and "The Recombination of Oxygen Atoms at Salt and Oxide Surfaces," *Proc. of the Royal Society*, series A, vol. 234, March 1956, pp. 489–515.

26 Reeves, R. R., Jr. and Harteck, P., "Utilization of Energy Stored in the Upper Atmosphere," AFOSR TR 57-50, ASTIA no. AD 136-421, July 1957.

27 Wahlen, R. J., Aerophysics Section, Bell Aircraft Corp., Private Communication.

28 Roginsky, S., Buben, N. and Schlechter, A., "Chemische Reaktionen in electrischen Entladungen. Recombination von Stickstoffatomen am Metallen," *Acta Physicochimica USSR*, vol. 6, no. 3, 1937, pp. 401–418, (for Part III); vol 10, no. 3, 1939, pp. 371–378, (for Part IV).

29 Wentink, T., Sullivan, J. O. and Wray K. L., "Nitrogen Atomic Recombination at Room Temperature," Letter to the Editor, current issue of *Journal of Chemical Physics*.

30 Glick, H. S. and Wurster, W. H. "Shock Tube Study of Dissociation Relaxation in Oxygen," *The Journal of Chemical Physics*, vol. 27, no. 5, Nov. 1957, pp. 1224-1226.

31 Feldman, S., "The Chemical Kinetics of Air at High Temperatures. A Problem in Hypersonic Aerodynamics," Heat Transfer and Fluid Mechanics Institute, Stanford University Press, 1957.

32 Camac, M., Camm, J., Feldman, S., Keck, J. and Petty, C., "Chemical Relaxation in Air, Oxygen and Nitrogen," IAS Preprint no. 802, Jan. 1958.

33 Demetriades, S. T. and Farber, M., "A Theoretical Study of the Recombination Kinetics of Atomic Oxygen," Aerojet-General Corp., Technical Note 21, AFOSR TN 58-18, ASTIA no. AD148057, Nov. 1957.

34 Keck, J., "A Statistical Theory of Chemical Reaction Rates," Avco Research Laboratory, Research Report 20, April 1958.

35 Adams, Mac C. and Probstein, R. F., "On the Validity of Continuum Theory for Satellite and Hypersonic Flight Problems at High Altitudes," JET PROPULSION, vol. 28, no. 2, Feb. 1958, p. 86.

36 Camac, M., Camm, J. Keck, J. and Petty, C., "Relaxation Phenomena in Air Between 3000 and 8000°K," Avco Research Laboratory, Research Report 22, March 1958.

Technical Notes

Liquid Propellant Inertia and Damping Due to Airframe Roll

HERBERT REISMANN[1]

The Martin Company, Denver, Colo.

Nomenclature

v = fluid speed
r = radial coordinate
a = radius of fluid cylinder
t = time
ω = frequency
v_0 = fluid speed at surface of fluid cylinder (at $r = a$)
$\bar{\rho}$ = mass density of fluid
μ = viscosity
ν = $\frac{\mu}{\bar{\rho}}$, kinematic viscosity
ρ = $\sqrt{\frac{\omega}{\nu}}\, r$, dimensionless radial coordinate
λ = $\sqrt{\frac{\omega}{\nu}}\, a$, dimensionless radius of fluid cylinder
τ = fluid shearing stress
I = effective moment of inertia
k = damping coefficient
i = $\sqrt{-1}$

Introduction

BALLISTIC missiles which obtain their propulsive thrust from a liquid propellant engine are characterized by a high mass ratio; i.e., the weight of the liquid propellant represents a high percentage of the total take-off weight. If one considers the rolling characteristics of such a missile in conjunction with, say, the design of a roll stabilization and/or control system, the following question must be answered: What is the effective moment of inertia, and how much damping is provided by the fluid? It is intuitively obvious that not all of the fluid will participate in the rolling motion of the airframe, and that the fluid stresses set up by this motion will result in a damping force acting on the airframe. Thus it is the purpose of this note to answer the following questions: To what degree does the liquid propellant in a rolling missile participate in its motion; what is its effective moment of inertia, and how much damping does it provide?

Analysis

We chose as our mathematical model a smooth walled tank of circular cross section and unit depth. Because of the manner of excitation (roll), it is reasonable to expect the fluid to respond in circular motion about the center of the tank. Thus the motion of a fluid particle is a function of its radial coordinate and time only.

The motion of a viscous fluid is characterized by the Navier-Stokes equations (see, for instance, (1))[2]. Neglecting compressibility, and assuming the motion to be independent of the polar angle, the Navier-Stokes equations in polar coordinates reduce to the following single partial differential equation (in dimensionless form)

$$\frac{1}{\omega}\frac{\partial v}{\partial t} = \frac{\partial^2 v}{\partial \rho^2} + \frac{1}{\rho}\frac{\partial v}{\partial \rho} - \frac{v}{\rho^2} \quad \ldots\ldots [1]$$

where the fluid shear stress is given by

$$\tau = \mu\sqrt{\frac{\omega}{\nu}}\,\rho\,\frac{\partial}{\partial \rho}\left(\frac{v}{\rho}\right) \quad \ldots\ldots [2]$$

For harmonic excitation of the missile in roll, we assume a velocity distribution of the form

$$v(\rho, t) = F(\rho)\cos \omega t + G(\rho)\sin \omega t \quad \ldots\ldots [3]$$

Substituting Equation [3] into Equation [1] and equating coefficients of cos ωt and sin ωt, respectively, we obtain

$$\frac{d^2F}{d\rho^2} + \frac{1}{\rho}\frac{dF}{d\rho} - \frac{F}{\rho^2} = G$$
$$\frac{d^2G}{d\rho^2} + \frac{1}{\rho}\frac{dG}{d\rho} - \frac{G}{\rho^2} = -F \quad \ldots\ldots [4]$$

Equations [4] can be combined into a single linear differential equation by letting

$$\bar{W} = F + iG$$

We thus obtain

$$\frac{d^2\bar{W}}{d\rho^2} + \frac{1}{\rho}\frac{d\bar{W}}{d\rho} + \left(i - \frac{1}{\rho^2}\right)\bar{W} = 0 \quad \ldots\ldots [5]$$

Equation [5] is the well-known Bessel differential equation of the first order. Its solution is given by

$$\bar{W}(\rho) = i^{-1}\bar{A}I_1(\rho i^{-1/2}) + i\bar{B}K_1(\rho i^{-1/2}) \quad \ldots\ldots [6]$$

where $\bar{A}$, $\bar{B}$ are arbitrary constants of integration, and I_1 and K_1 are known as the modified Bessel functions of the first and second kind, respectively, of the first order. Since it is awkward to manipulate Bessel functions with complex arguments, we note the following definition (see (2))

$$i^{-1}I_1(\rho i^{-1/2}) = \mathrm{ber}_1\,\rho - i\,\mathrm{bei}_1\,\rho$$
$$iK_1(\rho i^{-1/2}) = \mathrm{ker}_1\,\rho - i\,\mathrm{kei}_1\,\rho \quad \ldots\ldots [7]$$

The defining series expansions for the functions ber_1, bei_1, ker_1 and kei_1 are given in (2).

Let

$$\bar{A} = \alpha + i\beta$$
$$\bar{B} = \gamma + i\delta$$

and substitute, together with the defining Equations [7] into Equation [6]. Thus we can separate the real and imaginary parts of the complex function $\bar{W}$ and obtain

$$F(\rho) = \alpha\,\mathrm{ber}_1\,\rho + \beta\,\mathrm{bei}_1\,\rho + \gamma\,\mathrm{ker}_1\,\rho + \delta\,\mathrm{kei}_1\,\rho$$
$$G(\rho) = \beta\,\mathrm{ber}_1\,\rho - \alpha\,\mathrm{bei}_1\,\rho + \delta\,\mathrm{ker}_1\,\rho - \gamma\,\mathrm{kei}_1\,\rho \quad \ldots\ldots [8]$$

At the fluid-airframe interface there is no relative motion between the fluid and the airframe; i.e., the fluid sticks to the airframe, and the velocity of the fluid at that point is equal to the airframe velocity. In addition, since the airframe is in a state of pure rotation, the fluid velocity at the missile roll axis must vanish. Thus if the airframe is excited harmonically, the fluid velocity function must satisfy the following conditions

$$v(\lambda, t) = v_0 \sin \omega t$$
$$v(o, t) = 0 \quad \ldots\ldots [9]$$

Received March 26, 1958.

[1] Systems Analysis Staff, Denver Division. Member ARS.

[2] Numbers in parentheses indicate References at end of paper.

EDITOR'S NOTE: The Technical Notes and Technical Comments sections of JET PROPULSION are open to short manuscripts describing new developments or offering comments on papers previously published. Such manuscripts are published without editorial review, usually within two months of the date of receipt. Requirements as to style are the same as for regular contributions (see masthead page).

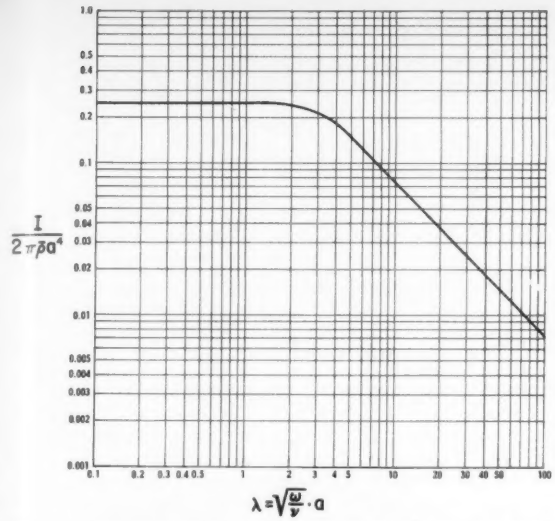

Fig. 1 **Dimensionless plot: Moment of inertia vs. frequency parameter**

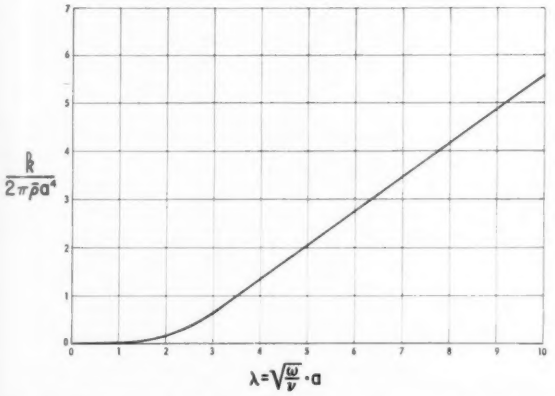

Fig. 2 **Dimensionless plot: Damping vs. frequency parameter**

Consequently, if we substitute Equation [8] into Equation [3] and impose condition [9] upon the result, we shall find that

$$\alpha = \frac{-v_o \, \mathrm{bei}_1 \lambda}{(\mathrm{ber}_1^2 \lambda + \mathrm{bei}_1^2 \lambda)}$$

$$\beta = \frac{v_o \, \mathrm{ber}_1 \lambda}{(\mathrm{ber}_1^2 \lambda + \mathrm{bei}_1^2 \lambda)}$$

$$\gamma = \delta = 0$$

and therefore

$$F(\rho) = \frac{v_o(\mathrm{ber}_1 \lambda \, \mathrm{bei}_1 \rho - \mathrm{bei}_1 \lambda \, \mathrm{ber}_1 \rho)}{(\mathrm{ber}_1^2 \lambda + \mathrm{bei}_1^2 \lambda)}$$

$$G(\rho) = \frac{v_o \, (\mathrm{ber}_1 \lambda \, \mathrm{ber}_1 \rho + \mathrm{bei}_1 \lambda \, \mathrm{bei}_1 \rho)}{(\mathrm{ber}_1^2 \lambda + \mathrm{bei}_1^2 \lambda)} \quad \ldots\ldots (10)$$

The torque exerted by the fluid upon the airframe is

$$\text{torque} = \begin{Bmatrix} 2\pi a^2 \tau(a) = 2\pi\omega\bar{\rho}a^3 \left[\frac{\partial}{\partial\rho}\left(\frac{v}{\rho}\right)\right]_{\rho=\lambda} \\ I\frac{v_o\omega}{a}\cos\omega t + \frac{kv_0}{a}\sin\omega t \end{Bmatrix} \quad \ldots\ldots [11]$$

where I is the effective moment of inertia of the fluid, and k represents the damping coefficient. Substituting Equation [3] together with Equation [10] into Equation [11] we obtain

$$\frac{Iv_o}{a} = 2\pi\bar{\rho}a^3\left[\frac{\partial}{\partial\rho}\left(\frac{F}{\rho}\right)\right]_{\rho=\lambda}$$

$$\frac{kv_o}{a} = 2\pi\omega\bar{\rho}a^3\left[\frac{\partial}{\partial\rho}\left(\frac{G}{\rho}\right)\right]_{\rho=\lambda}$$

$\ldots\ldots [12]$

and performing the required differentiations and substitutions in Equations [12] we obtain the results

$$\frac{I}{2\pi\bar{\rho}a^4} = \frac{(\mathrm{ber}_1 \lambda \, \mathrm{b\acute{e}i}_1 \lambda - \mathrm{bei}_1 \lambda \, \mathrm{b\acute{e}r}_1 \lambda)}{\lambda(\mathrm{ber}_1^2 \lambda + \mathrm{bei}_1^2 \lambda)} \quad \ldots\ldots [13]$$

$$\frac{k}{2\pi\mu a^2} = \frac{\lambda(\mathrm{ber}_1 \lambda \mathrm{b\acute{e}r}_1 \lambda + \mathrm{bei}_1 \lambda \, \mathrm{b\acute{e}i}_1 \lambda)}{(\mathrm{ber}_1^2 \lambda + \mathrm{bei}_1^2 \lambda)} - 1 \quad \ldots\ldots [14]$$

For sufficiently large values of λ we can replace the Bessel functions by their asymptotic approximations (see (2)). In this case formulae [13 and 14] reduce to

$$\frac{I}{2\pi\bar{\rho}a^4} = \frac{\sqrt{2}}{2}\frac{1}{\lambda} \quad \ldots\ldots [15]$$

$$\frac{k}{2\pi\mu a^2} = \frac{\sqrt{2}}{2}\lambda - 1 \approx \frac{\sqrt{2}}{2}\lambda \quad \ldots\ldots [16]$$

Conclusions

The degree of propellant participation in the rolling motion of the airframe is frequency dependent. Plots of Equations [13 and 14] are shown in Figs. 1 and 2, respectively. It is seen that the higher the frequency, the lower the effective propellant moment of inertia, whereas damping increases with rolling frequency. These remarks apply to relatively smooth tank walls. Appropriate adjustments in the application of this analysis must be made for tanks with wall protrusions.

The author wishes to thank J. C. Goodwyn, Chief, Systems Analysis Section, The Martin Company, Denver Division, for encouragement and permission to publish this note.

References

1 Lamb, Sir Horace, "Hydrodynamics," Dover Publication, New York, 6th ed., 1945.

2 Dwight, H. B., "Tables of Integrals and Other Mathematical Data," Macmillan Co., New York, Rev. ed., 1947.

Optical Determination of Orientation and Position Near a Planet[1]

ROBERT E. ROBERSON[2]

Autonetics Division of North American Aviation, Inc., Downey, Calif.

Introduction

THE visible horizon is the primary reference for establishing the vertical in marine navigation. It is natural to consider the analogous operation of establishing the direction to the center of a planet from a satellite or space ship by observation on the visible disk of the planet. This has, in fact, been proposed in astronautical literature (for example, in (1)[3]).

[1] Presented at the ARS Semi-Annual Meeting, Los Angeles, Calif., June 9–12, 1958.

[2] Chief, Astronautical Sciences. Member ARS.

[3] Numbers in parentheses indicate References at end of paper.

Exactly the same kind of device required to find the center of the disk would be expected to give the extent of the disk—its subtended angle—as well. Such a measurement has long been proposed (2) as a means of determining position, either relative to a close planet or to the sun.

The vertical, or direction to the planet's center, may be required for various reasons. In the case of a space vehicle approaching a planet and desiring to orbit or land, it is an important navigational orientation reference. It is important for the same reason in any ferry operation between the planet and an orbiting space station. For a satellite, the navigational problem may vanish, but the problem of a primary orientation reference system for instrumentation and communication then arises. In each case, the usefulness of the extent of the disk as a measure of position is clear.

The purpose of this note is to describe a rationale for determining orientation and position relative to a planet by observation of its disk. Specifically, the following measurement capability is assumed to exist aboard the vehicle. A physical device examines the intersection of the planet's face with the family of planes containing a reference axis on the vehicle—the latter forming an axis of rotation for an azimuthal mode of examination. In each plane, the angle can be measured between the reference axis and the edge of the disk.

Equations are developed which convert this measured angle into orientation and position information, at least in principle. They are derived purely on a geometric basis and are independent of the physical device used provided the subtended angle is available in each azimuth direction.

The present note is not concerned with the details of such a device, and thereby ignores some formidable practical problems. For example, if the edge of the disk is signaled by the albedo change between the planet and its space background, how is the case included where the planet has the appearance of a half-moon to the observer? It also leaves aside the problem of choosing a working spectrum for the device, which may be conceived to operate in the thermal, visible or even other portions of the electromagnetic radiation spectrum. Nevertheless, it is expected that the basic results developed here can be modified suitably to apply to cases where less information is present than we have assumed, but where advantage can be taken of some of the operating details of actual physical devices.

Nearly as important as the basic relationships used to infer orientation and position is the question of errors in the method. Some error sources are mentioned briefly. Most of these are stochastic; some depend on the particular mechanization used. One, however, is purely geometric and can be treated in detail, namely the planetary oblateness. It will be shown that this has a curious effect, leading to systematic errors in both orientation and position.

Basic Coordinate Systems

Choose axes x and y in the plane of the equator of the body to be observed and z along the polar axis so that xyz is a right-hand orthogonal system. Let the observer, i.e., the satellite or space ship, be situated at a radial distance ρ from the center of the body and at a geocentric latitude λ. Until the motion of the observer becomes a factor, there is no loss in generality in assuming that the observer is in the yz plane. Consider a set of reference axes $x'y'z'$ at the observer such that y' is along the outward-pointing geocentric radius, and x' is parallel to x. The geometry of the solution is shown in Fig. 1.

Two lines are of interest as seen from $x'y'z'$. One of these is the axis S_1 of the vehicle whose orientation, nominally vertical, it is desired to measure. The other is an arbitrary ray S_2 from the edge of the planet's disk to the observer. Let the former be characterized by angles α, β and the latter by θ, ψ as shown in Fig. 2.

The angle Ⓗ between S_1 and S_2 is the subtended angle seen relative to the vehicle's nominal vertical at the true azimuth

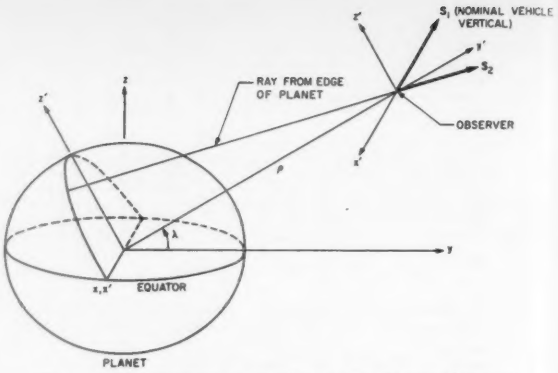

Fig. 1. The observer in relation to the observed planet

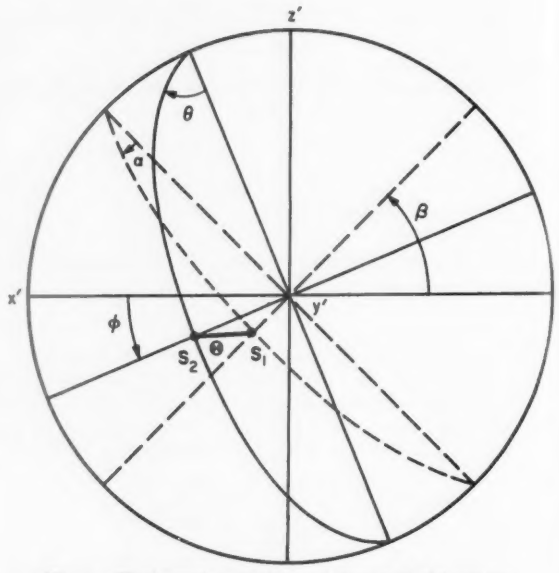

Fig. 2. Basic angle variables relative to $x'y'z'$ system

ϕ. It is not difficult to see that it is given by

$$\cos Ⓗ = \cos\theta\cos\alpha + \sin\theta\sin\alpha\cos(\phi - \beta) \quad [1]$$

If we suppose that the vehicle vertical has been established almost correctly so that α is a small angle, Ⓗ is approximately

$$Ⓗ = \theta - \alpha\cos(\phi - \beta) \quad [2]$$

It is not unreasonable to require that the axis of the sensing device be oriented approximately vertically—this is fairly easy to accomplish—so that attention can be confined here to the small α case.

Orientation and Position by Averaging

If the planet is a sphere with radius a, it is obvious that

$$\theta_0 = \arcsin(a/\rho) \quad [3]$$

should be used for θ in Equation [2].

Now Ⓗ given by Equation [2] is the output of a physical device, and is a function of the azimuth angle φ. Suppose that all values of φ can be examined rapidly enough that changes in α, β and vehicle position (although the latter is not important until an oblate planet is considered) are insignificant. Then the physical output Ⓗ can be operated on in various ways; specifically, it can be averaged with respect to φ in various ways. Suppose that the following quantities

can be formed by computation or filtering aboard the vehicle

$$\overline{\mathfrak{H}} = \left[\overset{\text{av}}{0 \leq \varphi \leq 2\pi}\right]\mathfrak{H}(\varphi) \qquad \mathfrak{H}_{23} = \left[\overset{\text{av}}{\pi/2 \leq \varphi \leq 3\pi/2}\right]\mathfrak{H}(\varphi)$$

$$\mathfrak{H}_{12} = \left[\overset{\text{av}}{0 \leq \varphi \leq \pi}\right]\mathfrak{H}(\varphi) \qquad \mathfrak{H}_{41} = \left[\overset{\text{av}}{3\pi/2 \leq \varphi \leq \pi/2}\right]\mathfrak{H}(\varphi)$$

$$\mathfrak{H}_{34} = [\pi \leq \varphi \leq 2\pi]\mathfrak{H}(\varphi) \qquad \ldots\ldots\ldots\ldots\ldots\ldots\ldots\ldots [4]$$

(The subscripts in the last four cases represent quadrants of φ values.)

Performing this averaging in Equation [2] and using Equation [3], it is easy to show that

$$a/\rho = \sin \overline{\mathfrak{H}} \ldots\ldots\ldots\ldots\ldots\ldots [5]$$

$$\alpha \sin \beta = \frac{\pi}{4}(\mathfrak{H}_{34} - \mathfrak{H}_{12})$$

$$\alpha \cos \beta = \frac{\pi}{4}(\mathfrak{H}_{23} - \mathfrak{H}_{41})$$

$$\ldots\ldots\ldots\ldots\ldots\ldots [6]$$

The distance ρ from the center of the planet to the observer is given directly by Equation [5], so $\overline{\mathfrak{H}}$ is a measure of relative position. For small α, the quantity $\alpha \sin \beta$ is just the angle of rotation of S_1 about the $-x'$ axis, and $\alpha \cos \beta$ about the $-z'$ axis, so that the two quantities are a measure of the angular misorientation of S_1 relative to the y' axis.

It is important to note in this connection that one really may desire these misorientation angles about body-fixed horizontal axes rather than x' and z', for if attitude control is desired the corrective action would take place about body-fixed axes. It can be shown, though, that this distinction does not vitiate the present results if the body-fixed horizontal axes are rotating about S_1 slowly relative to the speed at which the averaging over φ is accomplished. Although not crucial in the simple picture presented here, the distinction is nevertheless of genuine interest and will be treated elsewhere.

Errors in the Method

There are several obvious sources of error in the method described above. One is the instrument noise, depending on the details of the physical device observing the planet. It may be stochastic, or it may have systematic components, such as would be the case if it habitually triggered too early or too late in passing from regions of high to low albedo or vice versa. This source would also encompass imperfections in the averaging process leading to Equation [4].

Another potential source of error is attitude or radial motion of the vehicle while φ ranges over the values $[0, 2\pi]$. Its importance depends on both the instrument design which determines the φ-frequency and on the attitude and translational vehicle velocities. Unfortunately, it may not be able to make the effects arbitrarily small by increasing φ-frequency, because the sensitivity and some instrument errors may change adversely with increasing frequency. This source may be troublesome if one is trying to infer rates of change of radius or attitude with the present method.

Finally there is a class of errors which arise from the geometry of the planet's disk and the physics of its atmosphere. It is clear that the edge of the disk will have a location error in the presence of clouds or mountains, at least in the visible spectrum. Atmospheric refraction and scattering also may be troublesome. One error of this class is particularly interesting, that from any oblateness of the planet. It has systematic, pernicious components. These effects of oblateness are the concern of the remainder of the paper.

Oblateness Effects

In terms of the coordinate system xyz introduced previously, suppose that the body to be observed has the equation

$$(1 - \epsilon^2)(x^2 + y^2 - a^2) + z^2 = 0 \ldots\ldots\ldots [7]$$

where a is the equatorial radius, and $\epsilon^2 = 1 -$ (polar radius)$^2/a^2$. That is, it is an oblate spheroid with polar axis z and eccentricity ϵ. (Note that this is not ellipticity.) Using the transformation between xyz and $x'y'z'$ coordinates implied by the previous definitions, the equation of the ellipsoid as seen from the $x'y'z'$ system has the equation

$$(1 - \epsilon^2)(x'^2 - a^2) + (1 - \epsilon^2 \cos^2 \lambda)(y' + \rho)^2 + 2\epsilon^2 \sin \lambda \cos \lambda z'(y' + \rho) + (1 - \epsilon^2 \sin^2 \lambda)z'^2 = 0 \ldots\ldots\ldots [8]$$

Now if r represents distance from the $-y'$ axis in any plane defined by $\varphi = \text{const}$ (see Fig. 1), $x' = r \cos \varphi$, and $z' = -r \sin \varphi$. Therefore, the cross section of the ellipse in this plane has the equation

$$[1 - \epsilon^2(1 - \cos^2 \lambda \sin^2 \varphi)]r^2 - 2\epsilon^2 \sin \lambda \cos \lambda \sin \varphi r(y' + \rho) + (1 - \epsilon^2 \cos^2 \lambda)(y' + \rho)^2 = (1 - \epsilon^2)a^2 \ldots\ldots\ldots [9]'$$

At the same time, θ is defined as the angle between the $-y$ axis and the ray $r = -y' \tan \theta$ which is just tangent to the ellipse given by Equation [9].

A straightforward way to find θ is to substitute $r = -y' \tan \theta$ into [9], and then to require that the resulting quadratic in y' have only a single root. In this way, θ is found to satisfy

$$A \tan^2 \theta + 2\beta \tan \theta + C = 0 \ldots\ldots\ldots [10]$$

where

$$A = \left[1 - \frac{a^2}{\rho^2} + \epsilon^2\left(\frac{a^2}{\rho^2} - \cos^2 \lambda\right)\right]\left[1 - \epsilon^2(1 - \cos^2 \lambda \sin^2 \varphi)\right] - \epsilon^4 \sin^2 \lambda \cos^2 \lambda \sin^2 \varphi \ldots\ldots\ldots [11]$$

$$B = -\epsilon^2(1 - \epsilon^2)\frac{a^2}{\rho^2} \sin \lambda \cos \lambda \sin \varphi \ldots\ldots [12]$$

$$C = -(1 - \epsilon^2)\frac{a^2}{\rho^2}(1 - \epsilon^2 \cos^2 \lambda) \ldots\ldots\ldots [13]$$

We confine ourself to the case where ϵ^2 is small enough that ϵ^4 and higher order terms can be discarded. In this case, the solution [10] takes the form

$$\tan \theta = \pm \frac{a}{\sqrt{\rho^2 - a^2}} \mp \frac{a\epsilon^2}{2\sqrt{\rho^2 - a^2}}\left(\cos \lambda \sin \varphi \mp \frac{a}{\sqrt{\rho^2 - a^2}} \sin \lambda\right)^2 \ldots\ldots\ldots [14]$$

The upper algebraic sign must be chosen if θ is to remain a positive vertex semi-angle, the physical equivalent of the opposite sign being realized for $\varphi + \pi$. Using Equation [3] for θ_0, and continuing the same order of approximation in ϵ^2, Equation [14] gives

$$\theta = \theta_0 + \delta\theta \ldots\ldots\ldots [15]$$

where

$$\delta\theta = -\frac{\epsilon^2 a\sqrt{\rho^2 - a^2}}{2\rho^2}\left(\cos\lambda\sin\varphi - \frac{a}{\sqrt{\rho^2 - a^2}}\sin\lambda\right)^2 \quad \ldots [16]$$

Using Equation [16] for the oblateness error and performing the averaging of Equation [4], we obtain

$$\delta\overline{\mathfrak{y}} = -\frac{\epsilon^2 a\sqrt{\rho^2 - a^2}}{2\rho^2}\left(\frac{1}{2}\cos^2\lambda + \frac{a^2}{\rho^2 - a^2}\sin^2\lambda\right) \quad \ldots [17]$$

$$\delta\overline{\mathfrak{H}}_{12} = -\frac{\epsilon^2 a\sqrt{\rho^2 - a^2}}{2\rho^2}\left(\frac{1}{2}\cos^2\lambda - \frac{2a\sin\lambda\cos\lambda}{\pi\sqrt{\rho^2 - a^2}} + \frac{a^2}{\rho^2 - a^2}\sin^2\lambda\right)$$

$$\delta\overline{\mathfrak{H}}_{34} = -\frac{\epsilon^2 a\sqrt{\rho^2 - a^2}}{2\rho^2}\left(\frac{1}{2}\cos^2\lambda + \frac{2a\sin\lambda\cos\lambda}{\pi\sqrt{\rho^2 - a^2}} + \frac{a^2}{\rho^2 - a^2}\sin^2\lambda\right)$$

$$\delta\overline{\mathfrak{K}}_{23} = \delta\overline{\mathfrak{K}}_{14} = \delta\overline{\mathfrak{K}} \quad \ldots [18]$$

From Equation [5], $\delta\rho/\rho = -\sqrt{\rho^2 - a^2}\,\delta\overline{\mathfrak{K}}/a$, whence the position error arising from oblateness is

$$\frac{\delta\rho}{\rho} = \frac{\epsilon^2 a^2}{2\rho^2}\left[1 + \left(\frac{\rho^2 - 3a^2}{2a^2}\right)\cos^2\lambda\right] \quad \ldots [19]$$

From [6 and 18]

$$\delta(\alpha\sin\beta) = -\frac{\epsilon^2 a^2}{2\rho^2}\sin\lambda\cos\lambda \quad \ldots [20]$$

$$\delta(\alpha\cos\beta) = 0 \quad \ldots [21]$$

These results are easily interpreted. Equation [21] shows that there is no angular error about the z' axis from oblateness, as would be expected from symmetry considerations. Equation [20] shows that there is, however, an error about the x' (east to west) axis. It is positive about x' when the observer is in the northern hemisphere, negative in the southern hemisphere. Thus if $\alpha\sin\beta$ obtained from [6] were further averaged over an entire orbital revolution, this latter error would vanish in the average. The technique would not necessarily work for a nonorbiting vehicle, of course. On the other hand, the error in radial distance given by Equation [19] is an essential one, and cannot be removed by orbital averaging.

To give some idea of the magnitudes of these errors, consider observations on the Earth from a distance $\rho = \sqrt{3}\,a \approx$ 11,000 km and a latitude 45 deg N. We have $\delta\rho \approx 12$ km and $\delta(\alpha\sin\beta) \approx 0.547\,mr \approx 2'$. This angular error is a maximum with respect to λ and decreases with increasing ρ/a. One can ascertain from Equation [19] by properly grouping terms, that the relative error $\delta\rho/\rho$ is positive for all ρ and λ; also, that $\delta\rho/\rho \to (\epsilon^2\cos^2\lambda/4)$ as $\rho/a \to \infty$.

References

1 Stroud, W. G. and Nordberg, W., "Meteorological Measurements from a Satellite Vehicle," in "Scientific Uses of Earth Satellites," ed. J. A. van Allen, Univ. of Michigan Press, Ann Arbor, 1956, pp. 119–132.

2 Esnault, R. "Pelterie, L'Astronatique Complement," Paris, 1935, p. 87.

Motion of a Satellite With Friction

LEIF N. PERSEN[1]

Norwegian Institute of Technology, Trondheim, Norway

IN THE following, two examples of a satellite's motion under the action of frictional forces will be presented. They are taken from the author's lectures on applied mechanics and may be of interest because they show simple, exact solutions to apparently very difficult equations.

Received March 5, 1958.

[1] Associate Professor, Department of Applied Mechanics.

By the plane motion of a mass point the accelerations a_r and a_φ in the r- and φ-directions, respectively, are given by

$$a_r = \ddot{r} - r\omega^2 \quad \ldots [1]$$

$$a_\varphi = \frac{1}{r}\frac{d}{dt}(r^2\omega) \quad \ldots [2]$$

If the origin of the coordinate system is placed in the mass center of the Earth, the satellite will move under the action of a force P, acting in the direction toward the origin, of the magnitude

$$P = m\frac{\lambda}{r^2} \quad \ldots [3]$$

where m is the mass of the satellite. The equations of motion may now be written

$$\ddot{r} - r\omega^2 = -\frac{\lambda}{r^2} - F \quad \ldots [4]$$

$$\frac{1}{r}\frac{d}{dt}(r^2\omega) = -G \quad \ldots [5]$$

where F and G are the components of the frictional force in the r- and φ-directions, respectively. By neglecting friction these equations represent the equations of motion of planets and give ellipses, parabolas and hyperbolas as only possible orbits.

It is at present very difficult to give any reliable expression for the frictional forces resulting from the motion of a satellite; one has to make more or less reliable assumptions. If we suppose the friction to be caused by some sort of gas with very low density, it seems justifiable to assume the frictional force to be proportional to some power of the satellite's velocity, and also to assume the density of the gas to be decreasing with increasing distance from the origin. Two different assumptions for the frictional force made in accordance with this general point of view will now be treated, and exact solutions of Equations [4 and 5] will be established.

Case 1

It is assumed that the frictional force is proportional to the second power of the satellite's velocity and decreases as $1/r$ as r increases. In this way the variation of the density is taken into account to some extent. Equations [4 and 5] may then be written

$$\ddot{r} - r\omega^2 = -\frac{\lambda}{r^2} - k\frac{\dot{r}^2}{r} \quad \ldots [6]$$

$$\frac{1}{r}\frac{d}{dt}(r^2\omega) = -k\frac{r^2\omega^2}{r} \quad \ldots [7]$$

where k is a dimensionless "coefficient of friction." In those cases where the orbit of the satellite is close to a circle, F may be assumed to be negligible in comparison with G, without introducing an error of any importance. The last term in Equation [6] may thus be neglected. Remembering that

$$\frac{d}{dt} = \omega\frac{d}{d\varphi} \quad \ldots [8]$$

Equation [7] may be solved by simple integration rendering

$$r^2\omega = C_1 e^{-k\varphi} \quad \ldots [9]$$

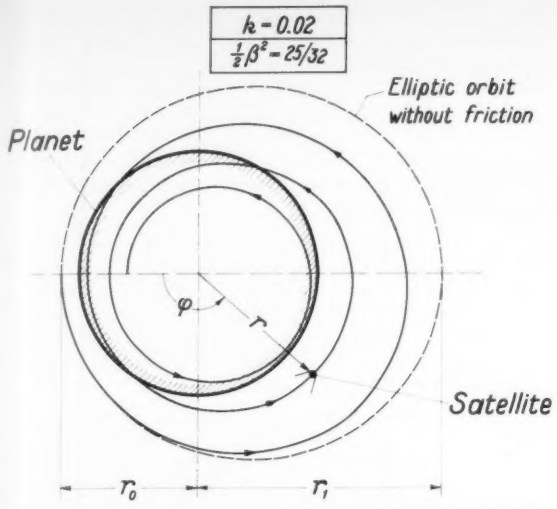

Fig. 1 Satellite orbit in case 1 with an unrealistically great value of k

where C_1 is a constant of integration. The time t is now replaced by φ as the independent variable of Equation [6] by means of the following expressions

$$\frac{d^2}{dt^2} = \omega^2 \frac{d^2}{d\varphi^2} + \epsilon \frac{d}{d\varphi} \qquad \epsilon = -\frac{1}{r}\left(kr\omega^2 + 2\omega^2 \frac{dr}{d\varphi}\right)$$

where the last expression is obtained from Equation [9]. In this way Equation [6] takes the form

$$\frac{d^2r}{d\varphi^2} - \frac{2}{r}\left(\frac{dr}{d\varphi}\right)^2 - k\frac{dr}{d\varphi} - r + \frac{\lambda}{C_1^2} r^2 e^{+2k\varphi} = 0 \quad \ldots [10]$$

This is a nonlinear differential equation with variable coefficients, which, however, may easily be transformed into the following linear equation

$$\frac{d^2\xi}{d\varphi^2} - k\frac{d\xi}{d\varphi} + \xi = \frac{\lambda}{C_1^2} e^{+2k\varphi} \quad \ldots [11]$$

with the solution

$$\xi = \frac{1}{r} = e^{\frac{k}{2}\varphi}\left[C_2 \sin\left(\varphi\sqrt{1 - \frac{k^2}{4}}\right) + C_3 \cos\left(\varphi\sqrt{1 - \frac{k^2}{4}}\right)\right] + \frac{\lambda e^{+2k\varphi}}{C_1^2(1 + 2k^2)} \quad \ldots [12]$$

where C_2 and C_3 are constants of integration to be determined by the initial conditions. Assuming these to be

$$r = r_0 \qquad \dot{r} = 0 \qquad \varphi = 0 \qquad \dot{\varphi} = \frac{v_0}{r}$$

and introducing the following numerical values

$$v_0^2 = \frac{16}{25}\frac{2gR^2}{r_0} \qquad \lambda = gR^2 \qquad k = 0.02$$

where R = radius of the Earth, the orbit of the satellite has been calculated and is shown in Fig. 1. The value of k is chosen unrealistically great to make the characteristic features of the curve come out more distinctly.

Case 2

The assumptions made in the first case are not satisfactory, because F has been neglected, and furthermore the variation of the density seems to be too small. If the motion of the satellite is regarded as the motion of a body in a gas with very low density, a Reynolds number may be written

$$Re = \frac{\rho v d}{\mu}$$

which, in spite of a very high velocity v, may be assumed to be small because of the extremely low value of ρ. This makes it tempting to assume the frictional force to be directly proportional to the velocity; and if, in addition, the variation of density is taken into account by assuming F and G decreasing with the second power of r, Equations [4 and 5] may be written

$$\ddot{r} - r\omega^2 = -\frac{\lambda}{r^2} - c\frac{\dot{r}}{r^2} \quad \ldots [13]$$

$$\frac{1}{r}\frac{d}{dt}(r^2\omega) = -c\frac{r\omega}{r^2} \quad \ldots [14]$$

where c may be regarded as a dimensional coefficient of friction. These equations may be solved in exactly the same way as those of the first case. By means of Equation [8] the solution of Equation [14] is found to be

$$r^2\omega = C_1 - c\varphi \quad \ldots [15]$$

from which the following relation may be derived

$$\epsilon = -\frac{1}{r^2}\left(c\omega + 2r\omega^2 \frac{dr}{d\varphi}\right)$$

With this expression for ϵ Equation [13] may be transformed into

$$\frac{d^2r}{d\varphi^2} - \frac{2}{r}\left(\frac{dr}{d\varphi}\right)^2 - r + \frac{\lambda r^2}{(C_1 - c\varphi)^2} = 0 \quad \ldots [16]$$

where the same procedure as that in the first case has been used. Introduction of $\xi = 1/r$ will further transform this equation into

$$\frac{d^2\xi}{d\varphi^2} + \xi = \frac{\lambda}{(C_1 - c\varphi)^2} \quad \ldots [17]$$

the solution of which is easily found to be

$$\xi = C_2 \sin\eta + C_3 \cos\eta - \frac{\lambda}{c^2}\left[\cos\eta\, Ci(\eta) + \sin\eta\, si(\eta)\right] \quad \ldots [18]$$

where Ci and si denote the cosine and sine integrals, respectively, and $\eta = (C_1/c - \varphi)$. The constants of integration C_1, C_2 and C_3 are now determined by the initial conditions of the first case. Furthermore the new nondimensional coefficient of friction κ defined by

$$c = \frac{1}{\kappa} v_0 r_0$$

and the abbreviation $\beta^2 = 2gR^2/v_0^2 r_0$ are introduced, whereupon the equation of the orbit may be written

$$\frac{r_0}{r} = \cos\varphi - \frac{1}{2}\kappa\beta^2 \sin\varphi + \frac{1}{2}\kappa^2\beta^2\left\{\left[Ci(\kappa) - Ci(\kappa - \varphi)\right]\cos(\kappa - \varphi) + \left[si(\kappa) - si(\kappa - \varphi)\right]\sin(\kappa - \varphi)\right\} \quad \ldots [19]$$

Also, in this case the orbits turn out to be elliptical spirals. Examples for different values of β and κ are given in Figs. 2 and 3.

It may be worth noticing that for the same initial value of the frictional force, the spirals of the two cases (Fig. 3) are not distinguishable in the scale to which the figure is drawn. Furthermore, it may be mentioned that the second case permits an easy determination of the number of revolutions

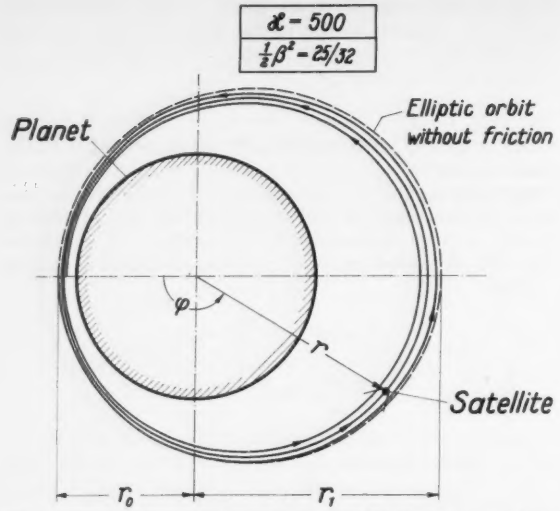

Fig. 2 Satellite's orbit in case 2. Height loss in percentage greatest in perigee

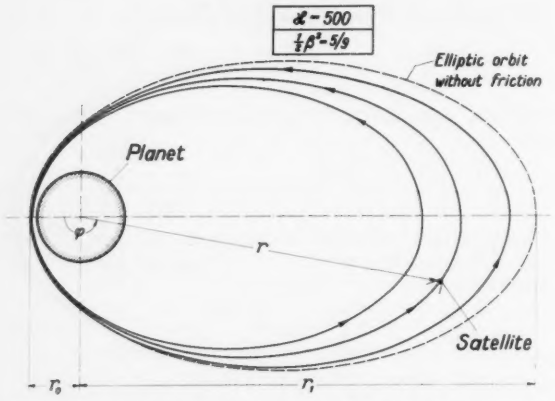

Fig. 3 Satellite's orbit in case 2. Height loss in percentage greatest in apogee

which the satellite will perform before reaching the origin. Once κ is known, this number is $\kappa/2\pi$.

It would have been interesting if these easy calculations had permitted a somewhat sensible determination of the lifetime of Sputnik I. From Equation [15] the following expression for the period is found

$$\tau = \int_0^{2\pi} \frac{r^2 d\varphi}{(C_1 - c\varphi)} \quad \ldots\ldots [20]$$

where $r = r(\varphi)$ has to be inserted from Equation [19]. Replacing c by $c = c_1 v_0 r_0$ will make τ a function of c_1, where c_1 is very small, and τ may be expanded into a power series in c_1

$$\tau = \tau_0 + \frac{\partial \tau}{\partial c_1}\bigg|_0 \cdot \frac{c_1}{1!} + \ldots .$$

where τ_0 denotes the period with no friction. This will give the following expression for the time-lag

$$\frac{\tau - \tau_0}{\tau_0} = \frac{\Delta\tau}{\tau_0} = \frac{c_1}{\tau_0}\frac{\partial \tau}{\partial c_1}\bigg|_0 \quad \ldots\ldots [21]$$

Using the data for Sputnik I,[2] this time-lag is $\Delta\tau/\tau_0 = 0.146666/5760$. The coefficient β may be calculated, giving $\beta^2 = 1.89888$ which further leads to

$$\frac{\partial \tau}{\partial c_1}\bigg|_0 = 14.079$$

whereupon $\kappa = 1/c_1 = 552{,}900$ is obtained from Equation [21]. The values of κ used for plotting the spirals in the diagrams shown are extremely small compared to this value. The given value of κ leads to 8800 revolutions before Sputnik I has reached the center of the Earth, but this is of no importance in connection with the lifetime of the satellite. Because of the extremely high value of κ, the *Ci*- and *si*-functions may be replaced by the asymptotic expansions, whereupon Equation [19] takes the form

$$\frac{r_0}{r} = \left(1 - \frac{1}{2}\beta^2\right)\cos\varphi - \frac{\beta^2}{\kappa}\sin\varphi + \frac{1}{2}\beta^2\left(1 - \frac{\varphi}{\kappa}\right)^{-2} \quad \ldots [22]$$

For $\varphi = 2n\pi$ (n = integer)

$$\frac{r_0}{r} = \left(1 - \frac{1}{2}\beta^2\right) + \frac{1}{2}\beta^2\left(1 - \frac{2n\pi}{\kappa}\right)^{-2} \quad \ldots\ldots [23]$$

this equation makes it possible to calculate r after n revolutions, or it may be used to obtain an approximate value for the number of revolutions after which r will have a given value. When the satellite starts to dive into the atmosphere, the present calculations cease to be valid, but from then on it is only a question of a few days until a satellite without any decelerating devices will burn out. Counting the lifetime of Sputnik I to the time when it starts diving into the atmosphere, and putting the thickness of the atmosphere at 50 km, Equation [23] gives $n = 1040$ and a "lifetime" $T_{50} = 70$ days. With an atmospheric thickness of 28 km, n becomes 1200, and the lifetime $T_{28} = 80$ days. If these calculations are realistic, one may expect that Sputnik I dived into the atmosphere and burnt out shortly after the period Dec. 29, 1957 to Jan. 8, 1958.

[2] "Radio Observations of the Russian Satellite," *Nature*, vol. 2, Nov. 1957, pp. 879–883.

On the Optimization of Physical Propulsion Systems[1]

ROBERT R. NEWTON[2]

The Johns Hopkins University, Silver Spring, Md.

Introduction

IN A rocket with chemical propulsion, the fuel performs two quite distinct functions: It supplies the mass which carries the momentum of the jet, and at the same time it supplies the kinetic energy which is involved in giving this momentum to the jet. For a single stage with a final mass of unity, initial mass M and an exhaust velocity c, the velocity in the absence of external forces is

$$v = c \ln M \quad \ldots\ldots [1]$$

In all experience to date, it has been desirable to make c as large as possible, in order to make M as small as possible. This situation arises because obtaining the values of M needed is the most serious problem in design, whereas the energy content of the fuel, so to speak, is free.

By a physical propulsion system for a rocket, we mean a system in which the functions of supplying mass and energy are separated, and are performed by different components of the system. In such systems, we are no longer necessarily limited to values of c of the order of 10^4 ft/sec, so that obtaining the values of M needed to achieve a high velocity may no longer be a serious problem. Instead, the limitation may be in either the power or the total energy which can be delivered by the source of energy.

These considerations suggest the following problem: If c is

Received May 7, 1958.

[1] This work was supported by the Bureau of Ordnance, Department of the Navy, Contract NOrd 7386.

[2] Physicist, Research Center, Applied Physics Laboratory. Member ARS.

regarded as a completely free parameter, is there any choice of c which leads to minimum energy or power, for a fixed value of v? We shall analyze this problem briefly in two special cases, first with no external force and second with a constant gravitational field. The analysis also applies, of course, to chemical rockets, if we regard either energy content or delivered power as more important than the mass of fuel.

Optimization With No External Forces

In this case, Equation [1] gives the final velocity, regardless of the thrust or power level at which the motor operates. We are therefore concerned only with minimizing the total energy demanded of the energy source. The energy source, carried on the rigid framework of the rocket, must give to the exhaust, of mass $M - 1$, the velocity c relative to that framework. The energy demand W is therefore equal to the kinetic energy of the exhaust relative to the rocket, and is

$$W = \tfrac{1}{2}(M - 1)c^2 \quad [2]$$

Substituting for c from Equation [1]

$$W = \tfrac{1}{2}v^2[(M - 1)/(\ln M)^2] \quad [3]$$

We wish to minimize W, for fixed v, which means minimizing the quantity in brackets.

Before doing this, we remark that the useful accomplishment of the rocket is to give unit mass a velocity v in a "fixed" coordinate system. It is therefore proper to define the energy output as $\frac{1}{2}v^2$, and to define the efficiency as

$$E = (\tfrac{1}{2}v^2)/W = (\ln M)^2/(M - 1) \quad [4]$$

The efficiency is zero when $M = 1$ and ∞; in the interval $(0, \infty)$, E has a single maximum, at

$$M_{opt} = 4.9214 \quad [5]$$

From this, we find

$$c_{opt} = 0.62751v \qquad E_{max} = 0.6476 \quad [6]$$

This case approximates the launching of an escape vehicle from a satellite. For this application, v is about 10^4 ft/sec, so the optimum exhaust velocity is about 6300 ft/sec.

In this analysis, the energy source is counted as part of the payload, and the kinetic energy given it as part of the useful output. In a more careful analysis, one would probably modify accordingly the definition of the output energy, but to do so would require knowing the relation between the mass and available energy of the energy source. Studying this relation is outside the scope of this note.

Optimization in a Gravity Field

If the rocket is required to achieve the velocity v while climbing vertically against gravity, the velocity is now given by

$$v = c \ln M - gt \quad [7]$$

Clearly, the maximum efficiency is achieved with $t = 0$; Equation [7] is then the same as Equation [1], and the earlier analysis applies, if maximum efficiency is the criterion of optimization.

However, achieving maximum efficiency in this case involves operation at an infinite power level. It is clearly of interest to investigate, instead, minimizing the power demand on the energy source. The power demand is

$$P = \tfrac{1}{2}\dot{m}c^2 = \tfrac{1}{2}Tc \quad [8]$$

where T is the thrust, and $\dot{m}$ is the mass flow rate. Assuming that P, T and c are constant, the minimum allowable value of T is Mg, since the rocket must be able to lift its initial weight. Combining Equations [7 and 8] with $T = Mg$, and using the fact that $t = (M - 1)/\dot{m} = (M - 1)c^2/2P$, we find that c must be a solution of the quadratic

$$[g(M - 1)/2P]c^2 - c \ln M + v = 0 \quad [9]$$

The discriminant of this quadratic gives the condition that

$$P(\ln M)^2/(M - 1) \geq 2gv \quad [10]$$

Since $2gv$ is fixed for a given application, the minimum value of P occurs when the equality holds, and also when $(\ln M)^2/(M - 1)$ is a maximum. So, again, we have the optimum value of M to be 4.9214. Other quantities of interest are

$$c = 1.2550v \qquad \dot{m} = 3.9214(g/v)$$
$$t = (v/g) \qquad P = 3.0883gv \quad [11]$$

In units of horsepower per lb, using the sea level value of g, the minimum power is

$$P = 0.005615v$$

For $v = 25{,}000$ ft/sec, this is 140.4 hp per lb of the final weight.

The value of t shows that the gravity loss equals the final velocity. Further, the value of c is just twice the value which gives maximum efficiency, so that the efficiency is only one fourth of the maximum or about 16.2 per cent. The distance of powered flight is

$$s = 0.24499v^2/g$$

For v as before, $c = 31{,}375$ ft/sec; $t = 776$ sec, and $s = 4.7552 \times 10^6$ ft, about 900 miles.

Summary and Comments

Regarding the exhaust velocity c as a free parameter, we have found the values of c which give maximum efficiency and those which require minimum power in climbing against gravity, for single-stage motors. We have found that the mass ratio should be 4.9214 for all cases considered, and that c should be proportional to the desired velocity. The value of c for the minimum power when climbing is twice the value for maximum efficiency, and the efficiency is one fourth of the maximum.

In launching a satellite, the minimum power is about 140 hp per lb, and the corresponding c is about 31,400 ft/sec. In launching an escape vehicle from a satellite, the optimum c is about 6300 ft/sec, and the minimum power is quite low (zero to the accuracy of the present treatment). Thus, we have an ironic situation: The only energy sources which, to date, can deliver the necessary power for launching a satellite are chemical, and they have c values far from optimum. However, for an escape vehicle, where power is not a limitation, chemical sources have about the optimum parameters.

One cannot conclude from this that chemical rockets should be used for an escape vehicle, because there are important considerations other than maximum efficiency. However, since chemical rockets do operate at about the maximum possible efficiency for this application, they need to be considered.

Measurement of Satellite Erosion Rates by the Backscattering of Beta-Rays

R. C. GOETTELMAN[1]

Stanford Research Institute, Menlo Park, Calif.

A sensitive method of measuring thickness changes, using beta-ray backscattering phenomena, is described. Experimental data and theory are used to show that the backscattering method is capable of detection of thickness changes characteristic of anticipated satellite erosion rates. The method is especially attractive since it does not physically alter the "skin" material surface, and therefore

Received May 7, 1958.

[1] Physicist, Atmospheric Chemical Physics Section.

should be representative of the actual satellite erosion rate. A null circuit is proposed which eliminates counting errors due to cosmic activity and provides a maximum sensitivity which responds to a 0.009-mil change in aluminum target thickness.

Introduction

ACCURATE measurement of surface erosion on orbiting vehicles is important for many reasons. In addition to its scientific value in adding knowledge about the universe, it has many practical applications.

Absorptivity and emissivity are directly dependent on the surface condition of a metal. The control of temperature within an instrumented or inhabited satellite or space ship is completely dependent on radiation losses and gains. Thus, in the design of a controlled temperature vehicle, the amount of surface erosion becomes important if long times of flight are expected.

At altitudes used for the employment of satellite systems we are concerned with free molecule flow, or superaerodynamics. In this realm two drag mechanisms operate: Newtonian (inelastic) reflections and specular (elastic) reflections of the gas molecules. Specular reflections are those in which the incident stream of particles is elastically reflected from the exposed body surface, and are directly dependent upon the "smoothness" of the reflecting surface, i.e., the roughness height (1).[2] Although only 3 to 10 per cent of the total molecules are specularly reflected (2) such reflections are important over long time intervals and when accurate calculations for re-entry vehicles are required.

Several erosion mechanisms (3) and erosion rates (3,4) have been suggested by researchers. Singer suggests a maximum erosion rate of 10μ (microns) per 1600 sec, while Whipple favors a rate of 2×10^{-13} gm/cm^2/sec (or 10^{-6} μ per 1600 sec for an aluminum target). This paper describes a beta-ray scattering technique which can be used to measure surface erosion rates between these two values.

Proposed Erosion Measuring Method

Several methods of erosion rate measurement have been suggested in the literature (3,5). One of these methods (3) utilizes the number of beta particles that are backscattered from a thin target as a direct indication of the material thickness. By observing the change in number of backscattered particles which results from the change in target thickness, it should be possible to determine the rate at which a physical process is removing material from the target surface, e.g., as in micrometeorite erosion. This paper describes the applicability of this process to satellite operation.

The principle advantages of the use of a beta-ray backscattering technique are its sensitivity, its stability and the fact that it operates without physically altering the measured surface.

The purely theoretical treatment of backscattering is quite complicated and not completely understood. Fortunately, thickness measurement by beta-ray backscattering has been employed sufficiently in industry and medicine for evolution of several useful empirical formulas. It is hoped that, by treating the results of some backscattering experiments with these formulas, enough confidence will be developed to show that we may extrapolate this technique for use between the erosion limits cited above.

Backscattering Experiments

A technique was developed at Stanford Research Institute, Menlo Park, California (6) for measuring thicknesses of ice by using the backscattering of beta-rays. It was shown that for thin targets the number of backscattered beta particles is proportional to the target thickness.

The essential elements of this system were a beam of beta-rays, a target area and a radiation detector. These are shown photographically in Fig. 1 and schematically in Fig. 2.

The beta source was a Tracerlab RA-1A Medical Applicator. The applicator was a beta-emitting plaque which contained strontium 90 in equilibrium with yttrium 90. Strontium 90 disintegrates with a half-life of 20 years, emitting particles of 0.65 mev to form yttrium 90. Yttrium 90 has a half-life of 62 hr and emits beta particles with a maximum energy

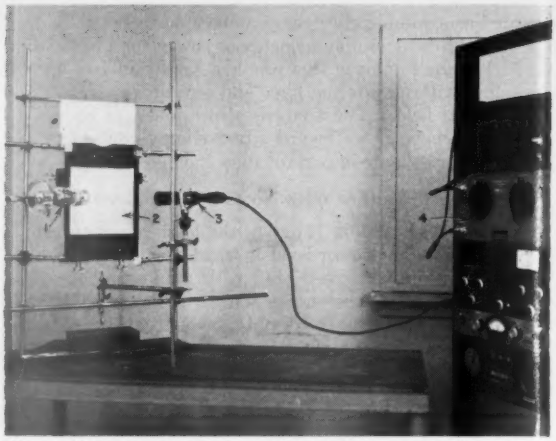

Fig. 1 Component arrangement for beta-ray scattering experiments: (1) Collimator and source, (2) scattering material (target), (3) detector, (4) scaling unit.

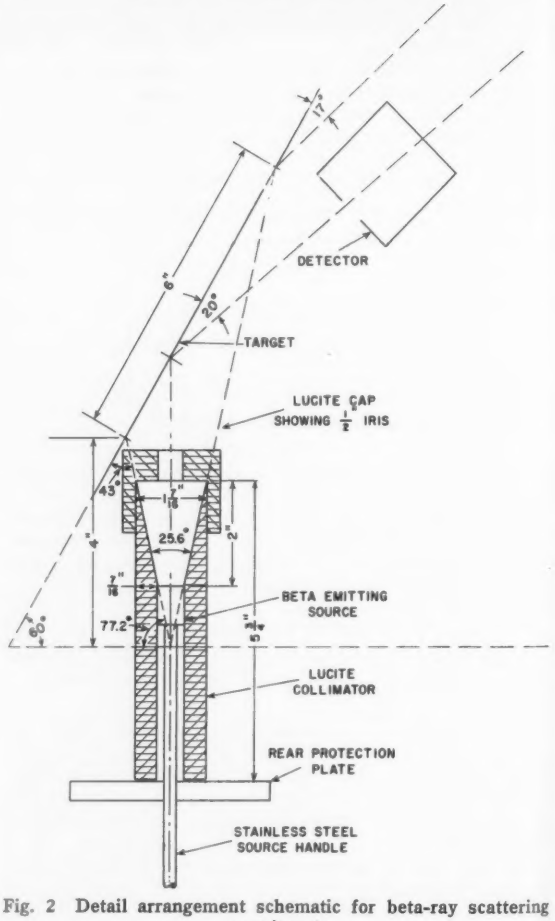

Fig. 2 Detail arrangement schematic for beta-ray scattering experiments

[2] Numbers in parentheses indicate References at end of paper.

of 2.16 mev to form the stable isotope, zirconium 90.

Fig. 3 shows that the number of backscattered beta particles (counts/min) increases with the target thickness. The counts per min tend to increase until a state of "saturation" predominates. At this point a further increase of target thickness does not noticeably increase the number of backscattered particles.

The two curves in Fig. 3 show the results of two different collimator "iris" openings. The point of saturation at constant source angle and distance, constant detector angle and distance, is nearly identical (about 56 mil for polyethylene) for the $\frac{1}{4}$- and $\frac{1}{2}$-in. iris openings. The only significant difference between the two curves is the improved sensitivity (change in counts/min per change in thickness) shown by the larger iris opening.

The importance of the saturation thickness is that it sets a "thickness limit" for any satellite skin in which we wish to use backscattering techniques. It is also reasonable to assume that target material, target thickness and beta particle energy will determine the amount of incident radiation scattered for detection.

Scattering Theory

"The scattering of swift electrons occurs in an absorber both by nuclear deflections and by inelastic collisions with atomic electrons" (7). At electron energies of 2 to 3 mev, the minimum distance of approach of the beta particles during collision with the target atoms is significantly greater than the radius of the nucleus. Thus, the only force acting is the inverse square coulomb force, so we may apply classical Rutherford scattering to our problem.

It can therefore be shown (7) that

$$\sigma_{(\text{backscatter})} = \pi \frac{Z^2 e^4}{E_2} \left[1 - \left(\frac{M_1}{M_2} \right)^2 \right] \quad \ldots\ldots [1]$$

where

Z = atomic number of the target material
E = energy of beta particles
M_1 = mass of the beta particles
M_2 = mass of the target material atoms
σ = Rutherford scattering cross section, cm²/atom, and

$$n = n_0 \sigma (N \Delta S) \quad \ldots\ldots [2]$$

where

n = number of particles scattered
n_0 = number of particles incident on the target
N = number of atoms, cm³
ΔS = target thickness, cm

We see that the assumption about the dependence of scattering on target material, target thickness and beta energy is supported by classical theory.

Empirical Formulas

Theoretically (8) saturation is reached if the target thickness is equal to half the range (R) of the beta particles. Practically, the maximum backscattering occurs at a thickness $d = 0.2R$. Saturation values are found to be independent of the particle energy between 0.3 and 2.3 mev. This can be explained by the fact that, for increasing energy, the decrease in scattering cross section, Equation [1], of the nuclei of the target material is compensated for by the increase in the number of nuclei encountered by the beta particles (because of the increase in range).

For energetic electrons the range is found empirically (9) to be

$$R_0 = 0.52\,E - 0.09 \quad \ldots\ldots [3]$$

where

R_0 = R times target density, gm/cm²
E = energy of beta particles, mev

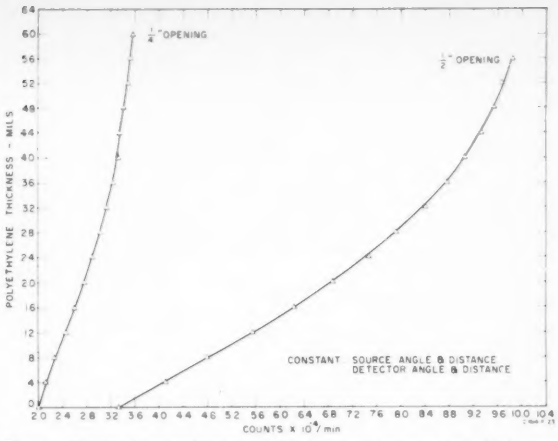

Fig. 3 Dependence of beta-ray backscattering on total thickness of polyethylene targets

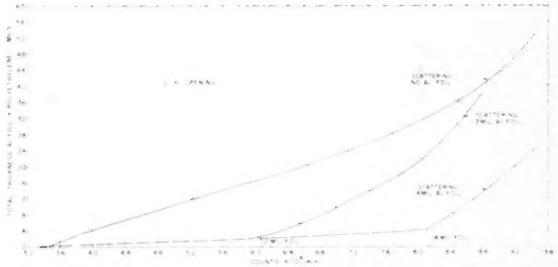

Fig. 4 Dependence of beta-ray backscattering on target material

Calculations

Comparing this theory with the results of the beta scattering experiments for polyethylene targets (6) we find: If E avg = 1.3 mev, i.e., E avg equals 0.6 E_{max} where E_{max} = 2.16 mev, then R_0 = 0.586 gm/cm², and $R = R_0$/density = 247 mil. Fig. 3 shows that saturation occurs at about 56 mil. Thus we see 56/247 = 0.22, or more properly, saturation thickness

$$d = 0.22R \quad \ldots\ldots [4]$$

which is in rather good agreement with the value above, i.e., $d = 0.2R$.

We may now with some confidence predict the saturation thickness (d) of aluminum and magnesium, two commonly used satellite materials. Using Equations [3 and 4], and E avg = 1.3 mev, we find the following results:

Material	Density gm/cm³	Range R mil	Saturation thickness d mil
polyethylene	0.93	247	56
aluminum	2.7	86	19
magnesium	1.8	128	28.5

Thus, if the strontium 90, yttrium 90 source were used, the maximum skin thickness would be restricted to about 30 mil for magnesium. Skin thickness in excess of the saturation thickness would not be prohibited however, if "windows," i.e., areas which had been machined to the proper depth, were provided for the beta scattering targets.

Fig. 4 shows the dependence of backscattering on the target density. The two curves indicate that aluminum is about twice as reactive (counts/min) as polyethylene at equal thicknesses. From Equation [2] we could expect magnesium to fall somewhere between these two curves. The slope of the aluminum-polyethylene curve suggests that, despite the high count rate, the counting tube was not overloaded in

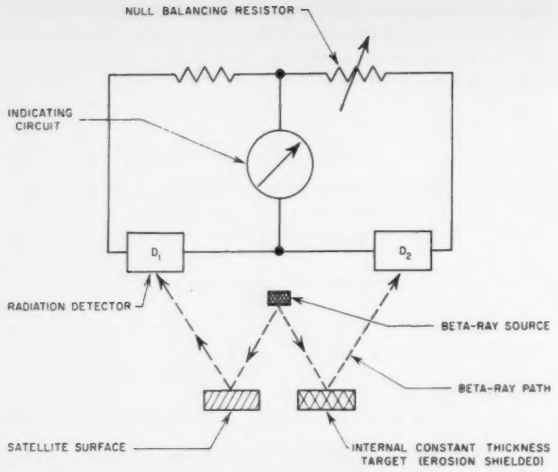

Fig. 5 Proposed circuit arrangement for increasing measuring sensitivity and excluding cosmic background

this region, an important fact when considering that the experimental saturation point might have been due to the tube and not the scattering mechanism being saturated.

At the speculated upper limit erosion rate of 10 μ per 1600 sec (3), or about 0.9 mil/hr, we see in Fig. 3 for the ½-in. iris curve, that the counting rate would have changed by about 5×10^2 counts/min for a polyethylene target whose thickness had changed by this amount.

We consider only the upper portion of the curve since the satellite skin would naturally be very near the saturation thickness for the particular material and beta-ray energies at the start of our observations. Since the aluminum response is about twice that of equal thicknesses of polyethylene, this erosion rate would produce a change of about 1×10^3 counts/min, and for a magnesium surface possibly 8×10^2 counts/min. If we postulate that the erosion rate is 0.01 to 0.001 of the upper limit of 0.9 mil/hr, we would expect a response change of only 1 to 10 counts/min for aluminum for each hour interval—a change too small to detect against natural cosmic background.

The obvious solution is less target thickness and longer intervals between samplings. Thus, a 4-mil thick window in an aluminum satellite would give a response change of 1×10^4 counts/min (Fig. 4) for every mil change in thickness. A 24 hr sample interval would show a response change of 240 counts/min for an 0.009-mil change in surface thickness.

At the lower erosion limit (4), which is equivalent to about 2.5×10^{-6} mil/day for an aluminum vehicle, it would require about 3600 days for the minimum response of a 0.009-mil depth change to become detectable.

By making use of a bridge-type arrangement such as is shown schematically in Fig. 5, we can improve the detection of response change. The signal obtained with this new arrangement corresponds to thickness change rather than total thickness, and excludes the cosmic radiation background.

An erosion rate of 0.009 mil/day (240 counts/min) observed by this method would require 12 years to completely erode away a 40-mil satellite.

Conclusions

Calculations based on experimental data have shown that beta-ray backscattering is a sensitive method for measuring the surface erosion of satellites by micrometeorites. Within the erosion rate limits envisioned by experimenters, the backscattering method adequately covers this range, leaving some doubt as to its value only at the extreme low limit. The principle value of the method is its ability to measure directly the change in thickness of a vehicle skin without physically influencing the material surface under observation.

References

1 Petersen, N. V., "Lifetimes of Satellites in Near Circular and Elliptic Orbits," JET PROPULSION, vol. 26, May 1956, p. 341.

2 Millikan, R. A., "Coefficients of Slip in Gases and the Law of Reflection of Molecules from the Surfaces of Solids and Liquids," *Physical Review*, vol. 21, 1923, pp. 217–230.

3 Singer, S. F., "The Effect of Meteoric Particles on a Satellite," JET PROPULSION, vol. 26, Dec. 1956, p. 1071.

4 Whipple, F., "The Meteoric Risk to Space Vehicles," Abstract from "First Look at American I.A.F. Papers," ASTRONAUTICS, Nov. 1957, vol. 2, no. 4, p. 72.

5 Swetnick, M. J., "Meteoric Abrasion Studies Proposed for Vanguard," *The Journal of Astronautics*, vol. IV, no. 1, Winter 1957, p. 69.

6 Poppoff, I. G. and Goettelman, R. C., "Techniques for Prevention and Removal of Ice on Radomes," Final Report prepared for Rome Air Development Center, Griffiss Air Force Base, New York.

7 Evans, R. D., "The Atomic Nucleus," McGraw Hill, New York, 1955, pp. 20, 76, 597.

8 Bleuler, E. and Goldsmith, G. J., "Experimental Nucleonics," Rinehart and Company, Inc., New York, 1952, p. 83.

9 Evans, R. D., "Advances in Biological and Medical Physics," ed. by Lawrence, J. H. and Hamilton, J. G., Academic Press Inc., New York, 1948, 1st ed., p. 160.

Flashback and Blowoff Limits of Unpiloted Turbulent Flames[1]

JOSEPH GRUMER[2]

Bureau of Mines, U. S. Department of the Interior, Pittsburgh, Pa.

Introduction and Summary

FLASHBACK and blowoff limits of laminar flames have been explained previously by a concept based on boundary velocity gradients (1).[3] This contribution has been most useful in treating gas appliance problems (2) but less so in applications dealing with turbulent flames. It has been shown that the critical boundary velocity gradient for blowoff can be the same for laminar and for unpiloted pipe flow turbulent flames (2,3,4). On the other hand, flashback and blowoff gradients have been reported to be greater in turbulent than in laminar flow (5 to 9,11). Elucidation of the causes of these differences could contribute to the understanding of turbulent combustion and to the design of industrial equipment and engines. These problems have not yet been treated comprehensively. In this note, the need for further study of stability limits of turbulent flames is indicated, and new data are presented on laminar tilted flame limits, and turbulent flashback and blowoff limits. Only unpiloted flames on unobstructed ports are discussed.

The mechanisms of flashback and blowoff of unpiloted turbulent flames have not yet been adequately elucidated. These instabilities stem from factors associated with the boundary laminar sublayer and with the core of the turbulent flow.

The Flashback Problem

1 Conceivably, in turbulent flow, one cannot distinguish between the flashback of tilted flames and true flashback. In laminar flow, the distinction is made readily (10). Consequently, a correlation should be attainable between tilted flame gradients in laminar flow and turbulent flashback gradients.

Von Elbe and Mentser (10) studied tilted flames in laminar

Received May 23, 1958.

[1] This research is supported in part by the American Gas Association (Project PDC-3-GU).

[2] Physical Chemist, Chief, Flame Research Section, Division of Explosives Technology. Member ARS.

[3] Numbers in parentheses indicate References at end of paper.

flow only. Following the general lines of their theory,[4] the tilted flame gradient in laminar flow is obtained by means of Equation [1]

$$K = \frac{g^2_{TL}}{\left(g^2_{TL} - \frac{16S_u^2}{R^2}\right)^{1/2}} \quad \ldots\ldots [1]$$

where K is the tilted flame gradient, which is a constant for the mixture, sec^{-1}; g_{TL} is the boundary gradient for the laminar flow prior to ignition, sec^{-1}; R, cm, is the radius, and S_u is the burning velocity, cm/sec. In turbulent flow[4]

$$K = \left(\frac{g^3_{TT}}{g_{TT} - \frac{0.0332 S_T^{1.75} \rho^{0.75}}{\sigma^{0.25}\eta^{0.75}}}\right)^{1/2} \quad \ldots\ldots [2]$$

Here K is as defined above; S_T is the turbulent burning velocity; g_{TT} is equivalent in turbulent flow of g_{TL} in laminar flow; σ, cm, is the major semi-axis of the tilted elliptical flame base (R is the minor semi-axis); ρ is the density, gm/cm^3, and η is the viscosity, poise. When R and σ are large, Equation [3] holds for laminar and turbulent flow

$$K = g_{TL} = g_{TT} \quad \ldots\ldots [3]$$

The thesis that turbulent flashback is really the flashback of tilted flames was tested by comparing the laminar tilted flame limits (10) with turbulent flashback limits (8) of hydrogen-oxygen flames. As shown in Fig. 1, the laminar tilted flame limits (10) fall on the turbulent flashback curve (8), indicating that turbulent flashback can be caused by flame tilt.

2 Another test of this concept was conducted employing slow-burning natural gas-air flames on much larger burners than those used in the hydrogen-oxygen tests. Measurements were made on three burners, 1.138, 1.435 and 1.914 cm in diameter, to obtain laminar tilted flame limits. Turbulent flashback was measured using 300-cm long tubes of 5.08 and 7.62 cm inside diameter. The data are given in Fig. 2.[5] There is no coincidence of laminar tilted flame limits and turbulent flashback limits, in contradiction to the results presented in Fig. 1. A possible explanation is now offered.

3 The turbulent flame stability gradients in Fig. 2 are numerically the same whether considered as tilted flame gradients or as turbulent flashback gradients. This is because Equation [3] applies for these large port diameters; actually no tilting of flames was observed before flashback. Next, consider that turbulent flames on the verge of flashback on wide diameter ports are short wide-angled flames. Photographs of such a flame are shown in Fig. 3 (the port is 7.62 cm, and the depth of focus of the optical system is about 3 cm). Many flame surfaces within the body of the turbulent stream appear ready to flash back, whereas the flame surfaces near the boundary of the stream (laminar sublayer) are nearly vertical. According to Equation [4] of (5), the sublayer thickness l should be about 0.06 cm

$$l = \frac{66R}{Re^{0.9}} \quad \ldots\ldots [4]$$

The photograph in Fig. 3 strongly suggests the possibility that on reducing the flow, the flame surfaces leading the flashback will not all be contained in the laminar boundary layer.

[4] Certain modifications and additions were made to the treatment presented by von Elbe and Mentser (10). In arriving at Equation [1], the sine of the angle of flame tilt was held to be equal to $[1 - (R/\sigma)^2]^{1/2}$ rather than $1.4[1 - (R/\sigma)]^{1/2}$. To arrive at Equation [2] the boundary velocity gradient for turbulent flow was equated to $\lambda \bar{U} Re/16R$, with $\lambda = 0.316/Re^{1/4}$. $\bar{U}$ is the average gas velocity, and Re is the Reynolds number.

[5] Efforts were made to induce flashback by flame tilt by fanning the base of the flame. These are all the points in Fig. 2 except those for the 5.08 cm burner. This variation in experimental procedure does not affect the conclusion that turbulent flashback gradients and laminar tilted flame gradients can be different.

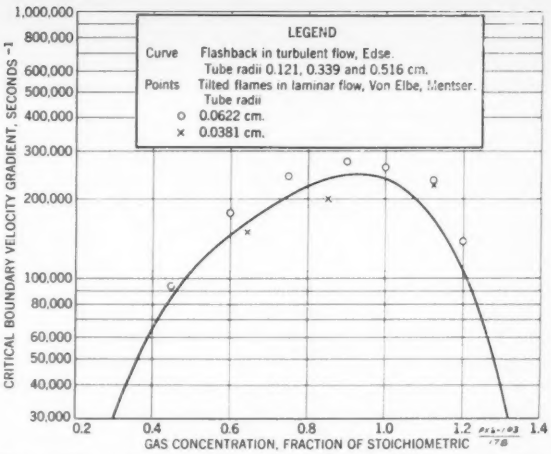

Fig. 1 Comparison of curve for flashback gradients in turbulent flow with points for tilted flame gradients in laminar flow: Hydrogen-oxygen mixtures

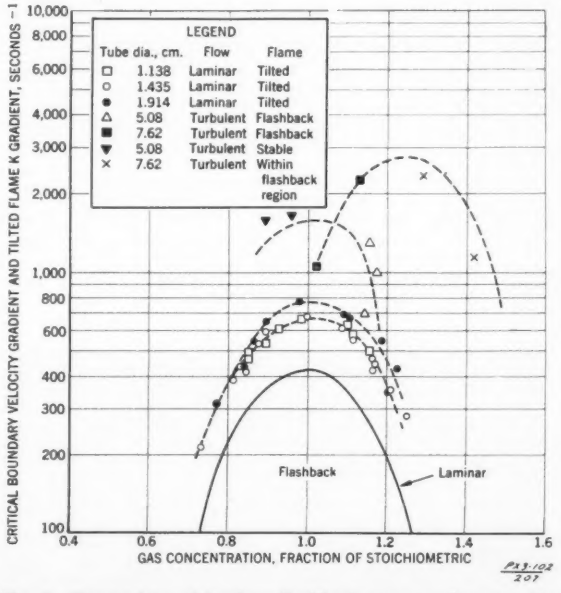

Fig. 2 Comparison of laminar flashback curve and curves for tilted flame K gradients for turbulent and laminar flow: Natural gas-air flames

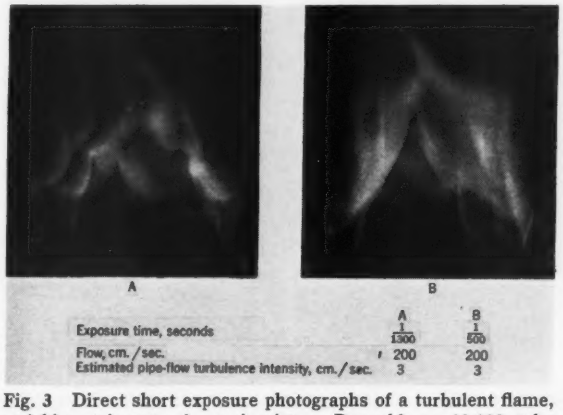

Fig. 3 Direct short exposure photographs of a turbulent flame, stoichiometric natural gas-air mixture, Reynolds no. 10,000, tube diam 7.62 cm

Correspondingly, turbulent flashback need not always be caused by conditions in the laminar sublayer of wide diameter ports. Conditions in the core of the stream may lead to instability. This possibility may explain the disagreement noted in paragraph 2.

The foregoing tilted flame theory involves the assumption that turbulent flashback is produced by events in the laminar sublayer. The sublayer is more likely to be significant on ports of small rather than large diameter. The natural gas-air turbulent flame tests were made with burners with diameters about 10 to 60 times those employed in the hydrogen-oxygen turbulent flame experiments. Equation [4] shows the sublayer thickness to be weakly dependent on port diameter and inversely proportional to roughly the average gas velocity.

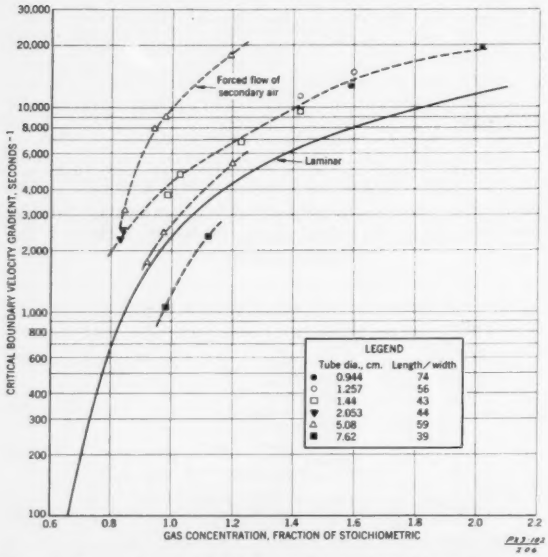

Fig. 4 Comparison of laminar and turbulent blowoff curves: Natural gas-air flames

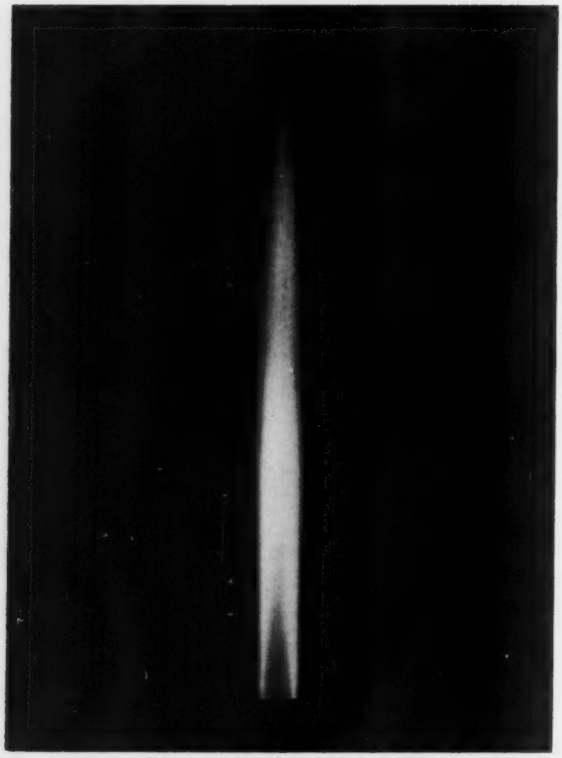

Fig. 5 Photograph of water-cooled skirt stabilized flame of stoichiometric natural gas-air

The Blowoff Problem

1 Blowoff gradients of unpiloted pipe flow turbulent flames also show that stabilization of turbulent flames is not always in the laminar boundary sublayer. Ample evidence that stabilization can occur in the laminar sublayer is recorded in (2,3,4 and 6). This is based on the equivalence of blowoff gradients in laminar and turbulent flow. But again there exists contrary evidence in (10) and in some of the data in Fig. 4.[6]

2 The volumetric flow at blowoff of pipe flow turbulent unpiloted flames was raised considerably by adding a cold, short, slightly but sharply expanded cylindrical section of tubing (a skirt stabilizer) atop a long pipe burner (12). The base of the flame was within the skirt stabilizer, generally about halfway up, the flame extending over virtually the entire inside diameter of the stabilizer. Flows were stabilized that were over 18 times the blowoff flow for a 300-cm long cylindrical pipe of the same diameter as the 15-cm long skirt stabilizer (7.6 cm ID). These skirt stabilizers were operated hot, water-cooled, and with inserts of varying geometry. In all instances, large gains in stability were obtained.

Fig. 5 is a photograph of the external portion of a 180,000 Reynolds number flame of a stoichiometric natural gas-air flame, stabilized on a 15-cm long water-cooled skirt of 7.62 cm ID atop a 300-cm length of 5.08-cm tubing. The flame base shows an interesting abrupt expansion at the exit of the skirt, which suggests that the cross-sectional area of the flame within the skirt is reduced by a boundary layer of burned gas along the wall. This inward thrust on the flame due to the confinement of burned gas by the wall of the skirt may be highly important in achieving the great gain in flame stabilization that this geometry provides.

Acknowledgment

The author is indebted for the new data presented in this paper to the efforts of Valeria R. Rowe, Margaret E. Harris and J. Kenneth Richmond, Joseph M. Singer and William F. Donaldson of these laboratories.

References

1 Lewis, B. and von Elbe, G., "Stability and Structure of Burner Flames," *Journal of Chemical Physics*, vol. 11, 1943, pp. 75–97.

2 Grumer, J., Harris, M. E. and Rowe, V. R., "Fundamental Flashback, Blowoff, and Yellow-Tip Limits of Fuel Gas-Air Mixtures," Bureau of Mines Report of Investigations 5225, 1956.

3 Wohl, K., Kapp, N. and Gazley, C., "The Stability of Open Flames," "Third Symposium on Combustion and Flame and Explosion Phenomena," Williams and Wilkins Co., Baltimore, 1949, pp. 3–21.

4 Bollinger, L. M. and Williams, D. T., "Experiments on Stability of Bunsen-Burner Flames for Turbulent Flow," NACA Tech. Note 1234, 1947.

5 Fine, B., "Further Experiments on the Stability of Laminar and Turbulent Hydrogen-Air Flames at Reduced Pressures," NACA Tech. Note 3977, 1957.

6 Fine, B., "Stability Limits and Burning Velocities for Some Laminar and Turbulent Propane and Hydrogen Flames at Reduced Pressure," NACA Tech. Note 4031, 1957.

7 Wohl, K., "Quenching, Flash-Back, Blow-Off—Theory

[6] Points shown as solid squares in Fig. 4 were obtained while fanning the flame, and those shown as the upper set of open triangles were obtained with a stream of secondary air around the flame. The improvement in stability occasioned by surrounding the base of the flame with a closely placed stream of secondary air is not necessarily a matter of reducing the boundary velocity gradient of the turbulent stream. Similar experiments in laminar flow have shown a decrease of stability.

and Experiment," "Fourth Symposium (International) on Combustion," Williams and Wilkins Co., Baltimore, 1953, pp. 68–89.

8 Edse, R., "Studies on Burner Flames of Hydrogen-Oxygen Mixtures at High Pressure," WADC Tech. Report 52–59, 1952.

9 Bollinger, L. E. and Edse, R., "Effect of Burner Tip Temperature on Flashback of Turbulent Hydrogen-Oxygen Flames," *Industrial and Engineering Chemistry*, vol. 48, 1956, pp. 802–807.

10 von Elbe, G. and Mentser, M., "Further Studies on the Structure and Stability of Burner Flames," *Journal of Chemical Physics*, vol. 13, 1945, pp. 89–100.

11 Boyer, M. H. and Friebertshauser, P. E., "An Investigation of the Behaviour and Reaction Mechanisms of Nitric Acid-Hydrocarbon Flames," *Combustion and Flame*, vol. 1, 1957, pp. 261–280.

12 Unpublished experiments, Bureau of Mines.

The Influence of the Launching Conditions on the Orbital Characteristics

GEZA S. GEDEON[1] and RICHARD E. DAWLEY[2]

Chance Vought Aircraft, Dallas, Texas

The relationship between the apogee and perigee altitudes and the burnout conditions are obtained from the equations of motion of a satellite orbiting in a vacuum around a spherical nonrotating Earth. This relationship is presented on a composite chart. It can be seen from the chart that for high reliability in achieving an orbit, high excess velocities are favorable.

Nomenclature

V = velocity
R = distance measured from the center of the Earth and a point in space
R_0 = radius of the Earth (here used as 3960 miles)
G = acceleration of gravity at sea level, 78,938 miles/hr^2
β = angle between radius and reference plane
ϕ = angle measured from the normal to the line connecting the point in space and the center of the Earth (deviation from local horizontal)
$\dot{R} = dR/dT$
$\ddot{R} = d^2R/dT^2$
$\dot{\theta} = d\theta/dT$

Subscripts

θ = in the direction of θ
B = burnout conditions
A = apogee
P = perigee
S = conditions for circular orbit

THE equation of motion in polar coordinates is

$$\ddot{R} = R(\dot{\theta})^2 - \frac{R_0^2 G_0}{R^2} \quad [1]$$

where

$R(\dot{\theta})^2$ = centrifugal acceleration
$\frac{R_0^2 G_0}{R^2}$ = gravitational acceleration
$\ddot{R}$ = resultant radial acceleration

These components of the accelerations are shown on Fig. 1.

Received May 27, 1958.

[1] Theoretical Aerodynamics Staff Engineer.

[2] Aerodynamics Design Engineer. Member ARS.

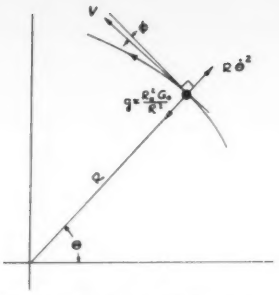

Fig. 1 Polar coordinate system

Since there are no tangential forces acting on the vehicle, the angular momentum is constant, i.e.

$$R^2\dot{\theta} = K \quad [2]$$

where K is a constant. Hence

$$\dot{\theta}^2 = \frac{K^2}{R^4} \quad [3]$$

The resultant radial acceleration $\ddot{R}$ may be expressed as

$$\ddot{R} = \dot{R}\frac{d\dot{R}}{dR} = \frac{1}{2}\frac{d(\dot{R})^2}{dR} \quad [4]$$

Using the above expression for $\ddot{R}$ and $\dot{\theta}$ in Equation [1], the equation of motion becomes

$$\frac{1}{2}\frac{d(\dot{R})^2}{dR} = \frac{K^2}{R^3} - \frac{R_0^2 G_0}{R^2} \quad [5]$$

Integration of Equation [5] yields

$$\frac{(\dot{R})^2}{2} = -\frac{1}{2}\frac{K^2}{R^2} + \frac{R_0^2 G_0}{R} + C \quad [6]$$

The angular momentum K and the constant of integration C can be evaluated at the burnout conditions. Thus

$$K = R^2\dot{\theta} = R_B(V_\theta)_B = R_B V_B \cos\phi_B \quad [7]$$

and

$$C = \frac{V_B^2}{2} - \frac{R_0^2 G_0}{R_B} \quad [8]$$

Using the above values for K and C, Equation [6] becomes

$$\frac{(\dot{R})^2}{2} = -\frac{1}{2}\frac{R_B^2 V_B^2 \cos^2\phi_B}{R^2} + \frac{R_0^2 G_0}{R} + \frac{V_B^2}{2} - \frac{R_0^2 G_0}{R_B} \quad [9]$$

The length of the radius vector to the apogee and perigee may be obtained from [9] since $\dot{R}$ is zero at these two orbital points. Therefore

$$R_{A,P} = \frac{\frac{R_0^2 G_0}{V_B^2} \pm \sqrt{\frac{R_0^4 G_0^2}{V_B^4} - \left(\frac{2G_0 R_0^2}{R_B V_B^2} - 1\right) R_B^2 \cos^2\phi_B}}{\frac{2G_0 R_0}{R_B V_B^2} - 1} \quad [10]$$

Equation [10] may be simplified by introducing the circular satellite velocity at the burnout altitude

$$(V_S)^2_B = \frac{R_0^2 G_0}{R_B} \quad [11]$$

Then

$$R_{A,P} = \frac{R_B}{2 - \left(\frac{V}{V_S}\right)^2_B}\left[1 \pm \sqrt{1 - \left(\frac{V}{V_S}\right)^2_B\left[2 - \left(\frac{V}{V_S}\right)^2_B\right]\cos^2\phi_B}\right] \quad [12]$$

The length of the radius vector to the apogee is obtained by using the positive sign on the radical, and the length of the radius vector to the perigee is obtained by using the negative sign on the radical.

Solutions of Equation [12] are illustrated on Fig. 2. To obtain the apogee and perigee altitudes from the initial conditions easily, Fig. 2 has two nomograms: One for converting the burnout velocity and the burnout altitude into the velocity ratio (V_B/V_S), and one for converting the radius ratio ($R_{A.P}/R_B$), and the burnout altitude into the apogee and perigee altitudes. An example illustrating the use of the figure is given on Fig. 2.

It can be seen from Fig. 2 that high excess launching speed increases the probability of obtaining an orbit. It is apparent that at high excess launching speeds the angular errors affect, mainly, the apogee altitude, whereas at launching speeds less than those required for a circular orbit, the angular errors affect mainly the perigee altitude.

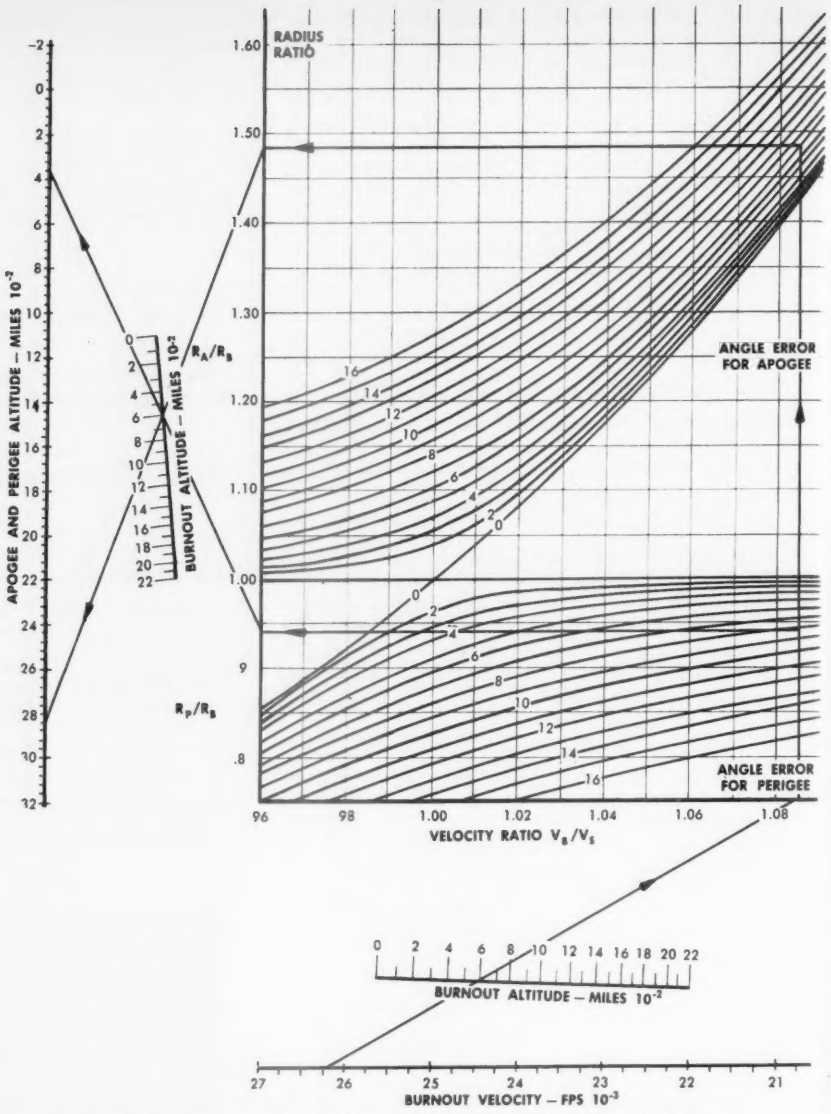

Fig. 2 Influence of launching conditions on the orbital characteristics

Thermodynamics of Al_2O_3

MILTON FARBER[1]

Hughes Tool Co., Aircraft Division, Culver City, Calif.

Introduction

THE utilization of aluminum as a propellant constituent is proceeding at an accelerated pace. The need therefore arises for performance calculations of propellant systems containing elemental aluminum and various components of aluminum. Early performance calculations considered the formation of either solid, liquid or gaseous aluminum oxide as the only combustion product of aluminum or its compounds. However, since the reactions of aluminum with the other combustion species can be quite involved, it is the purpose of this paper to discuss some of the significant reactions and to point out some of the thermodynamic relationships that are involved.

Theoretical Considerations

In most performance calculations of propellants containing aluminum or its compounds assumptions have been made that Al_2O_3 remains undissociated in the liquid stage at temperatures above 2500 K. Brewer and Searcy (1)[2] investigated the Al-Al_2O_3 system in an effusion cell. From the vapor pressure measurements, they obtained a boiling point of 3770 ± 200 K for Al_2O_3. Their evidence for the dissociation of Al_2O_3 to Al_2O and AlO at high temperatures has been substantiated by Hoch (2) and Cochran (3). From a combination of their work and values listed by Kelly (4) and NBS (5) and Brewer's Tables, some thermodynamic data have been deduced for the heats of formation of the dissociation products of Al_2O_3. A list of the heats of formation, entropies and specific heats (C_p) at standard conditions of these prod-

Received May 27, 1958.

[1] Head, Chemistry and Propellants Laboratory. Member ARS.

[2] Numbers in parentheses indicate References at end of paper.

ucts are presented in Table I. A value of 27 cal/deg/mole

Table I Thermodynamic properties of aluminum and its oxides

Compound	$H_f°$ 298 (kcal/mole)	$S°$** (cal/deg/mole)	C_p 298 (cal/deg/mole)	
Al(s)	0	6.77	5.82	
Al(l)	1.90	10.3	7.0	
Al(g)	77.4*	39.31	5.11	
Al_2O_3(s)	−399.1	12.5	18.88	
Al_2O_3(l)	−373	17.3	27	(estimate)
AlO(g)	9.5	52.14	7.4	(estimate)
Al_2O(g)	−34	65	9.6	(estimate)

* Measurements in an effusion cell by the author substantiate this value.

** Entropy and specific heat values are from Kelly (Bureau Mines Bulletin 477) and NBS tables (circular 500 NBS). Those for AlO(g) and Al_2O_3(l) have been estimated as described in the text.

for the specific heat of Al_2O_3 (l) at 298 K has been estimated from an examination of the literature for similar compounds and interpolation from a rule for estimating specific heats of liquids given by Wenner (6). This rule gives a value of 34 cal per mole for the C_p of Al_2O_3 (l) while Kopps' rule gives a value of 24.4 cal/deg/mole for C_p of Al_2O_3(s). Since the experimental value of the C_p at 298 K of Al_2O_3(s) is 18.9 cal/deg/mole the value obtained by Wenner's rule is undoubtedly too high and should be corrected to a lower value. Herzberg (7) gives a value of 978 cm^{-1} for ωe of AlO from which a value of 7.4 cal/deg/mole is calculated for C_p of AlO at 298 K. The C_p of Al_2O was estimated by adding the vibrational contribution of four degrees of freedom (assuming that the molecule is bent) to that of rotation and translation. Employing the AlO frequency as a first approximation for the Al_2O frequencies a value of 0.43 cal/deg/mole is obtained for the vibrational specific heat for each degree of freedom. The addition of 1.6 cal/deg/mole for the vibrational C_p yields a total specific heat of 9.6 cal/deg/mole for Al_2O(g) at 298 K.

Besides the straight decomposition of Al_2O_3 to elemental aluminum and its suboxides of Al_2O and AlO, the reactions of Al_2O_3 and the other combustion species must be considered. These include possible reactions with CO, CO_2, H_2O and solid C. Example calculations of the free energies of these reactions are presented for the combustion temperature range of 3000 K and in the vicinity of the boiling point, 3770 K, as an indication of the possible decomposition of Al_2O_3.

The Reactions of Al_2O_3 With Propellant Combustion Gases

The stability of Al_2O_3 at 3000 K is tested in reactions with H_2, CO and solid C.

1 The reaction of H_2 and Al_2O_3 may proceed as

$$2H_2 + Al_2O_3(l) = 2H_2O(g) + Al_2O(g)$$

$$\Delta H_{298} = +223.4 \text{ kcal} \quad \Delta S_{298} = 75.3 \text{ cal/K} \quad \Delta C_p = -15.4 \text{ cal/K}$$

$$\Delta F = 227{,}990 + 15.4\ T \ln T - 178.4\ T$$

$$\Delta F_{3000} = 62.8 \text{ kcal} \quad \Delta F_{3770} = 33.6 \text{ kcal}$$

$$K = \frac{P^2_{H_2O} P_{Al_2O}}{P^2_{H_2}}$$

$$K_{3000} = 2.7 \times 10^{-5} \quad K_{3770} = 1.1 \times 10^{-2}$$

The partial pressure of Al_2O becomes increasingly important above 3000 K.

2 The reaction of solid C and H_2 with Al_2O_3.

In some low temperature reactions or those in which large quantities of Al are added there is the possibility of the existence of solid carbon. Therefore its reaction with Al_2O_3 will be investigated in the following equilibrium at 2500 and 3000 K

$$C + H_2 + Al_2O_3(1) = CO + H_2O + Al_2O(g)$$

$$\Delta H_{298} = 254.8 \text{ kcal} \quad \Delta S_{298} = 107.4 \text{ cal/K} \quad \Delta C_p = -11.6 \text{ cal/K}$$

$$\Delta F = 258{,}260 + 11.6\ T \ln T - 185.1\ T$$

$$\Delta F_{2500} = 22.4 \text{ kcal} \quad \Delta F_{3000} = -18.4 \text{ kcal} \quad \Delta F_{3770} = -79.4 \text{ kcal}$$

$$K = \frac{P_{CO}\ P_{H_2O}\ P_{Al_2O}}{P_{H_2}}$$

$$K_{2500} = 1.09 \times 10^{-2}$$

From the above calculations it can be seen that the decomposition of Al_2O_3(l) with C and H_2 becomes considerable at temperatures above 2500 K. Although this temperature is below the average chamber temperature for hot propellant systems, it is probably an upper limit for systems containing solid carbon, since the source of carbon would be a fuel that would be stripped of its hydrogen atoms, resulting in low chamber temperatures.

3 The reaction of CO and Al_2O_3 can be considered as

$$2\ CO + Al_2O_3(1) = 2\ CO_2 + Al_2O(g)$$

$$\Delta H_{298} = 203.8 \text{ kcal} \quad \Delta S_{298} = 55.3 \text{ cal/K} \quad \Delta C_p = 13.8 \text{ cal/K}$$

$$\Delta F = 207{,}910 + 13.8\ T \ln T - 147.7\ T$$

$$K = \frac{P^2_{CO_2}\ P_{Al_2O}}{P^2_{CO}}$$

$$K_{3000} = 1.01 \times 10^{-7} \quad K_{3770} = 2.3 \times 10^{-5}$$

This calculation also gives a negligible vapor pressure of Al_2O_3 at 3000 K and at the boiling point.

Dissociation of Al_2O_3

Brewer and Searcy (1) indicate from their measurements that Al_2O_3 tends to dissociate to the suboxides at temperatures below its boiling point of 3800 K. A consideration of the extent of this dissociation is shown by the following reaction

$$Al_2O_3(1) = 2\ AlO(g) + O(g)$$

$$\Delta H_{298} = 456 \text{ kcal}$$

$$\Delta F = 443{,}000 + 12\ T \ln T - 212\ T$$

$$\Delta F_{3000} = 95 \text{ kcal} \quad \Delta F_{3770} = 16.4 \text{ kcal}$$

$$K = P^2_{AlO}\ P_O$$

$$K_{3000} = 1.14 \times 10^{-7} \quad K_{3770} = 1.12 \times 10^{-1}$$

This calculation shows that the pressure of AlO would be in the vicinity of 10^{-4} to 10^{-3} atm at 3000 K depending on the partial pressure of O in the gaseous species. However at temperatures near the boiling point the decomposition of Al_2O_3 is considerable.

Conclusions

The conclusions derived from the experimental measurements and the above calculations show that Al_2O_3 may be treated as an undissociated liquid resulting from the combustion of Al or Al compounds for the purpose of propellant performance calculations below 3000 K. At temperatures above 3000 K it will be necessary to calculate equilibrium constants for the various reactions and dissociations in order to determine the extent of the Al_2O_3 decomposition.

References

1 Brewer and Searcy, *Journal of the American Ceramic Society*, vol. 73, 1951, p. 5308.

2 Hoch, M. and Johnston, H. L., *Journal of the American Ceramic Society*, vol. 76, 1954, p. 2560.
3 Cochran, C. N., *Journal of the American Ceramic Society*, vol. 77, 1955, p. 2190.
4 Kelly, K. K., Bureau of Mines Bulletin no. 77.
5 National Bureau of Standards Tables, Circ. no. 500.
6 Wenner, R. R., "Thermochemical Calculations," McGraw-Hill, New York, 1941.
7 Herzberg, G., "Spectra of Diatomic Molecules," Van Nostrand, New York, 1950.

Characteristic Velocity as a Measure of Available Work

S. L. BRAGG[1] and H. RATCLIFFE[2]

Rolls-Royce Ltd., Derby, England

THE PURPOSE of this note is to demonstrate that the power available from a gas turbine is dependent primarily on the characteristic velocity of the entering gas, and is otherwise insensitive to gas properties, such as the specific heat ratio.

The power available from an ideal turbine passing a flow $\dot{M}$ of gas, at an initial total temperature T_1, and expanding the gas over a pressure ratio r (>1) is given by

$$550\,HP = \dot{M} C_p T_1 \left(1 - (r)^{\frac{1-\gamma}{\gamma}}\right) \quad [1]$$

where C_p is the specific heat of the gas at constant pressure, expressed in work units, and γ is the ratio of the specific heats of the gas.

In many cases, particularly where the turbine is driven by the products from a fuel rich gas generator, the exact composition and properties of the exhaust gases are unknown. Some clue to these is, however, given by the calculation, from the results of gas generator or turbine tests, of the characteristic velocity of the gases. This is defined by the relation

$$c^* = \frac{APg}{\dot{M}} \quad [2]$$

where A is the throat area choked by the flow $\dot{M}$ at total pressure P.

From the normal relations for isentropic choking flow of a perfect gas

$$\frac{\dot{M}\sqrt{RT}}{AP\sqrt{mg}} = \sqrt{\gamma}\left(\frac{2}{\gamma+1}\right)^{\frac{\gamma+1}{2(\gamma-1)}} = f(\gamma) \quad [3]$$

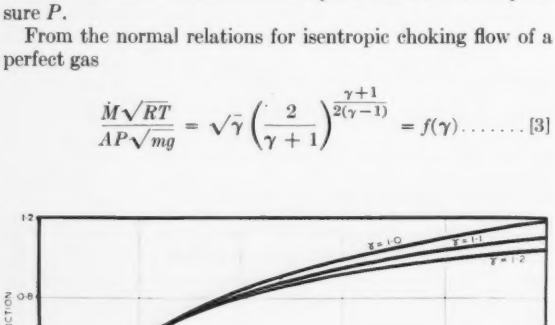

Fig. 1 Power function ($550\,HP\,g/\dot{M}\,c^{*2}$) against pressure ratio r

Received May 15, 1958.
[1] Supervisor, Performance Department, Rocket Division. Member ARS.
[2] Performance Engineer, Rocket Division.

where R is the universal gas constant in work units, and m is the molecular weight of the gas.

Also, for a perfect gas

$$\frac{R}{m} = \frac{\gamma - 1}{\gamma} C_p \quad [4]$$

Combining these equations, one obtains an expression for the power function

$$\frac{550\,HPg}{\dot{M}c^{*2}} = \frac{\gamma}{\gamma - 1}\left[1 - (r)^{\frac{1-\gamma}{\gamma}}\right][f(\gamma)]^2 \quad [5]$$

By a happy chance the expression on the right hand side is nearly independent of γ over the whole range normally of interest. It varies by less than 12 per cent as γ is increased from 1.0 to 1.2, at any particular value of r between 1 and 25.

Thus, to a sufficient approximation, the ideal turbine power is given by

$$\frac{550\,HPg}{\dot{M}c^{*2}} = f_2(r) \quad [6a]$$

or

$$HP = \dot{M}c^{*2} f_2(r)/550\,g \quad [6b]$$

Values for this function, based on a typical value of $\gamma = 1.13$ are given below.

r	1.0	1.5	2.0	3.0
$f_2(r)$	0	0.162	0.268	0.416
$\frac{\partial f_2(r)}{\partial \gamma}$	0	0.078	0.101	0.094
r	5.0	9.0	17.0	25.0
$f_2(r)$	0.592	0.782	0.974	1.083
$\frac{\partial f_2(r)}{\partial \gamma}$	0.020	−0.149	−0.402	−0.620

Since the ideal turbine horsepower can be obtained from Equation [6b] and compared with the horsepower actually produced on test, *it is possible to estimate turbine efficiency to within about ± 2 per cent without any more detailed knowledge of gas properties than is afforded by the direct calculation of the characteristic velocity.* Alternatively, the work available from a unit mass of gas expanding over a given pressure ratio is, to the same order of accuracy, directly proportional to the square of the characteristic velocity.

Toxicity and Personal Decontamination of Boron Hydride Propellant Fuels

SIDNEY ROTHBERG,[1] JOSEPH L. COLBOURN[2] and ROBERT SALVATORE[3]

Directorate of Medical Research, U. S. Army Chemical Warfare Laboratories, Army Chemical Center, Md.

The toxicities of the liquid boron hydride fuels (BHF) of the HEF-3 and HiCal class were determined for rats, guinea pigs, rabbits and cats by the intravenous, intraperitoneal, oral, ocular, inhalation and skin routes. The high toxicity of these compounds when applied to skin prompted a search for an effective decontaminant. A number of candidate materials were tested and found to be unsatisfactory. Rabbits and cats survived, however, when their skin was swabbed with a 2.8 per cent solution

Received June 2, 1958.
[1] Pharmacologist (Toxicology), Toxicology Division.
[2] Biologist, Toxicology Division.
[3] Enlisted Specialist (U.S. Army), Toxicology Division.

of ammonia water 15 minutes after application of four times the lethal dose of BHF.

Introduction

CURRENT interest in high energy propellant fuels has focused the attention of toxicologists on their potential hazard to health. The toxicities of the boron hydride fuels of the HEF-3 and HiCal class and procedures for their removal from the skin surface are the subjects of this report.

Borax and boric acid have long been known to be moderately toxic. Accidental deaths have occurred when boric acid was inadvertently administered to infants with their feeding formulas (1)[4] and when applied to extensive areas of skin in burn therapy (2,3,4). Krackow (5) has reported that decaborane, diborane and pentaborane are highly toxic compounds presenting a serious handling hazard by inhalation, oral ingestion and skin absorption. Other workers have reported on the toxicity of the boron hydrides (6,7,8,9).

Toxicity Studies

Toxicity studies were conducted on animals to find the LD50. This is the amount of material (in milligrams of fuel per kilogram of animal body weight) required to kill 50 per cent of the animals within a specified observation period, in this case, 24 to 48 hr. Intravenous and intraperitoneal toxicity experiments were carried out to ascertain the inherent toxicity of the fuels.

INTRAVENOUS TOXICITY The LD50 of BHF by intravenous injection was 13 mg/kg for rats and ranged from 4 to 6 mg/kg for rabbits. At these dosages, the animals were ataxic in 10 min, showed tonic and clonic convulsions in 15 to 20 min and prostration and death in 25 to 30 min.

INTRAPERITONEAL TOXICITY The LD50 of BHF by intraperitoneal injection ranged from 20 to 71 mg/kg for rats and 18 to 40 mg/kg for guinea pigs. In these animals, clonic convulsions were seen in 30 to 40 min and prostration followed by death in 45 to 120 min.

ORAL TOXICITY Oral toxicity was not directly measured, but an estimate of the toxicity of BHF by ingestion was obtained by administering the material into the stomach of rats by means of a flexible plastic tube. The LD50 was 40 ml/kg. Time of onset of toxic signs was somewhat longer by this route, clonic convulsions appearing in 3 to 4 hr and death in 3 to 5 hr.

INHALATION TOXICITY[5] The vapors of purified BHF are highly toxic, the LD50 being approximately 23 ppm for rats and 6 ppm for mice for a 4 hr exposure period.

EYE DAMAGE A very small amount (0.02 ml) of BHF was instilled into the eyes of normal rabbits. Five minutes later, the eyes were washed with physiological saline solution and examined daily for several weeks. All animals showed severe eye damage as characterized by iritis, conjunctival inflammation and edema, ulceration and corneal opacity. The opacity, which covered more than 75 per cent of the cornea, lasted longer than 16 days.

SKIN TOXICITY[6] BHF was applied to the skin of rats, guinea pigs, rabbits and cats. Local signs of poisoning appeared first. The skin immediately turned greyish-white at the site of application, where a vigorous reaction seemed to be taking place. Clonic convulsions appeared 3 to 6 hr later and death in 10 to 30 hr. LD50's were 317 to 502 mg/kg for rats, 158 to 251 mg/kg for guinea pigs, 57 to 105 mg/kg for rabbits and 126 mg/kg for cats.

Protection Offered by Rubber Gloves or Ointments

Experiments were performed to evaluate the protection afforded by surgical rubber gloves and protective skin creams. No evaluation was made of the protection afforded by heavier rubber or synthetic rubber gloves.

An application of 4 × LD50 (420 mg/kg) of BHF was made to the bare skin and to skin "protected" by a single layer of latex rubber from surgical gloves or by one of several silicone-containing ointments. In all cases, healthy clipped rabbits with intact skins were used. The unprotected animals died within 2 hr, the ointment-covered ones died in 3 to 48 hr and the rubber-covered ones in 72 to 96 hr, indicating that the toxic material eventually penetrated the ointment or the rubber. BHF caused the rubber to deteriorate to some extent, allowing penetration to occur during an overnight period of contact. All animals showed local signs of skin damage, convulsions and prostration prior to death. All control animals survived.

Skin Decontamination

Exploratory experiments were carried out on rabbits to screen a number of candidate skin decontaminants. Application of 4 × LD50 (420 mg/kg) of BHF was made on the back of each animal. Decontamination procedure[7] was carried out 30 sec later. Results, shown in Table 1, indicate a lack of effectiveness of most of the materials tested. The animals in this experiment generally showed signs of poisoning prior to death.

Table 1 Effect of candidate decontaminants after application of 4 × LD50 (420 mg/kg) of BHF to the skin of rabbits, exposure time: 30 sec

Candidate decontaminant	Approximate time of death(hrs)
none (controls)	1¾–2¾
water	1¾–2
acetone-alcohol (50–50)	1¾–2
cationic detergent (1 per cent triton X-400)	1¾–2
anionic detergent (1 per cent triton 300)	3–45
neutral detergent (1 per cent Tween)	2–5
gasoline	2–2¾
28 per cent tincture green soap—followed by water	48–116
sodium bicarbonate—5 per cent	2–3½
glycerine followed by sodium bicarbonate	1¼–27½
hard soap (castile)—followed by water	2½–3

Ammonia water was also tested as a decontaminant, based upon the fact that NH_3 reacts with decaborane to form hexaammoniates and diborane to form diammoniates. Results were encouraging; 29 out of 30 animals survived (Table 2). Even a weak solution (2.8 per cent) allowed 100 per cent recoveries, and none of the surviving animals showed local or systemic signs of poisoning. A yellow color appears when ammonia is applied to a contaminated area. This, it is presumed, is evidence of a chemical reaction.

Additional experiments were carried out to estimate the longest period of exposure which could be successfully decontaminated (Table 3). A 2.8 per cent solution (1:10 dilution of stock ammonium hydroxide) was selected as an effective, yet relatively nonirritating decontaminant. The results indicated that 4 × LD50 (420 mg/kg) can be decontaminated by a 2.8 per cent solution of ammonia water even after a 15 minute contact of BHF with the skin. Longer exposures prior to application of ammonia resulted in decreasing numbers of recoveries. All animals decontaminated with water after a 30 sec exposure died within 2 hr. Doubling the dose of BHF to 8 × LD50 (840 mg/kg) decreased the number of re-

[4] Numbers in parentheses indicate References at end of paper.

[5] The inhalation toxicity experiments were carried out by Leo Feinsilver, Gassing Branch, Chemical Warfare Laboratories.

[6] The high degree of skin toxicity might be better visualized if one were to convert mg to fl oz and extrapolate to humans. Thus, if BHF is as toxic to man as to rabbits, the LD50 for a 150 lb man would amount to ¼ oz.

[7] The procedure consisted in flushing with approximately 1300 ml of decontaminant while swabbing vigorously with cotton.

Table 2 Decontaminating effect of ammonia water after application of 4 × LD50 (420 mg/kg) of BHF to the skin of rabbits, exposure time: 30 sec

Agent	No. of animals	Decontaminant	Approximate time of death (hr) 24	48	72	96	120	144	168	No. of recoveries
BHF	10	14 per cent solution ammonia water	0	0	0	0	1	0	0	9
BHF	10	7 per cent solution ammonia water	0	0	0	0	0	0	0	10
BHF	10	2.8 per cent solution ammonia water	0	0	0	0	0	0	0	10
BHF	2	none	1	1	...	...	...	...	...	0
none	6	none	0	0	0	0	0	0	0	6

coveries somewhat, and 16 × LD50 (1680 mg/kg) reduced the number substantially.

Table 3 Decontaminating effect of 2.8 per cent ammonia water after application of 4 × LD50 (420 mg/kg) of BHF to the skin of rabbits

Agent	No. of animals	Exposure time (min)	Decontaminant	No. of recoveries
BHF	6	0.5	2.8 per cent solution NH_4OH	6
BHF	6	1.0	"	6
BHF	6	1.5	"	6
BHF	6	2	"	6
BHF	6	3	"	6
BHF	6	5	"	6
BHF	6	10	"	6
BHF	6	15	"	6
BHF	6	30	"	4
BHF	6	45	"	2
BHF	6	0.5	water	0
none	6	...	2.8 per cent solution NH_4OH	6

Studies with cats indicate that they can also be effectively decontaminated with ammonia.

Studies of the Decontaminating Action of Ammonia

BHF was mixed with an excess of ammonia water in test tubes and allowed to react for about 30 min. These mixtures were injected into the peritoneal cavity of guinea pigs or applied to the skin of rabbits. The resulting LD50's showed no decrease in lethality by these routes. It appears then that the addition of ammonia to the fuel may produce a reaction product, which although toxic and capable of penetrating skin, can be easily washed away.

Discussion

Boron hydrides of the HEF-3 and HiCal class are compounds which have a relatively high degree of toxicity by all the practical routes of entry into the body. Hence, it is necessary to take suitable measures to prevent accidental exposures, as for example, protective clothing. The area of operation should be well ventilated and protective masks readily available in the event of a spill. If, however, the skin does get splashed, immediate action is required. A simple application of ammonia water to the contaminated area is not sufficient, since the reaction product is toxic when left on skin. Copious flushing, along with swabbing is essential to remove the toxic material. Goggles should be worn to prevent splashing of the eyes with the ammonia water.

First Aid Decontamination Procedures

Immediate action is required in treating victims of accidental skin contamination with BHF. The following procedure is suggested:

1 Assure that both the victim and the person ministering to him are wearing goggles.

2 Flush contaminated skin with large amounts of 2.8 per cent ammonia water solution (preferably from a spray attachment) while swabbing vigorously with a ball of cotton or a sponge attached to a long holder.

3 Continue washing affected and adjacent areas until all of the BHF has been removed (at least 5 min).

4 Rinse thoroughly with a plain water shower to remove ammonia solution.

5 Follow up with soap and water, if available.

6 Report to plant physician for examination.

Conclusions

On the basis of the work described herein, it is concluded that:

1 Boron hydride fuels of the HEF-3 and HiCal class are highly toxic materials which present a serious health hazard by inhalation, oral ingestion, ocular contact and skin absorption.

2 A dilute solution (2.8 per cent) of ammonia water as a flushing agent is effective in removing these fuels from the skin of animals used in experiments; hence it is presumed to be effective for man.

3 Surgical glove material and the silicone-containing ointments used in this study provide only a limited degree of protection against BHF, the former being more effective than the ointments.

References

1 McNally, Wm. D. and Rust, C. A., "The Distribution of Boric Acid in Human Organs in Six Deaths Due to Boric Acid Poisoning," *Journal of the American Medical Association*, vol. 90, 1928, pp. 382–383.

2 Gettler, A. O. and St. George, A. V., "Toxicology in Children," *American Journal of Clinical Pathology*, vol. 5, 1935, p. 466.

3 Gissel, H., "Toxicity of Boric Acid," *Quart. Journal of Pharmacology* vol. 16, 1933, p. 714.

4 Kunkel, A. ., "Literature Survey on Toxicity of Boric Acid and Sodium Tetraborate (Borax)," Chem. Corps Medical Labs Special Report no. 2, Sept. 1950.

5 Krackow, E. H., "Toxicity and Health Hazards of Boron Hydrides," *AMA Archives of Industrial Hygiene and Occupational Medicine*, vol. 8, 1953, pp. 335–339.

6 Lowe, Harry J. and Freeman, Gustave, "Boron Hydride (Borane) Intoxication in Man," *AMA Archives of Industrial Health*, vol. 16, no. 6, Dec. 1957.

7 Long, J. E., Levinskas, G. J., Hill, W. H., and Svirbely, J. L., "Gas Mask Protection Against Diborane, Pentaborane, and Mixtures of Boranes," *AMA Archives of Industrial Health*, vol. 16, no. 5, Nov. 1957.

8 Wills, J. H., "Toxicity and Pharmacology of Boron Hydrides," MDSR no. 15, Army Chemical Center, Md., 1953.

9 Svirbely, J. L., "Acute Toxicity Studies of Decaborane and Pentaborane by Inhalation," *AMA Archives of Industrial Health*, vol. 10, 1954, pp. 298–304.

Technical Comments

Possibility of Aerodynamic Descent on the Moon

LANCE W. SMALL[1]

RECENT investigations of Elsmore[2] by use of radio astronomy have noticed an effect at certain wave lengths which implies refraction at the lunar disk. This refraction may be explained by assuming an atmospheric pressure of 10^{-12} atm on the moon. In this connection, Borst and Edwards[3] have suggested that such an atmosphere may be composed of the rare gases krypton and xenon.

If it were possible to glide into the moon without the excessive use of rocket braking, the vehicle used would either be smaller than those now planned or could utilize the power needed for braking for the trip home.

How does the lunar atmosphere compare with ours? Observations of Sputnik I have revealed that the ARDC atmosphere is too small by a factor of 40. This means that a satellite with a perigee altitude of 400 km initially will have its lifetime reduced by a factor of 40. Note that this applies to 400 km. The atmospheric pressure at 400 km would be $1.44 \times 10^{-8} \times 40$, that is, 5.8×10^{-9} millibars. On the moon the pressure would amount to 10^{-9} millibars. Therefore, the lunar atmosphere provides a greater drag by a factor of 5.

Also, if the mass of the lunar rocket is 10^4 greater than that of Sputnik I, the ballistic drag coefficient (mass/$Cd \times$ area where Cd is the drag coefficient) will be greater by a factor of 10^3. Thus, we have the possibility of aerodynamic descent on the moon. Of course, a winged vehicle would be better able to accomplish this.

Received March 24, 1958.

[1] Student, Roosevelt High School, Yonkers. Student Member ARS.

[2] Elsmore, B. and Whitfield, G., *Nature*, vol. 176, 1955, p. 457.

[3] Borst, L. and Edwards, W., *Science*, vol. 127, 1958, p. 325.

Solar Sailing—Practical Problems

S. W. GREENWOOD[1]

College of Aeronautics, Cranfield, England

IN A recent Technical Note, Garwin (1)[2] considers the solar radiation forces acting on sails in space, and accelerations theoretically possible with sails of given area and vehicles of given mass. As a result of his analysis he concludes that solar sailing is a practical method of propulsion within the solar system. In his examples he selects a thin sail made of plastic and aluminized on one side. It seems to me that before the method can be assessed as practical it is necessary to consider the following problems:

1 If all the incident solar radiation is reflected to produce maximum thrust, the temperature of the sail would on many occasions fall to near absolute zero owing to the radiation of energy from the shadow side. The problems arising here are the suitability of the material for operation at low temperatures, and effects produced by temperature cycling as the sail is furled and unfurled.

2 The sail is exposed to cosmic radiation, meteorite bombardment and the full spectrum of solar radiation. The material of the sail must be suitable for prolonged exposure to these conditions.

3 On occasions when the shadow side is emitting radiation, there is a force exerted on the sail opposite in direction to that produced by solar radiation.

Received May 5, 1958.

[1] Lecturer, Department of Aircraft Propulsion. Member ARS.

[2] Number in parentheses indicates Reference at end of paper.

Reference

1 Garwin, Richard L., "Solar Sailing—A Practical Method of Propulsion Within the Solar System," JET PROPULSION, vol. 28, March 1958, p. 188.

A Remark on an Iterative Method of Determining Equilibrium Compositions of Reacting Gases

J. L. SACKMAN[1]

Columbia University, New York, N. Y.

IN A recent article in this JOURNAL (1),[2] an iteration procedure for obtaining the roots of a system of simultaneous equations governing the equilibrium compositions of reacting gases was presented. It should be noted that the numerical procedure there presented is in reality an application of a method which has been well known in the field of numerical computations for a considerable period of time. It is commonly referred to as "the Newton method of approximation" (2). This method, as presented in (2), is briefly reviewed here for the special case of two simultaneous equations.

The roots of the simultaneous equations $F(x, y) = 0$ and $G(x, y) = 0$ are desired. Starting with an approximation $(x^{(n)}, y^{(n)})$, the next approximation $(x^{(n+1)}, y^{(n+1)})$ is determined in the following manner

$$x^{(n+1)} = x^{(n)} + \delta x^{(n)} \qquad y^{(n+1)} = y^{(n)} + \delta y^{(n)} \quad [1]$$

where $\delta x^{(n)}$ and $\delta y^{(n)}$ are obtained from the two simultaneous linear algebraic equations

$$\delta x^{(n)} F_{,x}(x^{(n)}, y^{(n)}) + \delta y^{(n)} F_{,y}(x^{(n)}, y^{(n)}) = -F(x^{(n)}, y^{(n)}) \quad [2]$$

$$\delta x^{(n)} G_{,x}(x^{(n)}, y^{(n)}) + \delta y^{(n)} G_{,y}(x^{(n)}, y^{(n)}) = -G(x^{(n)}, y^{(n)}) \quad [3]$$

The comma symbol denotes partial differentiation with respect to the indicated variable.

Consider now the system of Equations [1 to 6] of (1).

$$\sum_{i=1}^{6} p_i - p = 0 \quad [4]$$

$$(1 - 2\beta)p_{H_2O} + 2p_{O_2} - 2\beta p_{H_2} + (1 - \beta)p_{OH} + p_O - \beta p_H = 0 \quad [5]$$

$$p_O(p_{O_2})^{-1/2} = K_O \quad [6]$$

$$p_H(p_{H_2})^{-1/2} = K_H \quad [7]$$

$$p_{H_2}(p_{O_2})^{1/2}\,(p_{H_2O})^{-1} = K_{H_2O} \quad [8]$$

$$p_{OH}(p_{H_2})^{1/2}\,(p_{H_2O})^{-1} = K_{H_2O}^* \quad [9]$$

It is clearly seen that by using [6 to 9] to express four of the partial pressures in terms of the remaining two, this system of equations can immediately be reduced to one involving two simultaneous equations in two unknowns. To parallel

Received April 30, 1958.

[1] Instructor, Dept. of Civil Engineering, Institute of Flight Structures. Student Member ARS.

[2] Numbers in parentheses indicate References at end of paper.

the choice made in (1), p_{H_2O} and p_{O_2} are selected as the primary unknowns, and then [6 to 9] yield

$$p_O = K_O(p_{O_2})^{1/2} \quad [10]$$

$$p_{H_2} = K_{H_2O}p_{H_2O}(p_{O_2})^{-1/2} \quad [11]$$

$$p_H = K_H(K_{H_2O})^{1/2}\,(p_{H_2O})^{1/2}\,(p_{O_2})^{-1/4} \quad [12]$$

$$p_{OH} = K_{H_2O}{}^*(K_{H_2O})^{-1/2}\,(p_{H\,O})^{1/2}\,(p_{O_2})^{1/4} \quad [13]$$

In view of [10 to 13], Equations [4 and 5] may be written as

$$F(p_{H_2O}, p_{O_2}) = \sum_{i=1}^{6} p_i - p = 0 \quad [14]$$

$$G(p_{H_2O}, p_{O_2}) = (1 - 2\beta)p_{H_2O} + 2p_{O_2} - 2\beta p_{H_2} + (1 - \beta)p_{OH} + p_O - \beta p_H = 0 \quad [15]$$

It is now desired to locate the point of intersection of the two plane curves $F = 0$ and $G = 0$, and to this end Newton's method, as previously discussed, is employed. To utilize Equations [2 and 3] it is required to obtain F,p_{O_2}, F,p_{H_2O}, G,p_{O_2}, G,p_{H_2O}. These quantities are readily obtained from [14 and 15] and [10 to 13] by simple partial differentiation. For example

$$F,p_{H_2O} = \frac{\partial p_{H_2O}}{\partial p_{H_2O}} + \frac{\partial p_{O_2}}{\partial p_{H_2O}} + \frac{\partial p_{H_2}}{\partial p_{H_2O}} + \frac{\partial p_{OH}}{\partial p_{H_2O}} + \frac{\partial p_O}{\partial p_{H_2O}} + \frac{\partial p_H}{\partial p_{H_2O}} - \frac{\partial p}{\partial p_{H_2O}}$$

$$= 1 + 0 + \frac{p_{H_2}}{p_{H_2O}} + \frac{1}{2}\frac{p_{OH}}{p_{H_2O}} + 0 + \frac{1}{2}\frac{p_H}{p_{H_2O}} - 0 = A \quad [16]$$

In like manner

$$F,p_{O_2} = B \qquad G,p_{H_2O} = C \qquad G,p_{O_2} = D \quad [17]$$

It is also noted that

$$G(p_{H_2O}, p_{O_2}) = -E \quad [18]$$

where A, B, C, D, E are quantities defined in (1). (The expressions for C, D, E given in (1) appear to be in error. Assuming Equation [2] of (1) is correct, the multiplier in parentheses before p_{OH} should be $(1 - \beta)$ instead of $(1 - 2\beta)$ as is shown in (1) for C, D, E.)

These results are utilized in [1 to 3] to yield

$$p_{H_2O}^{(n+1)} = p_{H_2O}^{(n)} + \delta p_{H_2O}^{(n)} \qquad p_{O_2}^{(n+1)} = p_{O_2}^{(n)} + \delta p_{O_2}^{(n)} \quad [19]$$

$$A^{(n)}\delta p_{H_2O}^{(n)} + B^{(n)}\delta p_{O_2}^{(n)} = p - \sum_{i=1}^{6} p_i^{(n)} \quad [20]$$

$$C^{(n)}\delta p_{H_2O}^{(n)} + D^{(n)}\delta p_{O_2}^{(n)} = E^{(n)} \quad [21]$$

It is seen that [20 and 21] are exactly the Equations [22 and 23] of (1), thereby demonstrating that the method proposed in (1) is in actuality a specific application of Newton's method to the particular system of equations considered in (1). A discussion concerning convergence of Newton's method may be found in (2).

References

1 Chu, S. T., "An Iterative Method of Determining Equilibrium Compositions of Reacting Gases," Jet Propulsion, vol. 28, no. 4, April 1958, p. 252.

2 Willers, Fr. A., "Practical Analysis," Dover Publications, New York, 1948, pp. 223–225.

On a Generalized Optimization Procedure for N-Staged Missiles

M. ARENS[1]

Israel Institute of Technology, Haifa, Israel

REFERENCE (1)[2] established the general relation between weights of consecutive stages of a missile in drag-free space so that the launching weight be a minimum. It might be worth noting that the solution is implicitly contained in (2) where the more difficult problem of acceleration-limited stages is treated.

Using the notation of (1), the minimal solution must satisfy Equation [15] of (2), which with no restrictions on the permissible acceleration takes the form

$$\frac{M_{g_1}}{\bar{M}} \cdot \frac{M_{g_2}}{M_{g_1}} + \eta \frac{\partial\phi}{\partial\left(\frac{M_{g_1}}{M_{g_2}}\right)} = 0 \quad [1]$$

$$\frac{M_{g_1}}{\bar{M}} \cdot \frac{M_{g_3}}{\bar{M}_{g_2}} + \eta \frac{\partial\phi}{\partial\left(\frac{M_{g_2}}{M_{g_3}}\right)} = 0 \quad [2]$$

$$\frac{M_{g_1}}{\bar{M}} \cdot \frac{M}{\bar{M}_{g_N}} + \eta \frac{\partial\phi}{\partial\left(\frac{\bar{M}_{g_N}}{M}\right)} = 0 \quad [N]$$

$$\phi = \sum_{n=1}^{N} C_n \ln \frac{\frac{M_{g_n}}{M_{g_{n+1}}}}{1 - k_n + K_n \frac{M_{g_n}}{M_{g_{n+1}}}} - G = 0 \quad [N+1]$$

By solving for the Lagrangian multiplier η one obtains

$$\frac{M_{g_n}}{M_{g_{n-1}}} = \frac{C_{n-2}\,K_{n-1}\,(1 - K_{n-2})}{(1 - K_{n-2})\,(1 - K_{n-1})\,(C_{n-1} - C_{n-2}) + C_{n-1}\,K_{n-2}(1 - K_{n-1})} \frac{M_{g_{n-2}}}{M_{g_{n-1}}}$$

which is identical with Equation [13] of (1).

References

1 Weisbord, Leon, "A Generalized Optimization Procedure for N-Staged Missiles," Jet Propulsion, vol. 28, 1958, pp. 164–167.

2 Schurmann, Ernest E. H., "Optimum Staging Technique for Multistaged Rocket Vehicles," Jet Propulsion, vol. 27, 1957, pp. 863–865.

Received May 7, 1958.

[1] Research Associate, Department of Aeronautical Engineering.

[2] Numbers in parentheses indicate References at end of paper.

Comment on "A Practical Approach to Grain Design"

J. A. VANDENKERCKHOVE[1]

Université de Bruxelles, Brussels, Belgium

IN HIS interesting paper, Stone (1)[2] has proposed a method for the design of internal burning stars. This method is

Received June 24, 1958.

[1] Assistant. Consultant of the Poudreries Reunies de Belgique.

[2] Numbers in parentheses indicate References at end of paper.

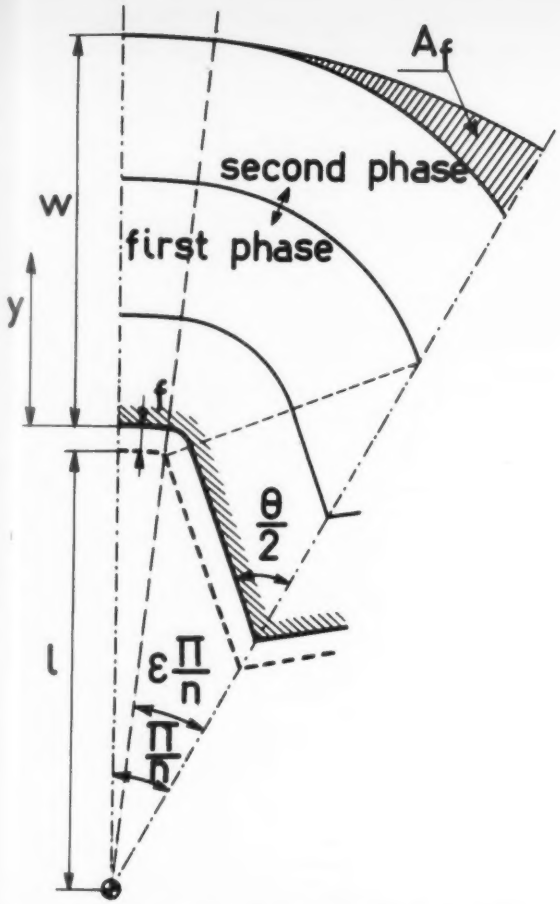

Fig. 1 Definitions of the design parameters of an internal burning star

limited to well-defined values of certain parameters (the fillet radius for instance) and does not take advantage of a few basic properties:

1 The fillet radius must not necessarily be imposed. Indeed, in view of the evolving nature of the combustion, the star with a fillet is identical to the star without a fillet which would have burnt on a distance equal to the fillet radius.

2 The star points are often cut at the outer diameters to increase the web or the port area and, overall, to reduce the sliver fraction. The amount cut can be expressed by the parameter ϵ defined on Fig. 1 (Stone is only concerned with the case $\epsilon = 1$.) This solution is of particular interest when tapered port areas are used.

3 The problem is complicated by taking the characteristic length equal to the grain outer diameter.

Indeed, for the same internal perforation, the web can be increased without changing the beginning of the thrust-time curve. By doing so in a region where the star points have disappeared, one generally introduces an increasing progressivity which fortunately can be easily neutralized by tapering the grain at the outer diameters.

Therefore a whole family of curves given by Stone can be replaced by one single curve independent of the fillet radius and of the web thickness, if the maximum radius of the basic perforation is taken as the characteristic length. Such a curve readily gives the variation of the burning area during combustion. In view of these remarks it seems possible to propose a much more general solution which is summarized in Figs. 1 to 4.

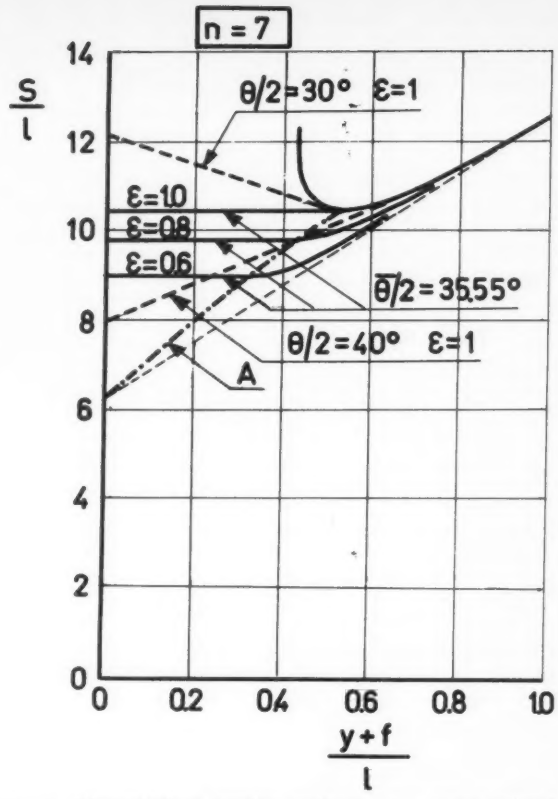

Fig. 2 Dimensionless burning perimeter of a seven-pointed star as a function of the reduced burnt distance

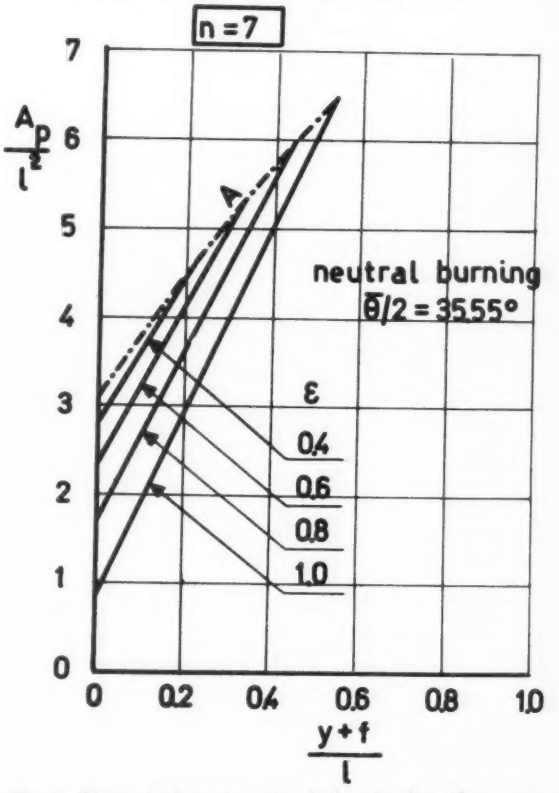

Fig. 3 Dimensionless port area during the first phase as a function of the reduced burnt distance. (Seven-pointed star and neutral first phase)

Table 1 Internal burning star

For $\dfrac{y+f}{l} \leq \dfrac{\sin \epsilon \dfrac{\pi}{n}}{\cos \dfrac{\theta}{2}}$ and $\dfrac{\theta}{2} \geq \epsilon \dfrac{\pi}{n}$

burning perimeter $$\frac{S}{l} = 2n\left[\frac{\sin \epsilon \frac{\pi}{n}}{\sin \frac{\theta}{2}} + \frac{y+f}{l}\left(\frac{\pi}{2} + \frac{\pi}{n} - \frac{\theta}{2} - \cot \frac{\theta}{2}\right) + (1-\epsilon)\frac{\pi}{n}\right]$$

neutral burning for $$\frac{\pi}{2} + \frac{\pi}{n} = \frac{\bar{\theta}}{2} + \cot \frac{\bar{\theta}}{2}$$

initial port area

$$\frac{A_p}{l^2} = n \sin \epsilon \frac{\pi}{n}\left[\cos \epsilon \frac{\pi}{n} - \sin \epsilon \frac{\pi}{n} \cot \frac{\theta}{2}\right] + (1-\epsilon)\pi + 2n\frac{f}{l}\left[\frac{\sin \epsilon \frac{\pi}{n}}{\sin \frac{\theta}{2}} + (1-\epsilon)\frac{\pi}{n} + 0.5\frac{f}{l}\left(\frac{\pi}{2} + \frac{\pi}{n} - \frac{\theta}{2} - \cot \frac{\theta}{2}\right)\right]$$

For $$\frac{y+f}{l} \geq \frac{\sin \epsilon \frac{\pi}{n}}{\cos \frac{\theta}{2}}$$

burning perimeter

$$\frac{S}{l} = 2n\left\{\frac{y+f}{l}\left[\frac{\pi}{n} + \sin^{-1}\left(\frac{l}{y+f} \sin \epsilon \frac{\pi}{n}\right)\right] + (1-\epsilon)\frac{\pi}{n}\right\}$$

final losses

$$\frac{A_f}{l^2} = \epsilon\pi\left(1 + \frac{y+f^2}{l}\right) - n\left\{\sin \epsilon \frac{\pi}{n}\left[\sqrt{\left(\frac{y+f}{l}\right)^2 - \sin^2 \epsilon \frac{\pi}{n}} + \cos \epsilon \frac{\pi}{n}\right] + \left(\frac{y+f}{l}\right)^2\left[\epsilon \frac{\pi}{n} + \sin^{-1}\left(\frac{l}{y+f} \sin \epsilon \frac{\pi}{n}\right)\right]\right\}$$

$$\sigma_f = \frac{\dfrac{A_f}{l^2}}{\pi\left(1 + \dfrac{y+f}{l}\right)^2 - \dfrac{A_{pi}}{l^2}}$$

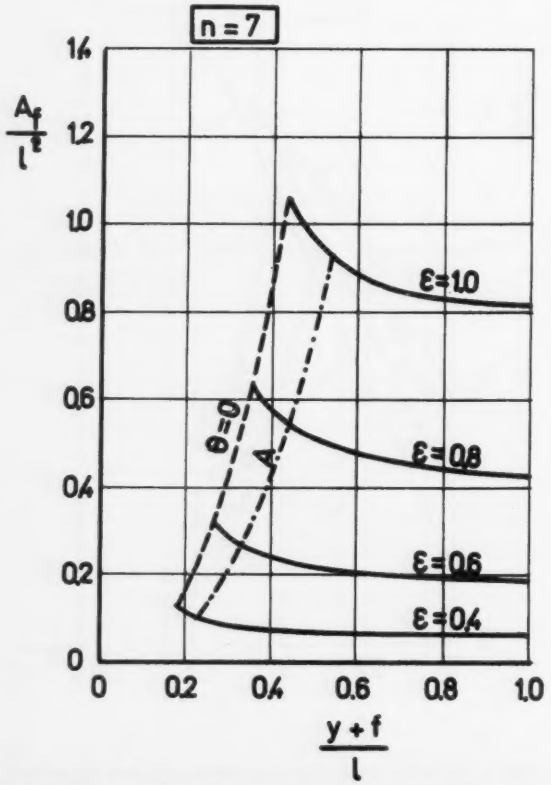

Fig. 4. Dimensionless sliver area of a seven-pointed star as a function of the reduced burnt distance

Fig. 1 represents a sector of an internal burning star, with the symbols defined. Table I gives the resulting equations which can be easily solved with a desk computer. The port area equation which is of particular interest for the grain designer is given rather than the loading fraction equation which is a byproduct. Figs. 2, 3 and 4 represent vs. the burnt distance y plus the fillet radius f, the burning perimeter S, the port area A_p during the first phase (during which the star points have not disappeared) and the final sliver area A_f during the second phase. These curves are given in a dimensionless form for different values of ϵ, in the case of the seven-pointed star ($n = 7$). Fig. 3 has been calculated for neutral burning during the first phase. Fig. 2 also represents in the case $\epsilon = 1$ a regressive and a progressive solution (in dotted lines) obtained by taking $\theta \neq \bar{\theta}$ during the first phase. The burning perimeter S varies linearly vs. y during the first phase and tangentially joins the curve describing the second phase (this curve is fully drawn in the case $\epsilon = 1$). Finally, the curve A represents the limit between the first and second phases for neutral burning during the first phase.

We believe that the method summarized above gives a simple, clear and useful picture which provides a maximum amount of information with the minimum number of graphs. The method can be readily extended in the case of the so-called wagon wheel design. A complete set of charts for n ranging from 3 to 12 has been prepared under an ARDC contract (2).

References

1 Stone, Max W, "A Practical Mathematical Approach to Grain Design," JET PROPULSION, vol. 28, no. 4, April 1958, pp. 236–244.

2 Vandenkerckhove, J., "Optimum Design of Solid Propellant Rockets," Université de Bruxelles: ARDC contract S.61(052) 58-13.

A Comment on Combustion Instability in Solid Propellant Rocket Motors

L. GREEN Jr.[1]
Aerojet-General Corp., Azusa, Calif.

and

W. NACHBAR[2]

Lockheed Aircraft Corp., Sunnyvale, Calif.

IN THEIR recent note describing experiments with a closed-end, tubular research burner, Price and Sofferis (1)[3] reported a "contention" of one of the writers to the effect that: "Changes in burning rate during unstable performance are favored by conditions of high quasi-steady stream velocity in the conduit of the burner." This report requires correction. On one hand, experience has been cited (2) that (other factors, such as mean chamber pressure, being constant) gross reaction irregularities (i.e., secondary peaks in the low response pressure vs. time history manifesting an increased propellant burning rate) generally tended to increase in severity and frequency of occurrence as the gas velocity leaving the aft end of side-burning charges was increased; i.e., as the throat to port area ratio was increased. It was surmised (2) that this effect might be attributed to the excitation and/or partial sustenance of combustion oscillations by fluid dynamically excited sound resulting from high velocity flow across a channel discontinuity, a possibility also noted by Price and Sofferis.

On the other hand, analytical results (2,3) indicate that a change in mean burning rate is favored by a high magnitude of both the mean value and the amplitude of the periodically fluctuating component of a parameter group involving the ratio $\rho_1 v_1/l$ (where ρ_1 is the chamber gas density, v_1 is the parallel stream velocity and l is a length parameter identified with the distance from the stream stagnation point to the station in question). This implies that changes in mean burning rate are consequently favored by a high mean value and by a high amplitude, in-phase fluctuation of gas pressure and of stream-wise velocity *gradient* as distinguished from a high stream velocity. These conditions would appear in the region of a stagnation point. This result is consistent with observations that the areas of locally excessive propellant burning rate, as revealed by interrupted burning experiments with conventional motors, are found near the stagnation point of the flow system. The analytical results do not conflict with the experimental observations of Price and Sofferis, which was the interpretation given (1), but are in agreement with their experiments, which showed that the observed instances of pronounced oscillations and changes in burning rate corresponded to instances of gas phase oscillation in those modes where the velocity nodes (and hence anti-nodes of pressure and axial velocity gradient) were located at or adjacent to burning propellant surfaces.

Recent observations by Price and Sofferis and others indicate that, under some conditions, gas phase oscillations can effect a *decrease* in mean propellant burning rate. This possibility has been considered in a re-examination of the behavior of the simplified analytical model (4). A principal assumption involved in the model is that the burning rate is an Arrhenius function of the surface temperature: $r = B \exp(-E/RT_s)$. The r vs. T_s curve is thus S-shaped, with zero slope at $T_s = 0$ and $T_s = \infty$, and with an inflection point at $T_s = E/2R$. For $T_s < E/2R$ the curvature is concave upward, for $T_s > E/2R$ it is concave downward. In the numerical example previously examined (3), the assumed values (taken as characteristic of a high energy, fast burning propellant) of $B = 100$ cm/sec and $E = 11{,}900$ cal/mole yielded a steady-state value of $T_{so} = 1150$ K. In this case $E/RT_{so} = 5.2$, and any fluctuations in T_s around this value of T_{so} (located in the region of upward concavity of the nonlinear Arrhenius curve) would effect an increase in mean burning rate, as averaged over a complete cycle.

However, if a different set of parameters (such as might characterize a slow burning but easily "activated" propellant of high flame temperature) were chosen, for example $E = 6000$ cal/mole and B small enough that the steady-state surface temperature is high enough to fall in the region of downward concavity (e.g., $T_{so} > 1500$ K), then oscillations in T_s about this value would effect a decrease in mean burning rate. The writers wish to emphasize this possibility here, since it was not noted in the original analysis (3) of the simplified model behavior.

Received Aug. 20, 1958.

[1] Head, Applied Research, Rover Projects. Member ARS.

[2] Head Applied Mechanics Section, Aerodynamics, Missile Systems Division.

[3] Numbers in parentheses indicate References at end of paper.

References

1 Price, E. W. and Sofferis, J. W., "Combustion Instability in Solid Propellant Rocket Motors," JET PROPULSION, vol. 28, 1958, pp. 190–192.

2 Green, L., Jr., "Observations on the Irregular Reaction of Solid Propellant Charges," JET PROPULSION, vol. 23, 1956, pp. 655–659.

3 Green, L., Jr., "Some Properties of a Simplified Model of Solid-Propellant Burning," JET PROPULSION, vol. 28, June 1958, p. 236.

4 Nachbar, W. and Green, L., Jr., "Analysis of a Simplified Model of Solid Propellant Resonant Burning," to be submitted for publication.

High Temperature Chemistry as Applied to Metal-Based Propellants

JOHN S. GORDON[1]

Thiokol Chemical Corp., Denville, N. J.

THE "last frontiers" of rocket propellant chemistry are high energy oxidizers and novel fuel structures containing light metals. These materials may find application in both liquid and solid rocketry. High energy oxidizers will contain oxygen and fluorine and as few other elements as possible; their combustion products are already well-known. Such is not the case (in varying degrees) for the combustion products of the light metals lithium, beryllium, boron, magnesium and aluminum. The status of these fuel elements may be summarized briefly.

Lithium: Excellent performance with fluorine-based oxidizers. Not outstanding with oxygen oxidizers. Density unattractive.

Beryllium: Performance probably excellent. High flame temperatures. Toxicity unattractive.

Boron: Extremely desirable in liquid fuels and solid fuel, binders. Complex combustion products due to trivalence.

Magnesium: Probably mediocre due to high atomic weight but no conclusive data yet.

Aluminum: Very attractive additive when oxidized by hydrogen peroxide or ammonium perchlorate, due to high heat of combustion to liquid Al_2O_3. Attractive density.

Silicon and higher: Poor energetics. Useful as central atoms in building novel molecular structures. Attractive densities occasionally occur.

The reduction-to-practice of these propellant families is being hindered by poor knowledge of the thermodynamic properties, heats of formation and molecular constants of the products of combustion of the metals in question. Improved

Received Aug. 20, 1958.

[1] Group Leader, Thermochemistry and Propellants Liaison, Chemistry Department, Reaction Motors Division. Member ARS.

data would be useful on the following gaseous species:

Li_2O, LiOH, LiO, LiCl, Li_2Cl_2, $Li_2(OH)_2$

BeO, BeF_2, $BeCl_2$, BeFCl, BeCl and corresponding Mg compounds

B_2O_2, HBO_2, $H_2B_2O_4$, H_3BO_3, OBF, OBCl, BF_2, BCl_2, FBCl, B_4O_5, $H_2B_4O_7$

Al_2O_2, Al_2O, AlO, $AlCl_2$, $AlCl_3$, Al_2Cl_2, AlF_2, AlF_3, AlF_2Cl, $AlFCl_2$, OAlCl, OAlF, AlC, AlN, $LiAlF_4$, $LiAlCl_4$

There is no present evidence for the gaseous HOAlO molecule, but this should be checked further. Work has been done in the Na_2O and NaOH liquid-vapor systems, and this should be extended to Li systems. Studies are also underway on determining unequivocally the structure and molecular constants of B_2O_3 and B_2O_2 gases. Most of this type of work is properly being done at universities and fundamental research institutions, because of the advanced techniques and interpretative thinking required.

Improved fundamental data along the lines suggested here will improve the reliability of the theoretical performance analyses being made by various agencies.

New Patents

George F. McLaughlin, *Contributor*

Control of reheat in turbojet engines (2,844,936). H. S. Fowler and D. A. J. Millar, Cyrville, Ontario, Canada, assignors to National Research Council.

Automatic variation of the nozzle area opening by an amount theoretically necessary to maintain the velocity of gases passing through the nozzle at a constant value.

Jet engine control (2,844,937). S. J. Mikina, Pittsburgh, Pa., assignor to the U. S. Navy.

Device for operating a fuel supply and a potentiometer for temperature control in response to the force of pressure from the compressor in excess of a predetermined pressure.

Fuel pressuring system for supersonic ramjet (2,844,938). J. P. Longwell, Scotch Plains, N. J., assignor to the U. S. Navy.

Projectile with outer and inner walls forming a tubular duct containing a diffuser. A compressible wall is located between the inner and outer walls, and a fuel chamber is defined by the diffuser wall and compressible wall. Vapor pressure compresses the compressible wall and forces fuel into the duct.

Tube-bundle combustion chamber (2,844,939). F. E. Schultz, Scotia, N. Y., assignor to General Electric Co.

Tubes secured together to form a hollow combustion chamber surrounded by a rubber coating forming a fluid impervious layer for preventing leakage of combustion gases between tubes. A binding means surrounds the coating for keeping it in contact with the tubes and for maintaining them in a predetermined shape.

Noise suppressors for jet engines (2,845,775). J. M. Tyler and R. E. Meyer, Glastonbury, Conn., assignors to United Aircraft Corp.

Hollow vanes, having large apertures on one side and small apertures in another. Vanes are rotatably mounted from movement in a clustered position downstream of an inner body within a jet engine tailpipe, outwardly to present the large apertures to the gas passage.

Protective device for jet engines (2,846,023). V. Milliman, San Diego, Calif., assignor to General Dynamics Corp.

Inlet for filtering foreign material from air entering a jet engine, consisting of a chamber with a top wall formed of coarser mesh than the other walls.

Vertical take-off and landing aircraft (2,846,164). E. Haberkorn, Dammarie-les-Lys, France, assignor to SNECMA Co.

Annular wing with flaps along the trailing edge pivotable to a retracted or extended position from both the outer and inner wing surfaces. Some of the flaps may be displaced longitudinally toward the trailing edge to form supports for the aircraft on the ground.

Impregnated ferrite (2,846,655). A. H. Iversen, Santa Monica, Calif., assignor to Hughes Aircraft Co.

Microwave ferrite element impregnated with a vitreous material along a predetermined direction so that the element is bonded and hermetically sealed at its surface.

Variable area convergent-divergent exhaust nozzle (2,846,843). D. B. Clark, G. S. Kelley and W. W. Mahnken, Union City, N. J., assignors to Curtiss-Wright Corp.

Regulation of the nozzle area so that increase in total pressure of the exhaust gases and decrease in static pressure of the surrounding atmosphere both effect an opening adjustment of the nozzle exit.

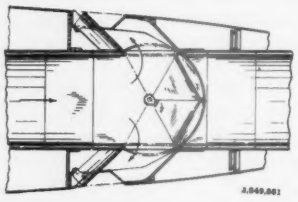

Aircraft reaction propulsion units (2,849,861). J. Gardiner and J. S. Wallett, Allestree, England, assignors to Rolls-Royce, Ltd.

Propulsion nozzle at the outlet of a jet pipe porting upstream to auxiliary ducting inclined forward to the flight direction to an outlet to the atmosphere. Gas flowing through the auxiliary duct produces a braking effect on the aircraft.

Variable area thrust deflector-augmenter for jet engines (2,846,844). N. W. O'Rourke, LaJolla, Calif., assignor to The Ryan Aeronautical Co.

Nozzle having complementary elements shiftable to vary the area of the primary orifice. Direction controlling deflectors, pivotally mounted, define a secondary orifice. The deflectors are connected to move the primary and secondary orifices in cross-sectional area.

Fuel system for gas turbine engines (2,846,846). F. C. Mock, South Bend, Ind., assignor to Bendix Aviation Corp.

Control of the rate of fuel feed to a gas turbine having means for avoiding compressor instability. Fuel is metered at a rate proportional to compressor inlet pressure and temperature. Effects of temperature on the rate of fuel feed are modified in the intermediate speed range.

Zero-length launcher (2,843,020). V. B. Bertagna and J. J. Pfarr, Inglewood, Calif., assignors to Northrop Aircraft, Inc.

Device for launching a missile. A frame structure spaced on a base and permitting a vehicle supporting a missile to advance within a passageway so the frame can be lowered to position for launching.

Angle mounted tip engine for aircraft sustaining rotor (2,843,210). R. K. Grove, Grosse Pointe Farms, Mich., assignor to Studebaker-Packard Corp.

Tip mounted aerodynamic pod secured to a propelling blade and enclosing a gas turbine. The exhaust discharge in a jet opening in the bottom of the pod is set in a direction rearward and slightly downward so as to produce a thrust having a positive blade twisting moment.

Composite aircraft system and method of flight (2,843,337). J. A. J. Bennett, San Mateo, Calif., assignor to Hiller Helicopters.

Rotary wing aircraft tug with jet engines at the rotor tips, and hollow legs and mechanism for detachable connection to a fixed wing aircraft. Landing of the composite aircraft is accomplished by the lift of the aircraft tug.

Circular wing aircraft having pressure induced radial airflow (2,843,338). H. F. Streib, Chula Vista, Calif.

An impeller directing a flow of air radially inwardly over the upper surface of a circular wing to create lift. Air is driven downwardly through a central circular opening to supplement the lift.

Jet aircraft (2,843,340). M. H. M. J. Wibault, Paris, France.

Propulsion system comprising a turbocompressor unit obliquely inclined with respect to the line of flight. Adjustable means permit deflecting the jet discharge from normal to a vertical downward direction so the jet and air stream produce a combined lifting force on the aircraft.

Mobile hydraulic catapulting apparatus (2,843,342). E. F. Ward, Pasadena, Calif., assignor to Task Corp.

Motorized vehicle with portable guide track sections adapted for assembly rearward of a gun for jetting liquid to guide a

EDITOR'S NOTE: Patents listed above were selected from the Official Gazette of the U.S. Patent Office. Printed copies of patents may be obtained from the Commissioner of Patents, Washington 25, D. C., at a cost of 25 cents each; design patents, 10 cents.

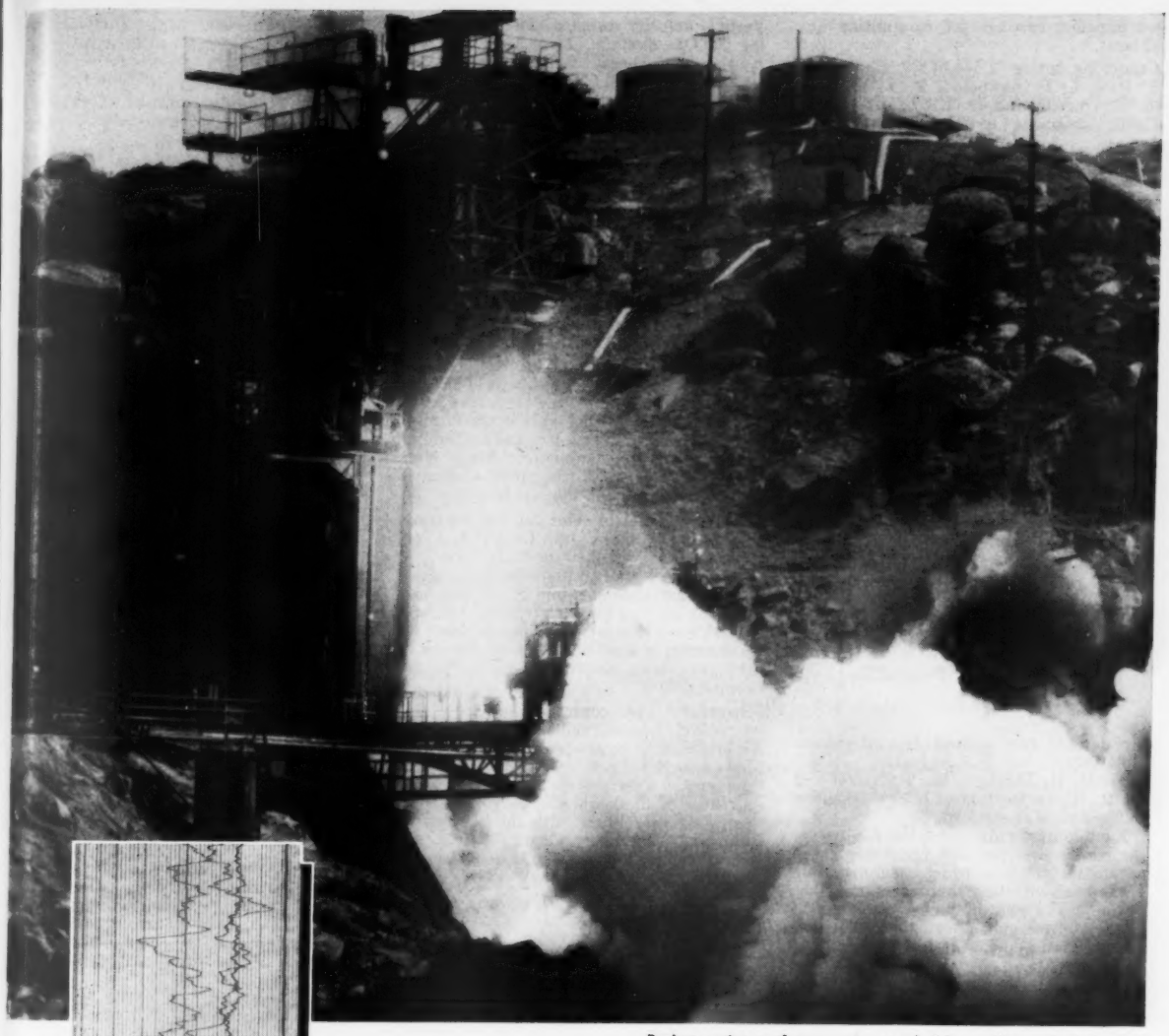

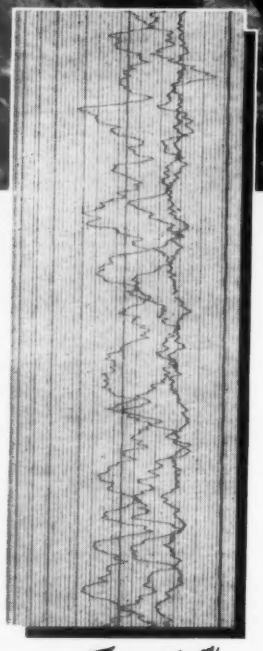

Now available on extra-thin base

Rocket engine performance is recorded by oscillograph at this test stand high in the Santa Susana Mountains. Test facilities are maintained by Rocketdyne, a division of North American Aviation, Inc.

Readout: *as you go*

Why wait for the answers?

You can *immediately* evaluate your test results if they are recorded on new Kodak Linagraph Direct Print Paper used in appropriate moving-mirror galvanometer oscillographs.

There is no need for development: Just run your test and read the records as they are being made. You'll get sharp, legible traces over a wide frequency range—0 to 3000 cps.

You can make pen or pencil notations on these records. And you can make the records permanent by fixation.

New Kodak Linagraph Direct Print Paper is available in 5″ x 200′, 6″ x 100′, 7″ x 200′, and 12″ x 200′ rolls. Other sizes on request. For complete details, write to:

EASTMAN KODAK COMPANY
Graphic Reproduction Division
Rochester 4, N. Y.

Kodak
TRADEMARK

jet impelled carriage for catapulting an aircraft.

Launching device (2,844,073). C. Ré, G. F. Rice, L. F. Birkeland, V. T. Koozin, G. C. Duncan and D. Kinda, Torrance, Calif., assignors to Royal Industries, Inc.

Ripple firing multiple rocket launcher. A series resistance circuit is provided for all rockets. Separate series-connected resistances are provided between each pair of adjacent connections with a fused circuit between each connection and the ground, including a fuse of lesser resistance adapted to burn through at a predetermined time interval.

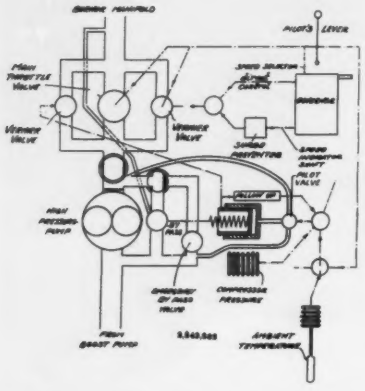

Air density fuel control for jet engine (2,849,862). C. H. Jorgensen, J. M. Barr, H. H. Dietrich, W. T. Nickel and M. R. Rowe, Rochester, N. Y., assignors to General Motors Corp.

Fuel control unit under the control by the pilot's lever and also under control of automatic devices which sense certain parameters affecting the operation of the engine. The pilot may change the status of the control unit so control by some or all automatic devices is removed.

Fast rising balloon (2,844,336). H. J. Mastenbrook, Falls Church, Va., assignor to the U. S. Navy.

High altitude spherical balloon with an inverted conical skirt attached at an angle to provide a couple to maintain stability during ascent but unrestrained in their natural ability to extend.

Aircraft control arrangement incorporating deflectable surface and boundary layer control jets (2,844,337). R. B. MacArthur and D. F. Swearingen, Hawthorne, Calif., assignors to North American Aviation, Inc.

Primary airfoil with a rearward opening recess within its trailing edge with nozzles for discharging air over the upper portion of the elevator or aileron when deflected.

Vertical velocity thrust control for hovering VTOL aircraft (2,844,338). I. W. Keith, San Diego, Calif., assignor to Ryan Aeronautical Co.

Sensitive vertical acceleration sensing means and signal and a velocity signal connected to an automatic throttle positioner with a signal delay means interposed.

Improved method and arrangement for starting reaction type propulsion units (2,840,987). D. J. Bloomberg and N. Burgess, Maderia, Ohio, assignors to General Electric Co.

Auxiliary reaction type propulsion unit having low energy starting characteristics and adapted to initiate the operation of several jet engines.

Fuel control apparatus for supersonic ramjet (2,840,988). J. P. Longwell, Westfield, N. J., assignor to the U. S. Navy.

Aerial missile with a body in the form of an elongated tubular duct, and containing a diffuser and combustor. Static and impact pressures in the duct control a flow control valve in the fuel feed line.

Multistage fuel injector for ramjet combustor (2,840,988). J. P. Longwell, Westfield, N. J., assignor to the U. S. Navy.

Set of fuel injection nozzles in an aerial missile arranged to inject fuel into airstreams passing through venturi throats. Nozzles are separated from each other by a distance of one-half the wave length of the periodic pressure fluctuation in the combustor.

Boundary layer control (2,841,344). M. Stroukoff, Lawrenceville, N. J.

Depression in the surface of a wing, between the leading and trailing edge portions. A series of high velocity jet streams of fluid are directed into a passageway associated with the depression, inducing boundary layer fluid into entrance openings fixed to the surface.

Jet propelled aircraft (2,841,346). W. E. Petter, Curdridge, England, assignor to Folland Aircraft, Ltd.

Fairing on the exterior of an engine mounted in a fuselage, extending aft from the air intake opening, providing a compartment for a landing gear unit or armament forward of the engine.

Fastening device (2,841,850). A. T. Zohorsky, Altadena, Calif., assignor to Aerophysics Development Corp.

Device for fastening together the adjacent edges of a material comprising a pair of strip members, the inner face of one strip in surface engagement with the outer face of the other. One strip has a row of projections and the other strip a row of recesses spaced along its length.

Radar tracking demonstrating and training instrument (2,841,884). H. P. Birmingham, Washington, D. C., assignor to the U. S. Navy.

Circuit for measuring the time duration that the deflection of a cathode ray beam is maintained within an octogonal area on the screen of a cathode ray tube.

Rear inlet annular diffuser (2,841,952). L. S. Billman, Lancaster, Calif., assignor to the U. S. Navy.

Ramjet aerodyne with a divergent-convergent fuselage. Air entering inlets in the path of travel flows through ducts, struts and complementary openings to the atmosphere. Air entering air inlet ducts may follow an unrestricted path to passageways to the fuel ignition means in the combustion chamber.

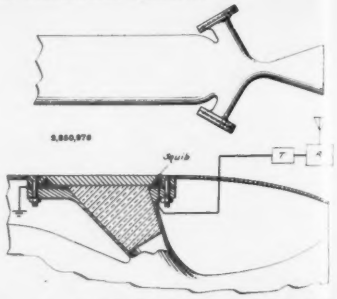

Thrust cancellation device (2,850,976). H. S. Seifert, Playa del Rey, Calif., assignor to the U. S. Army.

Device to control the trajectory of a solid propellant rocket without affecting a change in the characteristics of the motor design or in the propellant powder to initially propel the rocket in free flight. A neutralizing force overcomes the thrust of the main nozzle, operating with the least disturbance or transient force.

System for pressurizing the fluid propellant tank of a self-propelled missile (2,841,953). W. D. Teague, Jr., Alpine, N. J., assignor to the U. S. Army.

Diaphragm normally sealing a passageway between two compartments of a closed pressurizing chamber. A combustible charge in the first compartment moves a piston, ruptures the diaphragm and pressurizes the tank.

Directional control for jets (2,841,955). G. H. McLafferty, Manchester, Conn., assignor to United Aircraft Corp.

Converging-diverging diffuser downstream of the air intake, with partitions dividing the cooling duct into annular segments. Servos selectively close one or more valves in each segment to vary the flow direction from the main duct.

Guide vane arrangement for rocket missiles (2,842,058). N. E. G. Kuller, and K. J. T. Thorildsson, Bofors, Sweden, assignors to Aktiebolaget Bofors Corp.

Sheet metal vanes attached to a tubular rocket by protruding members and slots in releasably locking engagement.

Book Reviews

Ali Bulent Cambel, Northwestern University, *Associate Editor*

Gasdynamics, by A. B. Cambel and B. H. Jennings. McGraw-Hill Book Co., New York, 1958, 353 + xiii pp. text, 49 pp. tables and 11 pp. index. $11.

Reviewed by S. Kline
Stanford University

This book covers the elements of one-dimensional gasdynamics, combustion, aerothermochemistry and also an introduction to two- and three-dimensional flow problems. It is written at the advanced undergraduate level. The coverage and choice of material are excellent, and the text is very readable. For these reasons, and since no other book with such a coverage is available for the many courses in this area now developing within Mechanical and Aeronautical Engineering curricula, this book should be of considerable assistance to undergraduate instructors, and will also undoubtedly find a useful place as a reference book in some industrial situations.

A more detailed picture of the material included can be most readily obtained from the chapter headings; these are: 1 Basic Concepts of Gas Dynamics and Gas Properties; 2 Fundamental Equations of Steady Flow; 3 Isentropic Flow; 4 Diabatic Flow; 5 Flow With Friction; 6 Wave Phenomena; 7 Variable-Area Flow; 8 Thermochemistry;

TEST EQUIPMENT ENGINEER John W. Lloyd tells why his work on the B-70 Weapon System at IBM Owego affords him the creative engineering career he always wanted.

WHAT IT'S LIKE TO BE A CREATIVE ENGINEER AT IBM

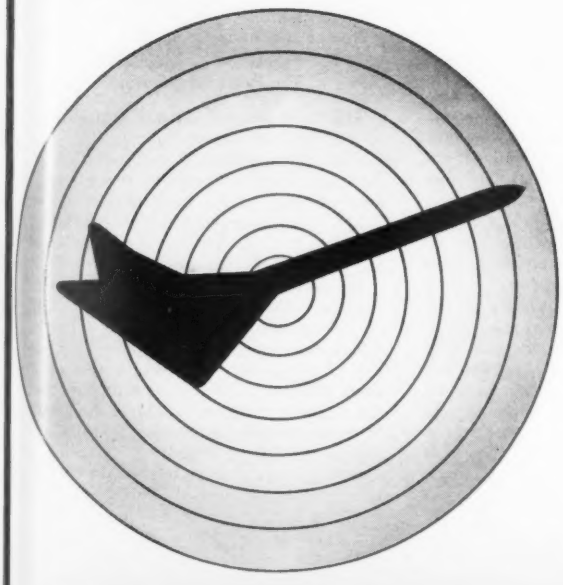

"Test equipment engineering," says John Lloyd, "is particularly stimulating when it's part of a project as new and important as the B-70, sometimes described as 'a huge flying computer.' Right now I'm coordinating the design of engineering support equipment for an advanced digital airborne computer, part of the B-70's bombing-navigational and missile guidance system. There's a minimum of routine. In order to design test equipment you must know — or learn — about the equipment to be tested; among these are radar, servo systems, digital and analog computers, inertial guidance. I see my professional growth assured as IBM continues to develop computers for airborne applications."

Challenging assignments now open

- **Airborne digital & analog computers**
- **Inertial guidance & missile systems**
- **Information & network theory**
- **Magnetic engineering**
- **Maintainability engineering**
- **Optics**
- **Radar electronics & systems**
- **Servomechanism design & analysis**
- **Theoretical physics**
- **Transistor circuits**
- **Units & systems test equipment**

There are other openings in related fields to broaden your skills and knowledge.

Qualifications:

B.S., M.S. or Ph.D. in Electrical or Mechanical Engineering, Physics, or Mathematics, **and proven ability** to assume a high degree of technical responsibility in your sphere of interest.

FOR DETAILS, just write, outlining background and interests, to:

Mr. P. E. Strohm, Dept. 572Y
International Business Machines Corp.
Owego, New York

IBM is a recognized leader in the rapidly expanding electronic computer field. Its products are used for both commercial and military applications. Continuous growth affords excellent advancement opportunities. The "small-group" approach assures recognition of individual merit. Company benefits set standards for industry, and **salaries are commensurate with your abilities and experience.**

IBM® MILITARY PRODUCTS

Plants and laboratories: Endicott, Kingston, Owego, Poughkeepsie, Yorktown, N. Y.; Lexington, Ky.; Rochester, Minn.; San Jose, Calif.

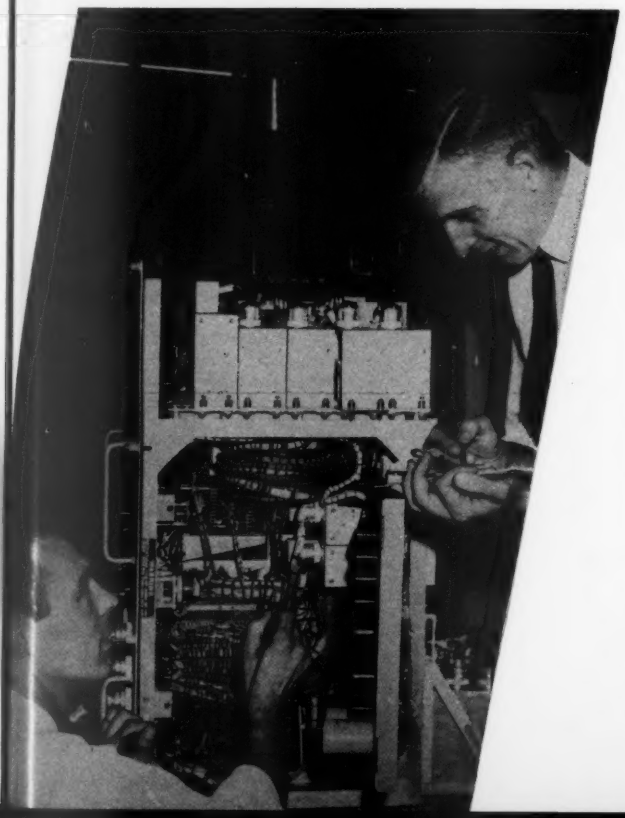

9 Introduction of Flames and Combustion; 10 Introduction to Multidimensional Flow; 11 Dimensional Analysis and Similitude; 12 Experimental Techniques and Measurements; 13 Aerothermochemistry. It should perhaps be noted that the authors use the term isentropic flow to mean what others have called introductory concepts of compressibility, and include such matters as the flow in nozzles with variable area in chapter 7. Chapter 7 also includes a very brief introduction to the now canonical methods of Shapiro and Hawthorne for one-dimensional flow with more than one effect occurring simultaneously at appreciable Mach numbers. In each case after the first few chapters, the authors carry the work considerably forward toward the best available modern results. For example, the chapter on wave phenomena includes a discussion of oblique shock waves and shock wave build-up; the chapter on thermochemistry includes discussions on reaction kinetics, disassociation, transport phenomena, etc., and the chapter on dimensional analysis includes not only the usual treatments of Buckingham and Bridgman, but the more powerful methods of Rayleigh, Kayser and Huntley, and a brief discussion on use of differential equations for such problems. Similar examples occur in all chapters beyond the first three. This reviewer feels that the inclusion of the three chapters on combustion are particularly useful and appropriate, and these will be doubly welcome since the senior author is well known for his many contributions and his grasp in this area. The inclusion of the material on combustion and on experimental methods with the more usual gasdynamics should provide a much more compact and usable text than has heretofore been available.

The knowledgeable reader will by now undoubtedly have asked himself the question, "How can so much material be placed in a single volume without some loss of rigor or completeness?" The answer, of course, is that it cannot. The present book in many instances provides only brief introductory treatments particularly of the more advanced topics, such as multidimensional flow and reaction chemistry. However, this is deemed appropriate for an undergraduate textbook since it provides the beginning student with at least a picture of the scope of present day knowledge. Also, by including in most instances the best modern references at the end of each chapter, the authors are able to make reference to appropriate treatments which are more complete and rigorous at many points, and thus give the student a good start on further work in any topics of particular interest or concern.

Also to some extent the concision of the present volume is achieved at the expense of thorough derivations and the sacrifice of a unified fundamental point of view. Different methodologies are adopted at different points in the text, and little is done to associate or rationalize them. The authors have a tendency to begin each section or example from the view that will lead them to the desired answer by the simplest and shortest means for the problem in question. While this is permissible and understandable for the advanced worker, it may cause some difficulty for beginning students who are attempting to find for themselves some unity and fundamental structure in this topic. This reviewer admits he is highly biased toward a uniform fundamental treatment of the expressions of continuity, momentum, energy and the Second Law of thermodynamics as the best rational means for construction of a uniform fundamental basis for gasdynamics, and many teachers may find the absence of such material in an introductory book far less vexatious than the writer. Despite this, the work would be improved, in the reviewer's opinion, by a more complete derivation of all the fundamental equations including more complete delineation of the conditions and restrictions surrounding their use, and by a more systematic methodology, both physical and mathematical, for introducing these equations in the examples given. Examples of this problem are the introduction of the momentum principle in various forms at various times with only a very short and incomplete discussion of the relation between momentum and Newton's Law of motion as applied to the system of fixed mass. In the most general momentum equation given (in chapter 10) the authors fail to note that the equation presented assumes the observer stands on the control volume and hence that the control volume must be such that its coordinates are inertial. Similarly, in the primary presentation of the energy equation, the discussion is restricted to steady, one-dimensional flow of a single stream, and the restrictions relating to the need for reversibility in the flow work term and in the use of an internal energy requiring only two independent intensive properties are not discussed. Admittedly, these are not matters that bother the average undergraduate, but despite this, both the precision of work and the information made available to the reader would be improved by their inclusion. It is also clear that the omission of discussion of these matters means that the book cannot be considered comparable in rigor to the recent advanced discussions of this topic, as for example those of Shapiro or of Liepmann and Roshko.

It is not to be inferred from these comments that the book contains technical errors; on the contrary, the results stated seem to be remarkably free from technical errors and misleading implications. Thus the comments offered in the previous paragraph concern methodology rather than fact and accordingly lie in the realm of opinion. The present version of the book already represents considerable improvement on these matters over an earlier draft seen by this reviewer, and the comments are offered in the hope that possible later editions of this useful work will be still further improved in the direction of combining maximum rigor and logical unity with the very readable, concise and extensive treatment given. The work would also be improved by inclusion of a few examples not entirely dependent on perfect gas behavior.

In summary then, the present volume is a contribution and should be of real aid in improving the effectiveness of teaching in advanced undergraduate courses on gasdynamics and combustion. It is not as rigorous as the best available monographs on these topics, but is nevertheless accurate and readable, and it provides a surprisingly good coverage of the material and introduction to the best modern results and references in a single compact volume. It is well worth the serious attention of anyone interested in a comprehensive introductory treatment in these areas for either educational or industrial purposes.

The Russian Literature of Satellites, Part I. Edited by A. V. Shpol'skii, International Physical Index, Inc., New York, 1958, x + 181 pp. $10.

Reviewed by F. J. KRIEGER
The Rand Corporation

This book is a collection of translations of the first six papers (pp. 1–122) of a special series published in *Uspekhi Fizicheskikh Nauk* (Progress in the Physical Sciences), vol. 63. no. 1a, Sept., 1957, pp. 1–144, commemorating the centennial of the birth of K. E. Tsiolkovskii, founder of the science of astronautics.

In the first paper, "Certain Variational Problems Associated with the Launching of an Artificial Earth Satellite," D. E. Okhotsimskii and T. M. Eneev examine the problems of: 1 Selecting the optimum mode of propellant consumption and the optimum program for thrust direction; 2 motion when the mode of propellant expenditure is specified; 3 guiding a satellite into its orbit while taking into account the variation of the gravitational field and the rotation of the Earth.

Using the methods of the calculus of variations (assuming a uniform gravitational field and constant acceleration), the authors establish that the most advantageous program for rocket thrust direction obtains when the tangent of the thrust angle is a linear function of time, and that the most advantageous mode of propellant expenditure is the instantaneous burning of all the propellant at some definite moment of flight.

The motion of a multistage rocket is considered in a uniform gravitational field (planar Earth), assuming that the rocket thrust is constant. The solution of the problem is given in analytical form. Graphs are included which make it possible to determine the various flight characteristics.

In an analysis of the more complex problem of rocket motion subject to the variation of the gravitational field and the rotation of the Earth, Okhotsimskii and Eneev show that the tangent of the thrust angle, giving the optimum program for rocket thrust direction, is expressed in terms of hyperbolic functions of time.

In the second paper, "Determining the Lifetime of an Artificial Earth Satellite and Investigating the Secular Perturbations of Its Orbit" by D. E. Okhotsimskii, T. M. Eneev and G. P. Taratynova, the variation of atmospheric density with altitude is approximated by exponential formulas fitted to the data presented in S. K. Mitra, "The Upper Atmosphere" (2d ed., 1952, p. 582). By assuming that

AERO-THERMODYNAMICISTS EXPLORE HIGH-SPEED RE-ENTRY

A report to Engineers and Scientists from Lockheed Missile Systems— where expanding missile programs insure more promising careers

Advanced weapon system technology has brought to the forefront problem areas requiring attention to interaction between aerodynamic and thermodynamic phenomena. Typical of these is the problem of high-speed atmospheric re-entry.

Expanding research and development activities have coincided with acceleration on top priority programs like our Polaris IRBM. At the same time, positions for qualified engineers and scientists have opened up that are unequalled in responsibility or in opportunities for moving ahead.

Positions in **aero-thermodynamics** include such areas as: aerodynamic characteristics of missiles at high Mach numbers; missile and weapon system design analysis; boundary layer and heat transfer analyses in hypersonic flow fields; and calculation of transient structural and equipment temperatures resulting from aerodynamic heating and radiation.

In addition, openings exist at all levels in **Gas Dynamics, Structures, Propulsion, Test Planning and Analysis, Test Operations, Information Processing, Electronics,** and **Systems Integration.** For these and other positions, qualified engineers and scientists are invited to write Research and Development Staff, Dept. 2511, 962 W. El Camino Real, Sunnyvale, California.

Lockheed / **MISSILE SYSTEMS DIVISION**

SUNNYVALE, PALO ALTO, VAN NUYS, SANTA CRUZ, VANDENBERG AFB, CALIFORNIA
CAPE CANAVERAL, FLORIDA • ALAMOGORDO, NEW MEXICO

Maurice Tucker, Aero-Thermodynamics Department Manager, right, discusses combined aero-thermodynamic re-entry body tests being conducted in Division's new "hot-shot" wind tunnel. Others are Dr. Jerome L. Fox, Assistant Department Manager, Thermodynamics, left, and Robert L. Nelson, Assistant Department Manager, Aerodynamics.

the Earth's gravitational field is central (i.e., the Earth is spherical) and neglecting the diurnal rotation of the atmosphere, the authors reduce the problem of determining the lifetime of a satellite to the integration of a system of two differential equations, the right-hand sides of which are expressed in terms of definite integrals whose integrand functions are known functions of the semilatus rectum, the eccentricity and the argument of latitude (i.e., the sum of the true anomaly and the argument of perigee). These functions are also independent of the aerodynamic drag coefficient c_x and of the satellite's design parameters (i.e., weight G and maximum cross-sectional area F).

The computational results, presented in both graphical and tabular form, give values for a quantity ν and for the initial perigee velocity as functions of the perigee and apogee altitudes. Satellite lifetime—in terms of the number of revolutions N—is obtained from the formula $N = \nu G/Fgc_x$, where g is the acceleration of gravity.

An analysis of the secular perturbations of orbital elements caused by other perturbing forces (e.g., the oblateness of the Earth and the diurnal rotation of the atmosphere) indicates that the perturbations are small and "that the method used in this paper to compute the lifetime is a sufficiently correct one."

It is interesting to compare the computed lifetime of a satellite with its actual lifetime. Sputnik I data published by TASS—perigee altitude 228 km, apogee altitude 947 km, diameter 58 cm, weight 83.6 kg—and a drag coefficient equal to 2 show that $\nu = 264$ and $N = 4260$ revolutions. This value of N is considerably higher than Sputnik I's actual lifetime of about 1400 revolutions or 92 days, indicating that the upper atmosphere is somewhat denser than heretofore supposed.

The third paper, "The Motion of an Artificial Earth Satellite in the Non-Gravitational Field of the Earth When Atmospheric Resistance Is Present" by G. P. Taratynova, and the fourth paper, "The Effect of Geophysical Factors on the Motion of a Satellite" by I. M. Iatsunskii, are ancillary, and in a sense complementary, to the second paper. They both take into consideration the basic perturbing forces caused by the oblateness of the Earth and by its atmospheric drag, including the diurnal rotation of the atmosphere with the Earth. Iatsunskii's paper discusses the possibility of determining the density of the air, the constants of the Earth ellipsoid and gravitational anomalies by means of satellite observations.

Although not concerned with satellites, the *pièce de résistance* of the collection is V. A. Egorov's paper, "Certain Problems of Moon Flight Dynamics." This paper is a result of a systematic investigation undertaken at the Steklov Mathematics Institute of the USSR Academy of Sciences in Moscow from 1953 to 1955 to find satisfactory solutions for the fundamental problems of the theory of flight dynamics, including the shape and classification of trajectories in the passive (unpowered) phase; possible trajectories for circumflight of the moon and return to the Earth; the minimum initial velocities required for reaching the moon; the problem of hitting the moon, and the very important problem of the effect of dispersion in the initial conditions on the characteristics of various moon-flight trajectories.

At the outset, Egorov reduces the problem of rocket flight to the moon to the circular restricted three-body problem by neglecting the oblateness of the Earth and the perturbations of the sun and the large planets. He also assumes that the rocket's flight trajectory begins outside the Earth's atmosphere at a height of several hundred kilometers.

The problem of minimum velocities Egorov solves by means of Jacobi's integral. He finds that the minimum velocity required to reach the moon (from an altitude of 200 km above the Earth's surface) is 10.84890 km/sec, and that required for a rocket to proceed to infinity is 10.84968 km/sec.

To determine minimum-velocity trajectories Egorov uses the method of numerical integration. These trajectories, although interesting academically, are of no practical interest because they remain approximate ellipses with a focus at the Earth's center for a long time, so that the rocket must make a large number of revolutions around the Earth (hundreds or more) before reaching the moon. Of more interest is the author's demonstration that the moon cannot possibly capture a projectile launched from the Earth on the first circuit of the trajectory, no matter what values of the initial conditions are specified.

Egorov describes a simple but accurate approximate method of analyzing approach trajectories based on the concept of separate "spheres of action" for the Earth and for the moon. Thus, it can be assumed the motion outside the moon's sphere of action occurs along a geocentric conic section, and the motion inside its sphere of action occurs along a selenocentric conic section. This method shows that motion relative to the moon along approach trajectories always takes place at velocities greatly exceeding the parabolic selenocentric velocities. Egorov also analyzes the evolution of a complete set of approach trajectories when the magnitude and direction of the initial velocity are varied.

In solving the problem of striking the moon, Egorov develops a method for determining the initial conditions that correspond to hitting the moon with a predetermined accuracy. He establishes that the deviation of the trajectory from the center of the moon is a quadratic, not a linear, function of small errors in the initial conditions. Similarly, in the problem of circumflight of the moon, he develops a method for determining the initial conditions for a return to Earth. Here the deviation of the return-flight trajectory from the center of the Earth is a quadratic function of the errors in the initial conditions. It is found that at a distance greater than the sphere of action of the moon (66,000 km), the accuracies required for a return to Earth would be no greater than in the problem of hitting the moon for the same initial velocity. Thus the problems of: 1 Hitting the moon and, 2 circumflight of the moon at a sufficiently great distance and returning to Earth without any correction during the passive (unpowered) phase of the motion are evidently technologically possible.

Egorov also examines three other problems: 1 The special problem of lunar circumflight, i.e., the determination of circumflight trajectories by which the rocket enters the Earth's atmosphere at a shallow angle; 2 the problem of whether or not it is possible to launch a projectile into the plane of the lunar orbit in such a way that it will periodically circumfly the moon, return to the vicinity of the Earth, and regularly give information about the moon (e.g., about its opposite side), this problem has not been previously treated in the literature; 3 the problem of accelerating or decelerating a cosmic rocket by means of the moon without making use of engine thrust.

In his paper, Egorov draws the following conclusion: For close circumflight of the moon (and especially for a shallow re-entry into the Earth's atmosphere) the accuracy requirements in the initial conditions are so stringent that a correction of the passive phase of the trajectory definitely seems necessary. For trajectories that hit the moon and for those that achieve distant circumflight of the moon, the accuracy requirements are moderate. Thus, it will be possible to achieve flights along these trajectories, without introducing any correction during the passive phase, as soon as rockets can achieve velocities of the order of the parabolic velocity.

The sixth paper, "The Use of Artificial Earth Satellites for Verifying the General Relativity Theory" by V. L. Ginzburg, is simply a résumé of a more comprehensive article published in *Uspekhi Fizicheskikh Nauk* (vol. 59, no. 1, 1956, pp. 11–49). The following four effects, which emerge from the general theory of relativity, are considered: 1 The rotation of a planet's perihelion around the sun; 2 the bending of light rays that pass close to the sun; 3 the gravitational shift of spectral lines; 4 the displacement of a planet's perihelion caused by the rotation of the sun. Ginzburg discusses the observational data obtained by astronomical methods to give a quantitative verification of the theory. He indicates how the use of artificial satellites will make it possible to verify the general theory of relativity (i.e., measure relativistic effects) more rapidly and with greater accuracy than heretofore.

In general, the quality of translation of the papers comprising the book is good. The editors have corrected numerous typographical errors in the original text but have made a few slips of their own, such as the persistent use of the word "perihelion" instead of "perigee" and of the redundant expression "conic cross section." In spite of its price (due to the enormous effort and expense of issuing such a translation), the book will undoubtedly be welcomed by the growing number of technical people who are seriously interested in problems involving the motion of a satellite (or lunar vehicle) and the scientific research that can be accomplished with it.

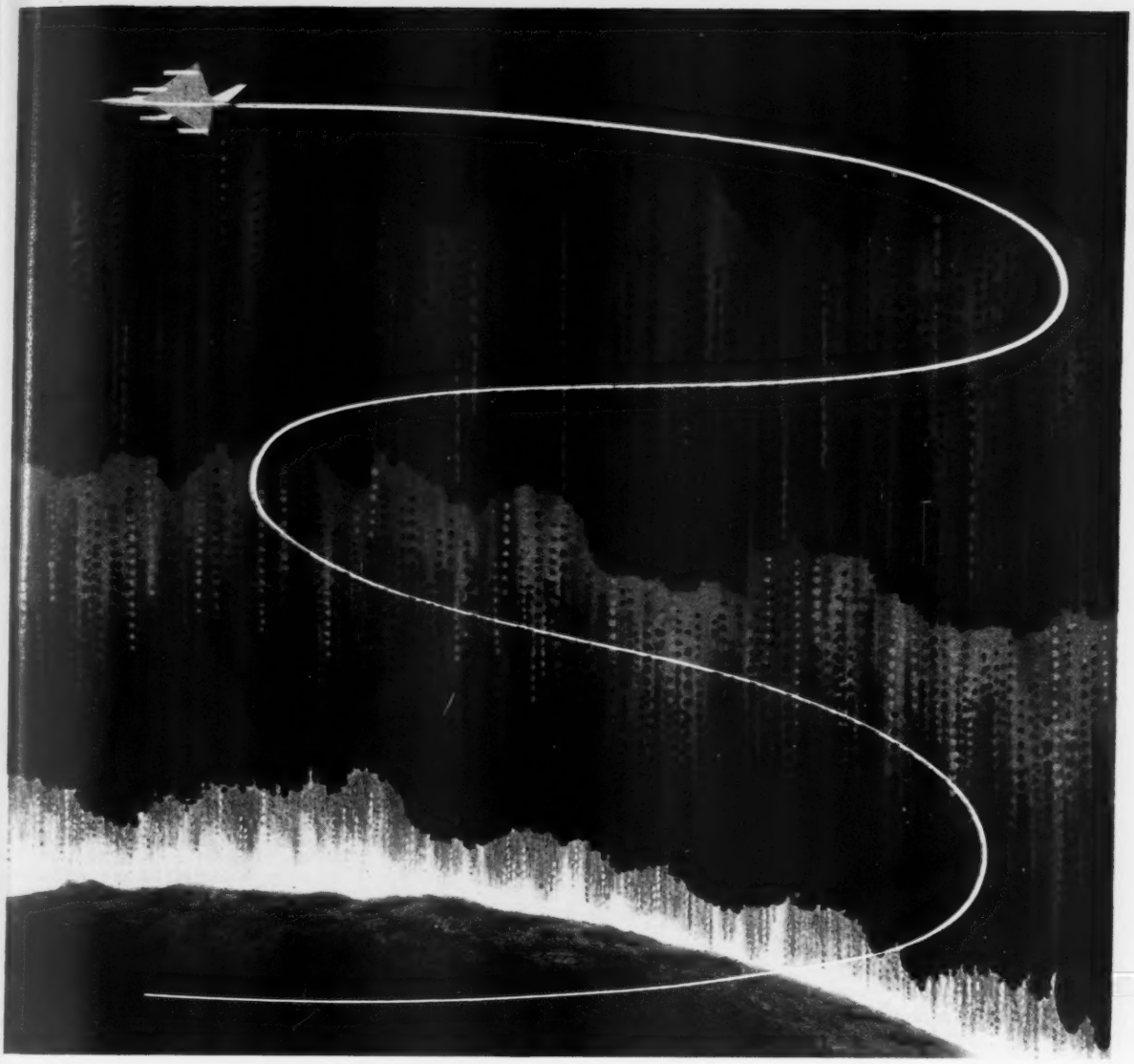

New extreme-high-temperature lubricants for missiles and supersonic aircraft **SHELL ETR GREASES**

One of the serious lubricating problems faced by designers of missiles and supersonic aircraft has been solved by scientists at Shell Research Laboratories.

The problem: to find a grease which would permit components to operate with certainty under extreme high temperatures. Co-operation with representatives of bearing manufacturers and military personnel resulted in a completely new class of greases—SHELL ETR GREASES.

These greases can easily withstand temperatures up to 600°F. They give superior lubricating performance because of a special thickener—an organic vat dye—which has exceptional heat stability and jelling efficiency.

If you are presently in the market for an ultra-high-temperature-range grease, we will be glad to provide more information on Shell ETR Greases.

SHELL OIL COMPANY

50 West 50th Street, New York 20, N.Y.
100 Bush Street, San Francisco 6, Calif.

SHELL

Technical Literature Digest

M. H. Smith, *Associate Editor,* **and M. H. Fisher,** *Contributor*

The James Forrestal Research Center, Princeton University

Jet and Rocket Propulsion Engines

Replacement of Piston Engines by Gas Turbines in Air Liners, by H. Sammons, *J. Roy. Aeron. Soc.*, vol. 62, no. 556, Feb. 1958, pp. 94–104.

Effect of Fuel Density and Heating Value on Ram-jet Airplane Range, by Hugh M. Henneberry, *NACA Res. Mem.* E51I21, Feb. 1952, 56 pp., diagrs., 3 tabs. (Declassified from Confidential by authority of NACA Res. Abstr. 123, p. 8, 1/7/58.)

Experimental Investigation of Turbojet-engine Multiple-loop Controls for Non-afterburning and Afterburning Modes of Engine Operation, by Donald B. Dirsch, Leon M. Wenzel and Clint E. Hart, *NACA TN* 4159, Jan. 1958, 61 pp., diagrs., tab.

Fundamental Rocket Research. Summary Report Covering the Period July 1, 1954, to July 1, 1956, by *American Machine & Foundry Co., Turbo Div., Rep. GA* 104 (*AFOSR TR*-56-55; *ASTIA AD* 110373), Aug. 1956, 64 pp., 26 figs.

Vapor Fuel Distribution Effects on Combustion Performance of a Single Tubular Combustor, by Richard J. McCafferty, *NACA Res. Mem.* E50J03, Dec. 1950, 27 pp. (Declassified from Confidential by authority of NACA Res. Abstr. 123, p. 7, 1/7/58.)

Preliminary Investigation of an Annular Turbojet Combustor Having a Catalytic-coated Linear, by Carl T. Norgren and J. Howard Childs, *NACA Res. Mem.* E53L07, Jan. 1954, 11 pp., diagrs. (Declassified from Confidential by authority of NACA Res. Abstr. 123, p. 10, 1/7/58.)

Solid Propellant Rocket Motors, by E. T. B. Smith, B.Sc., D.C.Ae., A.M.I. Mech. E., A.F.R. Ae.S., *J. Brit. Interplanet. Soc.*, vol. 16, Oct.–Dec. 1957, pp. 198–211.

The Calculation of Fuel Distribution in Step-rockets, by M. L. Williams, *J. Brit. Interplanet. Soc.*, vol. 16, Oct.–Dec. 1957, pp. 211–215.

Evaluation of an Automatic Inlet-pressure Control Valve for Study of Transient Engine Performance Characteristics, by Lewis E. Wellner, Robert J. Lubick and Harry E. Bloomer, *NACA Res. Mem.* E55L13, April 1956, 25 pp. (Declassified from Confidential by authority of NACA Res. Abstr. 124, p. 44, 2/10/58.)

Altitude Wind Tunnel Investigation of Tail Pipe Burner with Converging Conical Burner Section of J35-A-5 Turbojet Engine, by H. Carl Thorman and Carl E. Campbell, *NACA Res Mem.* E9I16, Feb. 1950, 60 pp. (Declassified from Confidential by authority of NACA Res. Abstr. 124, p. 40, 2/10/58.)

Altitude Performance and Operational Characteristics of 29 Inch Diameter Tail Pipe Burner with Several Fuel Systems and Fuel Cooled Stage Type Flame Holders on J35-A-5 Turbojet Engine, by Richard L. Golladay and Harry E. Bloomer, *NACA Res. Mem.* E50A19, April 1950, 57 pp. (Declassified from Confidential by authority of NACA Res. Abstr. 124, p. 41, 2/10/58.)

Effect of Diffuser Design, Diffuser-exit Velocity Profile, and Fuel Distribution of Altitude Performance of Several Afterburner Configurations, by E. William Conrad, Frederick W. Schulze and Karl H. Usow, *NACA Res. Mem.* E53A30, July 1953, 63 pp. (Declassified from Confidential by authority of NACA Res. Abstr. 124, p. 42, 2/10/58.)

Investigation of a Supersonic-compressor Rotor with Turning to Axial Direction, I—Rotor Design and Performance, by Edward R. Tysl, John F. Klapproth and Melvin J. Hartmann, *NACA Res. Mem.* E53F23, Aug. 1953, 36 pp. (Declassified from Confidential by authority of NACA Res. Abstr. 124, p. 42, 2/10/58.)

Investigation of a Supersonic-compressor Rotor with Turning to Axial Direction, II—Rotor Component Off-design and Stage Performance, by Melvin J. Hartmann and Edward R. Tysl, *NACA Res. Mem.* E53L24, March 1954, 31 pp. (Declassified from Confidential by authority of NACA Res. Abstr. 124, p. 42, 2/10/58.)

Design and Test of Mixed-flow Impellers, III—Design and Experimental Results for Impeller Model MFI-2A and Comparison with Impeller Model MFI-1A, by Joseph T. Hamrick, Walter M. Osborn and William L. Beede, *NACA Res. Mem.* E52L22a, March 1953, 34 pp. (Declassified from Confidential by authority of NACA Res. Abstr. 124, p. 41, 2/10/58.)

Design and Test of Mixed-flow Impellers, IV—Experimental Results for Impeller Models MFI-1 and MFI-2 with Changes in Blade Height, by Joseph T. Hamrick, William L. Beede and Joseph R. Withee Jr., *NACA Res. Mem.* E53L02, Feb. 1954, 32 pp. (Declassified from Confidential by authority of NACA Res. Abstr. 124, p. 42, 2/10/58.)

Design and Test of Mixed-flow Impellers, V—Design Procedure and Performance Results for Two Vaned Diffusers Tested with Impeller Model MFI-1B, by Joseph T. Hamrick and Walter M. Osborn, *NACA Res. Mem.* E55E13, July 1955, 32 pp. (Declassified from Confidential by authority of NACA Res. Abstr. 124, p. 43, 2/10/58.)

Design and Test of Mixed-flow Impellers, VI—Performance of Parabolic-bladed Impeller with Shroud Redesigned by Rapid Approximate Method, by Kenneth J. Smith and Walter M. Osborn, *NACA Res. Mem.* E55F23, Sept. 1955, 22 pp. (Declassified from Confidential by authority of NACA Res. Abstr. 124, p. 44, 2/10/58.)

Design and Test of Mixed-flow Impellers, VII—Experimental Results for Parabolic-bladed Impeller with Alternate Blades Cut Back to Form Splitter Vanes, by Walter M. Osborn, *NACA Res. Mem.* E55L15, March 1956, 13 pp. (Declassified from Confidential by authority of NACA Res. Abstr. 124, p. 44, 2/10/58.)

Design and Test of Mixed-flow Impellers, VIII—Comparison of Experimental Results for Three Impellers with Shroud Redesigned by Rapid Approximate Method, by Walter M. Osborn, Kenneth J. Smith and Joseph T. Hamrick, *NACA Res. Mem.* E56L07, Feb. 1957, 32 pp. (Declassified from Confidential by author-

EDITOR'S NOTE: Contributions from Professors E. R. G. Eckert, J. P. Hartnett, T. F. Irvine Jr. and P. J. Schneider of the Heat Transfer Laboratory, University of Minnesota, are gratefully acknowledged.

ity of NACA Res. Abstr. 124, p. 44, 2/10/58.)

Application of Radial-equilibrium Condition to Axial-flow Turbomachine Design Including Consideration of Change of Entropy with Radius Downstream of Blade Row, by James E. Hatch, Charles C. Giamati and Robert J. Jackson, *NACA Res. Mem.* E54A20, April 1954, 42 pp. (Declassified from Confidential by authority of NACA Res. Abstr. 124, p. 43, 2/10/58.)

Performance of a 16-inch Ram-jet Engine with a Can-type Combustor at Mach Numbers of 1.50 to 2.16, by Donald P. Hearth and Eugene Perchonok, *NACA Res. Mem.* E54G13, Aug. 1954, 30 pp. (Declassified from Confidential by authority of NACA Res. Abstr. 124, p. 43, 2/10/58.)

Effects of Inlet-air-flow Distortion on Steady-state Altitude Performance of an Axial-flow Turbojet Engine, by E(arl) William Conrad, Morgan P. Hanson and John E. McAulay, *NACA Res. Mem.* E55A04, Sept. 1955, 47 pp. (Declassified from Confidential by authority of NACA Res. Abstr. 124, p. 43, 2/10/58.)

Power Packages for Medium-sized Missiles, by A. E. Maine and E. Wall, *Missiles and Rockets,* vol. 3, no. 2, Feb. 1958, pp. 115–120.

Aerodynamics of Jet Propelled Vehicles

On the Numerical Calculation of Detached Bow Shock Waves in Hypersonic Flow, by P. R. Garabedian and H. M. Lieberstein, *J. Aeron. Sci.,* vol. 25, no. 2, Feb. 1958, pp. 109–116.

Estimating Aerodynamic Characteristic Times in Hypersonic Flow, by Sinclaire M. Scala, *J. Aeron. Sci.,* vol. 25, no. 2, Feb. 1958, pp. 131–132.

A New Method for Computing Drag Coefficients from Ballistic Range Data, by Alvin Seiff, *J. Aeron. Sci.,* vol. 25, no. 2, Feb. 1958, p. 133.

Stability of Bodies of Revolution Having Fineness Ratios Smaller Than 1.0 and Having Rounded Fronts and Blunt Bases, by Stanley H. Scher and James S. Bowman Jr., *NACA Res. Mem.* L52L08, Jan. 1953, 23 pp., diagrs., 5 tabs. (Declassified from Confidential by authority of NACA Res. Abstr. 123, p. 14, 1/7/58.)

A Flight Technique for the Measurement of Thrust Boundaries and of Drag Due to Lift, by H. D. Rylands, *North Atlantic Treaty Org., Advisory Group for Aeron. Res. and Dev., Rep.* 123, May 1957, 14 pp.

Aerodynamic Characteristics of a Rotating Model of the 5.0 Inch Spin Stabilized Rocket Model 32, by R. H. Heald, J. G. Logan Jr., H. Spivak and W. Squire, *Bur. Ordn., TN* 37, June 1957, 18 pp.

Summary of Flutter Experiences as a Guide to the Preliminary Design of Lifting Surfaces on Missiles, by Dennis J. Martin, *NACA TN* 4197, Feb. 1958, 21 pp. (Supersedes Res. Mem. L51J30.)

Heat Transfer and Fluid Flow

Heat Transfer in the Condensation of Metal Vapors: Mercury and Sodium up to Atmospheric Pressure, by Balabhadra Misra and Charles F. Bonilla, *Chem. Engng. Progr.,* vol. 53, 1957.

Effect of Agitation on the Critical Temperature Difference for a Boiling Liquid, by F. S. Pramuk and J. W. Westwater,

Chem. Engng. Progr., vol. 53, 1957.

Correlation of Maximum-heat-flux Data for Boiling of Saturated Liquids, by W. Rohsenow and P. Griffith, *Chem. Engng. Progr.*, vol. 53, 1957.

Some Experiments Related to the Noise from Boundary Layers, by Harvey H. Hubbard, *J. Acoust. Soc. America*, vol. 29, 1957.

Investigation of Burnout Heat Flux in Rectangular Channels at 2000 Psia, by H. S. Jacket, J. D. Roarty and J. E. Zerbe, *Westinghouse Electric Corp., Atomic Power Div.*, (*U.S. Atomic Energy Comm.*), WAPD-A2W (IM)-3, Dec. 1955.

Review of Boiling Heat Transfer with Particular Reference to Unstable Flow, by J. McNeillis, *Engng.*, vol. 183, 1957, p. 686.

Unsteady-state Heat Transfer to and from Gases in Laminar Flow, by T. D. Patten, *Chartered Mech. Engng.*, vol. 4, no. 6, June 1957.

Radial Temperature Distribution in an Annular Coolant Passage, by Henry Barrow, *The Engr.*, May 10, 1957, p. 713.

Convective Heat Transfer from High Temperature Air Inside a Tube, by H. E. Zellnick and S. W. Churchill, *ASME Paper* 57-HT-33 (*ASME-AIChE Heat Transfer Conference*, University Park, Pa., Aug. 11–15, 1957), Aug. 1957, 8 pp.

Gas Friction-Heat Transfer Charts for Ducted Flows, by S. V. Manson, *ASME Paper* 57-HT-34 (*ASME-AIChE Heat Transfer Conference*, University Park, Pa., Aug. 11–15, 1957), Aug. 1957, 3 pp.

Theoretical and Experimental Investigation of a Two Dimensional All Supersonic Diffusing Cascade at Mach Number 2.5, by E. Beder, *Propulsion Res. Corp.*, R-155, June 1955, 126 pp.

Systematic Investigations on Secondary Flow Losses in Cascades, by N. Scholz, *Braunschweig, Techn. Hochschule, Inst. für Stromungsmechanik, Rep.* 56/18a (*AFOSR-TR-57-39*; *ASTIA AD* 132400), March 1957, 61 pp.

Thermal Conductivity of Fluids: Nitric Oxide, by G. N. Richter and B. H. Sage, *Project Squid, Tech. Rep.* CIT-2-P (*ASTIA AD* 139905), Aug. 1957, 18 pp. (available only on microcard).

Thermal Conductivity of Pure Liquids, by W. J. Scheffy and E. F. Johnson, *Project Squid, Tech. Rep.* PR-71-M (*ASTIA AD* 142428), Aug. 1957, 19 pp. (available only on microcard).

Initial Inclination of the Mixing Boundary Separating an Exhausting Supersonic Jet from a Supersonic Ambient Stream, by Eugene S. Love, *NACA RM* L55J14, Jan. 1956, 30 pp. (Declassified from Confidential by authority of *NACA Res. Abs.* 121, p. 27, 11/4/57).

Preliminary Investigation of Performance of Variable-throat Extended-plug-type Nozzles over Wide Range of Nozzle Pressure Ratios, by Carl C. Ciepluch, H. George Krull and Fred W. Steffen, *NACA RM* E53J28, Feb. 1954, 35 pp. (Declassified from Confidential by authority of *NACA Res. Abs.* 121, p. 18, 11/4/57.)

Some Studies of Axisymmetric Free Jets Exhausting from Sonic and Supersonic Nozzles into Still Air and into Supersonic Streams, by Eugene S. Love and Carl E. Grigsby, *NACA RM* L54L31, May 1955, 178 pp. (Declassified from Confidential by authority of *NACA Res. Abs.* 121, p. 26, 11/4/57.)

Film Boiling from Vertical Tubes, by Y. Y. Hsu and J. W. Westwater, *ASME Paper* 57-HT-24 (*ASME-AIChE Heat Transfer Conference*, University Park, Pa., Aug. 11–15, 1957), Aug. 1957, 8 pp.

The Correlation of Nucleate Boiling Burnout Data, by P. Griffith, *ASME Paper* 57-HT-21 (*ASME-AIChE Heat Transfer Conference*, University Park, Pa., Aug. 11–15, 1957), Aug. 1957, 17 pp.

On the Stability of Boiling Heat Transfer, by Novak Zuber, *ASME Paper* 57-HT-4, (*ASME-AIChE Heat Transfer Conference*, University Park, Pa., Aug. 11–15, 1957), Aug. 1957, 4 pp.

Bubble Growth Rates in Boiling, by Peter Griffith, *ASME Paper* 57-HT-2 (*ASME-AIChE Heat Transfer Conference*, University Park, Pa., Aug. 11–15, 1957), Aug. 1957, 6 pp.

Description of Boiling Project Burnout Detector, by M. W. Raymond and J. M. Reynolds, *Mass. Inst. Tech., Heat Transfer Lab., Tech. Rep.* 11, July 1957, 6 pp.

Burnout in Forced Convection Nucleate Boiling in Water, by J. M Reynolds, *Mass. Inst. Tech., Heat Transfer Lab., Tech. Rep.* 10, July 1957, 17 pp.

The Correlation of Nucleate Burnout Data, by Peter Griffith, *Mass. Inst. Tech., Tech. Rep.* 9, March 1957, 15 pp., 2 figs.

Some Proposals Regarding the Definitions of Terms Relating to Various Flow Regimes of a Gas, by C. H. E. Warren and A. D. Young, *Gt. Brit., Aeron. Res. Council, Curr. Paper* 368 (formerly *A.R.C. Tech. Rep.* 19583), 1958, 6 pp. 1 fig.

Radiative Properties of High Temperature Air, by W. H. Wurster, H. S. Glick and C. E. Treanor, *Cornell Aeron. Lab., Inc., Rep.* QM-997-A-1, Sept. 1957, 28 pp., 15 figs.

Limited Investigation of Noise Suppression by Injection of Water into Exhaust of Afterburning Jet Engine, by Max C. Kurbjun, *NACA Res. Mem.* L57L05, Feb. 1958, 15 pp.

Theoretical Investigation of Subsonic Oscillatory Blade-row Aerodynamics, by Frank Lane and Manfred Friedman, *NACA TN* 4136, Feb. 1958, 64 pp.

The Effect of Inlet Circumferential Maldistribution on an Axial Compressor Stage, by R. C. Turner, J. Ritchie and C. E. Moss, *Gt. Brit., Aeron. Res. Council, Rep. & Mem.* 3066 (formerly *A.R.C. Tech. Rep.* 19047; *Natl. Gas Turbine Estab., Rep.* R. 203), 1958, 16 pp.

Thermodynamic and Transport Properties of Dissociated Hydrogen Mixtures, by Martin J. Reisfeld, *Atomic Energy Comm.*, LA-2123, June 1957, 23 pp.

Heat Transfer in Manhattan District and Atomic Energy Commission Laboratories: A Critical Survey, by W. B. Harrison, *Atomic Energy Comm.*, ORNL-156, Oct. 1948, 255 pp.

Use of a Free Molecular Probe in High Speed Rarefied Gas Flow Studies, by J. A. Laurmann and D. C. Ipsen, *Wright Air Dev. Center, Tech. Rep.* 57-440 (*ASTIA AD* 142109), Oct. 1957, 40 pp.

An Instrument for the Determination of Instantaneous Densities in a Flowing Gas, by Henry Lopez, *Rensselaer Polytech. Inst., Res. Div., TR AE* 5708, Jan. 1957, 49 pp.

The Thermal Conductivity of Nitrogen and Argon in the Liquid and Gaseous States, by H. Ziebland and J. T. A. Burton, *British J. of Appld. Phys.*, vol. 9, no. 2, Feb. 1958, pp. 52–59.

An Investigation of Droplet Oscillation During Mass Transfer, I. The Conditions Necessary, and the Source of the Energy for the Oscillations, by D. A. Haydon, *Proc. Royal Soc.*, Series A., vol. 243, no. 1235, Feb. 11, 1958, pp. 483–491.

An Investigation of Droplet Oscillation During Mass Transfer, II. A Dynamical Investigation of Oscillating Spherical Droplets, by T. V. Davies and D. A. Haydon, *Proc. Royal Soc.*, Series A., vol. 243, no. 1235, Feb. 11, 1958, pp. 492–499.

Experimental Verification of Nozzle Admittance Theory in Simulated Rocket Chamber, by Sotirios Lambiris, *Project Squid, Tech. Rep.* PR-74-R (*ASTIA AD* 147309), Nov. 1957, 81 pp. (available only on microcards).

Experimental and Theoretical Investigations of the Flow of Air Through Two Stage Compressors, by J. H. Horlock, *Gt. Brit. Aeron. Res. Council, Rep. & Mem.* 3031 (formerly *A.R.C. Tech. Rep.* 17517), 36 pp.

Hydromagnetic Effects on Stagnation Point Heat Transfer, by Joseph L. Neuringer and William McIlroy, *Republic Aviation Corp.*, Nov. 1957, 8 pp., 1 tab., 4 figs.

Theoretical Study of Magnetohydrodynamic Magneto-acoustic, and Magneto-elastic Phenomena, by Alfredo Banos Jr., *AFOSR-TR-57-35* (*ASTIA AD* 12-6561), May 1957, 30 pp.

Comparison of the Take-off Noise Characteristics of the Caravelle Jet Airliner and of Conventional Propeller Driven Airliner, by Laymon N. Miller and Leo L. Beranek, *Bolt Beranek and Newman, Inc.*, May 1957, 44 pp.

The Mixing of Unbounded Coaxial Compressible Streams, by D. Roger Willis and Irvin Glassman, *Project Squid, Tech. Rep.* PR-70-P (*ASTIA AD* 146039), Nov. 1957, 34 pp. (available only on microcards).

Pressure Temperature Relation for Constant Area Compressibility of a Gas Considering Heat Transfer and Friction with Constant Wall Temperature, by Franklin P. Durham, *Atomic Energy Comm.*, LA 2129, Jan. 1957, 81 pp.

Prediction of the Pressure Loss and Density Factors for Two Phase Annular Flow with or without Heat Generation, by J. C. Westmoreland, *Atomic Energy Comm.*, KAPL 1792, Feb. 1957, 35 pp.

A Method for the Calibration of Flexible Plate Supersonic Wind Tunnels and Calibration Results for the 12 Inch Wind Tunnel at the Jet Propulsion Laboratory, by G. G. Goranson, R. M. Barnett, R. E. Covey and H. N. Riise, *Calif. Inst. of Techn., Jet Propulsion Lab., Rep.* 20-110, June 1957, 78 pp.

Relativistic Magnetohydrodynamics, by Edward G. Harris, *Physical Rev.*, vol. 108, Dec. 15, 1957, pp. 1357–1360.

Hydrogen Flammability Data and Application to PWR Loss of Coolant Accident, by Z. M. Shapiro and T. R. Moffette, *Atomic Energy Comm.*, WAPD-SC-545, Sept. 1957, 23 pp.

Formulae and Approximations for Aerodynamic Heating Rates in High Speed Flight, by R. J. Monaghan, *Gt. Brit., Aeron. Res. Council, Current Paper* 260 (formerly *A.R.C. Tech. Rep.* 18567; *Roy. Aircr. Estab., TN Aero.* 2407), 1957, 31 pp., 19 figs.

Analysis of Incompressible, Nonviscous Blade-to-blade Flow in Rotating Blade Rows, by J. J. Kramer, *Trans., ASME*, vol. 80, no. 2, Feb. 1958, pp. 263–275.

Investigation of Burnout Heat Flux in Rectangular Channels at 2000 Psia, by H. S. Jacket, J. D. Roarty and J. E. Zerbe, *Trans., ASME*, vol. 80, no. 2, Feb. 1958, pp. 391–401.

Turbulent Heat Transfer in the Thermal Entrance Region of a Pipe with Uniform Heat Flux, by E. M. Sparrow, T. M. Hallman and R. Siegel, *Appld. Sci. Res.*, Section A, vol. 7, no. 1, 1957, pp. 37–52.

Analysis of Heat-driven Oscillations of Gas Flows, Part III—Characteristic Equation for Flame-driven Oscillation of the Organ-pipe Type, by H. J. Merk, *Appld. Sci. Res.*, Section A, vol. 7, no. 2-3, 1958, pp. 175–191.

Analysis of Heat-driven Oscillations of Gas Flows, Part IV—Discussion of the Theoretical Results Concerning Flame-driven Oscillations, by H. J. Merk, *Appld. Sci. Res.*, Section A, vol. 7, no. 2-3, 1958, pp. 192–204.

Statistical Mechanics of Transport Processes, XI, Equations of Transport in Multicomponent Systems, by Richard J. Bearman and John G. Kirkwood, *J. Chem. Phys.*, vol. 28, no. 1, Jan. 1958, pp. 136–145.

Theory of Stagnation Point Heat Transfer in Dissociated Air, by J. A. Fay and F. R. Riddell, *J. Aeron. Sci.*, vol. 25, no. 2, Feb. 1958, pp. 73–79.

Stagnation Point Heat-transfer Measurements in Dissociated Air, by P. H. Rose and W. I. Stark, *J. Aeron. Sci.*, vol. 25, no. 2, Feb. 1958, pp. 86–92.

An Approximation of the Boundary of a Supersonic Axisymmetric Jet Exhausting into a Supersonic Stream, by E. L. Love, *J. Aeron. Sci.*, vol. 25, no. 2, Feb. 1958, p. 130.

Heat Transfer Through Liquid Metals, by G. Braudeau, *Houille Blanche*, vol. 12, 1957, pp. 81–86 (in French).

Practical Calculation of Compressible Flow in Axial Turbines, by G. Cordes, *Technik*, vol. 12, 1957, pp. 279–284 (in German).

Engineering Data for Diphenyl Cooled Nuclear Reactors, by L. W. Froom and Kermit Anderson, *Nuclear Sci. and Engng.*, vol. 2, 1957, pp. 160–168.

Further Investigations of the Laminar-turbulent Transition in a Free Jet (Annular Nozzle), by O. Wehrmann and H. Fabian, *Hermann Fottinger-Inst. fur Stromunstech., Berlin Tech. U. Rep.* (*AFOSR TR* 57–31) (*AD* 126494), Dec. 1956, 1 vol.

On the Theory of Binary Fluid Mixtures, by F. J. Pearson and G. S. Rushbrooke, *Proc. Royal Soc.* (*Edinburgh*), Sect. A, 1955–57, pp. 305–317.

Combustion, Fuels and Propellants

Oriole . . . A Really Low-Cost Research Missile, *Missiles and Rockets*, vol. 2, Dec. 1957, pp. 86–87.

Mechanisms for the Formation of Ions in Flames, by H. F. Calcote, *Project Squid, Tech. Rep.* EXP-6-P (*ASTIA AD* 145989), Nov. 1957, 44 pp. (available only on microcards).

NACA Conference on Combustion; A Compilation of the Papers Presented by NACA Staff Members, by *NACA*, March 26, 1947, 77 pp. (Declassified from Confidential by authority of NACA Res. Abstr. 123, p. 18, 1/7/58.)

Studies in Bomb Calorimetry VIII—Design of Calorimeter Systems, by R. A. Mott, *Fuel*, vol. 37, Jan. 1958, pp. 3–18.

Stability of Propane-air Flames in Vortex Flow, by A. E. Potter Jr., E. L. Wong and A. L. Berlad, *NACA TN* 4210, Feb. 1958, 27 pp.

New Methods for the Measurement of Relative Ignitability and Ignition Efficiency, by Cecilio R. Grande, *Picatinny Arsenal, Samuel Feltman Ammunition Labs., Tech. Rep.* 2469, Feb. 1958, 1 vol.

Turbulent Burning Velocities of Natural Gas-air Flames with Pipe Flow Turbulence, by J. Kenneth Richmond, Joseph M. Singer, E. B. Cook, James R. Oxendine, Joseph Grumer, and David S. Burgess, *Bur. Mines, Div. Explosives Techn., Tech. Rep.* 1205 (*AFOSR-TN*-56-238, *ASTIA AD* 88358), Apr. 1956, 16 pp.

Combustion in Laminar Mixing Regions and Boundary Layers, by Donald Allen Dooley, *Calif. Inst. of Techn., Jet Propulsion Lab., Mem.* 20-151, June 1956, 244 pp.

Shock Waves and Flame Interaction, by George Rudinger, *Project Squid, Tech. Rep.* CAL-74-P (*ASTIA AD* 147699), Dec. 1957, 42 pp. (available only on microcards).

The Ignition of Combustible Mixtures by Hot Gases, by H. G. Wolfhard, *Project Squid, Tech. Rep.* BUM-24-P (*ASTIA AD* 147702), Dec. 1957, 27 pp. (available only on microcards).

The Study of Flow and Reaction Rates in Turbulent Flames, by R. P. Barbor, J. D. Larkin and C. W. Shipman, *Project Squid, Tech. Rep.* DEL-8-P (*ASTIA AD* 147703), Dec. 1957, 38 pp. (available only on microcards).

Theoretical Rocket Performance of JP-4 Fuel with Several Fluorine-oxygen Mixtures Assuming Equilibrium Composition, by Sanford Gordon, *NACA Res. Mem.* E57K22, Feb. 1958, 69 pp.

Infrared Analysis of Mixtures of Nitroglycerine and Ethylene Glycol Dinitrate, by Woodruff Huff, Michael Halik and Frank Pristera, *Picatinny Arsenal, Samuel Feltman Ammunition Labs., Tech. Rep.* 2472, Dec. 1957, 9 pp.

An Approximate Treatment of Hydrazine Decomposition in a Laminar Nonisothermal Flow, by Mitchell Gilbert, *Calif. Inst. Techn., Jet Propulsion Lab., Progr. Rep.* 20-336, July 1957, 25 pp.

Combustion of Elemental Boron. Summary Report for June–October 1957, *Experiment Inc., TM*-1009, 10 pp.

Phase Behavior in the Hydrogen Ammonia System, by H. H. Reamer and B. H. Sage, *Calif. Inst. Techn., Jet Propulsion Lab., Progr. Rep.* 20-237, Dec. 1957, 9 pp.

Experimental Thermal Conductivities of the $N_2O_4 = 2NO_2$ System, by Kenneth P. Coffin and Cleveland O'Neal Jr., *NACA TN* 4209, Feb. 1958, 22 pp.

Final Report Summarizing Research in Rate of High Speed Reactions, by Walter H. Wurster, *Cornell Aeron. Lab., Inc., Rep.* AD-959-A-2 (*AFOSR-TR*-58-8; *ASTIA AD* 148054), Jan. 1958, 11 pp., 8 figs.

Unified Theory of Internal Ballistics, by J. N. Kaper, *Quart. J. Mech. and Appl. Math.*, vol. 11, Part I, Feb. 1958, pp. 98–111.

Combustion Efficiency Performance of a Mil-F-5624 Type Fuel and Monomethylnaphthalene in a Single Vaporizing-type Combustor, by Anthony W. Jones and William P. Cook, *NACA Res. Mem.* E51K30, Feb. 1952, 26 pp., diagrs., photos., 2 tabs. (Declassified from Confidential by authority of NACA Res. Abstr. 123, p. 8, 1/7/58.)

Turbojet Combustor Efficiency with Ceramic-coated Liners and with Mechanical Control of Fuel Wash on Walls, by Helmut F. Butze and Edmund R. Jonash, *NACA Res. Mem.* E52125, Nov. 1952, 43 pp. (Declassified from Confidential by authority of NACA Res. Abstr. 124, p. 41, 2/10/58.)

Effectiveness of a Turbojet Tubular Combustor in Screening the Turbine from Foreign Objects, by Patrick T. Chiarito, *NACA Res. Mem.* E55E16, July 1955, 20 pp. (Declassified from Confidential by authority of NACA Res. Abstr. 124, p. 44, 2/10/58.)

Spontaneous Ignition Data of Hydrocarbons and Aviation Fluids, by E. M. Goodger, *Cranfield, Coll. of Aeron., Note* 68, Sept. 1957, 6 pp., 10 figs.

Report of Research and Technologic Work on Explosives, Explosions, and Flames; Fiscal Years 1953 and 1954, by Ruth F. Brinkley and Robert W. van Dolah, *Bur. Mines, Info. Circ.* 7804, Nov. 1957, 127 pp.

Preliminary Investigation of a Chemical Starting Technique for the Acid Gasoline Rocket Propellant System, by Glen Hennings and Gerald Morrell, *NACA Res. Mem.* E52K21, Jan. 1953, 23 pp. (Declassified from Confidential by authority of NACA Res. Abstr. 124, p. 41, 2/10/58.)

Methods for Calculating Thrust Augmentation and Liquid Consumption for Various Turbojet-afterburner Fuels, by James F. Morris, *NACA Res. Mem.* E-56A23, Oct. 1956, 73 pp. (Declassified from Confidential by authority of NACA Res. Abstr. 124, p. 44, 2/10/58.)

A Study of Sampling of Flame Gases, by C. Halpern and F. W. Ruegg, *J. Res., Nat. Bur. Standards*, vol. 60, no. 1, Jan. 1958, pp. 29–37.

How to Estimate Solid Propellant Rocket Performance, by Saxe Dobrin, *Aviation Age*, vol. 28, no. 8, Feb. 1958, pp. 70–73.

Materials of Construction

Electrical, Thermoelectric, Hardness and Corrosion Properties of Vanadium-base Alloys, by H. J. Cleary, *Nuclear Metals, Inc.* (*U.S. Atomic Energy Comm.*), NMI-1161, Sept. 1957, 1 vol.

Thermal and Electrical Conductivities of

Tungsten. Experimental Results on Single Crystals Compared with Theory, by J. DeNobel, *Physica*, vol. 23, March 1957, pp. 261–269 (in English).

Thermal and Electrical Resistivity of Some Tungsten Single Crystals at Low Temperatures and in Strong Magnetic Fields, by J. DeNobel, *Physica*, vol. 23, April 1957, pp. 349–358 (in English).

The Mechanical and Engineering Properties of Commercially Available Titanium Alloys, by H. V. Kinsey, *NATO, Advisory Group for Aeron. Res. and Dev., Rep.* 100, April 1957, 15 pp.

How to Design Radome Structures for High Speed Aircraft and Missiles, by R. M. Kubow and N. J. Linardos, *Aviation Age*, vol. 28, no. 8, Feb. 1958, pp. 74–79.

Instrumentation, Telemetering, Data Recording

Central Automatic Data Processing System, by the Staff of the Lewis Laboratory. Chapter I: General Description, by Bert A. Coss. Chapter II: Central Recording System, by Robert L. Miller. Chapter III: Automatic Voltage Digitizers, by Leonard Jaffe and Richard L. Smith. Chapter IV: Frequency Data, by John Ryskamp. Chapter V: Digital Automatic Multiple Pressure Recorder, by Leonard Jaffe, Arthur J. Gedeon and Richard N. Bell. Chapter VI: Playback and Control Room Equipment, by John Ryskamp, *NACA TN* 4212, April 1958, 96 pp.

New Breed of Microwave Tubes Spurs Radar, ECM, Scatter Designs, by James Holahan, *Aviation Age*, vol. 29, April 1958, pp.22–23, 157–164.

Closed Loop Instrument Systems Boost Performance, by V. A. Orlando, R. G. Jewell and D. W. Dibble, *Aviation Age*, vol.29, April 1958, pp.44–47.

Commutating Switches Critical for High Performance Telemetry, by George P. Bentley and Sumner Ackerman, *Aviation Age*, vol. 29, April 1958, pp. 70–72, 75–78.

Mechanoreceptors, Gravireceptors, by Hubertus O. Strughold, *J. Astronautics*, vol.4, no.4, Winter 1957, pp.61–63.

Cosmic Ray Instrumentation for the IGY Program, by Robert C. Haymes, *J. Astronautics*, vol. 4, no. 4, Winter 1957, pp. 64–68.

Reduced-size Satellite Transmitters Coming, by Raymond M. Nolan, *Missiles and Rockets*, vol. 3, April 1958, pp. 152–153.

An Engineering Approach to Cost Reduction as Applied to the Engine Analyzer, by J. Frank Morgan and William Van Rosenbergh, *Sperry Engng. Rev.*, vol. 11, Mar. 1958, pp. 22–26.

Development of the Calorimeter Heat Transfer Gage for Use in Shock Tubes, by Peter H. Rose, *AVCO Mfg. Corp., AVCO Res. Lab., Res. Rep.* 17, Feb. 1958, 49 pp.

The Satellite Tracking Camera, by Jospeh Nunn, *Inst. Aeron. Sci., Preprint* 794, Jan. 1958, 16 pp., 2 figs.

The Army Navy Instrumentation Program, by George W. Hoover, *Inst. Aeron. Sci., Preprint* 815, Jan. 1958, 9 pp.

The Air Force Instrument Development Program, by Marvin C. Demler, *Inst. Aeron. Sci., Preprint* 795, Jan. 1958, 15 pp., 43 figs.

Temperature and Pressure Corrections to be Applied to the Shielded Hot Wire Anemometer at Speeds for Which Natural Convective Cooling Is Negligible, by C. F.

Cowdrey, *Brit. J. Appld. Phys.*, vol. 9, Mar. 1958, pp. 112–116.

Strain-gage Principles, by M. A. Legette, *Instrs. & Automation*, vol. 31, Mar. 1958, pp. 447–449.

Strain-gage Instrumentation, by C. M. Hathaway, *Instrs. & Automation*, vol. 31, Mar. 1958, pp. 450–454.

Optical Strain-gage Standard, *Instrs. & Automation*, vol. 31, Mar. 1958, p. 455.

Sensitivity Ratings for Strain Gages, by Peter. K. Stein, *Instrs. & Automation*, vol. 31, Mar. 1958, pp. 456–561.

High-temperature Strain Gages, by Louis Herczeg and Paul Beckman, *Instrs. & Automation*, vol. 31, Mar. 1958, pp. 460–461.

Thermal Compensator for Bourdon Gauges, by Otto W. Heise, *Instrs. & Automation*, vol. 31, Mar. 1958, p. 473.

Methods of Testing Thermocouples and Thermocouple Materials, by William F. Roeser and S. T. Lonberger, *Nat. Bur. Standards, Circ.* 590, Feb. 1958, 21 pp.

Time Constants and Frequency Response of Coated Hot Wires Used as Turbulence Sensing Elements, by Avis Borden, *David Taylor Model Basin, Rep.* 952, June 1957, 48 pp.

Electronics: What's Coming After the Missile Age? by W. R. G. Baker, *Proc., Inst. Radio Engrs.*, vol. 46, Mar. 1958, pp. 534–537.

Thermoelectric Effects, by Frank E. Jaumot Jr., *Proc., Inst. Radio Engrs.*, vol. 46, Mar. 1958, pp. 538–554.

Unusual Propagation at 40 MC from the USSR Satellite, by H. W. Wells, *Proc., Inst. Radio Engrs.*, vol. 46, Mar. 1958, p. 610.

A Note on Some Signal Characteristics of Sputnik I, by J. D. Kraus and J. S. Albus, *Proc., Inst. Radio Engrs.*, vol. 46, Mar. 1958, pp. 610–611.

Intermetallic Semiconductors, by Henry T. Minden, *Sylvania Technologist*, vol. 11, Jan. 1958, pp. 6–9.

Apparatus for Producing and Measuring High-energy Electrical Discharges, by W. E. Richeson, *Rev. Sci. Instr.*, vol. 29, Feb. 1958, pp. 99–104.

Novel Circuit for Delivering Known Spark Energies, by T. A. Erikson, *Rev. Sci. Instr.*, vol. 29, Feb. 1958, pp. 173–174.

Piezoelectric Detector for Low-pressure Shock Waves, by Herbert T. Knight, *Rev. Sci. Instr.*, vol. 29, Feb. 1958, pp. 174–175.

Indium Resistance Thermometer, by G. K. White, S. B. Woods and F. Anglin, *Rev. Sci. Instr.*, vol. 29, Feb. 1958, pp. 181–182.

Backlighting the Shock Around a Moving Explosive Charge, by D. J. Hinz and J. Wenig, *Aberdeen Proving Ground, Ballistic Res. Labs., Mem. Rep.* 1110, Oct. 1957, 16 pp.

Aeronautical Studies in the Aeroballistic Range, by G. V. Bull, *Canadian Armament Res. and Dev. Estab., Rep.* 302/57, July 1957, 25 pp.

Comparison of Ballistic and "Breguet" Ranges, by D. Dembrow, *Johns Hopkins Unw., Appld. Phys. Lab.*, CF-222, March 1958, 8 pp., 5 figs.

Redesign Adapts Accelerometers to High Speed Use, by Daniel T. Gundersen, *Aviation Age*, vol. 29, May 1958, pp. 132–141.

Cyclops Cores Simplify Earth-satellite Circuits, by W. Matthews, R. W. Rochelle, C. B. House, R. L. Van Allen, D. H. Schaefer and J. C. Schaffert, *Electronics*, vol. 31, no. 9, Feb. 28, 1958, pp. 56–63.

Approximation Methods for the Calcula-

tion of Ultra-high-frequency Radio Wave Field Strength, Considering the Effects of Local Terrain, by A. N. Kalinin, *Radiotekhnika*, vol. 12, no. 4, April 1957, pp. 13–23 (in Russian).

A Method of Determining the Thermal Conductivity, Electrical Resistivity and Total and Spectral Emissivity of a Conducting Material at High Temperature from Electrical and Thermo-optical Measurements on a Heated Tube in a Vacuum, by Walter B. Powell, *Calif. Inst. of Techn., Jet Propulsion Lab., Progr. Rep.* 20-324, July 1957, 17 pp.

Experimental Investigation of the Surface Impact Pressure Probe Method of Measuring Local Skin Friction at Supersonic Speeds, by Charles J. Stalmach Jr., *Univ. of Texas, Defense Res. Lab.*, CF 2675 (DRL-410), Jan. 1958, 53 pp., 7 tabs., 36 figs.

A Contact Extensometer for the Recording of Flight Load Spectra, by O. Svenson, *NATO, Advisory Group for Aeron. Res. and Dev., Rep.* 121, May 1957, 10 pp.

A Study of Error Effects in Measuring Cyclic-temperature Heat-transfer Coefficients, by David A. Dingee and Joel W. Chastain, *Battelle Mem. Inst.* (*U.S. Atomic Energy Comm.*), BMI-1167, Feb. 1957, 1 vol.

Guidance Systems and Components

1958 Missile Guidance Roundup, by Heyward E. Canney Jr., *Missiles and Rockets*, vol. 3, no. 2, Feb. 1958, pp. 77–83.

How Industry Solved the Air-bearing Gyro Stabilization Problem, by John P. Jagy, *Missiles and Rockets*, vol. 3, no. 2, Feb. 1958, pp. 84–86.

Workhorse of Inertial Guidance, by Earl Finkle, *Missiles and Rockets*, vol. 3, no. 2, Feb. 1958, pp. 91–93.

Tracking Long-range Missiles, by Raymond M. Nolan, *Missiles and Rockets*, vol. 3, no. 2, Feb. 1958, pp. 125, 127.

Target Simulator Tests Beam-rider Missiles, by C. E. Hendrix, *Electronics*, vol. 31, no. 5, Jan. 31, 1958, p. 32.

Star Sensors for Automatic Navigation, by R. B. Horsfall, *Aviation Age*, vol. 29, April 1958, pp. 150–154.

Guiding the Terrier, by R. M. Nolan, *Ordnance*, vol. 42, March–April 1958, pp. 914–915.

An Analysis of the Optimization of a Beam Rider Missile System, by Marvin Shinbrot and Grace C. Carpenter, *NACA TN* 4145, Mar. 1958, 34 pp.

Proceedings, Guided Missiles Seminar: Guidance and Control, Sept. 2, 1956, *NATO Adv. Group for Aeron. Res. and Dev., AGARDograph* 21, Sept. 1956, 291 pp. Contents: **Weapons System Philosophy,** by George H. Clement, pp. 1–10; **ORO Weapon System Philosophy,** by Harlan C. Meal, pp. 11–28; **New Principles in the Design of Superior Communications, Navigation and Missile Guidance Systems,** by W. P. Lear Sr., pp. 29–38; **Guidance Techniques,** by Walter L. Webster Jr., pp. 29–56; **Considerations in the Choice of a Missile Guidance and Control System,** by Robert W. Mayer, pp. 57–66; **Inertial Navigation,** by Norman F. Parker and Charles P. Greening, pp. 67–86; **Aiding the Inertial Navigation System,** by William F. Ballhaus and Frederick Stevens Jr., pp. 87–100; **Linear Homing Navigation,** by Robert K. Roney, pp. 101–114; **Pitfalls in Missile Control,** by Robert L. Johnson, pp. 115–138; **The Effects of Airframe Characteristics on**

Control System Design, by F. E. Perry, pp. 139–152; **Geometrical Stabilization Based on Sevodriven Gimbals and Integrating Gyro Units,** by Charles S. Draper and Roger B. Woodbury, pp. 153–182; **Sampled Data Systems,** by John R. Ragazzini, pp. 183–228; **Digital Techniques in Missile Guidance Systems,** by Sidney Darlington, pp. 229–248; **The Use of Digital Computer Techniques in Missile Design and Control,** by D. H. Gridley, pp. 249–264; **The Application of Noise and Filter Theories to Guidance Problems,** by R. J. Parks and Robert M. Stewart, pp. 265–284; **Recent Developments in Fixed and Adaptive Filtering,** by A. G. Carlton and J. W. Folin Jr., pp. 285–300; **Practical Problems Encountered in Missile Guidance and Control Design,** by R. E. Whiffen, pp. 301–314; **Application of Methods of Science to the Problem of Reliability,** by C. Raymond Knight, pp. 315–330; **Reliability of Guided Missiles,** by Edwin A. Speakman, pp. 331–340; **Laboratory and Flight Evaluation of Airborne Guidance Systems,** by W. H. Clohessy, pp. 341–346; **Trends in Field Testing of Guided Missiles,** by Ernest A. Steinhoff, pp. 347–358; **Low Signal Level Missile Instrumentation,** by L. G. DeBey, pp. 359–374; **On the Way to Automated Processing of Flight Measurement,** by W. E. Klemperer, pp. 375–386; **Paper on the Guidance and Control of Missiles,** by Stephen Waldron, pp. 387–391.

Attenuation of Radio Waves as a Result of Boundary Layer Heating in Missiles Traveling at Supersonic Speeds, by Kilburn MacMurraugh, *NAVORD Rep.* 5816 (*NOTS* 1896), Jan. 1958, 18 pp.

Guidance and Control, by Peter A. Castruccio, *Aviation Age*, vol. 28, Mar. 1958, pp. 64–68.

Traveling Wave Slot Makes Novel X-band Beacon Antenna, by L. K. DeSize and L. J. Kuskowski, *Aviation Age*, vol. 28, Mar. 1958, pp. 188–192.

Atmospheric Angels Mimic Radar Echoes, by Vernon G. Plank, *Electronics*, vol. 31, Mar. 14, 1958, pp. 140–144.

Simple Plotter Analyzes Radar Noise Rapidly, by Daniel J. Zoll, *Electronics*, vol. 31, Mar. 14, 1958, pp. 162–164.

Inertial Guidance, by Walter Wrigley, Roger B. Woodbury and John Hovorka, *Inst. Aeron. Sci., SMF Fund Paper* FF-16, Jan. 1957, 69 pp.

Servomechanisms and Controls

The Improvement of Stabilization of Control Systems with Bounded Speed of the Servomotor by Means of a Memory Device, by V. A. Kotelnikov, *Automatika i Telemekanika*, vol. 18, no. 4, 1957, pp. 289–295 (in Russian).

Signal Stabilization of a Control System, by R. Oldenburger, *Automatika i Telemekanika*, vol. 18, no. 5, 1957, pp. 392–397 (in Russian).

The Synthesis of Linear Servosystems Using the Criterion of Minimum of Practically Critical Reproduction Error, by K. I. Kurakin, *Automatika i Telemekanika*, vol. 18, no. 5, 1957, pp. 402–408 (in Russian).

An Analog Study of a High-speed Recording Servomechanism, by J. W. Schwartzenberg, *Trans., ASME*, vol. 80, no. 2, Feb. 1958, pp. 490–496.

A Method for Designing a Sampling Servo System, by Saburo Kumagai and Akira Nishigori, *Osaka Univ., Technology Reps.*, vol. 7, March 1957, pp. 19–30.

Intelligence Sources for Guidance, by Arthur S. Locke, *Inst. Aeron. Sci., Preprint* 795, Jan. 1958, 15 pp., 43 figs.

The Development of the Talos Land Based System, by D. B. Holmes, *Inst. Aeron. Sci., Preprint* 804, Jan. 1958, 9 pp., 9 figs.

Report on the Endurance of Irreversible Servo Controls, by L. Vandenberghe, *NATO, Adv. Group for Aeron. Res. and Dev., Rep.* 128, May 1957, 6 pp. (in French).

Improvements of the Transient Response of Contractor Servomechanisms, by Yoshikazu Sawaragi and Hajime Akashi, *Proc., Japan, 6th Natl. Congr. for Appld. Mech.*, 1956, pub. 1957, pp. 461–464.

On the Self-excited Oscillations of a Non-linear Cascade Control System, by Yoshikazu Sawaragi, Yoshifumi Sunahara and Akira Someya, *Proc., Japan., 6th Natl. Congr. for Appld. Mech.*, 1956, pub. 1957, pp. 477–482.

Flight Vehicle Design and Testing

History of German Guided Missiles Development, by Th. Benecke and A. W. Quick, Brunswick, Germany, Appelhans, 1957, 420 pp. (*North Atlantic Treaty Organization, Advisory Group for Aeron. Res. and Dev., AGARDograph* no. 20.)

Rockets, Missiles and Space Vehicles, *Interavia*, vol. 13, no. 2, Feb. 1958, pp. 150–151.

NACA Hypersonic Rocket and High Temperature Jet Facilities, by Paul E. Purser and Aleck C. Bond, *NATO, Advisory Group for Aeron. Res. and Dev., Rep.* 140, July 1957, 13 pp.

Red Missile Arsenal, *Aviation Age*, vol. 29, April 1958, pp. 20–21, 94–96, 98–101.

Some Variation Problems Connected with the Launching of Artificial Satellites of the Earth, by D. E. Okhotsimskii and T. M. Eneev, *J. Brit. Interplanet. Soc.*, vol. 16, Jan.–Feb. 1958, pp. 263–294.

Rockets, Missiles and Space Vehicles, *Interavia*, vol. 13, March 1958, pp. 243–245.

Recoverable Boosters are Studied to Cut Manned Space Flight Cost, by D. C. Romick, R. A. Belfiglio and F. B. Sandgren, *Missiles and Rockets*, vol. 3, April 1958, pp. 95–96, 98, 100.

Role of Guided Missiles, by Dr. C. C. Furnace, *Ordnance*, vol. 42, March–April 1958, pp. 817–819.

Generalized Variational Approach to the Optimum Thrust Programming for the Vertical Flight of a Rocket, Part I: Necessary Conditions for the Extremum, by Angelo Miele, *Zeitschrift für Flugwissenschaften*, vol. 6, March 1958, pp. 69–77 (in English).

Guided Weapons and Aircraft—Some **Differences in Design and Development,** by J. E. Serby, *J. Roy. Aeron. Soc.*, vol. 62, Mar. 1958, pp. 187–202.

Application of the Electronic Digital Computer to the Solution of Flight Dynamics Problems, by Werner Niemz, *Zeitschrift für Flugwissenschaften*, vol. 6, Feb. 1958, pp. 47–52 (in German).

Missile Market Guide and Directory, *Missiles and Rockets*, vol. 3, No. 5, Mid-April 1958, 462 pp.

Effects of Size of Ballistic Missiles, by Oscar Scholze, *Raketentechnik und Raumfahrtforschung*, vol. 2, no. 1, 1958, pp. 2–8.

Entering the Atmosphere, by Terence Nonweiler, *Spaceflight*, vol. 1, no. 7, April

1958, pp. 238–240.

A Test and Launching Standard for the Vanguard Rockets, by Don Karshan, *Spaceflight*, vol. 1, no. 7, April 1958, pp. 253–257.

Motion of a Ballistic Missile Angularly Misaligned with the Flight Path upon Entering the Atmosphere and Its Effect upon Aerodynamic Heating, Aerodynamic Loads and Miss Distance, by H. J. Allen, *NACA TN* 4048, Oct. 1957, 66 pp.

A Study of the Motion and Aerodynamic Heating of Missiles Entering the Earth's Atmosphere at High Supersonic Speeds, by H. Julian Allen and A. J. Eggers Jr., *NACA TN* 4047, Oct. 1957, 61 pp.

New Methods in Heat Flow Analysis With Application to Flight Structures, by M. A. Biot, *J. Aeron. Sci.*, vol. 24, Dec. 1957, pp. 857–872.

Flight Measurements of Boundary-layer Temperature Profiles on a Body of Revolution (NACA RM-10) at Mach Numbers from 1.2 to 3.5, by A. G. Swanson, J. J. Buglia and L. T. Chauvin, *NACA TN* 4061, July 1957, 40 pp.

Theory and Apparatus for Meaurement of Emissivity for Radiative Cooling of Hypersonic Aircraft with Data for Inconel and Inconel X, by William J. O'Sullivan Jr., and William R. Wade, *NACA TN* 4121, Oct. 1957, 48 pp.

Interception Problems for Surface to Air Missiles, by James Hay Stevens, *Aeronautics*, vol. 38, Mar. 1958, p. 27.

Ballistic Missiles, by Terence R. F. Nonweiler, *Aeronautics*, vol. 28, Mar. 1958, pp. 28–31.

Instruments of Interception (Missile Catalogue), *Aeronautics*, vol. 28, Mar. 1958, pp. 38–40.

A Note on Goddard's Problem, by G. Leitmann, *Astronautica Acta*, vol. 3, no. 4, 1957, pp. 237–240.

Space Flight

A Note on Space Travel in a Gravitational Field, by E. Newton Rowland, M. A., Ph.D., *J. Brit. Interplan. Soc.*, vol. 16, Oct.–Dec. 1957, pp. 216–221.

Effects of Acceleration on the Human Frame, by Wg. Cdr. F. Latham, *J. Brit. Interplan. Soc.*, vol. 16, Oct.–Dec. 1957, pp. 222–224.

Gravitational Torque on a Satellite Vehicle, by Robert E. Roberson, *J. Franklin Inst.*, vol. 265, Jan. 1958, pp. 13–22.

The True Nature of the Boiling of Body Fluids in Space, by Capt. Julian E. Ward, *J. Aviation Medicine*, vol. 27, Oct. 1956, pp. 429–439.

Astrophysics, Aerophysics

A Continuously Recording Automatic Auroral Radar, by A. G. McNamara, *Canadian J. Physics*, vol. 36, Jan. 1958, pp. 1–8.

On the Theory of Propagation of Electromagnetic Waves Along a Curved Surface, by James R. Wait, *Canadian J. Physics*, vol. 36, Jan. 1958, pp. 9–17.

A Large-area Liquid Scintillation Counter and Some Measurements on High-energy Cosmic-ray Particles, by C. H. Millar, E. P. Hincks and G. C. Hanna, *Canadian J. Physics*, vol. 36, Jan. 1958, pp. 54–72.

Further Interactions of the Heavy Nuclei of the Cosmic Radiation, by V. Y. Rajopadhye and C. J. Waddington, H. H. Wills Phys. Lab., Bristol (England), *Philosophical Mag.*, 8th Series, vol. 3, Jan. 1958, pp. 19–32.

Nuclear Propulsion

Stability of the Pinch, by Marshall Rosenbluth, *Atomic Energy Comm.*, LA-2030, June 1956, 36 pp.

Conceptual Design of an Advanced Engineering Test Reactor, by R. G. Mallon, J. Saldick and R. E. Gibbons, *Atomic Energy Comm.*, NYO-4849, March 1957, 124 pp.

A Selection Study for an Advanced Engineering Test Reactor, Aeronutronic Systems, Inc., *Atomic Energy Comm.*, AECU-3478, March 1957, 142 pp.

Dynamic Simulation of a Fast Reactor System, by Richard G. Olson, *ASME, Paper* 57-NESC-25 (*AIEE, Paper* 57-402; *Nuclear Engng. Sci. Conf.*, 2nd, March 11–14, 1957), 10 pp.

Control Problems in Sodium Cooled Graphite Moderated Reactors, by J. E. Owens, *ASME, Paper* 57-NESC-77 (*Nuclear Engng. Sci. Conf.*, 2nd, March 11–14, 1957), 11 pp.

Solid State Neutron Flux Measuring System, by Truman S. Gray, William M. Grim Jr., Frank S. Replogle and Richard H. Spencer, *ASME, Paper* 57-NESC-35 (*AIEE, Paper* 57-407; *Nuclear Engng. Sci. Conf.*, 2nd, March 11–14, 1957), 8 pp.

The Development of a Thermal Neutron Flux Measuring Instrument, by C. V. Weaver, C. K. Smith and J. W. Chastain, *ASME, Paper* 57-NESC-39 (*AIEE, Paper* 57-406; *Nuclear Engng. Sci. Conf.*, 2nd, March 11–14, 1957), 8 pp.

Energy Exchange between Electron and Ion Cases through Coulomb Collisions in Plasmas, by A. A. Dougal and L. Goldstein, *Phys. Rev.*, vol. 109, no. 3, Feb. 1, 1958, pp. 615–624.

Electron-electron Interaction and Heat Conduction in Gaseous Plasmas, by L. Goldstein and T. Sekiguchi, *Phys. Rev.*, vol. 109, no. 3, Feb. 1, 1958, pp. 625–629.

Controlled Thermonuclear Reactions; a Conference Held at Berkeley, Calif., Feb. 20–23, 1957, by *Atomic Energy Comm., TID*-7536 (Part I), Sept. 1957, 41 pp.

Waves in a Plasma in a Magnetic Field, by Ira B. Bernstein, *Atomic Energy Comm.*, NYO 7897, April 1957, 41 pp.

An Energy Principle for Hydromagnetic Stability Problems, by I. B. Bernstein, E. A. Frieman, M. D. Kruskal and R. M. Kulsrud, *Atomic Energy Comm.*, NYO-7896, March 1957, 26 pp. (Appendix to NYO-7315.)

Exact Non-linear Plasma Oscillations, by Ira B. Bernstein, John M. Greene and Martin Kruskal, *Atomic Energy Comm.*, NYO-7898, June 1957, 19 pp.

An Energy Principle for Hydromagnetic Stability Problems, by I. B. Bernstein, E. A. Frieman, M. D. Kruskal and B. M. Kulsrud, *Atomic Energy Comm.*, NYO-7315, March 1957, 56 pp.

Conference on the Utilisation of Heat from Nuclear Reactors Held at Harwell on 18th Jan. 1957, *Gt. Brit., Atomic Energy Res. Estab., AERE* CE/R 2257 (Rev. Ed.), 1957, 88 pp.

Report on a Conference on Neutron Source Preparation and Calibration Held at Buckland House on the 8th and 9th of July 1954, by D. J. Littler, *Gt. Brit., Atomic Energy Res. Estab., AERE* NP/R 1577, 1957, 57 pp.

Two-dimensional Diffusion Theory Analysis of Reactivity Effects of a Fuel-plate-removal Experiment, by Edward R. Togsky, James P. Cusick and Donald Bogart, *NACA TN* 4164, Jan. 1958, 30 pp.

Index to Advertisers